Downstream processing of lentiviral vectors with focus on steric exclusion chromatography

Von der Naturwissenschaftlichen Fakultät der

Gottfried Wilhelm Leibniz Universität Hannover

zur Erlangung des Grades

Doktorin der Naturwissenschaften (Dr. rer. nat.)

genehmigte Dissertation

von

Jennifer Julia Labisch, M.Sc.

2023

Referent: Prof. Dr. rer. nat. Thomas Scheper

Korreferent: Prof. Dr. rer. nat. Sascha Beutel

Tag der Promotion: 15.03.2023

Zusammenfassung

Lentivirale Vektoren (LV) werden zur Übertragung therapeutischer Gene für die Gen- und Zelltherapie eingesetzt, vornehmlich für die Therapie mit chimären Antigenrezeptor-T-Zellen. Das Marktwachstum führt zu einer steigenden Nachfrage nach LV. Die geringe LV-Stabilität stellt Anforderungen an einen schonenden Prozess. Bestehende Verfahren müssen stark optimiert werden und die Erforschung neuer, alternativer Methoden ist unerlässlich.

In einem ganzheitlichen Ansatz fokussiert sich die Arbeit auf gefundene Schwachstellen und stellt für die Klarfiltration, die Analytik und die chromatographische Reinigung neue Ansätze vor. Im ersten Teil dieser Arbeit wurde eine vakuumbasierte Klärungsmethode mit Kieselgur für LV etabliert, die durch Suspensionszellkultur hergestellt wurden. Diese Klärungsmethode ermöglichte eine schnelle Filtration mit hohem Durchsatz und verbesserte die Handhabung durch den Wegfall des Zentrifugationsschritts und die Erhöhung der Filterkapazität. Die Klarfiltration von LV legte damit die Grundlage für nachfolgende Chromatographiestudien.

Um den analytischen Probendurchsatz zu verbessern und die Prozessentwicklung zu beschleunigen, befasste sich der zweite Teil dieser Arbeit mit der Entwicklung eines Hochdurchsatzassays mit automatisierter Erfassung und Auswertung zur Bestimmung des infektiösen Titers, welcher für umhüllte virale Vektoren die wichtigste Prozessgröße darstellt. Transduzierte Zellen werden hierbei durch immunologische Detektion in einem Echtzeit-Lebendzell-Analysesystem mit softwarebasierter Bildauswertung quantifiziert.

Der dritte und vierte Teil befasste sich mit der sterischen Ausschlusschromatographie (SXC). Es konnte gezeigt werden, dass die Mischstrategie der Puffer und die Flussrate für den thermodynamisch getriebenen Prozess der Verarmungsinteraktion zwischen den LV und der Membran entscheidend sind. Weiterhin wurde identifiziert, dass die Parameter PEG Konzentration und Größe entscheidend für den Erfolg sind und dementsprechend optimiert werden müssen. Die Visualisierung der LV auf der Membran zeigte, dass hauptsächlich die oberste Membranlage für die Abscheidung genutzt wurde. Daher war die oberflächenspezifische Flussrate für die Hochskalierung entscheidend. Das mechanistische Verständnis des Prozesses und die Prozessoptimierungen ermöglichten reproduzierbar hohe LV-Wiederfindungen und die Entfernung von Verunreinigungen.

Schlagwörter: Lentivirale Vektoren, Klarfiltration, Sterische Ausschlusschromatographie, Analytik infektiöser Titer

Abstract

Lentiviral vectors (LV) are widely used to deliver therapeutic genes for gene therapy and gene-modified cell therapy and have shown success in chimeric antigen T cell therapies. The ongoing market growth leads to an increasing demand for purified LV which requires efficient downstream processes. Due to the lower stability of LV, new demands are placed on the process. Existing unit operations must be greatly optimized and research into new, alternative methods is essential.

In a holistic approach, the work focused on identified bottlenecks and presents new approaches for clarification, analytics, and chromatographic purification. In the first part of this work, a vacuum-based clarification method with diatomaceous earth was improved for LV which were produced by suspension cell culture. This clarification method allowed fast and high throughput clarification and improved handling by eliminating the centrifugation step and increasing filter capacity. Thus, clarification of LV with diatomaceous earth laid the foundation for subsequent chromatography studies.

To improve the analytical sample throughput and accelerate process development the second part of this thesis deals with the development of a high throughput assay with automated readout and analysis for the determination of the infectious titer, which is the key process variable for enveloped viral vectors. For this purpose, transduced cells are quantified by immunological detection in a real-time live-cell analysis system using software-based image evaluation.

Eventually, the third and fourth parts focused on steric exclusion chromatography. It could be demonstrated that process parameters like the buffer mixing strategy and flow rate are crucial for this thermodynamically driven process of depletion interaction between the LV and the membrane. Moreover, it was shown that an ideal PEG molecular weight and concentration must be identified. The visualization of the LV on the membrane showed that the LV were mainly found on the first membrane layer after loading. Therefore, the surface area-specific flow rate was crucial for scale-up. The mechanistic understanding of the process and the process optimizations enabled reproducibly high LV recoveries and removal of impurities.

Keywords: Lentiviral vectors, clarification, steric exclusion chromatography, infectious titer analytics

Danksagung

An dieser Stelle möchte ich mich herzlich bei allen Personen bedanken, die mich in den letzten Jahren bei dieser Arbeit sowohl fachlich auch als persönlich unterstützt haben.

Zuerst möchte ich mich bei Herrn Prof. Dr. Thomas Scheper für die Möglichkeit bedanken mein Promotionsthema zu bearbeiten, sowie für die Übernahme des Erstgutachtens und die Zeit, mir Rückmeldung zu geben und die Ergebnisse meiner Arbeit zu bewerten. Darüber hinaus möchte ich mich bei Herrn PD Dr. Ulrich Krings für die Übernahme als weiteren Prüfer und bei Herrn PD Dr. Sascha Beutel für die Übernahme des Korreferats und den Prüfungsvorsitz bedanken.

Weiterhin möchte ich mich bei Dr. Karl Pflanz und Dr. Franziska Bollmann für ihre Anregungen, fachlichen Diskussionen und Unterstützung während meiner Promotion bedanken. Auch der LEAD Arbeitsgruppe möchte ich danken für die gute Zusammenarbeit, insbesondere Florian Hebenstreit, Marius Iseke, Dr. Andreas Pickl, Klaus Schöne und Dr. Sandra Söderholm. Bei allen Kollegen und Kolleginnen, mit denen ich im S2 Labor arbeiten durfte, vor allem bei Katja, Diana, Sinan, Katrin und Jana, möchte ich mich für die wunderbare Atmosphäre und die Zusammenarbeit im Labor bedanken.

Ein weiteres großes Dankeschön geht an die Doktoranden aus dem gemeinsamen Büro, insbesondere Lucas, Sascha und Fabian. Die fachlichen Diskussionen, aufbauende Gespräche und geteilte Frustration haben diese Zeit immens bereichert.

Mein besonderer Dank gilt meinen Studenten Philip Wiese, Meriem Kassar und Richard Paul, die ich während meiner Promotion betreut habe und von denen ich ebenso viel lernen durfte. Es war mir eine große Freude sie zu betreuen und sie bei ihrem Abschluss des Studiums zu begleiten und zu unterstützen.

Ich danke meinen Freundinnen, die mir geholfen haben, die Verbindung zur Welt außerhalb meiner Forschung aufrecht zu erhalten. Abschließend möchte ich mich bei meinen Eltern Margarete und Waldemar, bei Michael, bei Kamilla, bei meinem Bruder Matthias und meinen Großeltern Gisela, Peter und Irena für ihre Unterstützung bedanken. Insbesondere möchte ich mich bei Alex bedanken für die Geduld, den Zuspruch und den Glauben an mich.

Table of contents

1 Introduction

Gene therapy and gene-modified cell therapy are rapidly growing fields in the pharmaceutical industry that hold great potential to cure a wide range of diseases by delivering a therapeutic gene into the respective target cells [1]. Currently, more than 3,000 gene therapy clinical trials are ongoing using various delivery systems including the physical administration of naked nucleic acids or the use of viral vectors [2]. Immunotherapy with chimeric antigen receptor (CAR) T cells is a well-known gene-modified cell therapy with five commercially approved products to date [3–5]. Lentiviral vectors (LV) are a commonly used vector to transfer the gene coding for the CAR to T cells, which renders the generated CAR-T cells specific to tumor antigens. LV are especially useful for this application as they stably integrate its genome into the target cell genome, thereby enabling long-term expression of the transgene [6]. Extensive engineering of LV improved their efficiency and biosafety such that the first pediatric patient with acute lymphoblastic leukemia has now been cancer-free for ten years following LV-mediated CAR T-cell therapy [7].

During the upstream process, LV are produced by mammalian cells which secrete the LV into the medium [8]. The downstream process aims to remove the impurities while concentrating the vector and maintaining its activity. The cell and gene therapy market growth leads to an increasing demand for viral vectors and hence efficient downstream processes and respective analytics. The transfer of existing methods in protein purification for the purification of LV is difficult because the biomolecules have different properties and different demands on the process. This requires a significant optimization of existing unit operations; or exploring new, alternative approaches for the downstream process.

As the industry moves towards LV production with suspension culture, the classical laboratory-scale approach of centrifugation and filtration holds difficulties when dealing with the increased impurity load. The use of filter aids could be a promising alternative. LV typically show high susceptibility towards buffer components of classical chromatography modes like ion exchange or affinity chromatography. Therefore, there is a need to explore and develop alternative chromatography methods that preserve viral infectivity. High throughput virus analytics represents one of the major bottlenecks in viral vector process development and new methods are constantly being developed as there is no universal solution due to the heterogeneous properties of the different vector types.

2 Scope of the research

The aim of the thesis was to improve the laboratory-scale downstream process of LV in terms of an efficient clarification process and to gain a greater mechanistic understanding of steric exclusion chromatography (SXC) that would enable its implementation for LV purification. Besides general SXC process optimization, gaining insights into the scalability of the unit operation was targeted. An additional goal was to advance and automate the LV infectious titer analytical assay, which in turn would aid in accelerating process development.

First, a suitable clarification method needs to be developed to obtain clarified LV material produced by suspension mammalian cell culture, which is free of cells, cell debris, and larger contaminants, which would otherwise burden the subsequent downstream processing steps. Next, to perform process development, which generates a high number of samples, respective analytics need to be developed alongside. The success of process development steps can only be evaluated with respective analytics which enables reliable high throughput analysis, especially of the infectious LV titer as this is a key characteristic for fragile enveloped viral vectors. Subsequently, the chromatography step of LV processes needs to be improved, since classical chromatography techniques have limitations regarding the preservation of LV infectivity. The development of alternative chromatography techniques, like steric exclusion chromatography (SXC), is necessary. The lack of mechanistic understanding of SXC needs to be addressed to develop a purification protocol for LV and a scale-up solution for SXC.

In summary, the aim of this dissertation was the implementation of an alternative clarification approach, infectious titer analysis strategy, and chromatography method for LV to overcome various limitations of the existing downstream process and analytical methods.

3 Theoretical background

3.1 Lentiviral vectors and their applications

Viruses are infectious particles comprising genetic material (DNA or RNA) surrounded by a protein coat that is sometimes additionally coated by a membrane. Viruses are obligate intracellular parasites that use the host cell machinery for their replication and are therefore the underlying reason for a range of diseases [9–11]. Profound knowledge of virus biology made it possible to make use of their natural ability to efficiently transduce host cells in gene therapy and gene-modified cell therapy. The engineered viral vectors are used as therapeutic gene delivery vehicles [1,12]. Viral vectors currently used for gene transfer in gene therapy and gene-modified cell therapy clinical trials include adenoviruses, γ-retroviruses, lentiviruses (LV), adeno-associated viruses (AAV), vaccinia viruses, poxviruses, herpes simplex viruses, and others (listed from highest to lowest number of clinical trials), with LV accounting for 331 clinical trials (10.1%) [2], of these 331 clinical trials around 60% comprise chimeric antigen receptor (CAR) T cell therapies.
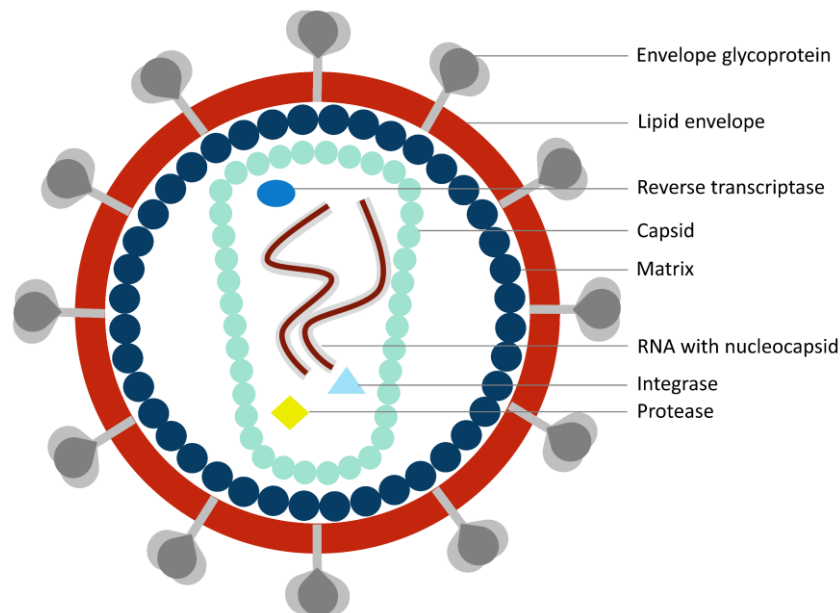
Figure 1: Scheme of lentiviral vector structure, adapted from [13,14].

Lentiviral vectors used for cell and gene therapy applications are most commonly derived from the human immunodeficiency virus HIV-1 which belongs to the *retroviridae* family [10]. The virus particles have a diameter of approximately 100 nm and are schematically depicted in Fig. 1. The conical viral capsid contains the viral genome complexed with the nucleocapsid proteins, and the enzymes reverse transcriptase, integrase, and protease. The capsid is

surrounded by an envelope membrane lined from the inside with a layer of matrix proteins. Glycoproteins are located in the envelope membrane [13,15]. A lentiviral particle has a single-stranded RNA genome with a size of up to 10 kb that is reverse transcribed into DNA and then stably integrated into the host cell genome through reverse transcriptase and integrase enzymes which are provided in the viral particle [16]. Hence, LV do not directly deliver DNA, but their RNA genome is converted into DNA via reverse transcription, and the stable integration into the host cell genome enables the stable expression of the gene of interest. The envelope membrane makes the LV extremely sensitive. Several factors like high temperature (time-dependent decay), freeze and thaw cycles, pH, shear stress, and salt concentration were reported to reduce LV infectivity [17–20].

The stable expression of the integrated transgene makes them a suitable tool for CAR-T cell therapies, which is to date the major application of LV [21]. A general flow scheme of CAR-T cell therapy is depicted in Fig. 2.
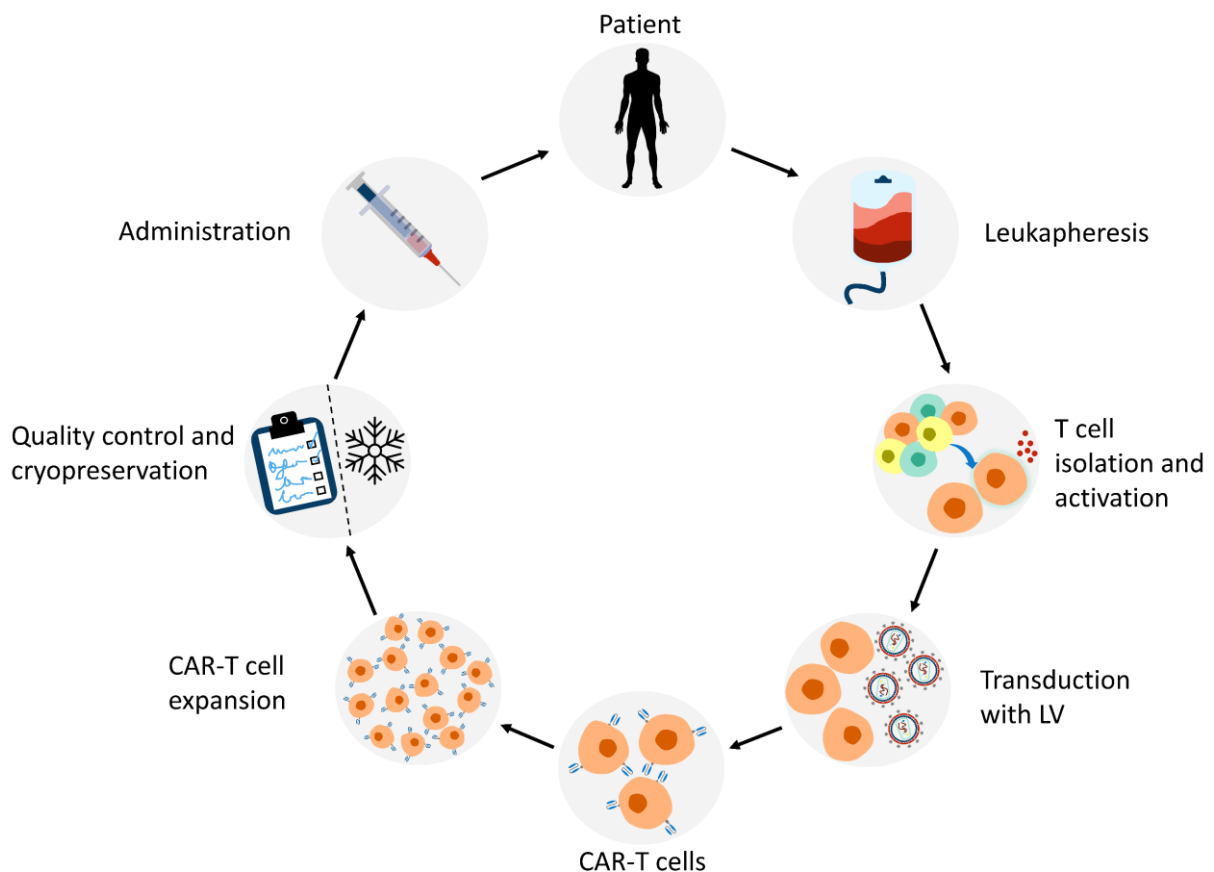

Figure 2: Workflow of autologous CAR-T cell therapy bioprocess, adapted from [6,22].

In CAR-T cell therapy, the patient's T cells are isolated and transduced with a viral vector *ex vivo* which transfers the genetic information for the CAR. The hereby generated CAR-T cells can target tumor antigens that are not naturally recognized by their endogenous T-cell

receptors. After expansion, the CAR-T cells are administered back to the patient and can recognize and kill tumor cells [6,12,23]. Five commercially available CAR-T cell therapies are currently approved of which three use LV for the transduction of the T cells for the treatment of blood cancers, including lymphomas, some forms of leukemia, and multiple myeloma [3–5]. Moreover, an LV-mediated genetic modification of autologous hematopoietic stem cells for the treatment of beta-thalassemia, a rare genetic blood disease, was recently approved that replaces a missing or mutated gene, hence this is the first approved LV gene therapy application [24].

Clinical trials using LV target the treatment of a range of diseases, including cancers, immune disorders, metabolic disorders, and rare congenital diseases [1,12]. Moreover, new potential applications for LV in vaccination, cell-type differentiation, and gene editing are currently being investigated [13,25–29].

According to market research analyses the global viral vector manufacturing market is approximately worth USD 646 million in 2021 with a projected value of USD 2,677 million in 2030 and an estimated annual growth rate of 16% over the next decade. With 10% adenoviral vectors hold the largest market share of the vector manufacturing market in 2021, however, in 2030 it is expected that lentiviral vectors will hold the greatest share with 19% [30]. The expected market growth leads to increasing demand for efficient viral vector manufacturing and consequently to a need for process development to implement such [31].

3.2 Upstream processing of lentiviral vectors

The easiest to develop and most widely used method for viral vector production is the transient transfection of mammalian cells with multiple plasmids [32]. Different transfection reagents can be used, like calcium phosphate, polyethyleneimine, and lipofectamine, to name the most common ones [33]. Typically, split genome packaging constructs of three to four plasmids (Fig. 3) are used to reduce the likelihood of recombination events that would lead to the generation of replication-competent viral vectors. The generation of replication-competent LV poses a safety concern as most LV used, are derived from the pathogenic human immunodeficiency virus 1 (HIV-1). The third-generation system with four plasmids is widely used and comprises the packaging plasmids with the *gag-pol* genes coding for the LV enzymes and structural proteins, a plasmid with the *env* gene coding for the envelope protein, mostly pseudotyped with the glycoprotein from the vesicular stomatitis virus (VSV-G), a plasmid with

the *rev* gene coding for the regulatory protein Rev, and the vector plasmid coding for the transgene [34,35].

This method offers maximum flexibility but at a large scale, high costs for the needed plasmid DNA and transfection reagents and batch variability are faced. Stable producer cell lines can be a solution to overcome cost and variability hurdles, however, some vector components, like the VSV-G envelope protein, are toxic for the cells, favoring an inducible producer cell line, and the development of a stable producer cell line is time-consuming and somewhat costly [35,36].

Traditionally the human embryonic kidney 293 (HEK293) or HEK293 T cells are used as they can be transfected easily and adapted to different culture strategies [33]. The HEK293 T cells express the SV40 large T-antigen yielding higher titers [37]. Typically, these cells are grown adherently in T-flasks, cell stacks, or factories. For large-scale production of adherent cell cultures scale-out approaches are used, adding more cell factories, cell stacks, or roller bottles to increase the culture area [38].

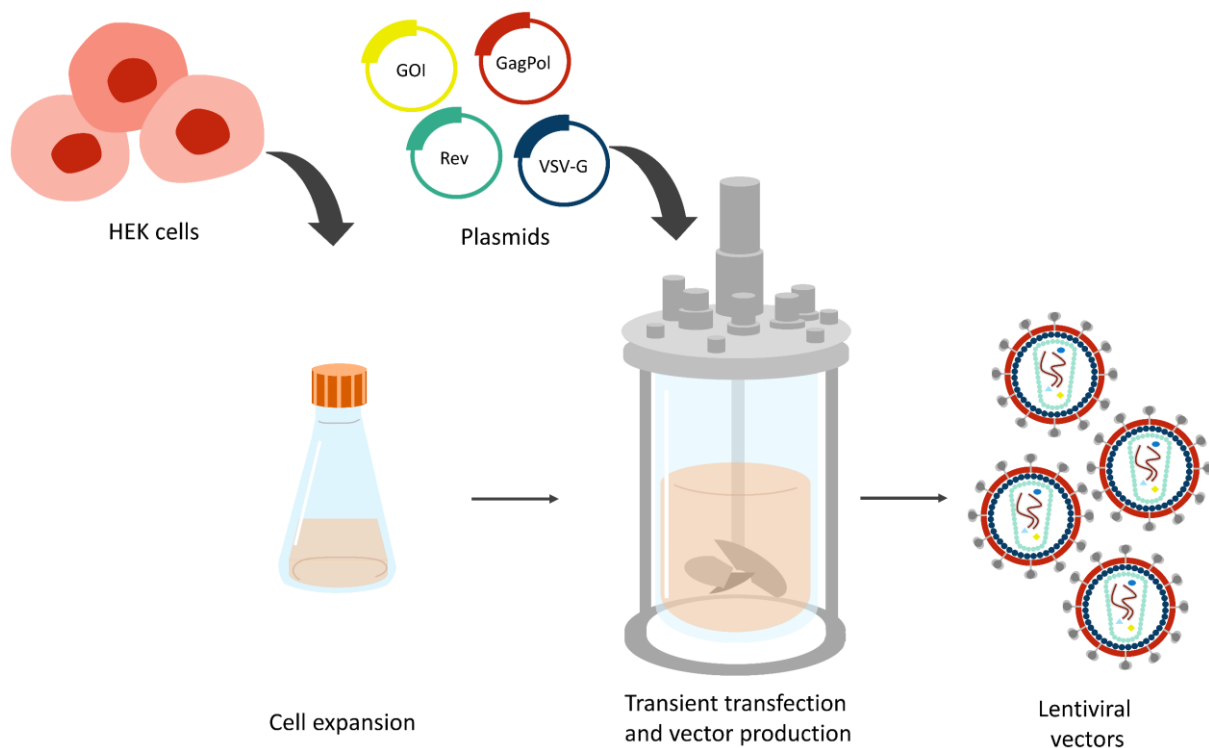**Figure 3:** Lentiviral vector batch production by transient transfection of HEK cells in a stirred tank bioreactor with multiple plasmids.

Monitoring and controlling process parameters in such culture systems are limited but offered in fixed-bed bioreactors [39,40] or hollow fiber bioreactors [41]. However, the adaption of the HEK cells to growth in suspension allows easy scale-up of viral vector production in stirred tank

bioreactors [32] (Fig. 3). Suspension cultures can be grown serum-free, reducing costs and the risk of contamination. Moreover, material and time consumption is lower compared to adherent cell cultures [37,42]. Hence, the trend goes towards LV production in suspension culture, especially because it facilitates Good Manufacturing Practice (GMP) and can advance industrial scale vector manufacturing [43]. LV production in suspension culture raises the hurdles for downstream processing as the feed has a higher impurity load compared with LV feeds produced in adherent cell culture.

3.3 Downstream processing of lentiviral vectors

After the upstream process, a series of downstream processing (DSP) steps follow that aim to increase the purity and maintain the potency of the viral vector material [14]. The viral vector material contains product-related and process-related impurities. Product-related impurities are variants of the viral vector product including inactive particles, broken particles, and vector fragments, as well as viral vector aggregates. Process-related impurities are derived from the upstream or downstream process itself and comprise media components, host cell-related molecules (cell debris, host cell DNA, and proteins), plasmid DNA, transfection reagents, nucleases, and buffers. When the viral vector is used as a pharmaceutical, the impurities must be removed down to a certain level set by regulatory authorities to ensure the safety of the product [44,45]. The DNA concentration measured after DSP operations aims to demonstrate the removal of host cell DNA and plasmid DNA. As the LV has an RNA genome, free viral RNA is not measured with the DNA quantification techniques. The acceptable remaining impurity levels are <10 ng DNA per dose for parenteral inoculation or <100 µg DNA per dose for oral administration with a DNA size of <200 base pairs [46,47]. The acceptable host cell protein limits are set by individual case reviews by regulatory authorities. For monoclonal antibody products, it is usually <100 ppm and can serve as a guideline [48].

Downstream processing of lentiviral vectors is a challenging task and requires a special set of considerations due to the low stability of the particles, their large size, and their complex structure [45]. There is no platform solution available for the DSP of LV and different combinations of unit operations are feasible [32] (Fig. 4).
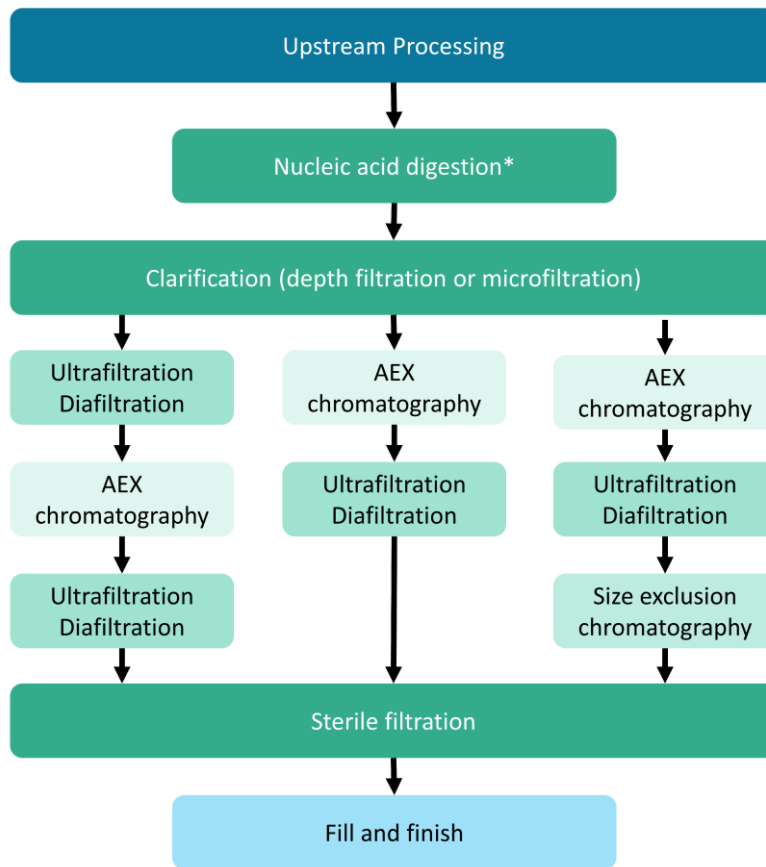
Figure 4: Downstream processing workflow of LV illustrating different sequences of unit operations. *The nuclease digestion can be implemented at different stages of the process, adapted from [45,49].

Several DSP steps are conducted to achieve purification, concentration, and stability of the LV sample. The DSP begins with the harvest of the LV from the cell culture. Lentiviral vectors bud from their host cells and are found in the supernatant [8]. Therefore, no cell lysis is required, and the clarification step is performed to remove cells and cell debris. A detailed description of the clarification step is provided in Section 3.3.1. Intermediate purification with chromatography and/or ultrafiltration is performed to purify and concentrate the vector sample, followed by a polishing step for concentration and buffer exchange to formulate the LV for improved vector stability. Common chromatography techniques for LV are described in more detail in Section 3.3.2. Finally, the LV product undergoes sterilizing filtration before the fill and finish step. A nucleic acid digestion step can be implemented at different phases of the DSP, with varying impacts on the execution of the DSP [32,49,50].

3.3.1 Clarification of lentiviral vectors

Diverse technologies for viral vector clarification exist either based on centrifugation or filtration. The overall objective of the clarification step is the removal of large impurities, e.g., cells and cell debris, and the reduction of the supernatant turbidity while recovering the vector product. Typically, two operations called primary clarification and secondary clarification are required. Primary clarification aims to remove larger impurities like cells and cell fragments, on the other hand, secondary clarification is used for the removal of colloidal matter and smaller impurities, including aggregates [51].

Centrifugation has been extensively used as a primary clarification step in combination with microfiltration as a secondary clarification step, especially for small-scale studies [43,49,52–54]. The advantage of centrifugation in handling high solid loads opposes the disadvantages of high investment and limited scalability [55]. For large-scale manufacturing, the centrifugation step is aimed to be fully replaced by filtration processes as they facilitate seamless scalability [51].

Filtration unit operations can be performed as a secondary clarification step after centrifugation (for a laboratory scale) or as both, a primary and secondary clarification step. When operating LV filtration, a suitable membrane chemistry should be selected to avoid LV adsorption to the membrane. As the LV is negatively charged at neutral pH it will likely adsorb to positively charged surfaces, which must be avoided [45]. Materials like polypropylene, polyethersulfone, or synthetic filters are widely for viral vector purification, as they enable the full transmission of the vector across the membrane while also excluding many impurities [56]. Clarifying filtration techniques comprise normal flow filtration (dead-end filtration), or tangential flow filtration (crossflow filtration) [57]. The different filtration technologies are described in the following.

Normal flow microfiltration membranes have a low dirt-holding capacity, thus being mainly used for secondary clarification [55]. Normal flow microfiltration membranes used for LV processing have moderately large pore sizes between 0.45 to 0.8 µm as smaller pore sizes result in early filter clogging and high product loss due to the large size of the LV [8]. If the LV is produced by adherent cell culture, the supernatant can be easily separated from the live cells, which remain attached to the surface of the cell culture vessel, and only a smaller amount of dead cells and cell debris is found in the supernatant. A single normal flow

microfiltration step of the supernatant derived from adherent cell culture may be sufficient given that a comparatively clear supernatant with a small amount of cells and cell debris is applied to the filter [58–60]. For the clarification of suspension cultures, the cells must be separated from the supernatant by centrifugation before the filtration step, otherwise, a large amount of cells in the supernatant leads to filter clogging. A potential method of omitting centrifugation of the suspension culture-derived material is the use of filter aids like diatomaceous earth in combination with normal flow microfiltration [61]. The highly porous and rigid structure of the diatomaceous earth forms a nearly incompressible porous cake allowing liquid flow with a reduced risk of filter clogging [62]. In a laboratory scale, this is typically performed by mixing the suspension culture with the filter aid and applying it on a bottle-top vacuum filter, whereas further scale-up solutions for clarification with diatomaceous earth are provided by FILTROX with the filter aid directly incorporated inside the filter device [63].

Another option for the primary clarification step is to perform tangential flow filtration (TFF) with microfiltration membranes in a flat-sheet cassette or a hollow fiber format. The product (viral vector) passes through the membrane and is recovered in the permeate, while cells and cell debris are retained [55,64], however TFF for LV clarification was not yet reported [49]. TFF-based primary clarification has the advantage of having the feed material flowing across the membrane surface, which is minimizing filter cake formation. Clogging of the membrane pores by filter cake formation needs to be avoided since it reduces the actual membrane pore size leading to increased virus retention [8]. Due to its long processing time and higher shear stress, the use of TFF for primary clarification of enveloped viral vectors may reduce infectious titers and respective yields.

The tangential flow depth filtration is a new clarification mode that uses a depth filter in a hollow fiber format that is operated in a TFF mode. Thereby, the cell culture feed is passed through a tubular depth filter in tangential mode. In contrast to hollow fibers, the membrane has an isotropic pore structure and an approximately 25 times higher wall thickness which serves as a depth filter [65].

Another possibility to minimize filter clogging besides using TFF or the use of filter aids is the use of normal flow depth filters. They are often made of a cascade of membranes with decreasing pore sizes with a final pore size of 0.45 µm. Large impurities like cells and cell debris

are retained at the first filter of larger pore size, while smaller impurities are retained at the smaller pore size filter. The filter train, therefore, reduces the risk of filter blocking [66–69].

3.3.2. Common chromatography techniques for lentiviral vectors

Four basic chromatography matrices exist: resins, membranes, monoliths, and nanofibers (Fig. 5). Each matrix supports different purification needs and has unique features.

Resins are porous, spherical particles and can be made for instance of agarose, dextran, cellulose, polystyrene, and polyacrylamide [70]. Resins with a defined diameter and pore size are packed into a column [71]. For the separation of biomolecules with resins, the underlying mass transfer is based on diffusion into the pores where many functional groups are located, hence slow flow rates are applied. The resin pores commonly have a size of 20-40 nm resulting in a significantly reduced dynamic binding capacity and poor mass transfer when applied to large biomolecules [72]. Therefore, resins are not widely used for the chromatography-based purification of large enveloped viral vectors, such as LV, aside from a small number of research examples. These research studies used affinity resins for LV purification either using histidine-tagged LV with immobilized metal affinity chromatography [73], desthiobiotinylated LV [74], or an LV with biotin mimicking peptide [75] with streptavidin affinity chromatography, or heparin pseudo affinity chromatography [76,77]. The separation of biomolecules is based on specific interactions between the target molecule (which may be coupled to a tag) and the ligand. Affinity tags and ligands pose a regulatory concern due to possible ligand leakage, the toxicity of desorption reagents, and ligands from animal sources like heparin that complicate the clinical use of the LV purified by these methods [34,50]. Moreover, immobilized metal affinity chromatography faced issues with retrovirus stability because the desorption reagent imidazole reduces retrovirus infectivity [78]. As a consequence of the limited mass transfer using resins and the susceptibility towards the desorption reagents, LV recoveries purified by affinity chromatography were moderate ranging from 38% to 68% [73–77]. Moreover, by the introduction of a tag to the envelope protein, the viral infectivity or tropism can be altered [49]. Besides affinity purification techniques, resins are employed in size exclusion chromatography (SEC) for LV polishing [58,79,80] which separates feed components based on their size and hence, their retention time through a packed column [81]. The low capacity of SEC columns, the slow flow rate, and the dilution of the vector sample are the major

drawbacks of SEC, which is why TFF ultrafiltration and diafiltration are preferred as a polishing step, especially at larger process scales [49,79].
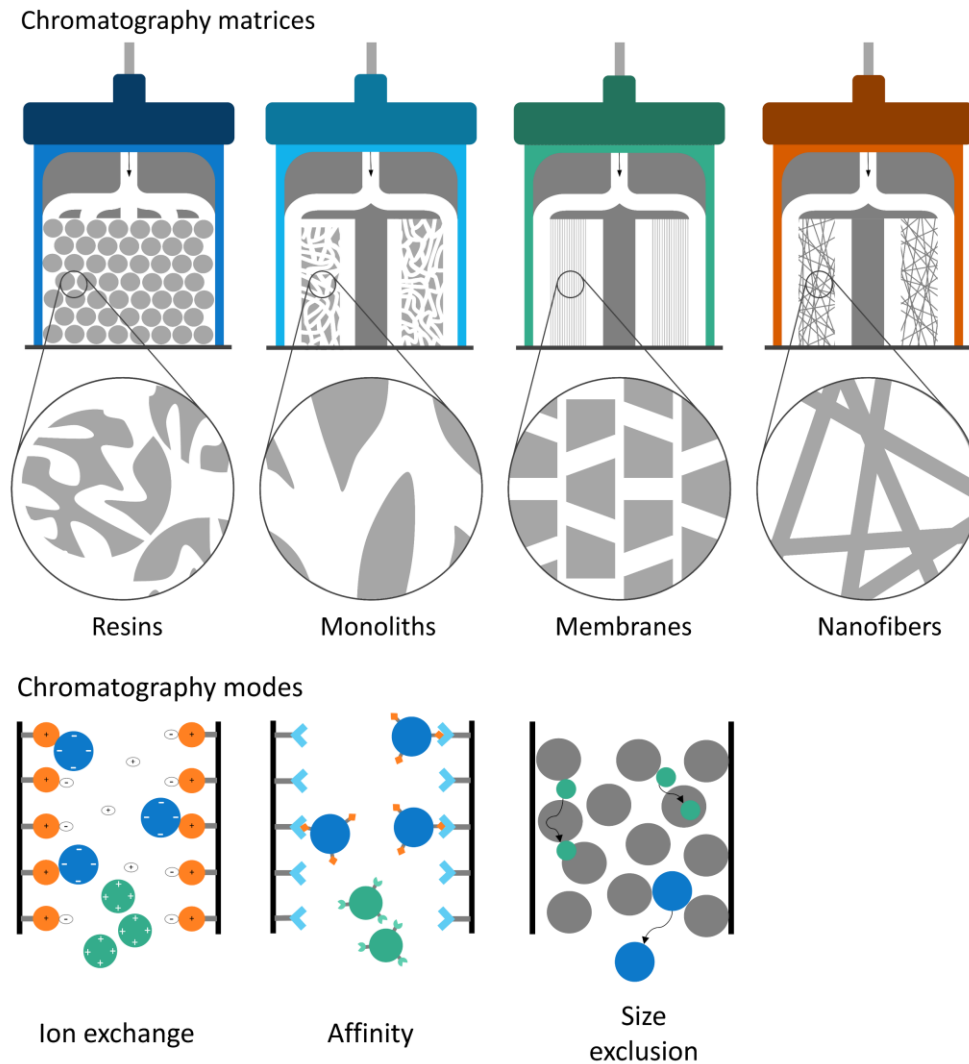
Figure 5: Chromatography matrices and chromatography modes used for lentiviral vector purification and polishing, adapted from [82].

Membrane chromatography matrices are made of different polymers that form large pores, such as polyacrylamide hydrogel, modified polyethersulfone, or regenerated cellulose. Membrane channel sizes of 5 µm to 0.65 µm allow for flexible selection that fits to the virus size. Also, the membrane bed height can be easily adjusted by the number of membrane layers. Small-scale membrane chromatography units hold several stacked membrane layers that form a thin column of a few millimeters in thickness with a frontal (axial) dead-end flow directed from the top [83]. Larger devices are either based on a capsule format with a rolled-up membrane with a radial feed flow from the external to the internal fluid channel [84] or a flat-sheet cassette module [85]. The mass transfer is based on convection, thus high flow rates can

be applied [71,86]. Membrane chromatography offers the possibility to be operated in a single-use manner which reduces labor and costs compared to resin chromatography, as no column packing must be performed and higher flow rates can be applied reducing process time [83,86]. Membranes are widely used for LV purification, mainly by employing anion-exchange chromatography, which is based on electrostatic interactions of the LV and the positively charged ligands coupled to the membrane, as LV has a negative charge at physiological pH [58]. Most frequently clarified LV material is directly loaded onto AEX membranes in small-scale studies [18,43,67,80,87–92]. Some large-scale DSP protocols suggest performing the chromatography step for LV after clarification as well [34], but more recently a study reported loading of concentrated LV material to the AEX membrane after TFF [68]. Adjustment of the starting material with sodium chloride (NaCl) to reduce protein binding during loading showed increased membrane capacity and product purity [68,93]. The elution is typically performed by increasing the NaCl concentration to 0.4-2 M. The major concern of increasing the salt concentration is the high susceptibility of lentiviral vectors toward high salt concentrations, resulting in a loss of LV infectivity [18,20,94]. This problem is addressed by immediate dilution of the elution fraction to reduce the conductivity or a directly succeeding ultrafiltration and diafiltration step for desalting and buffer exchange [43,67,87,89]. These pre-treatments (conductivity adjustment before loading) and post-treatments (dilution of elution sample) increase the buffer consumption and can reduce the achieved concentration factor of the LV by AEX [50]. Infectious LV recoveries between 28% and 90% have been reported for the AEX step with the majority of the studies yielding a recovery between 30% and 60% [18,43,67,68,80,88–91,95,96]. If reported at all, protein removal by AEX was 95-99% and removal of contaminating DNA (host cell DNA, plasmid DNA) was 70-95% [68,89,95].

Another chromatography matrix that enables convective mass transport are monoliths. They are made of a continuous polymer block with wide, interconnected channels; thus, monoliths have a high porosity [70,71]. As membranes, monoliths have proven to be suitable for large biomolecules such as viral vectors because the large channels have sizes of 2 to 6 µm, thus allowing easy access to the binding sites and providing high mass transfer [44,97,98]. Ion exchange monoliths [58,67,95] and some affinity monoliths [75,99] have been used to purify LV. LV recoveries of AEX and affinity chromatography using monoliths are comparable with membrane chromatography using the same capture chemistries.

A less frequently used stationary phase is nanofibers which are arranged randomly forming a large surface that is functionalized. The nanofibers can be made of nylon, glass, or cellulose, among others. Like membranes and monoliths, nanofibers offer convective mass transport [100]. Their applicability for LV purification was so far demonstrated in one study using them for AEX [101].

An in-depth review of chromatography methods for LV will be published soon in the book "Bioprocess development and analytics for viral vector-based therapeutics" (see publication list, page 110 f.).

3.3.3 Steric exclusion chromatography

Steric exclusion chromatography (SXC) relies on the principle of depletion interaction to separate biomolecules. Depletion interaction was first introduced by Asakura and Oosawa [102] and later investigated in detail by Vrij [103] describing polymer molecules, for example, polyethylene glycol (PEG), as penetrable hard spheres. The term "penetrable hard spheres" means that the polymer molecules can overlap each other but when interacting with colloidal particles they act as hard spheres. Upon addition of the polymer, which is arranged in a random coil structure in solution, to a solution containing colloidal particles, depletion interaction may occur. The underlying mechanism is based on the steric exclusion of the polymer from the surface of the colloidal particles, which is inaccessible to the center of gravity of the polymer, resulting in the formation of effective depletion zones (Fig. 6) [104]. The depletion zones have a lower polymer concentration compared to the bulk solution [105].
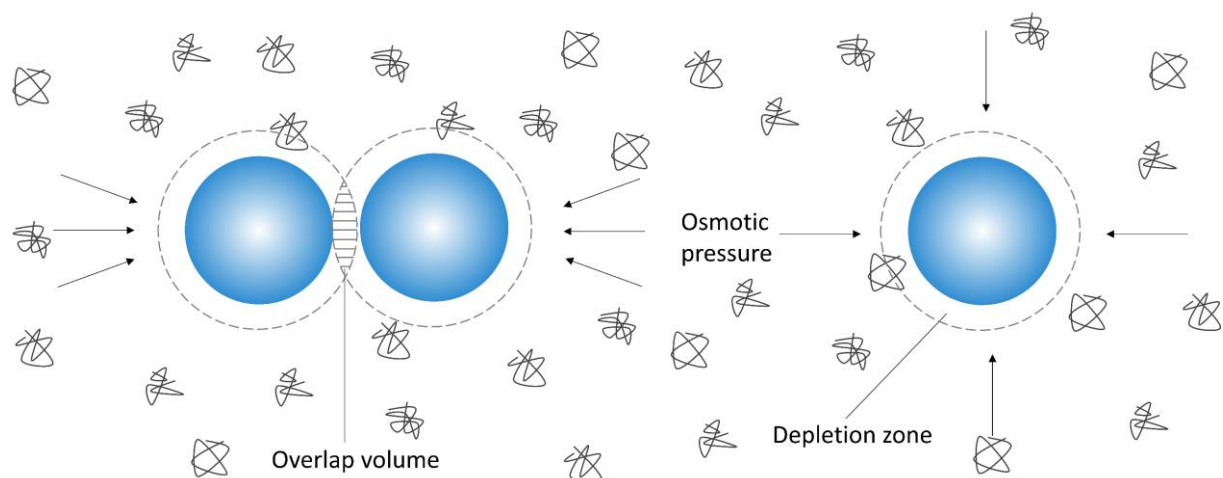

Figure 6: Depletion interaction of colloidal particles (blue spheres) in a polymer solution. The polymer molecules are arranged in a random coil structure, adapted from [104].

The steric exclusion of the polymers leads to a loss of conformational entropy of the polymer chains. The increased free energy of the polymers creates a thermodynamically unfavorable state. When two colloidal particles come close to each other so that their depletion zones overlap, the total excluded volume is reduced, and the excess water is transferred to the bulk solution reducing the free energy as this volume is now available for the polymer chains [104,106]. Single spheres experience an isotropic osmotic pressure due to the polymer concentration difference between the depletion layer and the bulk solution. When two colloidal particles are close to each other, the polymer molecules are unable to penetrate the gap and the osmotic pressure becomes anisotropic. An anisotropic pressure means in this case that the osmotic pressure around the particles is higher than between them, resulting in the weak attraction of the colloidal particles [107]. Polymer solutions can be classified according to their concentration regimes. In dilute polymer solutions, the polymer chains do not interact with one another. The depletion layer thickness in a dilute polymer solution is about the radius of the polymer forming a penetrable hard sphere. The range and strength of interaction depend on the polymer size and polymer concentration, respectively [104].

SXC exploits the depletion interaction mechanism for the purification of biomolecules, such as viruses, using a hydrophilic stationary phase and PEG as a polymer. PEG is an inert polymer with high biocompatibility and high water solubility that has found versatile applications in the pharmaceutical industry [108]. PEG is mixed with the virus solution and loaded onto the hydrophilic stationary phase. Depletion zones form around the stationary phase and the virus surface, from which PEG is sterically excluded. The thermodynamically unfavorable increase in free energy promotes the physical reorganization of the viral particles. Depletion interaction may occur between the viruses and the stationary phase or between viruses with one another. During the loading phase, the virus is then precipitated on the stationary phase and can be eluted by using a buffer without PEG that reverses the association of the virus with the stationary phase (Fig. 7). The SXC method does not require high buffer conductivities or a pH change for elution because it is not based on a chemical interaction but is a thermodynamically driven process. Hence, mild elution conditions can be used and SXC can be applied to different biomolecules [105,109].
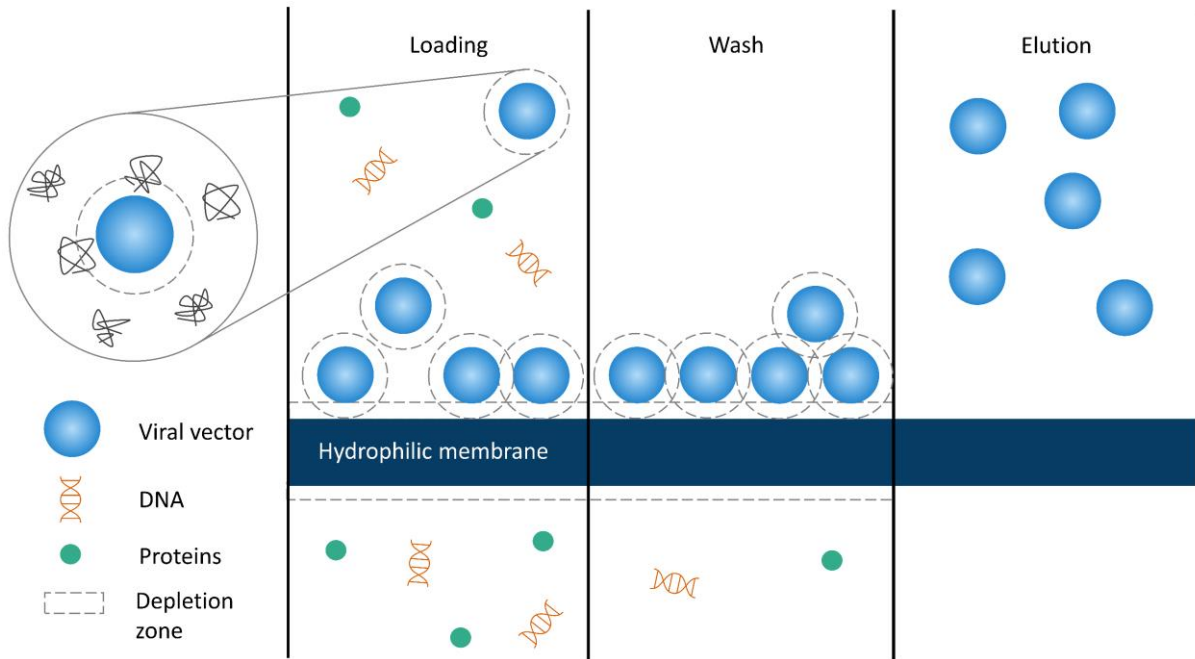
Figure 7: Steric exclusion chromatography procedure using a hydrophilic membrane as a stationary phase, adapted from [105,110].

The optimal PEG molecular weight and concentration depend on the size of the biomolecule to be purified. PEG precipitation enables size-based separation with large biomolecules being preferentially precipitated by lower concentrations of low molecular weight PEGs, and small biomolecules precipitate with higher concentrations of higher molecular weight PEGs [111]. Therefore, the optimal concentration and molecular weight combination of PEG has to be identified in order to be able to achieve a state where depletion zones are formed around the largest biomolecules in the solution (i.e., the virus) but not around contaminating smaller molecules like host cell proteins and host cell or plasmid DNA. Through this approach, the removal of these contaminations is possible via SXC.

After the description of depletion interaction by Asakura, Oosawa, and Vrij, PEG was utilized for the precipitation of proteins [112]. The first description using depletion interaction in the context of SXC was published by Lee et al. who purified IgM and bacteriophage M13K07 with OH-monoliths. Other publications describe the purification of serum proteins [113], RNA molecules [114], and IgG [109] by SXC. More recently SXC gained interest in the field of virus purification. SXC has been used to purify a variety of viruses with regenerated cellulose membranes as stationary phases, including AAV [115], baculovirus [116], influenza A virus [110], influenza A virus defective interfering particles [117], Orf virus [118,119], and hepatitis C virus [120]. All these studies using SXC to purify viruses were performed on a small scale and

reported successful virus purification. So far, no study describing the purification of LV by SXC was published.

3.4 Lentiviral vector analytics

Analytical tools are crucial for the manufacturing and process development of viral vectors and are performed for process monitoring and batch release. The product characterization can be divided into four key specifications: the potency, purity, safety, and identity of the product (Fig. 8). To ensure consistent product quality and safety, it must be reliably monitored that the specifications are met as defined by regulatory guidelines [32,50]. Since the use of LV for gene and cell therapy applications is relatively new and the knowledge is steadily increasing, the regulations will likely increase in the future making regular checks on current guidelines essential [121].
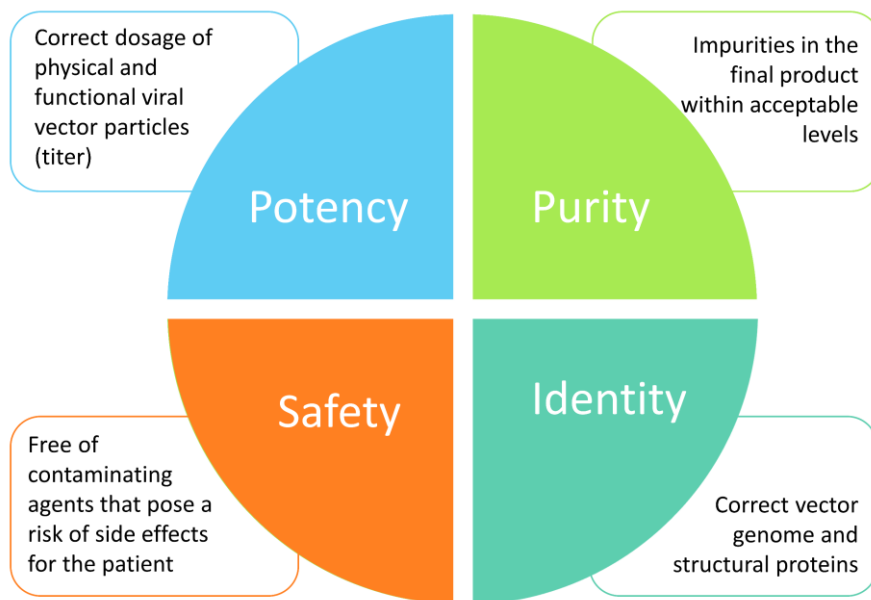
Figure 8: Categories of product characterization and quality criteria for viral vector products

To assess the potency of a viral vector the total particle titer and the infectious titer are determined. The methods most widely used to measure the total particle titer quantify vector particle components, like structural proteins or the vector genome. These can be done by the p24 enzyme-linked immunosorbent assay (ELISA) [122], or quantitative polymerase chain reaction (qPCR) [123–125]. However, methods quantifying the vector genome would omit empty particles. Other methods of measuring physical particles are nanoparticle tracking analysis, tunable resistance pulse sensing, and transmission electron microscopy [126,127], among others. The measurement of the infectious titer requires infection of a suitable cell line

and subsequent measurement of the transgene expression which can be performed by reverse transcriptase qPCR [128,129], digital droplet PCR [130], or flow cytometry [36,131,132] if the LV comprises a fluorescent marker gene or when a protein is expressed that can be labeled by a fluorescence-tagged antibody [122]. The infectious titer is the more important titer specification, especially for enveloped viral vectors that have limited stability. Only by measuring the infectious titer, it is possible to find out if a certain operation unit has preserved the functionality of the virus.

The infectious titer is generally lower than the particle titer, and the ratio of total to infectious viral particles depends on the virus type. For LV a wide range of the total particle titer to the infectious titer ratio of 10^2 to 10^7 [133,134] was reported with a common ratio of 10^3 [49]. There are several reasons for the high ratio. The total particle titer includes all vector forms (infectious, defective, empty, free viral proteins or nucleic acids), and the infectious titer only includes functional particles [130]. Out of these functional particles, not all particles will successfully infect a target cell due to diffusion limitation, temperature-dependent decay in suspension due to low LV stability, or abortive infection [133].

Profound knowledge of the impurities is important to ensure the product's quality and safety. The impurities have different origins, as they can derive from the process or the product. Process-related impurities can derive from the culture medium components, the producer cell (e.g., host cell DNA and proteins), the transient transfection method (e.g., plasmid DNA, transfection reagents), or the purification (e.g., nucleases). Product-related impurities are molecular variants of the product that do not have the properties of the desired product, like defective particles or aggregates. It is more difficult to remove product-related impurities as they have similar characteristics to functional vector particles [45,135]. The purity can be analyzed by either examination of the total protein (e.g., by Bradford assay) and total DNA content (e.g., by PicoGreen assay), or the determination of a specific protein concentration (e.g., by ELISA), or a specific DNA concentration (e.g., by qPCR) for example for host cell protein and host cell DNA [50]. The LV genome is made of RNA and is not detected by DNA quantification methods.

Other contaminants which could pose a risk to patients, e.g., mycoplasma, endotoxins, and other viral and microbial agents, are not intended to be part of the manufacturing process but can be adventitiously introduced. The absence of these contaminants must be demonstrated

to ensure product safety [49]. Moreover, the formation of replication-competent LV that might originate from several recombination events within the cells has to be determined for an LV product [136,137]. The identity of the viral vector product can be confirmed by sequencing the vector genome and identifying structural vector proteins by Western Blotting [32].

Depending on whether analytics is needed for process development or manufacturing, different requirements for analytical assays exist. During process development, small-scale screening experiments result in a high number of samples. Hence, high-throughput methods with short handling times and a small, required sample volume are needed. Full assay validation and qualification according to regulatory guidance are required for manufacturing purposes. Thus, the assay accuracy, specificity, linearity, range, and detection limit are of main importance and all product characteristics (potency, purity, safety, and identity) are analyzed. During process development, the focus is predominantly on potency and purity analysis [138].

4 Research results

The objective of this dissertation was to develop an alternative clarification approach, infectious titer analysis strategy, and chromatography method for LV to overcome the limitations of the existing downstream process and analytical methods. For this purpose, the experimental work of the thesis was divided into four parts: a new simplified clarification approach for lentiviral vectors using diatomaceous earth improves throughput and safe handling (Section 4.1), infectious titer determination of lentiviral vectors using a temporal immunological real-time imaging approach (Section 4.2), steric exclusion chromatography of lentiviral vectors using hydrophilic cellulose membranes (Section 4.3), and scaling up of steric exclusion membrane chromatography for lentiviral vector purification (Section 4.4). All parts were published in four different peer-review journals.

Chromatography studies require clarified LV material, which is free of cells, cell debris, and larger contaminants. Previous small-scale studies performed centrifugation and subsequent filtration of the supernatant; however, the material was obtained by adherent cell culture [43,49,52–54]. Due to the limited scalability of adherent cell cultures, the trend goes towards suspension culture-produced LV, which in turn raises the hurdles for the DSP as the suspension culture feed has a higher impurity load.

The conventional approach of centrifugation with subsequent filtration revealed several drawbacks for clarification of suspension cell culture derived LV, therefore a clarification method with diatomaceous earth for LV clarification using a Design of Experiment (DoE) approach was developed in the first part of this thesis. This DoE had the purpose to understand how this clarification method, classically used for protein clarification, has to be adopted for LV clarification. It was found that the selection of an appropriate DE concentration results in a trade-off between LV recovery and impurity removal and filtration time, as the infectious LV titer was reduced, but the impurity removal and filtration time improved when the DE concentration was increased. Moreover, the clarification method using diatomaceous earth was compared to the conventional clarification approach consisting of centrifugation and subsequent filtration of the supernatant. A comprehensive performance evaluation based on the LV titer, filtration time, turbidity reduction, impurity removal, filter capacity, and handling, was performed. The clarification with DE highly increased filter capacity and reduced handling time and material consumption compared to the centrifugation-based clarification approach.

However, the recovered infectious titer was lower when using DE, but as the clarification with DE offers a more convenient and robust lab scale clarification method for LV, this can outweigh the drawback [139].

During the clarification study, the infectious titer assay was identified as being another critical bottleneck because the determination of the infectious titer was very laborious and greatly limited the number of samples that could be analyzed. The infectious titer of LV is the most important characteristic to be monitored during process optimization or manufacturing, because of the low stability of enveloped viral vectors. As only infectious particles are functional it is important to preserve the infectious potential of the vector. The laborious flow cytometry-based infectious titer assay originally performed, required a lot of manual handling steps. For this reason, priority was given to the need to first improve the throughput and quality of the analytics before conducting further process optimization studies.

The goal of the second part of the experimental work was to develop a largely automated assay that quantifies the transduced cells by immunological detection in a real-time live-cell analysis system using image-based software evaluation. An automated data analysis was established, and an extensive assay characterization of the newly developed assay was performed. Besides, a comparison with the flow cytometry-based assay was conducted to evaluate the performance of the developed infectious titer assay.

The newly developed infectious titer assay showed good inter- and intra-assay precision and the LV titers determined with the developed immunological real-time imaging assay were not significantly different from the flow cytometry method. Moreover, lower standard deviations between replicates, a broader linear range, and the possibility of a flexible readout for the real-time imaging method as the data is acquired over time, were the identified advantages of the new method. The main goal of significantly increasing the sample throughput was achieved and demonstrated by a comprehensive LV stability study, analyzing the effects of temperature, salt concentration, freeze and thaw cycles, and shear stress on LV infectivity. Significant effects of high temperatures, high salt concentrations, and extensive exposure to shear stress on LV infectivity were determined [140].

Chromatography of large enveloped viral vectors remains a challenge. Although literature reported moderately high LV recoveries and high impurity removals with AEX (Section 3.3.2), we were not able to reproduce this data at our site. Testing the commercially available AEX

modules we achieved only an infectious LV titer recovery of 20-30% with Sartobind Q and D and 45% with Mustang Q. The protein depletion was <90% and DNA depletion >30% (data not shown). This demonstrated that investigation into new chromatography techniques is necessary to improve both, LV titer recovery and impurity removal. Therefore, the third part of this thesis deals with the implementation of a chromatography mode not previously used for lentiviral vectors, namely steric exclusion chromatography (SXC).

To this end, it was first necessary to gain an understanding of which process parameters are critical to achieving effective depletion attraction between LV and membrane, which can be reversed during elution. The analyzed parameters were the mixing strategy of the PEG buffer with the LV solution, the PEG size and concentration in the PEG buffer, as well as the flow rate. In addition, other important aspects such as system pressure, loading capacity, and residual PEG concentration were highlighted to help obtain a better comprehension of the process operation.

A dynamic in-line mixing strategy (1:1 mixing of PEG buffer with LV feed), the use of PEG 4000 in a final concentration of 12.5%, and a flow rate of 7 mL·min^{-1} were identified as ideal process conditions resulting in an LV particle and infectious titer recovery of 86% and 88%, respectively while removing approximately 80% total protein and dsDNA (host cell DNA, plasmid DNA). Overloading the membrane was found to lead to almost complete product loss, hence monitoring pressure increase was important. A residual PEG concentration in the eluate of 7.6 g·L^{-1} was measured, which could potentially be removed in subsequent DSP steps due to the pronounced size difference of LV and PEG molecules [141].

Furthermore, in the fourth part of the thesis, a scale-up approach of SXC was investigated. To understand scaling needs, first, a visualization of the LV adsorption behavior inside the devices was performed. This showed that the LV is mainly located on the upper two membrane layers with only low to no amounts detectable on the lower membrane layers. For this reason, increasing the membrane surface area of the first membrane layer while keeping the number of membrane layers constant was aimed for the scale-up. To identify required scaling conditions, different device scales were used with the aim to obtain comparable results.

The optimal process conditions for the small-scale device identified in the third part of this work were applied to a device with a four-fold larger membrane area. Unexpectedly, the LV recoveries were low (~10%), indicating that the process conditions were not suitable for the

larger device. Based on the finding that the LV was mainly captured on the upper membrane layers, the flow rate was scaled with the membrane surface area, which results in the same flow velocity through the pores when the fluid is equally distributed. By applying the same surface area-specific flow rate to the large device, the LV recoveries increased significantly to 73% and were not significantly different from the recoveries obtained with the small device at the same surface area-specific flow rates. To proof the concept of scaling the flow rate according to the membrane surface area of the first layer, further scale-down experiments with an axial device and scale-up experiments with a radial 5'' capsule were performed. The results showed that a critical minimum surface area-specific flow rate is required, and thus reproducible results could be obtained for four different module sizes with an overall scaling factor of 98.

Moreover, different configurations of the axial flow device lid geometry were tested. A lid structure was preferred which enabled a uniform liquid flow distribution across the membrane and thus uniform LV loading, which in turn led to higher LV recoveries and smaller standard deviations.

4.1 A new simplified clarification approach for lentiviral vectors using diatomaceous earth improves throughput and safe handling

The clarification step is at the interface between the upstream and the downstream process. The performance of the clarification step influences the subsequent downstream processing steps, as effective removal of large contaminants is essential [55]. Only limited literature on LV clarification is available with most laboratory-scale studies reporting centrifugation of the supernatant of an adherent cell culture with subsequent filtration without further optimization [43,49,52–54]. Applying this described workflow to suspension culture-based upstream processes can be challenging, as suspension culture broth has a higher cell density and therefore a higher impurity load to be removed during DSP [38,142]. Centrifugation and vacuum filtration are not only labor intensive but also require inconvenient handling with the risk of spillage when filter clogging occurs as reported in a study comparing different vacuum filtration units using centrifuged supernatant of an LV suspension culture [143].
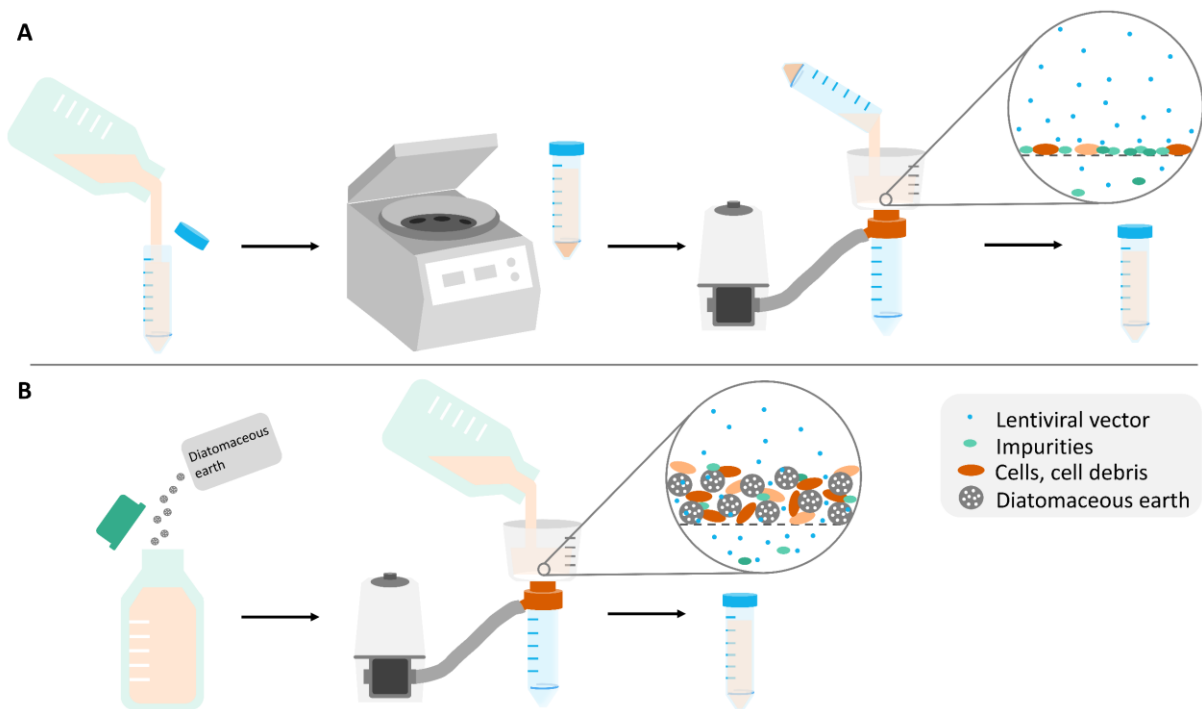
Figure 9: Overview of the microfiltration approaches for LV clarification performing (A) centrifugation of cell culture broth and subsequent filtration of the supernatant, or (B) mixing of cell culture broth with diatomaceous earth and direct filtration. Filter cake visualization adapted from [144].

Therefore, the first part of the research results of this work addresses the lab scale clarification of lentiviral vectors produced by a suspension HEK293 cell culture, first, to obtain clarified material of high quality for subsequent downstream processing steps, and second, to improve

the handling and throughput of the clarification step. In this publication, the standard clarification approach of centrifugation and subsequent vacuum filtration of the supernatant was compared with a single-step clarification using diatomaceous earth (DE) as a filter aid (Fig. 9). DE is a mineral microfossil of diatomaceous algae having a high permeability and porosity [145]. The use of DE avoids the need for a centrifugation step, as the cell culture broth is mixed directly with DE and then applied to a vacuum filtration unit. The DE forms a porous filter cake that allows liquid flow and prevents filter clogging [146].

Different DE concentrations and contact times of the LV solution with DE were screened in a Design of Experiment (DoE) approach in combination with a 0.45 µm polyethersulfone bottle-top microfilter. It was shown that a higher DE concentration reduced the filtration time and the turbidity, while the contact time had only a minor reinforcing effect on turbidity reduction. However, the infectious LV titer was reduced with increasing DE concentration, probably due to adsorption effects. The selection of an appropriate DE concentration results in a trade-off between LV recovery and impurity removal and filtration time. An ideal DE concentration of 6-12 g·L^{-1} was determined when high LV recovery is considered to have the highest priority. Next, two different membrane structures were compared. The use of an asymmetrical over a symmetrical membrane structure increased filter capacity for both filtration methods, as the asymmetrical membrane has a depth filter-like structure that has higher permeability and reduces filter cake formation. The LV recovery was unaffected by the membrane structure. An asymmetrical membrane resulted in higher final turbidity of the filtrate when centrifugation and filtration were performed, whereas the turbidity reduction was not affected by the membrane structure for clarification performed with DE and filtration. In general, we observed that the method consisting of centrifugation with subsequent filtration yielded higher LV recoveries but resulted in a lower impurity removal and longer handling time compared to using DE and filtration.

To summarize, clarification with DE highly increased filter capacity compared to the centrifugation-based clarification approach, while reducing handling time and material consumption, and increasing sample throughput. A rather low DE concentration must be selected to avoid LV loss. By implementing a method that makes use of DE for clarification, the safe handling of the LV solution was improved and offered a convenient and robust lab-scale clarification method for LV.

A new simplified clarification approach for lentiviral vectors using diatomaceous earth improves throughput and safe handling

Jennifer J. Labisch [a,b,*], Franziska Bollmann [b], Michael W. Wolff [c], Karl Pflanz [b]

[a] Institute of Technical Chemistry, Leibniz University Hannover, Callinstr. 5, 30167, Hannover, Germany
[b] Research & Development, Sartorius Stedim Biotech GmbH, August-Spindler-Str. 11, 37079, Goettingen, Germany
[c] Institute of Bioprocess Engineering and Pharmaceutical Technology, University of Applied Sciences Mittelhessen (THM), Wiesenstr. 14, 35390, Giessen, Germany

ARTICLE INFO

ABSTRACT

Lentiviral vectors have proven their great potential to serve as a DNA delivery tool for gene modified cell therapy and gene therapy applications. The downstream processing of these vectors is however still a great challenge, particularly because of the low stability of the virus. Harvesting and clarification are critical and until now insufficiently characterized steps for lentivirus processing. To address this bottleneck, we analyzed whether lentiviral vectors produced by transient transfection of HEK293 T/17 SF suspension cells can be efficiently clarified with a lab-scale method with the filter aid diatomaceous earth (DE) and bioburden reducing membrane filters achieving high lentivirus recoveries.

Using a design of experiment approach we found that higher DE concentrations are advantageous for a higher turbidity reduction and shorter filtration times, but at the same time LV titer decreases with increasing DE concentration. A DE concentration of 9 g/L was identified with a DoE as a robust set-point. Clarification with DE was compared with for lab-scale traditionally employed centrifugation and subsequent bioburden reduction filtration of viral vectors. The use of DE allows to perform a harvest and clarification process, which does not only facilitate faster and safer virus handling, but enables a lower material consumption due to the extremely increased filter capacity, thus representing an efficient and robust lab-scale clarification process.

1. Introduction

Viruses are highly important tools in medicine and have become more relevant with the advent of gene therapy. Gene therapy has a significant therapeutic potential for the treatment of many hereditary as well as acquired diseases (Segura et al., 2011). In contrast to other retroviral vectors which can transduce only dividing cells, lentiviral vectors (LV) have the ability to transduce non-dividing cells as well (Mátrai et al., 2010), thus offering a wide range of applications for LV in gene modified cell therapy and gene therapy (Aiuti et al., 2013; Cartier et al., 2009; Cavazzana-Calvo et al., 2010; Mátrai et al., 2010; Maude et al., 2014; Milone and O'Doherty, 2018; Turtle et al., 2016). LV are widely used for cancer immunotherapies introducing genes for a chimeric antigen receptor (CAR) into T cells. This enhances the specificity of T cells to redirect them to target antigens overexpressed on cancer cells that are not recognized by their endogenous receptors. The patient's T cells are modified to express a CAR construct and after *ex vivo* cell expansion are re-infused back to the patient (Miliotou and Papadopoulou, 2018; Milone and O'Doherty, 2018).

Today, there are three thousand clinical trials with viral vectors registered as ongoing, among which about 10 % are conducted with lentiviral vectors (John Wiley and Sons, Inc et al., 2019). The promising prospect of the ongoing clinical trials on gene therapy (Hanna et al., 2017; Herzog et al., 2010) means that there is a strong demand for scalable and cost-effective methods for production and purification of viral vectors. Especially the downstream process is considered to be a major bottleneck for the commercialization of gene therapies (Ruscic et al., 2019). Lentiviral vectors are spherical, enveloped particles with a diameter of 80−120 nm and are extremely labile. Therefore, it is mandatory to design downstream processing (DSP) strategies that suit the physicochemical properties of the vector (Segura et al., 2006).

Lentiviral vectors are typically produced by transient transfection of HEK293 T cells (Merten et al., 2014) with multiple vector plasmids (Sakuma et al., 2012). The viral vector is released into the supernatant. The LV is an enveloped virus, which buds through the membrane of the host cell thereby acquiring their lipid bilayer. For the membrane fission

step Gag molecules recruit factors of the cellular endosomal sorting complexes required for transport (ESCRT) pathway (Votteler and Sundquist, 2013). The first DSP step, is the separation from the cells of the cell culture broth and clarification of the supernatant (Rodrigues et al., 2007). At harvest the cells reach a density $1-5\cdot10^6$ cells/mL for a batch process and $10-20\cdot10^6$ cells/mL for a perfusion process with a viability of 60–80 % (Manceur et al., 2017; Merten et al., 2014; Segura et al., 2007). Clarification has so far received little consideration and is performed as an obligatory step before other LV DSP steps to reduce bioburden and to increase capacity of further downstream steps, which have gotten more attention in terms of process development and optimization, such as ultrafiltration (Cooper et al., 2011; Geraerts et al., 2005; Papanikolaou et al., 2013) or chromatography (Cheeks et al., 2009; Chen et al., 2010; Kutner et al., 2009; Mekkaoui et al., 2018; Olgun et al., 2019; Segura et al., 2005, 2007; Yu and Schaffer, 2006).

Currently there is no established method for LV clarification to be considered as the gold standard. Clarification in a laboratory scale is typically performed by centrifugation of the fermentation broth, complemented with subsequent microfiltration of the supernatant (Bauler et al., 2020; Rodrigues et al., 2007; Segura et al., 2011). For microfiltration of LV a pore sizes of 0.45 μm is typically used (Bauler et al., 2020; Reeves and Cornetta, 2000), since viral particle loss was reported with smaller pore sizes (Segura et al., 2013). For scales greater than 1 L, a single microfiltration step is preferred, because centrifugation is poorly scalable (Besnard et al., 2016). However, this can lead to rapid clogging of the membrane. A possible approach to perform microfiltration in a single step is the use of filter aids (Doran, 2013). Filter aids like diatomaceous earth (DE) are skeletal remains of diatoms with a highly porous structure. DE forms a nearly incompressible porous cake and its high porosity allows liquid to flow around the particles preventing filter clogging (Grauf et al., 2018). Besides its use in blood and plasma fractionation, DE was established for the clarification of protein expressing high-density mammalian cell broths (van der Meer et al., 2014). The process was not adapted for LV yet, which is crucial, since a 1:1 transfer is unlikely due to the distinct bio- and physicochemical properties of the molecules. To our knowledge, clarification of lentiviral vectors has not yet been analyzed with the use of the filter aid DE.

Although, comprehensive studies on the clarification of viral vectors are rarely published in literature (Besnard et al., 2016), there is a need to optimize this step to minimize loss of the viral vector from the beginning of the whole downstream process. Inappropriate clarification processes can rapidly result in filter clogging, which reduces the actual pore size of the filter leading to virus retention (Segura et al., 2011) and thus reduced product yields. This work investigates the effect of DE on clarification performance and whether the usage of DE can effectively provide a LV clarification process, which is both easy to handle and yields high LV titers.

2. Materials and methods

2.1. HEK293T/17 SF cell expansion

Suspension HEK293T/17 SF cells (ACS-4500, ATCC) were expanded in CD293 medium (Thermo Fisher Scientific) supplemented with 10 μL/mL Insulin-Transferrin-Selenium (ITS; Thermo Fisher Scientific) and 8 mM glutamine (Thermo Fisher Scientific) in disposable non-baffled shake flasks of a size range from 125 mL to 1000 mL (Corning). Cells were passaged in a 2–3 day rhythm when reaching a cell density above $1\cdot10^6$ cells/mL. Before and after passaging the cells, the cell density and viability was determined (see section 2.7). Shake flasks were inoculated with a viable cell density of $2-3\cdot10^5$ cells/mL in 37.5 mL medium for a 125 mL shake flask (75 mL medium for a 250 mL shake flask, 150 mL medium for a 500 mL shake flask and 300 mL medium for a 1000 mL shake flask). Cultivation was performed at 37.0 °C, 8 % CO_2 and 130 rpm in an orbital shaking incubator (Sartorius).

2.2. Lentiviral vector production

Third generation lentiviral vectors were produced by transient transfection of suspension HEK293 T/17 SF cells with multiple plasmids in a UniVessel® single-use (SU) 2 L bioreactor (Sartorius). One day before inoculation, the UniVessel® SU 2 L was filled with 1.25 L Free-Style293 medium (Thermo Fisher Scientific) supplemented with 10 μL/mL ITS and antifoam C (Sigma Aldrich) at a final concentration of 0.025 %. Cultivation parameter set-points were 37.0 °C, 30 % dissolved oxygen, pH 7.1 and stirring speed of 190 rpm. Process control was performed with a BIOSTAT® DCU (Sartorius). The next day, the bioreactor was inoculated with 180 mL HEK293 T/17 SF cell solution to a final cell density of $1\cdot10^6$ cells/mL. Two 125 mL shake flasks were inoculated with the same cell density as a positive reference control (virus production in shake flask) and a negative control (30 mL each). 24 h later, transfection with PEIpro DNA transfection reagent (Polyplus) and four plasmids in a ratio of 4:1 was performed. 0.5 μg total plasmid amount per $1\cdot10^6$ cells in a ratio of 5:2.5:1:1 (pALD-Lenti-anti-CD19-CAR-EGFRt : pALD-GagPol-A : pALD-VSV-G-A : pALD-Rev-A, Aldevron) were prepared in 100 mL production medium (1.5 mL for the shake flask controls). In a separate reaction tube PEIpro was diluted in the same volume of production medium. Diluted PEIpro was added to the diluted DNA, gently mixed and incubated for 15 min at room temperature. The mixture was added to the cells. A negative control without using a transfection reagent was prepared and treated equally as the virus production cultures. $7-8$ h after transfection anti clumping agent (Thermo Fisher Scientific) was added at a 1:500 (v/v) dilution and sodium butyrate (Sigma Aldrich) was added at a final concentration of 10 mM. Additionally, antifoam C was added to give a final concentration of 0.025 %.

2.3. Harvest and DNA digestion

The lentivirus was harvested 72 h post transfection. DENARASE® (c-Lecta) and $MgCl_2$ (Carl Roth) were added to the cell culture broth (37 °C) one hour before harvesting at a final concentration of 10 U/mL and 2 mM, respectively. After nucleic acid digestion, the lentivirus containing cell culture broth was directly clarified.

2.4. Clarification

Clarification of 50 mL LV culture broth samples was performed with Sartoclear Dynamics® Lab V50 0.45 μm polyethersulfone (PES) version (Sartorius) with DE concentrations between 5 g/L to 40 g/L according to manufacturer's instructions. The filtration setup is shown in Fig. 1. The detailed acceptance criteria for the DE material are listed in the validation guide, which can be found on the manufacturer's homepage. Additionally, clarification of 50 mL cell culture broth was performed without DE in a two-step method of 5 min centrifugation at 800 x g and subsequent filtration through a Sartolab® RF50 with 0.45 μm PES membrane (Sartorius). Two distinct 0.45 μm PES membranes were compared with each other; a symmetrical and an asymmetrical type. For filter capacity determination, clarification was performed until filter clogging occurred and filtrate volume was determined.

2.5. Design of experiment

A design of experiment (DoE) based approach was performed to analyze the effect of the factors DE concentration and contact time of the lentivirus containing cell culture with DE on the responses infective LV titer, turbidity and filtration time, respectively. To this end, the DE concentration was varied between 5 g/L, 12.5 g/L and 20 g/L and contact time between 0 min, 10 min and 20 min. The experiments were planned as a full factorial design and evaluated using the MODDE® software (Version 12.1, Sartorius) with four center points, resulting in a total of 12 experiments.
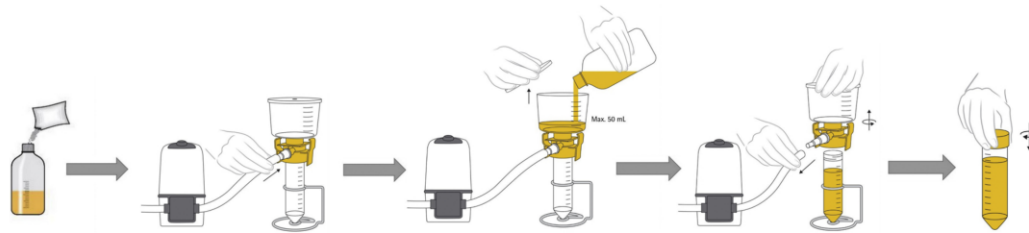
Fig. 1. Filtration setup with the filter aid diatomaceous earth. The filter aid is poured into the cell culture broth and mixed. The solution is filled into the funnel of the filtration device which is connected to a vacuum pump. After filtration is completed the vacuum tube is disconnected and the funnel unscrewed. The collection tube can be stored until further use.

2.6. Turbidity measurement

The turbidity of the bulk solution and the filtrates was measured using an Orion™ AQUAfast AQ3010 turbidity meter (Thermo Fisher Scientific) and is given in nephelometric turbidity units (NTU). The measurement was performed according to manufacturer's instructions.

2.7. Cell density and viability measurement

For determination of cell concentration and viability Cedex HiRes Analyzer (Roche) was used. Measurements were performed according to manufacturer's instructions.

2.8. Infectious LV titer determination

For quantification of the infectious lentiviral vector titer, adherent HEK293 T cells (ACC 635, DSMZ) were infected with serially diluted LV samples and the expression of the EGFRt-transgene-fusion protein was detected by flow cytometry. One day before infection $6 \cdot 10^4$ cells/well were seeded in 0.5 mL Dulbecco's modified Eagle medium (DMEM; Thermo Fisher Scientific) + 10 % fetal calf serum (FCS; Sigma Aldrich) (v/v) in a tissue culture (TC) treated 24-well plate (Greiner Bio-one). Cells were incubated at 37 °C and 5 % CO_2 in a static incubator (Sartorius). On the day of infection, culture medium was removed from the HEK293 T cells and the cells were transduced by transferring 0.5 mL of diluted virus solution. A negative control of the respective LV batch was analyzed as well. 8 µg/mL polybrene (Sigma Aldrich) were added to each well and the plate was incubated as before. 18 h post infection, the medium was removed and replaced with fresh culture medium without polybrene. 72 h post infection the expression of the gene-of-interest was analyzed by flow cytometry. First, the culture medium was removed from the cells, 200 µL trypsin-EDTA (Thermo Fisher Scientific) was pipetted to each well and incubated for 5 min at 37 °C. The enzymatic reaction was stopped by adding 500 µL culture medium, subsequently the plate was centrifuged at 300 x g for 5 min and the supernatant was removed. Cells were resuspended in 150 µL PBS and transferred to a non-TC 96-well plate with conical bottom (Sartorius). The 96-well plate was centrifuged and the supernatant was discarded. To discriminate viable and dead cells, 100 µL of a 1:1000 dilution (in PBS) of the fixable fluorescent dye Zombie NIR™ (BioLegend) was added to each well and incubated for 10 min in the dark. After another centrifugation step and removal of the supernatant, 100 µL Roti®-Histofix 4 % (Carl Roth) was added to the cells and incubated for 15 min. The supernatant was removed from the wells after centrifugation and cells were washed with 150 µL PBS. Hereafter, centrifugation of the plate was performed, the supernatant was removed and the cells were incubated for 30 min with an anti-human EGFRt phycoerythrin (PE) conjugated antibody (R&D Systems) at a 1:200 dilution in 40 µL staining buffer (1 % Bovine serum albumin (Carl Roth) in PBS). The cells were washed with 100 µL staining buffer. After each washing step the plate was centrifuged and the supernatant aspirated. Finally, the cells were resuspended in 40 µL

staining buffer and flow cytometry was performed with an iQue ScreenerPlus flow cytometer (Sartorius). The obtained data was analyzed using the integrated ForeCyt 7.0 software. The percentage of EGFRt positive cells of viable single cells was determined. For calculation of the infective titer the virus dilution yielding between 5−20 % positive cells was selected. The functional lentiviral titer given in transducing units (TU) per mL was calculated using the following formula:

$$Infectious\ titer = \frac{P \cdot N \cdot D}{V \cdot 100}$$

With P being the percentage of positive cells, N being the number of cells at the time of transduction, D is the dilution factor of the LV used for infection and the transduction volume V in mL.

2.9. Total protein quantification

The Pierce™ Coomassie Bradford protein assay kit (Thermo Fisher Scientific) was used, according to the manufacturer's instructions, to quantify total protein concentrations. Standards and samples were analyzed in duplicates in transparent 96-well microtiter plates (Greiner Bio-one). The absorbance was read at 595 nm with a FLUOstar Omega plate reader (BMG Labtech). The obtained standard curve was fitted by linear regression.

2.10. Total dsDNA quantification

The dsDNA content was determined with the Quant-iT™ Pico-Green™ dsDNA assay (Thermo Fisher Scientific). The assay was performed according to manufacturer's instructions. Standards and samples were analyzed in duplicates. A 96-well black microplate (Corning) was used to perform the assay. Excitation was done at 480 nm and the fluorescence emission intensity was measured at 520 nm with a FLUOstar Omega plate reader. The obtained standard curve was fitted by linear regression.

3. Results

3.1. Evaluation of the impact of a filter aid on the processing time

Evaluation of the handling time for clarification of 50 mL lentivirus solution was compared by performing a single-step clarification with 5 g/L DE and a 0.45 µm PES filter or centrifugation with subsequent microfiltration of the supernatant through the same filter, which is often a lab-scale standard method. The entire processing time was broken down into preparation time (i.e. measuring culture volumes, removing supernatant after centrifugation, weighing of DE and addition of DE to the cell suspension), centrifugation time and filtration time and the results are shown in Fig. 2. The handling time for the conventional clarification method was about 8.5 min. During clarification of the centrifuged supernatant filter clogging occurred after approximately
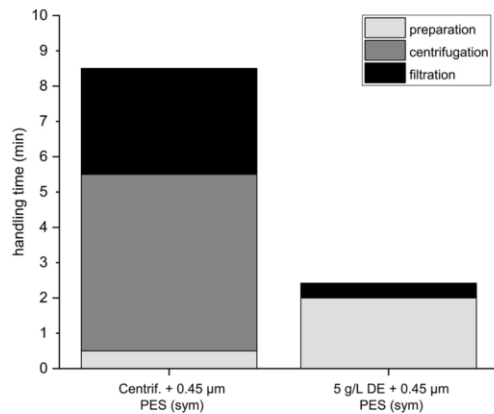
13

Fig. 2. Comparison of clarification methods regarding their processing time. The preparation, centrifugation and filtration time needed to clarify 50 mL mammalian cell culture containing lentiviral vectors with a total cell density of $1.1 \cdot 10^6$ cells/mL and a turbidity of 141 NTU using the conventional method of centrifugation combined with microfiltration or using 5 g/L diatomaceous earth (DE) and microfiltration for clarification. For both methods symmetrical (sym) 0.45 μm polyethersulfone (PES) membrane filters were used. Mean, N = 3.

25 mL. Hence, using a second microfilter was required and the remaining unfiltered solution had to be transferred to the second filter, which was laborious and complicated the overall handling. Using the same microfilter with 5 g/L DE reduced the total preparation time due to the lack of a need for a centrifugation step and resulted in a handling time of about 2.4 min. The use of 5 g/L DE reduced the handling time 3.5-fold compared to a standard centrifugation and microfiltration method.

3.2. Analysis of the effects of DE on lentivirus clarification performance by DoE

The use of diatomaceous earth was hypothesized to lead to a higher turbidity reduction by removal of impurities due to retention by the porous structure of DE or adsorption of contaminants. With the intention of assessing potential adsorption and retention effects of the lentivirus by DE, filtrations with different DE concentrations were analysed. Preliminary experiments were performed to screen a wide range of DE concentrations from 5 to 60 g/L. Here, a DE concentration between 5−20 g/L, which is lower than the DE concentration of 40 g/L commonly used for protein clarification of a typical fed-batch high-density cell cultures, was identified as a suitable concentration range for further optimizations, due to a higher LV particle titer recovery (data not shown).

With the aim to investigate the effect of DE on LV clarification, the factors DE concentration (5−20 g/L) and contact time (0−20 min) with DE were selected for a Design of Experiment (DoE) approach. The experiments were planned as a full factorial design without replicates and evaluated using the MODDE® software. Contact time with DE could possibly be relevant if several samples of LV-containing broth have to be clarified at once and if they are e.g. filtered successively and not simultaneously and the operator prepares all samples in advance rather than one by one. The total cell density of the cell culture broth used for the filtrations of the DoE was $3.7 \cdot 10^6$ cells/mL with a turbidity of 382 NTU.

The DoE resulted in good models for each of the responses with R2 = 0.96 and Q2 = 0.88 for the turbidity, R2 = 0.82 and Q2 = 0.75 for the infective LV titer, R2 = 0.98 and Q2 = 0.97 for the filtration time. R2 indicates how well the model fits the data and Q2 how well the model predicts new data with a maximum value of 1 for both coefficients. The

effect of each factor on the responses was assessed by analysis of the regression coefficient plot (Fig. 3A) and the response contour plot (Fig. 3B). The regression coefficient plots indicate how the two factors of the model influence the responses. The response contour plots show the dynamic of each response depending on the set-points of the factors. Fig. 3 shows that the responses infectious titer and filtration time are only affected by the factor DE concentration. With increasing DE concentration the infectious titer is reduced linearly. For the filtration time a quadratic term for the DE concentration exists, leading to a decrease of filtration time with increasing DE concentration of the tested concentration range. The turbidity was linearly reduced with increasing contact time of the sample with DE. Furthermore, with increasing DE concentration the turbidity was reduced (quadratic term), with the latter being the factor with the greater effect.

The design space is "the multidimensional combination and interaction of input variables (e.g., material attributes) and process parameters that have been demonstrated to provide assurance of quality" (U.S. Department of Health and Human Services et al., 2009). The design space of the process was estimated and is shown in Fig. 4. The green region of the graph has a low probability of failure and is named design space (Eriksson, 2008). The calculation for the design space is consider the model error as well as the precision of set-points (e.g. considering the calibration error). The response specifications were set to a moderate target turbidity (15 NTU) and filtration time (35 s) and to a high infectious LV titer ($1.9 \cdot 10^7$ TU/mL), which was our major interest for the clarification step. In Fig. 4 the green area indicates a probability of failure of 0.5 % for all responses. That means when selecting parameter combinations within the green area in less than 0.5 % of the process the specification will not be met for at least one of the responses. A DE concentration between 6−12 g/L yields acceptable process response values with a low probability of failure independent of the selected contact time. The optimizer function of MODDE® was used to find a robust set-point with the following criteria: Maximizing infective LV titer and minimizing turbidity and filtration time. The calculated robust set-point is located in the center of the design space with 9 g/L DE and an incubation time of 14.67 min. The robust set-point outlines, that a far lower DE concentration, compared to the DE concentration of 40 g/L recommended for protein clarification, is optimal to achieve a high LV titer.

3.3. Comparison of microfilter membrane structures and clarification methods

Two 0.45 μm PES membrane microfilters were analyzed, having either a symmetrical or asymmetrical membrane structure. The two membranes were compared with each other to investigate whether the use of asymmetrical membranes increases filter capacity and LV titer recovery due to its higher permeability, which could potentially reduce virus entrapment. Clarification was performed either with 5 g/L DE or with the standard method by centrifugation of the cell culture broth and subsequent filtration. Resulting infectious LV titers, as well as turbidities of the filtrates are shown in Fig. 5. According to Fig. 5, no significant impact of a symmetrical and an asymmetrical membrane structure on the infectious LV titer could be observed for both of the methods. When comparing the two clarification methods, the two-step clarification method combining centrifugation and filtration leads to a significantly higher infectious LV titer. After clarification with DE, the infectious LV titer was about 65 % of the titer obtained with the standard method centrifugation and clarification. However, centrifugation and filtration results in a significantly higher final turbidity of 30–43 NTU depending on the membrane structure. This corresponds to a turbidity reduction of 89–92 % compared to the starting material, whereas with DE turbidity is reduced by 95 % down to 1820 NTU. When filtrating the centrifuged supernatant the turbidity is with a difference of 12.67 NTU significantly ($p \leq 1$ %) higher with the use of an asymmetrical membrane compared to the symmetrical membrane. When using 5 g/L DE the turbidity of the

14
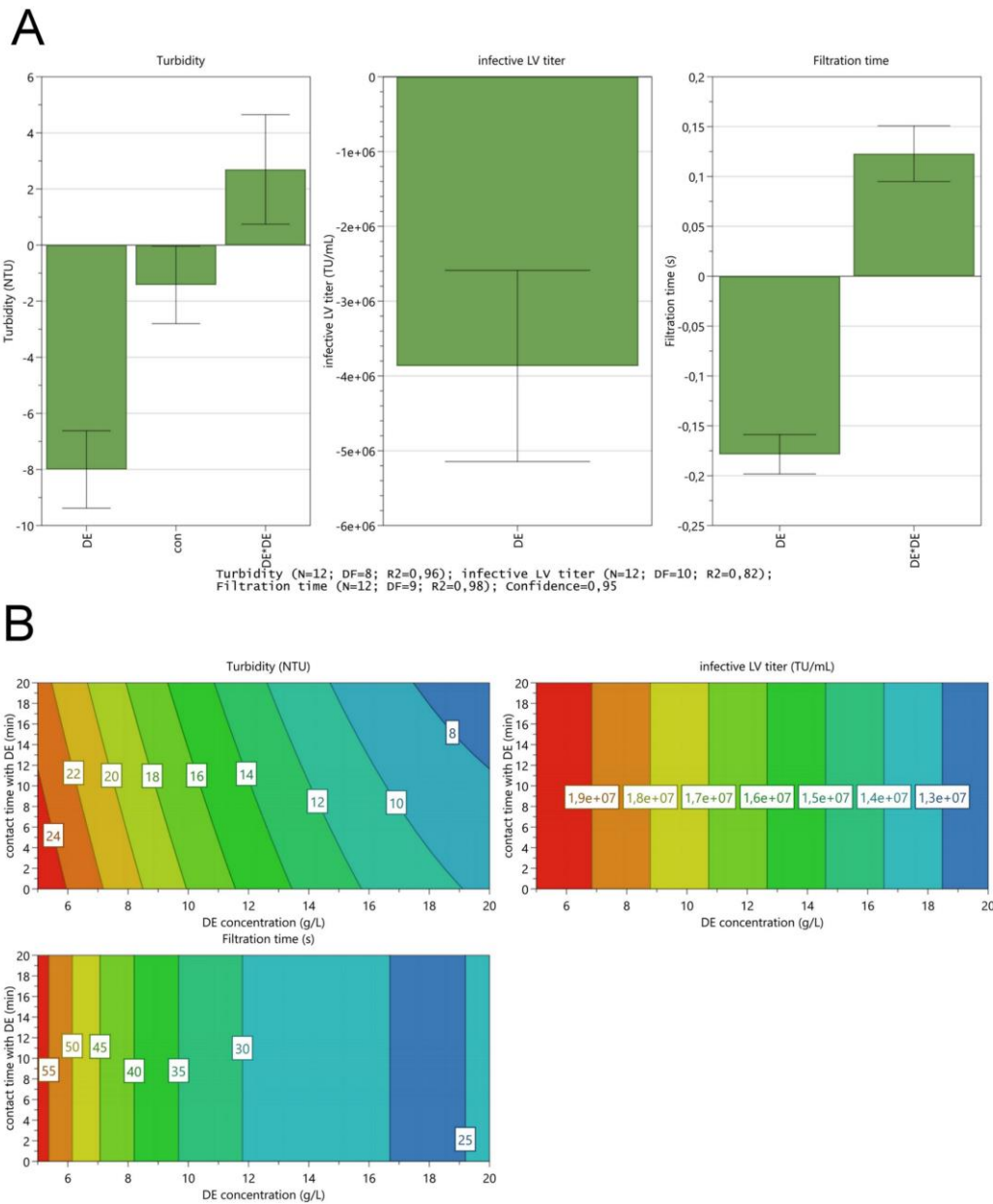
Fig. 3. Effects of diatomaceous earth (DE) on lentivirus clarification performance. Regression coefficient plot (A) and response contour plot (B) for the factors DE concentration (DE) and incubation time (time) on the responses turbidity, filtration time, and infectious lentiviral vector (LV) titer.

filtrates differs only by 2.55 NTU between the two membrane types, which is not a significant difference. This shows that there is no significant difference in final NTU using DE in combination with different membrane structures, whereas the latter has a great impact on final NTU when no DE is used. Moreover, filter clogging occurred after 15 mL for the symmetrical membrane and after 33 mL for the asymmetrical membrane when using it in combination with standard centrifugation method. This means, that four symmetrical or two asymmetrical filter devices would have been necessary to filtrate the target volume of

50 mL. Whereas, only one filter device was needed when using DE, since no filter clogging was observed when filtrating 50 mL.

3.4. Impurity removal capacity by different concentration of DE

The potential to remove process related impurities was analyzed by total protein and dsDNA quantification and the results are listed in Table 1. Several DE concentrations have been tested and compared to the standard method of centrifugation with subsequent filtration. It

15
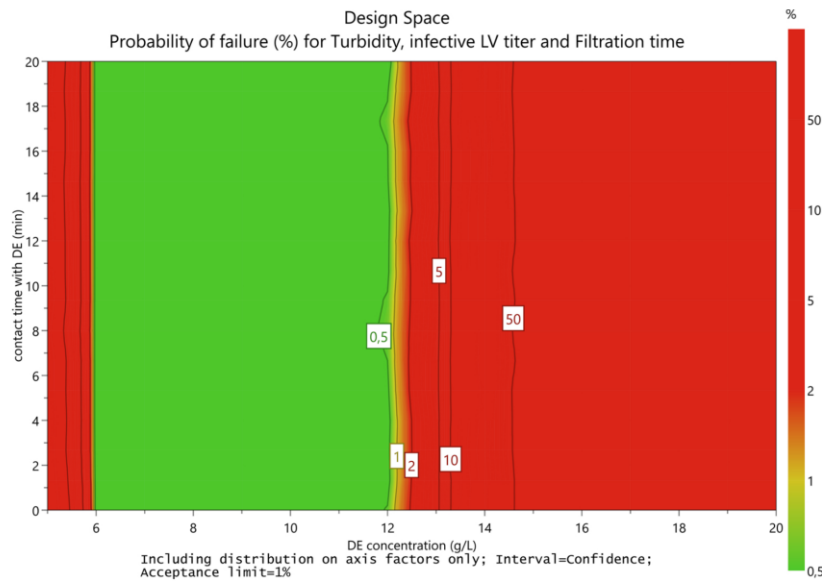
Fig. 4. Design space for clarification of lentiviral vectors (LV) with diatomaceous earth (DE). Design space showing the probability of failure in % to meet the response specifications for turbidity, filtration time and infectious LV titer.
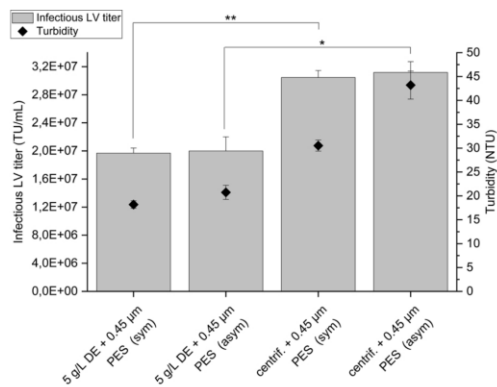
Fig. 5. Effects of clarification methods and membrane structures on turbidity and infectious lentiviral vector (LV) titer. Turbidity and infectious lentiviral vector titer after clarification with 5 g/L diatomaceous earth (DE) using either a symmetrical (sym) or asymmetrical (asym) 0.45 µm polyethersulfone (PES) membrane or by centrifugation of the culture broth and filtration through the same filter types. The LV containing cell culture broth had a cell density of $3.7 \cdot 10^6$ cells/mL and a turbidity of 398 NTU at the time of harvest. Mean ± standard deviation, N = 3, data was analyzed with unpaired t-test (* p ≤ 5 %, ** p ≤ 1 %).

should be investigated whether the use of DE has an advantage in terms of process related impurity removal towards the standard method and whether low DE concentrations yield a sufficient impurity reduction level.

According to Table 1, the use of 5 g/L DE with 0.45 µm PES (sym) membrane filter resulted in a lower impurity concentration in the filtrate compared to centrifugation combined with filtration with the same membrane. A DE concentration of up to 10 g/L DE resulted in reduced protein and dsDNA concentration, but higher DE concentrations between 10 g/L and 40 g/L did not lead to any further improvement of impurity removal.

Table 1

Impurity concentration and removal of different clarification methods. Analyzed clarification methods were clarification with DE and centrifugation with subsequent clarification of the supernatant. Microfilter PES membranes had a symmetrical (sym) structure. Total protein and dsDNA concentration are given as mean ± standard deviation, N = 3.

Clarification method	Total protein concentration (µg/mL)	dsDNA concentration (ng/mL)	Removal of protein (%)	Removal of dsDNA (%)
5 g/L DE +0.45 µm PES (sym)	101.4 ± 8.1	144.7 ± 1.2	21.2 ± 6.3	26.3 ± 0.6
10 g/L DE +0.45 µm PES (sym)	45.1 ± 6.7	116.9 ± 5.2	65.0 ± 5.2	40.4 ± 2.6
40 g/L DE +0.45 µm PES (sym)	52.1 ± 6.3	114.0 ± 3.3	59.4 ± 5.0	41.9 ± 1.7
Centrifugation +0.45 µm PES (sym)	117.9 ± 6.3	151.0 ± 1.6	8.3 ± 4.9	23.0 ± 0.8

3.5. Determination of filter capacities and the effects of the use of a filter aid

Filter capacity is an important criteria when selecting the appropriate filter for a specific production process. A high filter capacity can reduce costs and foot-print of a viral vector downstream process. Filter aids can significantly increase filter capacities due to an increased porosity of the filter material. In this experiment filter capacities have been determined by using only a minimal DE concentration of 5 g/L for clarification with a 0.45 µm PES membrane filter (either symmetrical or asymmetrical membrane structure), or by performing centrifugation and subsequent filtration of the supernatant through the same membrane types. Filtration was performed until filter clogging occurred. The lentivirus containing cell culture broth used for filter capacity determination had a total cell density of $3.7 \cdot 10^6$ cells/mL and a turbidity of 398 NTU at the time of harvest. The filtrate volumes until filter clogging

16

occurred and respective volumetric flow rates are listed in Table 2.

Performing the conventional lab-scale method of centrifugation for cell removal and clarification of the supernatant resulted in rapid filter clogging. The used filtration device Sartolab® RF50 is designed to filtrate up to 50 mL. This volume was not reached with the conventional method. Using 5 g/L DE as a filter aid increased the maximal filtration volume immensely and exceeded the maximal filtration volume of the used filtration device more than 2-fold. Moreover, the asymmetrical structure of the microfilter allowed filtration of an even larger sample volume.

The filter capacities for the different clarification processes were calculated and are shown in Fig. 6. According to Fig. 6, filter capacities were low when performing conventional clarification by centrifugation and subsequent filtration with 7 L/m² for the symmetrical and 15 L/m² for the asymmetrical membrane. Filter capacities increased 8.5-fold when using 5 g/L DE in combination with the symmetrical membrane and 4-fold when using the asymmetrical membrane structure to about 60–63 L/m². The asymmetrical PES membrane structure had a significantly higher membrane capacity compared to the symmetrical PES membrane for both methods.

4. Discussion

4.1. Evaluation of the impact of a filter aid on the processing time

The handling time is an important factor to obtain an efficient downstream process. Since rapid filter clogging occurred when performing the standard method of centrifugation and subsequent microfiltration, a second filter was required and the remaining solution had to be transferred to the second filter. This not only leads to a doubled material consumption, but also means complicated and unsafe handling for the user due to the risk of spillage of the lentiviral vector. In contrast, clarification with DE offered a safe and easy handling procedure for the user with less material consumption. Besides that, clarification is significantly accelerated when using DE compared to the two-step classical method of centrifugation and filtration. This is beneficial not only in terms of efficiency, but also to recover infectivity of the fragile lentiviral vector, which has a high decay rate (Higashikawa and Chang, 2001; Segura et al., 2005) and should therefore be processed in a short time frame at room temperature.

4.2. Analysis of the effects of DE on lentivirus clarification performance by DoE

With the DoE approach the DE concentration and incubation time were identified as factors affecting clarification performance in terms of turbidity reduction, filtration time and recovery of infectious LV titer. Although the design space is quite large, the operator should consider that higher DE concentrations reduce the LV titer. A reduced LV recovery may occur due to retention of the LV by the highly porous structure of DE containing up to 8090 % voids (Bakr, 2010) with pore sizes of about 1.522 μm (Wypych, 2016). With a size of about 80–120 nm (Segura et al., 2006) the lentiviral vector should be able to diffuse into the pores of DE. Another aspect to consider is the positive charge of DE which might result in adsorption of the negatively charged LV (Besnard et al., 2016). If the major aim of the operator is a short filtration time and high turbidity reduction, higher DE concentrations
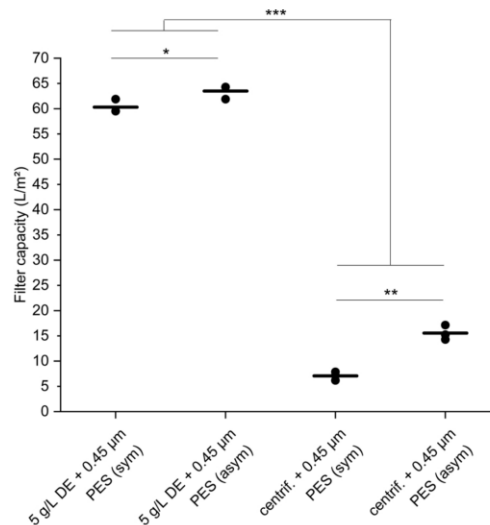

Fig. 6. Filter capacity determination for different clarification processes and membrane structures. Capacities of filters (in L /m²) used for clarification either by 5 g/L diatomaceous earth (DE) and 0.45 μm polyetherfulfone (PES) (symmetrical or asymmetrical structure) or by centrifugation and subsequent microfiltration of the supernatant through the same membrane filters. N = 3, mean is shown as horizontal line, data was analyzed with unpaired *t*-test (* p ≤ 5 %, ** p ≤ 1 %, *** p ≤ 0.1 %).

would provide this. This correlation can be associated to possible retention of impurities by the porous structure of DE (Bakr, 2010). The robust set-point identified with the Optimizer function of MODDE® software suggests to use an incubation, because the robust set-point is positioned in the center of the design space area with the lowest probability of failure and having the largest distances to its boundaries. The only positive effect of the incubation time on clarification performance was observed for the final turbidity. However, this effect was slight, therefore it is not recommended to let the lentiviral vector incubate with DE, if this can be avoided. Depending on the major interest of the operator (high reduction of turbidity, fast filtration or high lentivirus titer recoveries) a suitable DE concentration should be selected.

Moreover, the operator may have to adjust the DE concentration to the characteristics of his cell culture broth to be clarified. The HEK293 T cell density at time of transfection is typically between $8 \cdot 10^5$ cells/mL and $1.5 \cdot 10^6$ cells/mL (Merten et al., 2016). When producing the lentivirus in a classical batch process the cell density would reach approximately up to $5 \cdot 10^6$ cells/mL at time of harvest (Merten et al., 2014). These cell densities are far lower compared to the ones of classical protein production processes. Typical protein-producing cell cultures, like CHO cell lines, result in higher final cell densities of about $20 \cdot 10^6$ to $30 \cdot 10^6$ cells/mL for high density cell cultures in a 10–14 day fedbatch process (Yongky et al., 2019) for which the use of filter aids for clarification has great benefits. The wet cell weight (WCW) of a CHO cell culture of $25 \cdot 10^6$ cells/mL is about 8 % (w/v). A DE concentration of about 50 % of the wet cell weight is recommended to use (van der Meer

Table 2
Filtrate volumes until the occurrence of filter clogging and volumetric flow rates by performing different clarification strategies. Analyzed clarification methods were clarification with 5 g/L DE versus centrifugation and subsequent filtration of the supernatant. PES membranes had either a symmetrical (sym) or asymmetrical (asym) structure. Filtered volumes are given as mean ± standard deviation, N = 3.

	5 g/L DE +0.45 μm PES (sym)	5 g/L DE +0.45 μm PES (asym)	Centrifugation +0.45 μm PES (sym)	Centrifugation +0.45 μm PES (asym)
Filtrate volume (mL)	126.7 ± 2.9	133.3 ± 2.9	14.8 ± 1.8	32.7 ± 3.1
Volumetric flow rate (L/m²h)	921.1 ± 61.3	1304.4 ± 286.6	631.5 ± 119.4	935.4 ± 112.4

17

et al., 2014), which would result in this case in a DE concentration of 40 g/L. The cell density and WCW was far lower for our lentiviral vector production protocol than for a typical therapeutic protein production process, with a maximum total cell density of $3.7 \cdot 10^6$ cells/mL and a WCW of 1.3 %. Hence, a lower DE concentration range appears to be more suitable for the lentivirus clarification. Half of the highest WCW obtained in this study would correspond to a DE concentration of 6.5 g/L. The experiment showed, that even a lower DE concentration of 5 g/L was sufficient to avoid filter clogging.

4.3. Comparison of membrane structures and clarification methods regarding lentivirus recovery, impurity reduction and filter capacity

Comparison of the filter capacities of the different clarification methods highlighted the increase of filter capacity when using DE compared to a classical centrifugation plus microfiltration approach. Since the filter capacity highly depends on the characteristics of the cell culture broth, mainly cell density and viability (Immarino et al., 2007), results will vary from batch to batch. In our experiment the target volume for the filtration device of 50 mL was exceeded about 2.5-fold. This illustrates the robustness of the method, where a successful filtration of 50 mL culture volume with 5 g/L DE can be expected even with varying LV batches. The classical lab scale clarification method of centrifugation and filtration, however, seems to be more susceptible to batch variabilities, since filter clogging occurred after varying volumes depending on the LV batch. In contrast, clarification with 5 g/L DE was always successful. For a lentivirus containing cell culture with a low total cell density of $1.1 \cdot 10^6$ cells/mL and a turbidity of 141 NTU, filter clogging of the centrifuged supernatant already occurred after 25 mL, whereas for the two LV batches with approximately $3.7 \cdot 10^6$ cells/mL and a turbidity around 380–390 NTU, filter clogging occurred already after 15 mL using a symmetrical 0.45 μm PES membrane in both cases. Since the cells are completely removed during centrifugation, filter clogging depended on the turbidity of the supernatant with higher turbidities indicating more impurities that can potentially block the filter membrane. The robustness of the classical clarification method may therefore be rated as lower. On one hand, performing membrane filtration in a cross-flow filtration mode could possibly increase the filter capacity when filtrating the LV supernatant after centrifugation, since cross-flow filtration minimizes filter cake formation and consequently delaying filter blockade. On the other hand, cross-flow filtration increases shear stress which is a disadvantage when working with enveloped fragile viruses like LV. During dead-end filtration, exposure time to shear stress is short since the LV undergoes a rapid single pass (Besnard et al., 2016). Therefore, we assume, that dead-end filtration is a milder operation mode for the clarification process.

Impurity reduction increased with increasing concentration of DE, although between 10 g/L and 40 g/L there could not be observed any further improvement of impurity removal. Compared to centrifugation and microfiltration the use of DE resulted in a higher impurity removal, but with 5 g/L DE only slightly performing better. Hence, in order to achieve a sufficient impurity reduction level higher DE concentrations should be used.

Filter capacities were higher with an asymmetrical membrane structure. This can be explained by the depth filter-like structure of the membrane. The pore size at the surface site of the membrane is greater than 0.45 μm, but decreases towards the filtrate site where the pores have a size of 0.45 μm. In contrast, the symmetrical membrane has a consistent pore size from the surface site to the filtrate site. The asymmetrical membrane is more permeable overall and is known to have higher capacities (Gottschalk, 2009; Li et al., 2009), which was observed in this study as well. However, a disadvantage of a higher permeability of the asymmetrical membrane is that the degree of contaminant removal, e.g. turbidity, is lower, allowing more impurities to pass the membrane. The difference in filtrate turbidity between the two membrane structures is much more pronounced when filtrating the

centrifuged supernatant (12.67 NTU difference) than with clarification using DE. For the latter method, the turbidities differ only by 2.55 NTU. This could be explained by the possibility that mainly DE is involved in depletion of impurities and the membrane structure effects are less visible than with the standard method. The final turbidity was lower when DE was used, although a turbidity below 10 NTU, which is commonly targeted, could not be achieved with low DE concentrations, like 5–10 g/L. Hence, to achieve this, a second microfiltration step would be necessary or the use of higher DE concentrations of about 20 g/L as predicted by the DoE model. At the same time LV titer would decrease with increasing DE concentration, thus the operator needs to consider his main objectives and find a compromise between these two conditions.

5. Conclusion

Suspension based upstream processes for the production of lentiviral vectors have become of high interest in the last few years. Although clarification has so far received little attention during LV DSP optimization, it is a critical step for the purification of viral vectors and has a strong impact on product yield and process reproducibility (Besnard et al., 2016). In this work, the main goal was to analyze the effect of applying a filter aid, like DE, on clarification of lentiviral vectors produced by transient transfection of HEK293 T suspension cells.

We could show that turbidity was reduced more efficiently with the use of DE. Higher DE concentrations are beneficial for a higher impurity reduction and to achieve shorter filtration times, but at the same time LV titer decreases with increasing DE concentration, thus the operator needs to consider his main objectives. A DE concentration of 9 g/L was identified as a robust set-point and incubation time with DE should be avoided. Besides an improved turbidity reduction, clarification with the filter aid DE has other advantages that may offset the virus titer loss. Clarification with DE allows the operator to perform a clarification process, which does not only facilitate faster and safer handling, but enables a lower material consumption due to the extremely increased filter capacity, thus representing an efficient and robust clarification process. The use of an asymmetrical membrane structure further increases filter capacity, but leads to a reduced removal of impurities. Usage of DE for the clarification of lentiviruses produced in suspension culture may become a commonly applied laboratory method in the future. In terms of scalability lab scale virus clarification can be covered with the Sartolab MultiStation which can hold six bottle top filters for filtration of 1 L virus solution each, allowing simultaneous clarification of 6 L. Currently the connection of 2 L bottle top filters is under development, which would then facilitate clarification of up to 12 L. Certainly vacuum filtration has its limitations here and for larger volumes other solutions must be found. An application for other viral vectors is conceivable and should be investigated.

CRediT authorship contribution statement

Jennifer J. Labisch: Conceptualization, Methodology, Investigation, Formal analysis, Visualization, Writing - original draft. Franziska Bollmann: Supervision, Writing - review & editing. Michael W. Wolff: Supervision, Writing - review & editing. Karl Pflanz: Supervision, Project administration.

Declaration of Competing Interest

The authors report no declarations of interest.

Acknowledgements

18

thank Andreas Pickl and Klaus Schöne for the fruitful discussions and Florian Hebenstreit for the assembly of the filters. Assistance with the DoE provided by Timo Schmidberger was greatly appreciated.

References

Aiuti, A., Biasco, L., Scaramuzza, S., Ferrua, F., Cicalese, M.P., Baricordi, C., Dionisio, F., Calabria, A., Giannelli, S., Castiello, M.C., Bosticardo, M., Evangelio, C., Assanelli, A., Casiraghi, M., Di Nunzio, S., Callegaro, L., Benati, C., Rizzardi, P., Pellin, D., Di Serio, C., Schmidt, M., Kalle, C., Gardner, J., Mehta, N., Neduva, V., Dow, D.J., Galy, A., Miniero, R., Finocchi, A., Metin, A., Banerjee, P.P., Orange, J.S., Galimberti, S., Valsecchi, M.G., Biffi, A., Montini, E., Villa, A., Ciceri, F., Roncarolo, M.G., Naldini, L., 2013. Lentiviral hematopoietic stem cell gene therapy in patients with Wiskott-Aldrich syndrome. Science (New York, N.Y.) 341 (6148), 1233151. https://doi.org/10.1126/science.1233151.

Bakr, H.E.G.M., 2010. Diatomite: its characterization, modifications and applications. Asian J. Mater. Sci. 2 (3), 121–136. https://doi.org/10.3923/ajmskr.2010.121.136.

Bauler, M., Roberts, J.K., Wu, C.-C., Fan, B., Ferrara, F., Yip, B.H., Diao, S., Kim, Y.-I., Moore, J., Zhou, S., Wielgosz, M.M., Ryu, B., Throm, R.E., 2020. Production of lentiviral vectors using suspension cells grown in serum-free media. Mol. Ther. Methods Clin. Dev. 17, 58–68. https://doi.org/10.1016/j.omtm.2019.11.011.

Besnard, L., Fabre, V., Fettig, M., Gousseinov, E., Kawakami, Y., Laroudie, N., Scanlan, C., Pattnaik, P., 2016. Clarification of vaccines: an overview of filter based technology trends and best practices. Biotechnol. Adv. 34 (1), 1–13. https://doi.org/10.1016/j.biotechadv.2015.11.005.

Cartier, N., Hacein-Bey-Abina, S., Bartholomae, C.C., Veres, G., Schmidt, M., Kutschera, I., Vidaud, M., Abel, U., Dal-Cortivo, L., Caccavelli, L., Mahlaoui, N., Kiermer, V., Mittelstaedt, D., Bellesme, C., Lahlou, N., Lefrère, F., Blanche, S., Audit, M., Payen, E., Leboulch, P., l'Homme, B., Bougnères, P., Kalle, C., Fischer, A., Cavazzana-Calvo, M., Aubourg, P., 2009. Hematopoietic stem cell gene therapy with a lentiviral vector in X-linked adrenoleukodystrophy. Science (New York, N.Y.) 326 (5954), 818–823. https://doi.org/10.1126/science.1171242.

Cavazzana-Calvo, M., Payen, E., Negre, O., Wang, G., Hehir, K., Fusil, F., Down, J., Denaro, M., Brady, T., Westerman, K., Cavallesco, R., Gillet-Legrand, B., Caccavelli, L., Sgarra, R., Maouche-Chrétien, L., Bernaudin, F., Girot, R., Dorazio, R., Mulder, G.-J., Polack, A., Bank, A., Soulier, J., Larghero, J., Kabbara, N., Dalle, B., Gourmel, B., Socie, G., Chrétien, S., Cartier, N., Aubourg, P., Fischer, A., Cornetta, K., Galacteros, F., Beuzard, Y., Gluckman, E., Bushman, F., Hacein-Bey-Abina, S., Leboulch, P., 2010. Transfusion independence and HMGA2 activation after gene therapy of human β-thalassaemia. Nature 467 (7313), 318–322. https://doi.org/10.1038/nature09328.

Cheeks, M.C., Kamal, N., Sorrell, A., Darling, D., Farzaneh, F., Slater, N.K.H., 2009. Immobilized metal affinity chromatography of histidine-tagged lentiviral vectors using monolithic adsorbents. J. Chromatogr. A 1216 (13), 2705–2711. https://doi.org/10.1016/j.chroma.2008.08.029.

Chen, R., Folarin, N., Ho, V.H.B., McNally, D., Darling, D., Farzaneh, F., Slater, N.K.H., 2010. Affinity recovery of lentivirus by diaminopelargonic acid mediated desthiobiotin labelling. J. Chromatogr. B Analyt. Technol. Biomed. Life Sci. 878 (22), 1939–1945. https://doi.org/10.1016/j.jchromb.2010.05.019.

Cooper, A.R., Patel, S., Senadheera, S., Plath, K., Kohn, D.B., Hollis, R.P., 2011. Highly efficient large-scale lentiviral vector concentration by tandem tangential flow filtration. J. Virol. Methods 177 (1), 1–9. https://doi.org/10.1016/j.jviromet.2011.06.019.

Doran, P.M., 2013. Bioprocess engineering principles, 2nd ed. Academic Press, Waltham. https://doi.org/10.1016/C2009-0-22348-8. Mass., 1 online resource.

Eriksson, L., 2008. Design of Experiments: Principles and Applications, 3rd rev. And Enl. Umetrics Academy, Umeå, Sweden. https://doi.org/10.1002/cem.686 ed. ed 459 pp.

Geraerts, M., Michiels, M., Baekelandt, V., Debyser, Z., Gijsbers, R., 2005. Upscaling of lentiviral vector production by tangential flow filtration. J. Gene Med. 7 (10), 1299–1310. https://doi.org/10.1002/jgm.778.

Gottschalk, U., 2009. Process Scale Purification of Antibodies. John Wiley & Sons, Hoboken, N.J xxvi, 430 str.

Grauf, M., Lagrange, B., Schöne, K., 2018. Simplified small-scale harvest of CHO cells for mAb analytics. Genet. Eng. Biotechnol. News 38 (5), 22–23. https://doi.org/10.1089/gen.38.05.07.

Hanna, E., Rémuzat, C., Auquier, P., Toumi, M., 2017. Gene therapies development: slow progress and promising prospect. J. Mark. Access Health Policy 5 (1), 1265293. https://doi.org/10.1080/20016689.2017.1265293.

Herzog, R.W., Cao, O., Srivastava, A., 2010. Two decades of clinical gene therapy–success is finally mounting. Discov. Med. 9 (45), 105–111.

Higashikawa, F., Chang, L., 2001. Kinetic analyses of stability of simple and complex retroviral vectors. Virology 280 (1), 124–131. https://doi.org/10.1006/viro.2000.0743.

Immarino, M., Nti-Gyabaah, J., Chandler, M., Roush, D., Göklen, K., 2007. Impact of cell density and viability on primary clarification of mammalian cell broth: an analysis using disc-stack centrifugation and charged depth filtration. Bioprocess Int. 38–50.

John Wiley & Sons, Inc, 2019. Gene Therapy Trials Worldwide. John Wiley & Sons, Inc, Hoboken, NJ, USA. Journal of Gene Medicine. http://www.abedia.com/wiley/vectors.php. Accessed 5 May 2020.

Kutner, R.H., Puthli, S., Marino, M.P., Reiser, J., 2009. Simplified production and concentration of HIV-1-based lentiviral vectors using HYPERFlask vessels and anion exchange membrane chromatography. BMC Biotechnol. 9, 10. https://doi.org/10.1186/1472-6750-9-10.

Li, W., Duclos-Orsello, C., Ho, C.-C., 2009. Theoretical analysis of the effects of asymmetric membrane structure on fouling during microfiltration. AIChE J. 55 (6), 1434–1446. https://doi.org/10.1002/aic.11763.

Manceur, A.P., Kim, H., Misic, V., Andreev, N., Dorion-Thibaudeau, J., Lanthier, S., Bernier, A., Tremblay, S., Gélinas, A.-M., Broussau, S., Gilbert, R., Ansorge, S., 2017. Scalable lentiviral vector production using stable HEK293SF producer cell lines. Hum. Gene Ther. Methods 28 (6), 330–339. https://doi.org/10.1089/hgtb.2017.086.

Mátrai, J., Chuah, M.K.L., VandenDriessche, T., 2010. Recent advances in lentiviral vector development and applications. Mol. Ther. J. Am. Soc. Gene Ther. 18 (3), 477–490. https://doi.org/10.1038/mt.2009.319.

Maude, S.L., Frey, N., Shaw, P.A., Aplenc, R., Barrett, D.M., Bunin, N.J., Chew, A., Gonzalez, V.E., Zheng, Z., Lacey, S.F., Mahnke, Y.D., Melenhorst, J.J., Rheingold, S.R., Shen, A., Teachey, D.T., Levine, B.L., June, C.H., Porter, D.L., Grupp, S.A., 2014. Chimeric antigen receptor T cells for sustained remissions in leukemia. N. Engl. J. Med. 371 (16), 1507–1517. https://doi.org/10.1056/NEJMoa1407222.

Mekkaoui, L., Parekh, F., Kotsopoulou, E., Darling, D., Dickson, G., Cheung, G.W., Chan, L., MacLellan-Gibson, K., Mattiuzzo, G., Farzaneh, F., Takeuchi, Y., Pule, M., 2018. Lentiviral vector purification using genetically encoded biotin mimic in packaging cell. Mol. Ther. Methods Clin. Dev. 11, 155–165. https://doi.org/10.1016/j.omtm.2018.10.008.

Merten, O.-W., Schweizer, M., Chahal, P., Kamen, A.A., 2014. Manufacturing of viral vectors for gene therapy: part I. Upstream processing. Pharm. Bioprocess. 2 (2), 183–203. https://doi.org/10.4155/pbp.14.16.

Merten, O.W., Hebben, M., Bovolenta, C., 2016. Production of lentiviral vectors. Mol. Ther. Methods Clin. Dev. 3, 16017. https://doi.org/10.1038/mtm.2016.17.

Miliotou, A.N., Papadopoulou, L.C., 2018. CAR T-cell therapy: a new era in cancer immunotherapy. Curr. Pharm. Biotechnol. 19 (1), 5–18. https://doi.org/10.2174/1389201019666180418095526.

Milone, M.C., O'Doherty, U., 2018. Clinical use of lentiviral vectors. Leukemia 32 (7), 1529–1541. https://doi.org/10.1038/s41375-018-0106-0.

Olgun, H.B., Tasyurek, H.M., Sanlioglu, A.D., Sanlioglu, S., 2019. High-grade purification of third-generation HIV-based lentiviral vectors by anion exchange chromatography for experimental gene and stem cell therapy applications. Methods Mol. Biol. (Clifton, N.J.) 1879, 347–365. https://doi.org/10.1007/7651_2018_154.

Papanikolaou, E., Kontostathi, G., Drakopoulou, E., Georgomanoli, M., Stamateris, E., Vougas, K., Vlahou, A., Maloy, A., Ware, M., Anagnou, N.P., 2013. Characterization and comparative performance of lentiviral vector preparations concentrated by either one-step ultrafiltration or ultracentrifugation. Virus Res. 175 (1), 1–11. https://doi.org/10.1016/j.virusres.2013.03.015.

Reeves, L., Cornetta, K., 2000. Clinical retroviral vector production: step filtration using clinically approved filters improves titers. Gene Ther. 7 (23), 1993–1998. https://doi.org/10.1038/sj.gt.3301328.

Rodrigues, T., Carrondo, M.J.T., Alves, P.M., Cruz, P.E., 2007. Purification of retroviral vectors for clinical application: biological implications and technological challenges. J. Biotechnol. 127 (3), 520–541. https://doi.org/10.1016/j.jbiotec.2006.07.028.

Ruscic, J., Perry, C., Mukhopadhyay, T., Takeuchi, Y., Bracewell, D.G., 2019. Lentiviral vector purification using nanofiber ion-exchange chromatography. Mol. Ther. Methods Clin. Dev. 15, 52–62. https://doi.org/10.1016/j.omtm.2019.08.007.

Sakuma, T., Barry, M.A., Ikeda, Y., 2012. Lentiviral vectors: basic to translational. Biochem. J. 443 (3), 603–618. https://doi.org/10.1042/BJ20120146.

Segura, M., Kamen, A., Trudel, P., Garnier, A., 2005. A novel purification strategy for retrovirus gene therapy vectors using heparin affinity chromatography. Biotechnol. Bioeng. 90 (4), 391–404. https://doi.org/10.1002/bit.20301.

Segura, Md.L.M., Kamen, A., Garnier, A., 2006. Downstream processing of oncoretroviral and lentiviral gene therapy vectors. Biotechnol. Adv. 24 (3), 321–337. https://doi.org/10.1016/j.biotechadv.2005.12.001.

Segura, M.M., Garnier, A., Durocher, Y., Coelho, H., Kamen, A., 2007. Production of lentiviral vectors by large-scale transient transfection of suspension cultures and affinity chromatography purification. Biotechnol. Bioeng. 98 (4), 789–799. https://doi.org/10.1002/bit.21467.

Segura, M.M., Kamen, A.A., Garnier, A., 2011. Overview of current scalable methods for purification of viral vectors. Methods Mol. Biol. (Clifton, N.J.) 737, 89–116. https://doi.org/10.1007/978-1-61779-095-9_4.

Segura, M.M., Mangion, M., Gaillet, B., Garnier, A., 2013. New developments in lentiviral vector design, production and purification. Expert Opin. Biol. Ther. 13 (7), 987–1011. https://doi.org/10.1517/14712598.2013.779249.

Turtle, C.J., Hanafi, L.-A., Berger, C., Gooley, T.A., Cherian, S., Hudecek, M., Sommermeyer, D., Melville, K., Pender, B., Budiarto, T.M., Robinson, E., Steevens, N.N., Chaney, C., Soma, L., Chen, X., Yeung, C., Wood, B., Li, D., Cao, J., Heimfeld, S., Jensen, M.C., Riddell, S.R., Maloney, D.G., 2016. CD19 CAR-T cells of defined CD4+: CD8+ composition in adult B cell ALL patients. J. Clin. Invest. 126 (6), 2123–2138. https://doi.org/10.1172/JCI85309.

U.S. Department of Health and Human Services, Food and Drug Administration, Center for Drug Evaluation and Research (CDER), Center for Biologics Evaluation and Research (CBER), 2009. Guidance for Industry: Q8(R2) Pharmaceutical Development. ICH.

van der Meer, T., Minow, B., Lagrange, B., Krumbein, F., Rolin, F., 2014. Diatomaceous earth filtration: innovative single-use concepts for clarification of high-density mammalian cell cultures. Bioprocess Int. 2014.

Votteler, J., Sundquist, W.I., 2013. Virus budding and the ESCRT pathway. Cell Host Microbe 14 (3), 232–241. https://doi.org/10.1016/j.chom.2013.08.012.

Wypych, G., 2016. Handbook of Fillers, fourth edition. ChemTec Publishing, Toronto.

Yongky, A., Xu, J., Tian, J., Oliveira, C., Zhao, J., McFarland, K., Borys, M.C., Li, Z.J., 2019. Process intensification in fed-batch production bioreactors using non-perfusion seed cultures. mAbs 11 (8), 1502–1514. https://doi.org/10.1080/19420862.2019.1652075.

Yu, J.H., Schaffer, D.V., 2006. Selection of novel vesicular stomatitis virus glycoprotein variants from a peptide insertion library for enhanced purification of retroviral and lentiviral vectors. J. Virol. 80 (7), 3285–3292. https://doi.org/10.1128/JVI.80.7.3285-3292.2006.

35

4.2 Infectious titer determination of lentiviral vectors using a temporal immunological real-time imaging approach

Appropriate analytical methods are critical for DSP development. The analytics of viral vector samples are a major bottleneck in process development, since many of the existing analytical assays are time-consuming, and thus, slow down product and process development. Refinement of the critical quality attributes of viral vectors in recent years emphasized the need for faster and more accurate analytical assays [32,147].

During the previous part of the research, which focused on clarification, an infectious titer assay with a flow cytometry readout was identified as the decisive step that greatly slowed down the downstream process development. Therefore, before starting further development work on DSP steps, improving the infectious titer assay by increasing throughput and reducing handling, while maintaining the accuracy of the titer determination, was tackled.

To accelerate CD19 CAR LV infectious titer determination, an assay based on an automated real-time imaging live-cell analysis system was implemented (Fig. 10).
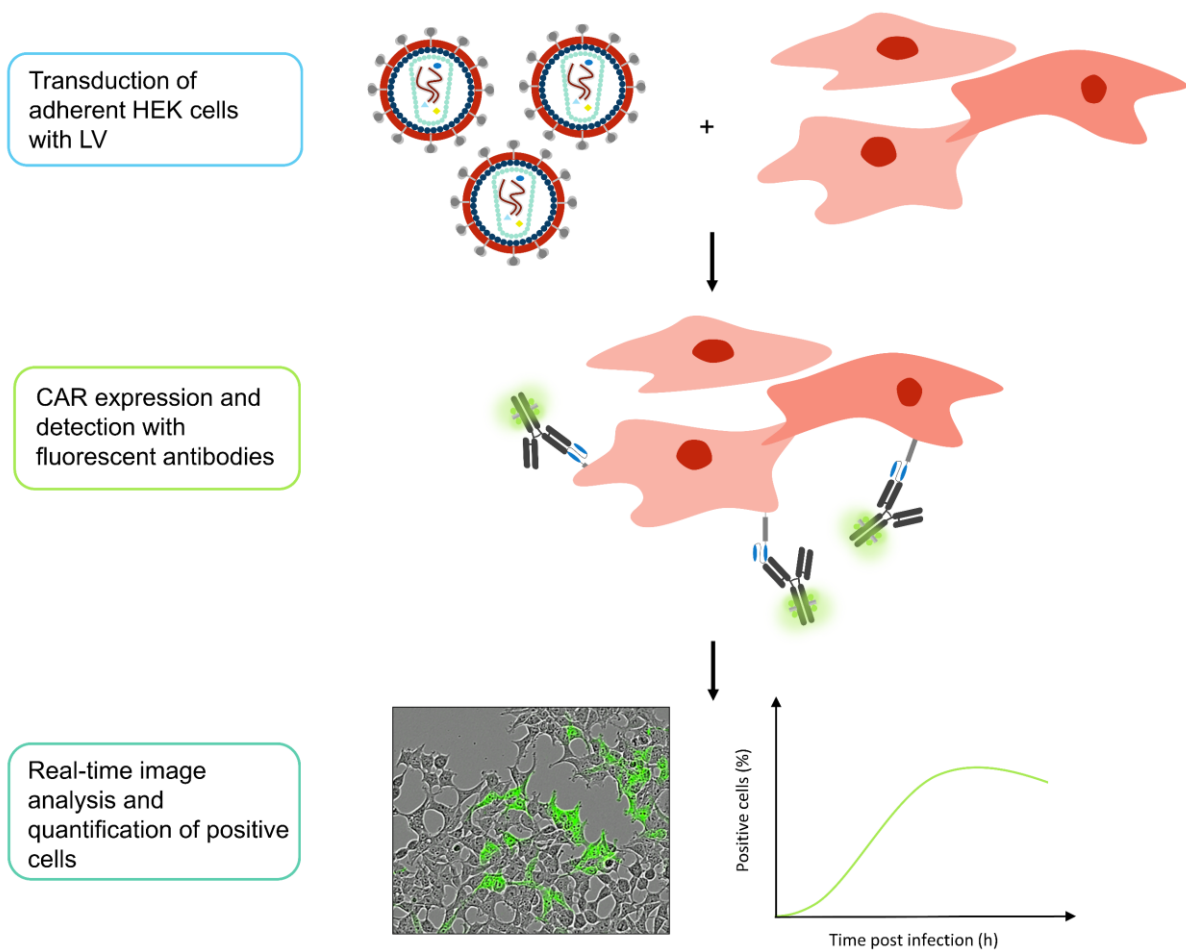
Figure 10: Schematic visualization of the developed assay for infectious titer determination of lentiviral vectors by an immunological real-time imaging approach.

The method was compared with the previously used flow cytometry-based infectious titer assay which required a lot of manual pipetting, centrifugation, and staining steps to obtain the assay readout that limited the number of samples per week and operator to a maximum of 24 samples analyzed in duplicates. Considering the inclusion of several dilutions per sample to be able to select the appropriate dilution that was in the range of the analytical assay, later on, this further reduced the number of samples that could be analyzed to below 10 samples.

The new infectious titer assay protocol is based on real-time imaging of cells inside a static incubator. Adherent HEK293T cells were seeded into 96-well plates and images were acquired every 2 h automatically. The implemented software allowed for the segmentation of phase contrast and fluorescence images. After transduction of the cells by the LV samples, the cells were stained with an anti-CD19 CAR antibody emitting green fluorescence when bound to an infected cell that expressed the CD19 CAR transgene (Fig. 10). The throughput was increased as six 96-well plates could be analyzed simultaneously and all centrifugation steps and many pipetting steps were eliminated.

The developed immunological real-time imaging assay determined LV titers that were not significantly different from the flow cytometry method, and at the same time had lower standard deviations between replicates. Furthermore, the assay possesses a broader linear range, which increases the likelihood that an applied LV dilution lies within this range. Most likely the reduction of pipetting steps and the possibility to use electronic multi-channel pipettes led to the decrease in the standard deviations. Moreover, the newly developed infectious titer assay showed good inter- and intra-assay precision. The main difference between the two assays is an endpoint readout for the flow cytometry assay and a flexible readout for the real-time imaging method as the data is acquired over time and the operator can select the optimal point of readout, thereby preventing titer determination at an unfavorable time point.

The decreased labor of the immunological real-time imaging infectious titer assay highly increased sample throughput. This was proven by a comprehensive LV stability study, analyzing the effects of temperature, salt concentration, freeze and thaw cycles, and shear stress on LV infectivity. Viral vector stability studies are seldom found in literature due to the high number of samples that need to be analyzed. The LV stability study conducted showed a significant effect of high temperatures, high salt concentrations, and extensive exposure to shear stress on LV infectivity.

PLOS ONE

Infectious titer determination of lentiviral vectors using a temporal immunological real-time imaging approach

Jennifer J. Labisch [1,2]*, G. Philip Wiese [1,3], Kalpana Barnes[4], Franziska Bollmann[5], Karl Pflanz[1]

1 Lab Essentials Applications Development, Sartorius Stedim Biotech GmbH, Göttingen, Lower Saxony, Germany, 2 Institute of Technical Chemistry, Leibniz University Hannover, Hannover, Lower Saxony, Germany, 3 Faculty of Mathematics, Computer Science and Natural Sciences, RWTH Aachen University, Aachen, North Rhine-Westphalia, Germany, 4 BioAnalytics Applications, Essen BioScience, Royston, Hertfordshire, United Kingdom, 5 Segment Marketing Viral-based Therapeutics, Sartorius Stedim Biotech GmbH, Göttingen, Lower Saxony, Germany

* jennifer.labisch@sartorius.com

Abstract

The analysis of the infectious titer of the lentiviral vector samples obtained during upstream and downstream processing is of major importance, however, also the most challenging method to be performed. Currently established methods like flow cytometry or qPCR lack the capability of enabling high throughput sample processing while they require a lot of manual handling. To address this limitation, we developed an immunological real-time imaging method to quantify the infectious titer of anti-CD19 CAR lentiviral vectors with a temporal readout using the Incucyte® S3 live-cell analysis system. The infective titers determined with the Incucyte® approach when compared with the flow cytometry-based assay had a lower standard deviation between replicates and a broader linear range. A major advantage of the method is the ability to obtain titer results in real-time, enabling an optimal readout time. The presented protocol significantly decreased labor and increased throughput. The ability of the assay to process high numbers of lentiviral samples in a high throughput manner was proven by performing a virus stability study, demonstrating the effects of temperature, salt, and shear stress on LV infectivity.

Introduction

Most lentiviral vectors used for therapeutic applications are based on the human immunodeficiency virus (HIV) type 1 which belongs to the *Retroviridae* family and the genus *Lentivirus* [1]. Lentiviral vectors (LV) are efficient gene delivery vehicles playing an important role for advanced therapy medicinal products (ATMPs), that include gene therapy and gene-modified somatic cell therapy products [2]. The aim of ATMPs is to replace disease-causing mutated genes or to deliver a gene for the expression of therapeutic proteins. Lentiviral vectors represent the most frequently used viral gene delivery platform for the *ex vivo* generation of chimeric antigen receptor (CAR)-T cells for cancer immunotherapies [3]. Antigens with a high coverage on

tumor cells are selected as targets for the CAR constructs to enhance T cell specificity [4]. CD19 is the most widely used target in CAR-T cell therapy to treat B cell lymphomas [5,6]. Five CAR-T cell therapy products are currently approved by the Food and Drug Administration, with Kymriah™, Breyanzi®, and Abecma® relying on lentiviral vector-mediated gene transfer [7–9].

The increasing demand of lentiviral vectors due to the high gene-modified cell therapy and gene therapy market growth leads to supply shortfalls [10,11]. A significant bottleneck for viral vector process development and production is the vector quality control. To speed up the upstream and downstream development of lentiviral vector production process, reliable and efficient assays for their quantification are required. A method for fast and precise determination of lentiviral vector infectious titers is desperately needed for process development and process optimization, where typically a high number of samples are generated. Process development is decelerated by labor-intensive and time-consuming virus titer assays. Typically, virus quantification methods aim to determine either the total viral particle (VP) titer or the infectious virus particle titer given in transducing units (TU) per mL [11]. Infectious titer is more meaningful as it measures the number of virus particles that can infect target cells [12]. HEK293T cells are typically used as target cells for LV infectious titer determination [13–18]. The infectious titer of lentiviral vectors can be determined by transduction of cells followed by quantification of the proviral DNA copy number by quantitative polymerase chain reaction (qPCR) [14,19,20]. However, qPCR overestimates the titer since the DNA copy of the lentiviral RNA genome that is inserted into the host cell genome yields varying expression levels depending on the chromatin region [15]. To overcome this drawback, measurement of the transgene expression at the mRNA level by reverse transcription qPCR (RT-qPCR) is an alternative, but requires a time-consuming RNA extraction step [19]. Another commonly used technique for infectious titer determination is flow cytometry. With this technology the expression of the gene of interest or a reporter gene, such as the green fluorescent protein (GFP) is measured [15]. Using GFP as a reporter gene has the advantage of eliminating staining steps, however, the usage of lentiviral vectors transferring the gene for GFP is limited to *in vitro* and preclinical *in vivo* research. In the case of lentiviral vectors used for therapeutic applications such as CAR-T cell therapy, the expressed CAR construct is detected by a fluorophore-conjugated antibody during flow cytometry analysis or by measuring the mRNA expression of the transgene with RT-qPCR [19,21]. These assay formats are multi-step processes, generally time consuming and results are obtained after four to five days [21,22]. Furthermore, both methods lack the ability for high-throughput sample processing that can be easily implemented at a relatively low cost.

To address the bottleneck of current analytical methods for viral vectors, we developed a new immunological real-time imaging method to quantify the infectious titer of anti-CD19 CAR lentiviral vectors using the Incucyte® S3. The principle of this approach is shown in Fig 1.

The introduction of a temporal readout simplified the workflow, increased throughput, and reduced labor. The applicability of the established method for lentiviral vector infectious titer quantification was shown by studying the stability of lentiviral vectors towards external influences. A comparison of the different workflows for infectious LV titer determination, either by flow cytometry, RT-qPCR, or by the newly developed real-time imaging approach is shown in Fig 2.

Materials and methods

Lentiviral vector production

Third generation lentiviral vectors were produced by transient transfection of suspension HEK293T/17 SF cells (ACS-4500, ATCC) with four plasmids in an Ambr® 250 Modular
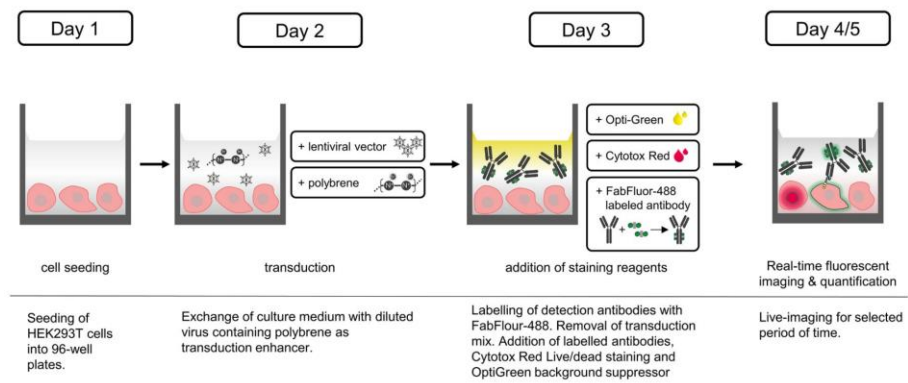
Fig 1. Schematic workflow of the infectious titer assay performed with the Incucyte® S3. HEK293T cells were seeded into a 96-well plate on day 1. The next day, the cells were transduced with diluted lentiviral vector and the transduction enhancer polybrene. 24 h post-infection the transduction mix was removed and replaced by a mixture of staining reagents containing FabFluor-488 labeled anti-FMC63 scFv antibody, Cytotox Red, and Opti-Green background suppressor. Dead cells were stained by Cytotox Red. Infected cells expressing the anti-CD19 CAR were stained by the FabFluor-488 labeled anti-FMC63 scFv antibody. Viable non-infected cells remained unstained. Quantification was performed by real-time fluorescence imaging from days 3-5.

https://doi.org/10.1371/journal.pone.0254739.g001
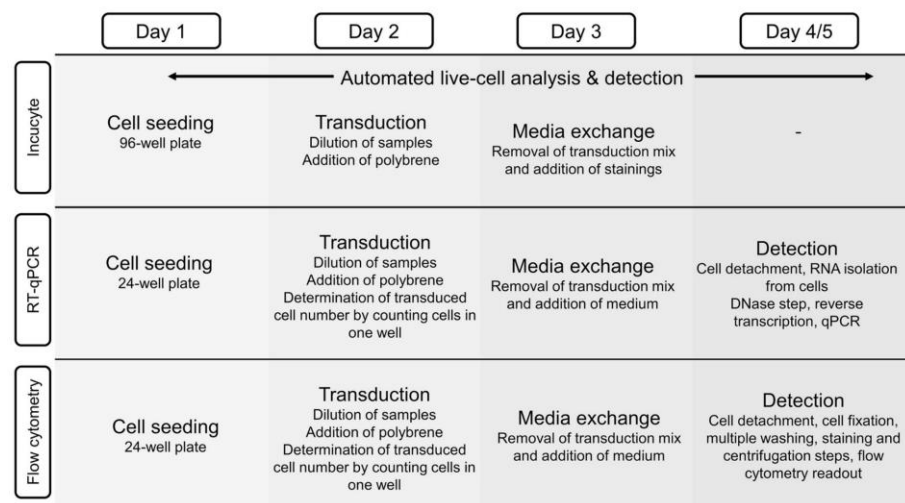
Fig 2. Workflow comparison of lentiviral vector (LV) infectious titer determination methods. One day after cell seeding, cells are transduced with LV and transduction enhancer; measurement of cell number may be required to determine the cell number at time of transduction. On the third day the transduction mix is removed and replaced by growth medium and the staining mixture for the Incucyte® method. While the Incucyte®-based assay continually detects transduced cells with no further action required, the flow cytometry and RT-qPCR based assays require intensive handling for the final (endpoint) readout on day 4 or 5.

https://doi.org/10.1371/journal.pone.0254739.g002

bioreactor system (Sartorius). The cultivation parameters were: Temperature of 36.8°C, 30% dissolved oxygen, pH 7.1, and stirring speed 400 rpm. The plasmids and transfection method are described in detail in Labisch et al [23].

Lentiviral vector harvest and clarification

The lentiviral vector was harvested 72 h post-transfection. DENARASE® (c-Lecta) and $MgCl_2$ (Carl Roth) were added to the cell culture broth one hour before harvest at a final concentration of 10 U/mL and 2 mM, respectively. After nucleic acid digestion, the lentiviral vector containing cell culture broth was directly clarified with Sartoclear Dynamics® Lab V50 (0.45 µm polyethersulfone membrane version) with 5 g/L diatomaceous earth (Sartorius). The lentiviral vector was aliquoted and stored at -80°C.

Infectious titer determination using flow cytometry

To quantify the infectious lentiviral vector titer by flow cytometry, adherent HEK293T cells (ACC 635, DSMZ) were infected with serially diluted LV samples and the expression of the EGFRt-transgene-fusion protein was detected. $6 \cdot 10^4$ cells/well were seeded in 0.5 mL Dulbecco's modified Eagle medium (DMEM; Thermo Fisher Scientific) + 10% fetal calf serum (FCS; Sigma Aldrich) (v/v) in a tissue culture (TC) treated 24-well plate (Greiner Bio-one). Cells were incubated at 37°C and 5% CO_2 in a static incubator (Sartorius) for one day. To infect the cells, culture medium was removed, and the cells were transduced by transferring 0.5 mL of diluted virus solution containing 8 µg/mL polybrene (Sigma Aldrich). A negative control of the respective LV batch was analyzed as well. 18 h post infection, the medium was removed and replaced with fresh culture medium. 72 h post infection the expression of the gene-of-interest was analyzed by flow cytometry. First, cells were detached by incubation with 200 µL trypsin-EDTA (Thermo Fisher Scientific) for 5 min at 37°C. The enzymatic reaction was stopped by adding 500 µL culture medium, subsequently the plate was centrifuged at 300 x g for 5 min and the supernatant was removed. Cells were resuspended in 150 µL PBS and transferred to a non-TC 96-well plate with conical bottom (Sartorius). The 96-well plate was centrifuged, and the supernatant was discarded. To discriminate viable and dead cells, 100 µL of a 1:1000 dilution (in PBS) of the fixable fluorescent dye Zombie NIR™ (BioLegend) was added to each well and incubated for 10 min in the dark. After another centrifugation step and removal of the supernatant, 100 µL Roti®-Histofix 4% (Carl Roth) was added to the cells and incubated for 15 min. The supernatant was removed from the wells after centrifugation and cells were washed with 150 µL PBS. Hereafter, centrifugation of the plate was performed, the supernatant was removed and the cells were incubated for 30 min with an anti-human EGFRt phycoerythrin (PE) conjugated antibody (R&D Systems) at a 1:200 dilution in 40 µL staining buffer (1% Bovine serum albumin (Carl Roth) in PBS). The cells were washed twice with 100 µL staining buffer. After each washing step the plate was centrifuged and the supernatant aspirated. Finally, the cells were resuspended in 40 µL staining buffer and flow cytometry was performed with an iQue ScreenerPlus flow cytometer (Sartorius). The obtained data was analyzed using the integrated ForeCyt 8.0 software. The percentage of EGFRt positive cells of viable single cells was determined. Samples were analyzed in duplicates if not indicated otherwise. The functional lentiviral titer, given in transducing units (TU) per mL, was calculated using the following formula:

$$Infectious\ titer\ =\ \frac{P_1 \cdot N \cdot D}{V \cdot 100} \tag{1}$$

41

Where P_1 is the percentage of positive (live) cells, N is the number of cells at the time of transduction, D is the dilution factor of the LV used for infection, and the transduction volume V in mL.

Infectious titer determination using the Incucyte® S3

For quantification of the infectious virus titer with the Incucyte® S3 (Sartorius), adherent HEK293T cells (ACC 635, DSMZ) were infected with serially diluted LV samples and the expression of the CD19-CAR was measured (Fig 1). 6×10^3 cells were seeded (using Picus® NxT 50–1200 µL, 12-channel, multi-dispense mode, speed: 1, Sartorius) in DMEM + 10% FCS (Sigma Aldrich) in a TC-treated, poly-L-lysine (Sigma Aldrich) coated black 96-well plate with clear bottom (Corning). A positive control for a live/dead cell staining was prepared by adding Triton X-100 (Carl Roth) at a final concentration of 0.005% to the cells. Untreated cells were used as a negative control for the live/dead staining. The cells were incubated at 36.5˚C and 5% CO_2 in the Incucyte® S3 which was located within a static CO_2 incubator (PHCbi). Each well was analyzed every 2 h, taking four images at a 10x magnification with the phase contrast channel, the red and green fluorescence channel. 24 h after cell seeding the culture medium was removed and replaced by 50 µL diluted LV samples (Picus® NxT 5–120 µL, 8-channel, speed: 1, Sartorius). Polybrene was added at a final concentration of 8 µg/mL to each well. A negative control of the corresponding virus batch was included. Samples were analyzed in triplicates if not indicated otherwise.

To stain the infected cells, the test antibodies were labeled with FabFluor-488 (Sartorius) in a reaction tube before addition to the cells. The anti-FMC63 scFv mouse IgG1 antibody (Acro-Biosystems) binding the CD19-CAR construct was used at a final assay dilution of 1:200 and the final concentration of FabFluor-488 was 2.5 µg/mL. A negative isotype control antibody (1 µg/mL) and a positive control anti-transferrin-receptor antibody (3 µg/mL) (R&D Systems), both a mouse IgG1 subtype, were labeled at a 1:3 molar ratio with FabFluor-488. The test antibodies were incubated with Fab-Fluor-488 for 15 min at 37˚C in the dark. 24 h post-infection the medium was removed (Picus® NxT 5–120 µL 8-channel, speed: 1, Sartorius) and 150 µL fresh medium with previously prepared staining reagent mixtures, containing FabFluor-488 labeled test antibody, Cytotox Red (Sartorius) and Opti-Green background suppressor (Sartorius) in final concentrations of 250 nM and 0.5 mM, respectively, were added to the cells (Picus® NxT 10–300 µL, 8 channel, speed: 1, Sartorius). Afterwards, the plate was placed into the Incucyte® S3. Imaging was continued as described above for 5 days.

The Incucyte® analysis software was used to determine the phase contrast area as well as the dead cell area, stained by Cytotox Red, and the area of infected cells, indicated by a Fab-Fluor-488 labeling over time. The percentage of positive cells P_2 was determined by dividing the FabFluor-488 labeled cell's area A_{FF488} by the phase contrast area A_C.

$$P_2 = \frac{A_{FF488}}{A_C} * 100 \tag{2}$$

The number of cells at the time of transduction N was calculated based on a correlation of the phase contrast area and the number of cells seeded per well determined by an offline cell count analysis. To do so, the samples of different cell counts were analyzed offline with a Cedex HiRes analyzer, followed by seeding of the cells into a 96-well plate and subsequent measurement of the phase contrast area with the Incucyte® S3.

$$N = \frac{C - b}{m} \tag{3}$$

42

C is the measured phase contrast area in percent, b is the y-intercept, and m is the slope of the linear regression of cell count and phase contrast area. With the aid of the determined values from Eqs 2 and 3, the infectious titer was calculated using Eq 1.

The percentage of infected cells can be assessed either accounting for all cells or just for live cells when an additional live/dead cell staining is performed. Cells that are infected but dead, emit a green and red fluorescent signal. These cells are detected by an overlap analysis. The overlap analysis module of the Incucyte® S3 software enables calculation of the infectious titer including positive viable cells. Dead cells emit a red fluorescence signal, due to the Cytotox Red staining and can thereby be excluded from the analysis.

The area of cells that are both infected but dead (A_{PD}) was subtracted from the FabFluor-488 labeled area A_{FF488} to obtain the area of infected viable cells. This area was divided by the total area of viable cells, which was calculated by subtracting the area of dead cells A_D from the phase contrast area at readout time A_C. This gives the percentage of positive viable cells P_3.

$$P_3 \quad = \quad \frac{A_{FF488} - A_{PD}}{A_C - A_D} * 100 \tag{4}$$

P_3 was used to calculate the infectious titer with Eq 1 accounting just for positive viable cells, whereas P_2 was used to calculate the titer accounting for all cells.

Segmentation of phase contrast and fluorescence images

The segmentation adjustment to bias the segmentation between cells and background was set to 1.0. The minimum area was set to 170 μm² which leads to exclusion of smaller objects from the analysis e.g. cell debris. The outlines of the confluence mask were refined by applying a clean-up filter of -2 pixels. HEK293T cells that were infected by the LV and expressed the CAR construct could be detected in the green fluorescence channel after binding of a FabFluor-488 labeled anti-FMC63 scFv antibody. The optimal dilution of the anti-FMC63 scFv antibody was chosen to give maximal intensity without excessive background intensity. The edge split filter was deactivated to enable the determination of the green positive area. The background was subtracted from the images by setting the top-hat filter to the radius of the largest fluorescent object. Objects brighter than the specified threshold were detected in the background-subtracted image. The optimal settings were determined to be a top-hat filter radius of 20 μm, a threshold of 1.3 green calibrated units (GCU), a clean-up filter of -1 pixel, and a minimum area filter of 35 μm². For detection of dead cells, the top-hat filter was set to a radius of 20 μm, and a threshold of 0.3 red calibrated units (RCU) was selected. An area filter of 35–1400 μm² lead to recognition of objects only in the specified size range. The minimum thresholds of the FabFluor-488 mask and the Cytotox Red mask were set according to the positive and negative controls of the FabFluor-488 and Cytotox Red staining, thus false positives and unspecific binding events would not significantly affect the calculated titers. The IgG1 isotype antibody and the matrix control containing no LV gave no FabFluor-488 signal and served as negative controls. The anti-transferrin-receptor IgG1 antibody confirmed successful FabFuor-488 labeling of the antibodies (S1 Fig).

Lentiviral vector stability study

The lentiviral vector was frozen by placing the samples into a -80˚C refrigerator. The samples were thawed rapidly in a water bath at 37˚C. The freeze and thaw procedures were repeated for multiple freeze and thaw cycles. To study the infectivity loss upon temperature exposure, the lentiviral vector was incubated at 4˚C, 22˚C, and 37˚C for 24 h, 48 h, and 72 h. An untreated sample served as a negative control. The effect of salt on LV infectivity was analyzed

by incubating the LV with 0.2, 0.4, 0.6, 0.8, and 1 M of NaCl in PBS for 1 h at 4°C. Incubation was stopped by diluting to 0.1 M NaCl. A sample without NaCl treatment incubated for 1 h at 4°C served as a negative control. Shear stress caused by pumping was analyzed. A tube (#16, 3.2 mm x 1.6 mm, Watson Marlow) was connected to a peristaltic pump 120U/DV (Watson Marlow) and a reservoir containing 30 mL of the lentiviral vector sample. The sample was pumped at 19.5 mL/min or 78.2 mL/min for 10 min or 30 min in a cycle. A sample incubated for 10 min or 30 min at room temperature served as a negative control. All experiments were performed in triplicates. Each replicate was analyzed in duplicates in the Incucyte® S3.

Statistical analysis

The statistical significance of between-group differences was evaluated by using unpaired Student's t-tests (two-tailed) with OriginPro® 2020 (OriginLab). Differences among more than two groups were evaluated by one-way ANOVA with Holm-Sidak post-hoc test for multiple comparisons with SigmaPlot 14.5 (Systat).

Results

Segmentation of phase contrast and fluorescence images

Part of the development of the infectivity assay for lentiviral vectors with the Incucyte® S3 was defining the analysis parameters for segmentation of phase contrast and fluorescence images. The image analysis software of the Incucyte® S3 allows to process kinetic data from three channels in real-time. High definition phase contrast images were captured and segmented to return a value of total cell area (Fig 3A). The green and red fluorescent images were segmented and yielded area metrics for positively infected cells expressing the CAR construct (Fig 3B) and dead cells respectively (Fig 3C).

Determination of the linear range and precision of the Incucyte®-based infectious titer assay

To identify the linear range of the assay in regard to the normalized positive area of the infected cells, HEK293T cells were infected with serially diluted lentiviral vector. The measurement showed a time-dependent and concentration-dependent effect (Fig 4). For all experiments, a readout time was defined for each curve, which corresponded to the maximum signal over the measured period.

To determine the linear range of the flow cytometry and the Incucyte® S3 based methods, cells were transduced with a twofold serial dilution of the LV. With the flow cytometry readout, a logarithmic trend (Fig 5A) across the dilution range was observed and a linear range for dilutions between 1:128 and 1:512 with an R^2 of 0.98 (Fig 5B). The Incucyte®-based method showed a logarithmic trend as well (Fig 5C). A linear range was observed for dilutions between 1:64 and 1:512 with an R^2 of 0.96 (Fig 5D). According to the linear range of the Incucyte® S3 infectious titer assay, the lower limit of detection (LLOD) and the upper limit of detection correspond to a normalized positive area of 31% and 70%, respectively.

The inter-assay precision between three independently performed assays was analyzed by calculating the standard deviation (SD) and coefficient of variation (CV) (Table 1). The performed assays included the following variations: Day-to-day variation, technician-to-technician variation and batch-to-batch variation of the working cell bank used.

The Incucyte® S3 infectious titer assay resulted in an inter-assay CV ranging from 2.21% to 12.29% for the LV dilution factors of 2 to 256. The CV should be below 15% for samples above the LLOD. At the LLOD (1:512 dilution) the CV was 20.7%, which is slightly higher than the
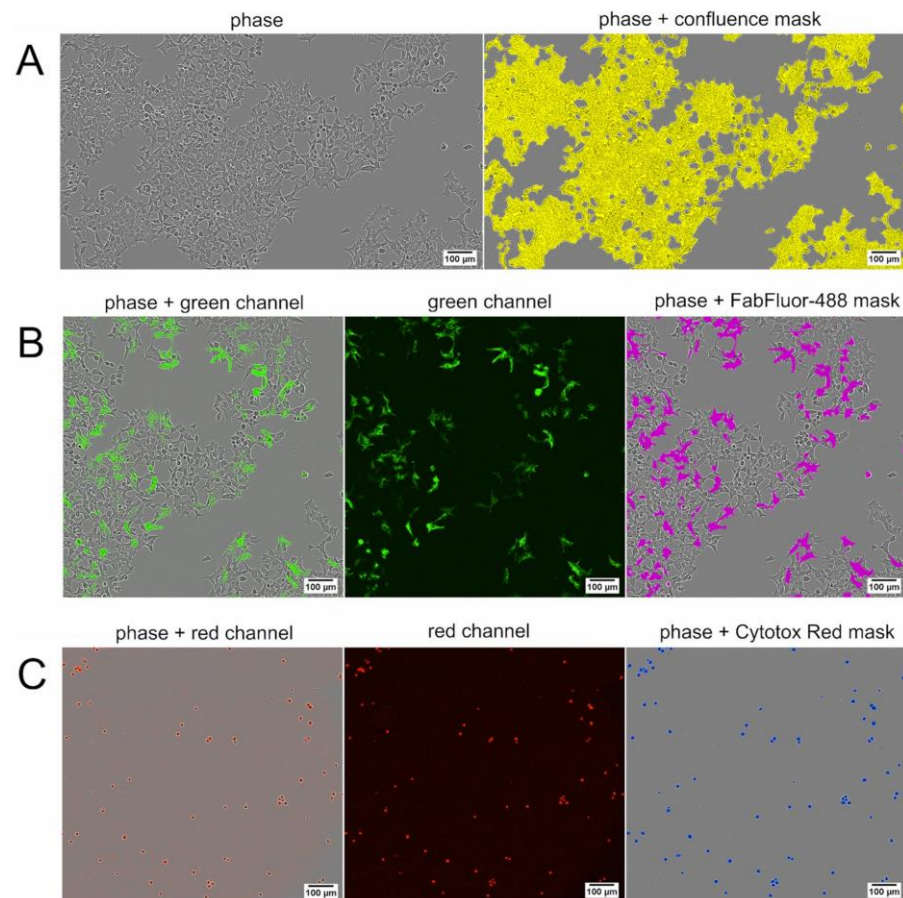
Fig 3. Detection masks for infective titer calculation. (A) Phase contrast image of HEK293T cells (left), merged with phase contrast area analysis mask in yellow (right). (B) HEK293T cells infected with lentiviral vector at a 1:625 dilution. The expressed CAR-construct was stained with an anti-FMC63 scFv antibody labeled with FabFluor-488. Phase contrast image merged with green fluorescence channel (left), background corrected green fluorescence channel (middle), and phase contrast image merged with green fluorescence analysis mask in magenta (right). (C) Live/dead staining positive control cells treated with 0.005% Triton X-100 and stained with Cytotox Red. Phase contrast image merged with red fluorescence channel (left), background corrected red fluorescence channel (middle), and phase contrast image merged with red fluorescence analysis mask in blue (right). All images were taken at 10x magnification.

accepted CV of up to 20% for the LLOD [24]. For LV dilutions below the LLOD, the CV increased. The Z'-factor is a statistical characteristic giving an indication of assay quality in high throughput screening assays and does find applicability in image-based high throughput analysis assays [25]. A Z'-factor between 0 and 0.5 gives a marginal assay and a Z'-factor between 0.5 and 1 gives an excellent assay [26]. The Z'-factor of the inter-assay experiment was ≥ 0.58 for the LV dilution factors between 2 and 256. At the LLOD and below, the Z'-factor was below 0.5. The intra-assay precision was determined for a high, medium and low LV concentration of a distinct LV sample with randomly positioned samples on a 96-well plate

45
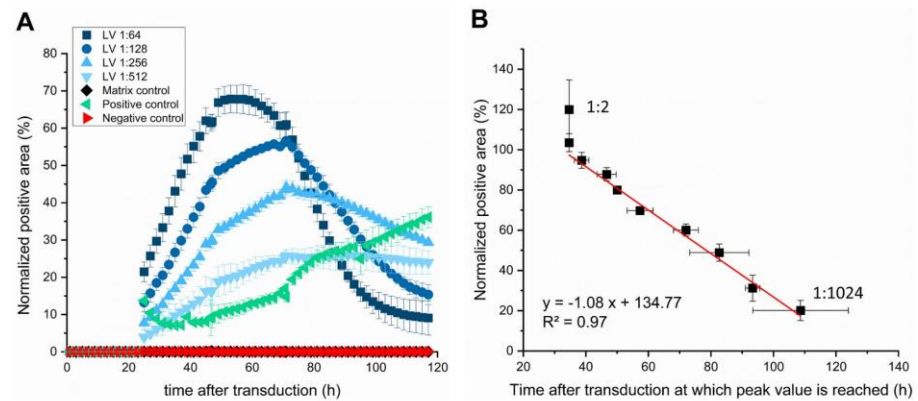
Fig 4. Time course series of normalized positive cell area. (A) The FabFluor-488 positive area was normalized to the phase contrast area over time after transduction. The IgG1 isotype negative control and the lentiviral vector (LV) negative control (matrix) showed no FabFluor488 signal. The anti-transferrin-receptor IgG1 positive control antibody confirmed successful FabFluor488 labeling of the test antibodies. Matrix control overlaps with the negative control. Data represent the mean ± standard deviation of three technical replicates. (B) Normalized FabFluor488 peak value vs. time at which this value is reached. The datapoint in the upper left with the highest normalized positive area represents the 1:2 LV dilution. The other datapoints represent two-fold serially diluted LV up to a dilution of 1:1024 with the lowest normalized positive area and the longest time after which the peak value is reached. Data represent the mean ± standard deviation of three biological replicates.

with 10 replicates for each LV sample (Table 1). The intra-assay CV was below 9.53% for all sample concentrations. The Z'-factor for the intra-assay experiment was > 0.71 for all samples. The measured values were independent of the position of the samples on the plate.

Comparison of infective titer calculation approaches and titration methods

After characterizing the assay and identifying its linear range, the infectious titer was calculated. To calculate the infectious titer with Eq 1, the number of cells at the time of transduction was determined. Various samples of different cell concentrations were prepared, and the total cell density was measured by the Cedex HiRes® Analyzer (Roche). Cells were seeded in triplicates into a 96-well plate with a density between 2200-53400 cells/well and the phase contrast area was monitored every 30 min over 12 h with the Incucyte® S3. Cells were fully attached after 7 h. The phase contrast area (confluence) 7 h after seeding was plotted against the cell number seeded per well (Fig 6A). The measured confluence showed a linear correlation to the seeded cell number. Linear regression of the measurements resulted in a coefficient of determination (R^2) of 0.99.

To assess the accuracy of the assay results, the titer of a single lentiviral vector batch was determined by the flow cytometry and by the Incucyte® protocol for three independent biological replicates (Fig 6B). The titers were calculated for dilutions of a lentiviral vector sample that were in the linear range of the respective method. The infective titer obtained by the Incucyte® protocol was $1.70 \times 10^7 \pm 0.68 \times 10^7$ TU/mL and $2.45 \times 10^7 \pm 1.23 \times 10^7$ TU/mL for the flow cytometry-based protocol. The functional titers were not significantly different. The infectious titer was calculated either including all cells or viable cells. With the infectious titer assay performed with the Incucyte® a $99.9 \pm 0.1\%$ viability of the cells was determined over the whole time course. The infectious LV titers calculated with the two different approaches (Fig 6B) did not differ significantly (unpaired t-test). For this reason, the infective titer was
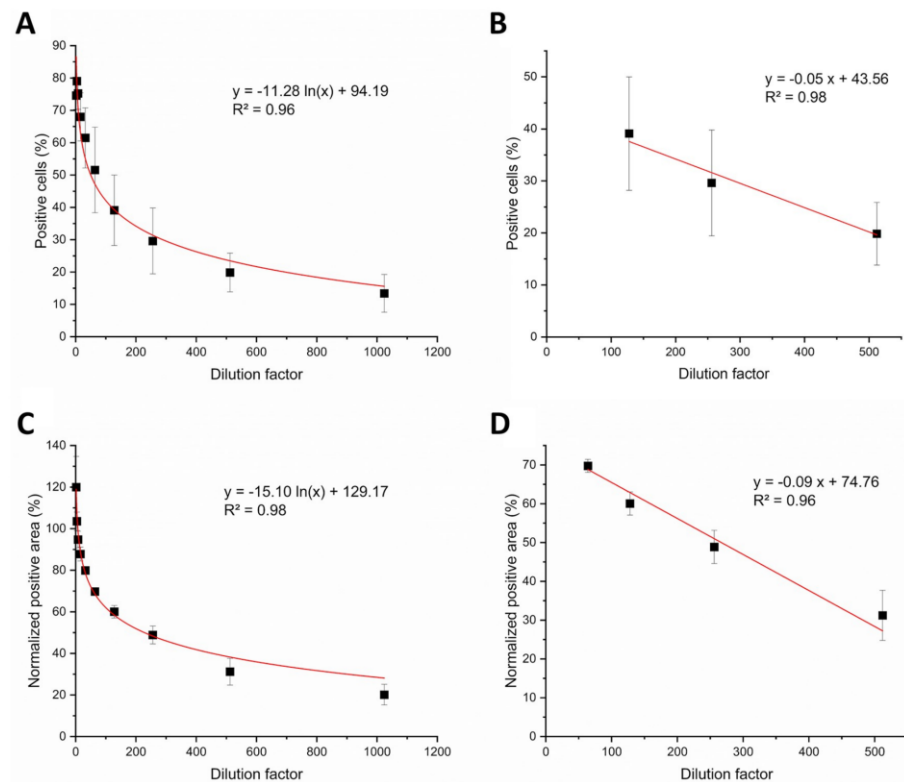
Fig 5. Linear range of the infectious titer assays. The number of positive cells detected via flow cytometry (A & B) and the FabFluor-488 positive area determined with the Incucyte® S3 (C & D) were plotted against dilution factors from a serially diluted lentiviral vector. A logarithmic trend was observed across the whole range of dilutions using the Incucyte® readout with an R^2 of 0.98 (C) and the flow cytometer readout with an R^2 of 0.95 (A). A linear dependence was determined for dilutions from 1:64 to 1:512 for the Incucyte® assay with an R^2 of 0.96 (D) and from 1:128 to 1:512 for the flow cytometer assay with an R^2 of 0.988 (B). Data represent the mean ± standard deviation of three biological replicates.

https://doi.org/10.1371/journal.pone.0254739.g005

calculated for all cells in further experiments. With the flow cytometry protocol, the cell viability at the time of readout (72 h post-infection) was 88.3 ± 4.4%.

Application of the newly established infectious titer assay protocol to investigate lentiviral vector stability

During downstream processing (DSP) the LV can be exposed to different physical conditions. It is, therefore, necessary to investigate which process parameters affect the infectious titer. According to current literature it is known that lentiviral vector is prone to damage and loss of infectious titer by several external factors, including temperature, pH, conductivity and shear stress [27]. In this study we analyzed the impact of several physical conditions on the infectivity of a vesicular stomatitis virus glycoprotein (VSV-G) pseudotyped HIV-1 derived LV (Fig 7). Several freeze and thaw cycles were performed, and the LV was exposed to different

47

Table 1. Inter-assay and intra-assay precision of the Incucyte® infectious titer assay.

	Sample dilution factor	Mean	SD	CV (%)	Z' factor
Inter-assay precision [a]	2	119.97	14.74	12.29	0.58
	4	103.53	4.46	4.30	0.81
	8	94.75	3.97	4.19	0.81
	16	87.76	3.29	3.75	0.81
	32	79.94	1.77	2.21	0.85
	64	69.76	1.67	2.39	0.84
	128	60.06	3.00	4.99	0.74
	256	48.86	4.28	8.76	0.60
	512	31.23	6.47	20.70	0.15
	1024	20.14	4.98	24.71	-0.12
Intra-assay precision [b]	16	75.45	2.53	3.35	0.89
	128	40.98	3.91	9.53	0.71
	512	20.79	1.85	8.91	0.72

Mean of normalized positive area is given in %, standard deviation (SD), coefficient of variation (CV), and Z'-factor.

[a] n = 3,

[b] n = 10.

temperatures for different incubation times. Moreover, the impact of exposure to salt and shear stress by a peristaltic pump was analyzed.

The LV samples were thawed rapidly in a water bath at 37°C and then stored for 1 day at -80°C between each freeze and thaw cycle. The LV maintained its activity over four freeze and thaw cycles (Fig 7A). Thermostability is an important aspect to consider when manufacturing the LV. The purification process is mostly performed at room temperature because it is more economical. Process operations at lower temperatures would require cooling of the instrument and the LV feed or working in a cold room. Stability of LV at a temperature of 37°C are mainly of interest during its upstream processing or during the workflow of an infectious titer assay, where cells are incubated with the virus at 37°C for about 24 h. In our study we identified that the LV infectious titer was not significantly affected by storage at 4°C over an incubation
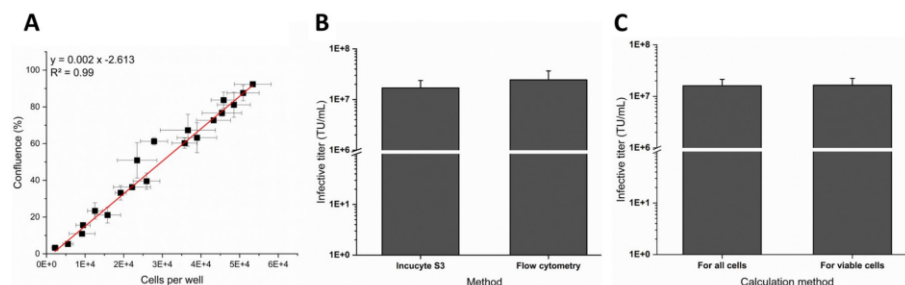
Fig 6. Infectious titer calculation. (A) Correlation of cell count and cell confluence. The cell confluence measured 7 h after cell seeding with the Incucyte® was plotted against the cell count seeded per well as determined by the Cedex HiRes® Analyzer. Mean ± standard deviation, linear regression fit applied (red line) with $R^2 = 0.99$. (B) Infective titer for viable cells determined by the Incucyte® S3 and by flow cytometry. (C) Infective titer for three samples of different virus dilutions within the linear range of the Incucyte®-based assay calculated either for all cells or for viable cells. Data represent the mean ± standard deviation of three biological replicates.
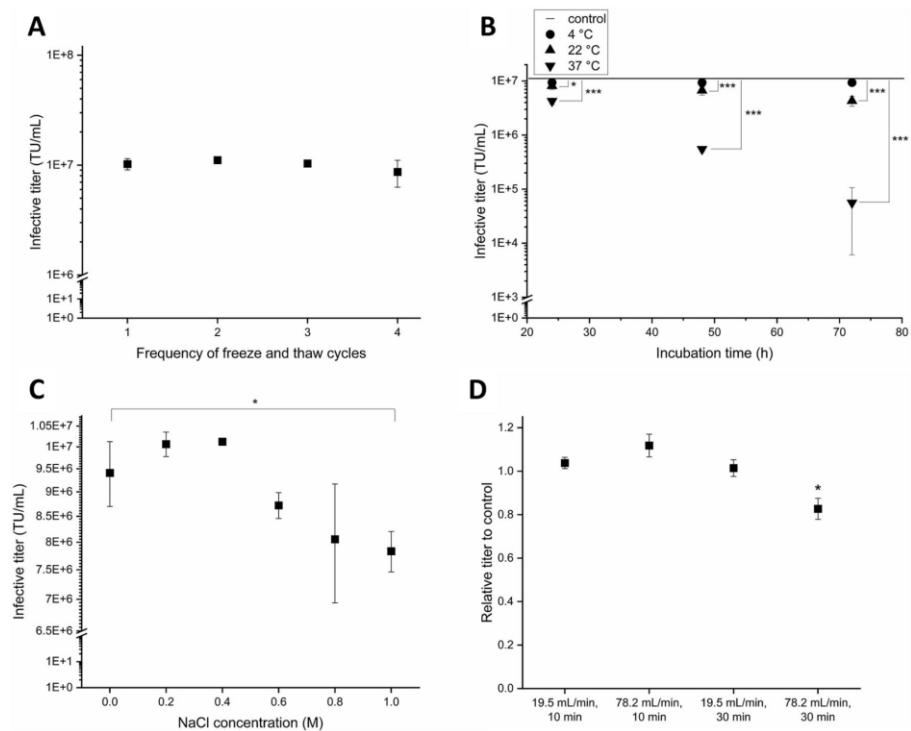
Fig 7. Investigation of external factors on lentiviral vector stability. Assessment of the influence of repeated freeze and thaw cycles (A), storage at different temperatures over time (B), control line represents non-treated LV sample, different sodium chloride (NaCl) concentrations (C) and shear stress induced by a peristaltic pump (D) on lentiviral vector (LV) infectivity. Experiments were performed in biological triplicates. Data represent the mean ± standard deviation. P-values are indicated as follows: * $p \leq 0.05$; ** $p \leq 0.01$; *** $p \leq 0.001$.

https://doi.org/10.1371/journal.pone.0254739.g007

period of 72 h (Fig 7B). At 22°C and 37°C the LV infectivity decreased significantly for all investigated incubation times. LV half-lives were calculated from a 4-point kinetic experiment. At room temperature, a decay of infectious titer over time was observed with a half-life of 75.3 ± 12.1 h. The LV half-life at 37°C was 37.0 ± 11.8 h.

Sodium chloride is often used for elution of the virus during its purification by ion exchange chromatography, with typical concentrations in a range between 1 M and 1.5 M [28,29]. In our study, the infectious titer decreased between 0.6 and 1 M NaCl (Fig 7C) after incubation for 1 h at 4°C. When compared with the no NaCl control sample, the samples exposed to 1 M showed a significant decrease of LV infectivity by 17%.

Shear stress induced by continuously pumping the virus through a tube with a peristaltic pump reduced LV infectious titer significantly by 17% when applying a flow rate of 78.2 mL/min for 30 min (Fig 7D). A shorter time period or lower flow rate did not significantly reduce LV infectivity. A flow rate of 78.2 mL/min applied for the duration of 10 min corresponds to a 78-fold transport of one milliliter through the pump. Within a duration of 30 min, 1 mL is transported 20 times (at flow rate of 19.5 mL/min) or 26 times (at a flow rate of 78.2 mL/min)

49

through the pump, within a duration of 10 min 1 mL of virus is transported 7 times (at 19.5 mL/min) through the pump.

Discussion

Immunological real-time imaging approach for infectious titer determination

We developed an immunological real-time imaging protocol for CAR-based lentiviral vector infectious titer determination. The extracellularly expressed protein is bound and stained via labeled antibodies enabling the quantification of lentiviral vectors used for CAR-T cell therapies. The presented protocol is not limited to lentiviral vectors and could be performed with other viral vectors that transfer a gene of interest coding for an extracellular protein or a cell surface receptor, but clearly finds its limitation for genes of interest, that do not code for a receptor or protein located on the cell surface. Moreover, the FabFluor label system is currently applicable for IgG1, IgG2a and IgG2b with a mouse Fc part. For research and development applications, viral vectors transferring the gene for GFP are frequently used [15]. The infectious titer determination for GFP-based viral vectors can be performed with the presented protocol by replacing the staining step by a simple media exchange. Real-time imaging techniques have previously been used to assess the transduction efficiency based on the expression of GFP or other fluorescent reporter proteins by determining the percentage of positive cells or the green object count [30–36]. In contrast to these methods, the workflow presented in this study allows for the determination of the infectious viral titer which is an important value for quality control in upstream and downstream processes of viral vectors. Stewart *et al.* used the Incucyte® for infectious titer determination of hepatitis C virus by an endpoint measurement after fixation and staining [37]. The evolution of the Incucyte® platform and associated software and reagents has enabled a kinetic approach for titer determination described in our article. To our knowledge, detection of transduced cells expressing a cell surface receptor with a real-time live-cell analysis system to determine infectious viral titers has not been published yet. For accurate titer calculation, the number of cells at the time of transduction must be precisely determined. For flow cytometry protocols the cell number is often determined by detaching the cells of one well before transduction. The measured cell count is then assigned to all wells. A small variance of the cell count between different wells is likely to occur. It is more exact to measure the cell count for each well, which is not possible with flow cytometry or a PCR-based method. For our protocol it was not possible to use the Cell-by-Cell analysis software module of the Incucyte®, due to the low cell boundary contrast of HEK cells. The use of this analysis module is possible for other cell types with a higher cell boundary contrast. This would allow to determine the number of cells at time of transduction and the number of positive cells. We addressed this problem and correlated an off-line measured cell count and the phase contrast area detected by the Incucyte® for a precise cell count determination for individual wells. The correlation of phase contrast area and cell count can be quickly performed for any cell line used for the infectious titer assay. Besides, we expect limitations when working with suspension cells. Suspension cells could be used but require an optimization of plate coating and pipetting steps to avoid loss of cells.

It is good scientific practice to determine the infectious lentiviral titer for viable cells only. In our study using HEK293T as target cells, the difference between the infectious titer determined from only viable cells versus all cells was not significant. This can be explained by the observed high cell viability. The high viability during the Incucyte® based assay is due to the gentle protocol, which does not require any centrifugation, washing, or fixation steps that are usually performed during the flow cytometry protocol. With flow cytometry, generally a lower

50

cell viability during the readout was detected. We assume this is due to the handling of the cells according to the protocol.

For accurate infectious titer calculation, the LV sample needs to be diluted such that the percentage of positive cells is within the linear range of the respective titration method. The infective titer protocol based on the Incucyte® had a broader linear range compared to the flow cytometry protocol. The Incucyte®-based protocol showed good inter-assay and intra-assay precision and an excellent Z'-factor for the linear range. The calculated infective titers determined by the Incucyte® had a smaller standard deviation compared with the flow cytometry method, meaning that a greater variation between replicates was observed for the flow cytometry protocol. Although statistical analysis indicated that the calculated titers do not significantly differ between the two methods, we consider the determined titer with the Incucyte® to be more accurate for the reasons outlined above.

The major advantages of the Incucyte® approach are the simple protocol and the temporal readout. The operator can track the percentage of transduced cells whilst the experiment is running and decide for the optimal readout time. Flow cytometry and qPCR rely on an endpoint measurement where the optimal readout timepoint can be easily missed. We have observed that after reaching a maximum, the normalized FabFluor-488 area decreases. Cell surface receptor-mediated antibody internalization could be a reason for a decreasing normalized FabFluor-488 area [38]. The integrated FabFluor-488 intensity over time showed an equivalent time course, indicating that the signal decreases after reaching a maximum (S2 Fig). Upon internalization of the antibody, the FabFluor-antibody complex emits little or no fluorescence due to the lower intracellular pH. Microscopic analysis showed that cell clusters, that were fully detected by the FabFluor analysis mask at the time of the peak intensity, were not fully detected by the mask at later time points due to lower fluorescence intensity in some areas (S3 Fig). This also supports the hypothesis of antibody internalization.

For the operator, the real-time imaging approach means a significant reduction in workload, as fixation, multiple washing, staining, and centrifugation steps, that are typically performed for a flow cytometry based readout [23], are not required. These steps are the rate-limiting steps of the flow cytometry protocol and severely constrain the number of samples that can be analyzed within one week. Automation of the protocol by using a pipetting robot is hardly possible due to the need for multiple centrifugation steps and the risk of aspirating the cell pellet. Furthermore, the investment and footprint of a pipetting robot is high. The handling time was significantly reduced with the Incucyte® real-time imaging approach, eliminating the need for fixation, washing and centrifugation steps. Thereby, a higher throughput was enabled with the possibility to measure up to six 96-well plates simultaneously within one week.

Virus stability study

We investigated factors affecting lentiviral vector stability. In an experiment to evaluate the effect of repeated freezing and thawing of lentiviral vectors, no loss of infectious titer was observed over four cycles. This allows for LV being stored between DSP steps at -80°C for later analytical testing. In contrast in a comparable study using VSV-G pseudotyped LV produced by TE671 cells an infectivity reduction by freeze and thaw cycles with a half-life of 3.8 cycles was observed. The same study reported half-lives of 10.4 h at 37°C, approx. 50 h at 20°C and 200 h at 4°C [39]. The half-lives at 37°C and 20°C are shorter than the ones determined in our study with 37 h at 37°C and 75 h at 22°C. Dautzenberg *et al.* reported a half-life of 35 h at 37°C for a VSV-G pseudotyped LV produced in adherent 293T cells [40], which is similar to the half-life determined in our study. An aspect to consider is the buffer in which the LV is

formulated. The half-lives determined by Dautzenberg *et al.* are greater than those reported by Higashikawa and Chang. This may be due to the different buffer conditions used, as this is consistent with the reported increase in thermostability of lentiviral vectors in the presence of FCS [41]. The LVs used in our study and by Dautzenberg *et al.* were derived from similar cell lines, whereas Higashikawa and Chang did not use a HEK293-based cell line. LV particles produced with different cell lines have a distinct viral envelope constituents profile depending on their producer cell line. The viral envelope composition was reported to affect LV infectivity [42,43]. Besides the formulation aspect, this may be an explanation for greater susceptibility of lentiviral vectors to thermal exposure and freeze and thaw cycles.

We observed an infectivity loss of 17% after incubation with 1 M NaCl for 1 h, which is consistent with the data of Zimmermann *et al.* who determined an infectivity loss of 16% of VSV-G pseudotyped LV after incubation with 1 M NaCl for 1 h [44]. The effect of salt on another retrovirus was analyzed by Segura *et al.* A VSV-G pseudotyped moloney murine leukemia retrovirus (MLV) lost 50% infectivity after 1 h incubation with 1 M NaCl [45]. This highlights limited comparability of different retroviral vectors, even though they have the same envelope protein. The observed loss of infectious lentiviral titer due to exposure to high salt concentrations corresponds to the low recoveries reported for anion exchange chromatography during DSP [27].

Peristaltic pumps are frequently used during DSP, e.g. during clarification when the virus suspension is pumped through a filter. The number of passages of the virus suspension through the pump was observed to be the critical factor for infectivity reduction. When 1 mL was transported either 7 or 26 times through the pump, the infectivity was not affected independent of the applied flow rate. However, after 78 circulation cycles the infectivity was reduced significantly by 17%. A limitation of the circulation cycles of the viral vector through the system should therefore be considered. The negative impact of shear forces on LV infectivity is often mentioned as an important factor [46]. The stability of VSV-G pseudotyped LV towards shear forces has been previously analyzed during ultracentrifugation. About 54% of the infectious titer was recovered after ultracentrifugation demonstrating the effect of shear forces [47]. Ruscic *et al.* [18] investigated potential losses of RDpro pseudotyped LV infectivity through shear stress applied by the chromatography device by letting the LV pass through the system without capture. They have reported no significant loss of infectious LV in the chromatography system, consequently, no impact of shear forces generated in the system was observed. Control experiments are indispensable to estimate the LV loss caused by the system itself.

The LV stability study, which resulted in a total of 78 samples emphasizes the major advantage of the newly established Incucyte®-based infectious titer assay in terms of sample throughput. All samples were analyzed within one week in technical duplicates. The flow cytometry protocol was not performed because the analysis of the samples would have taken 4-7 weeks. Due to the high amount of labor needed to perform infectious titer assays with methods established so far, stability studies were rarely performed and published in the literature. The Incucyte® protocol enables the operator to quickly perform infectious titer assays, resulting in the ability to test even more conditions during process development or to assess the most optimal formulation of the final virus product in reduced time.

In conclusion, we developed an immunological real-time imaging method to quantify the infectious titer of anti-CD19 CAR lentiviral vectors using the Incucyte® S3. The newly established method decreased labor profoundly and thus increased throughput. The real-time imaging and analysis capabilities of the Incucyte® enable an accurate and precise measurement of the infectious LV titers. The broad linear detection range of this method is advantageous and is well suited for analyzing a variety of samples, such as for virus stability studies.

Supporting information

S1 Fig. Positive and negative controls of the staining protocol. Top row: Phase contrast image of HEK293T cells merged with green channel. Bottom row: Phase contrast image merged with FabFluor-488 mask in magenta. Left column: Anti-transferrin-receptor IgG1 antibody labeled with FabFuor-488 as a positive control. Middle column: IgG1 isotype antibody labeled with FabFuor-488 as a negative control. Right column: Matrix control containing no lentiviral vector with anti-FMC63 scFv antibody labeled with FabFluor-488. All images were taken at 10x magnification.
(TIF)

S2 Fig. Total FabFluor-488 integrated intensity of HEK293T cells infected by several lentiviral vector dilutions over time. FabFluor-488 fluorescence intensity was analyzed on three independently infected plates (A-C). Lentiviral vector (LV) dilutions were between 1:2 and 1:1024. Low virus dilutions showed a higher integrated intensity, its peak is reached earlier, and the signal decreases earlier compared to high virus dilutions. The negative controls (matrix and medium control) gave no signal.
(TIF)

S3 Fig. FabFluor-488 mask over time. HEK293T cells after infection with a 1:2 diluted lentiviral vector and staining 24 h post-infection. Phase contrast image were merged with FabFluor-488 mask, shown in magenta. Yellow arrow indicates a fully detected cell cluster 66 h post-infection that is not fully detected by the FabFluor-488 mask at later time points (90 h and 98 h post-infection). Normalized positive areas were 90.5% (A), 68.8% (B) and 63.3% (C) for the representative images.
(TIF)

S1 Table. All data used for figures, tables, and statistical analyses.
(XLSX)

Acknowledgments

Author Contributions

Conceptualization: Jennifer J. Labisch.

Formal analysis: Jennifer J. Labisch, G. Philip Wiese.

Investigation: Jennifer J. Labisch, G. Philip Wiese.

Methodology: Jennifer J. Labisch.

Project administration: Karl Pflanz.

Supervision: Kalpana Barnes, Franziska Bollmann, Karl Pflanz.

Visualization: Jennifer J. Labisch, G. Philip Wiese.

Writing – original draft: Jennifer J. Labisch.

Writing – review & editing: Kalpana Barnes, Franziska Bollmann.

References

1. Vargas JE, Chicaybam L, Stein RT, Tanuri A, Delgado-Cañedo A, Bonamino MH. Retroviral vectors and transposons for stable gene therapy: advances, current challenges and perspectives. J Transl Med. 2016; 14:288. https://doi.org/10.1186/s12967-016-1047-x PMID: 27729044.

2. Hanna E, Rémuzat C, Auquier P, Toumi M. Advanced therapy medicinal products: current and future perspectives. J Mark Access Health Policy. 2016; 4. https://doi.org/10.3402/jmahp.v4.31036 PMID: 27123193.

3. Rininger J, Fennell A, Schoukroun-Barnes L, Peterson C, Speidel J. Capacity analysis for viral vector manufacturing: Is there enough. Bioprocess Int. 2019; 2019. Available from: https://bioprocessintl.com/manufacturing/emerging-therapeutics-manufacturing/capacity-analysis-for-viral-vector-manufacturing-is-there-enough/.

4. Miliotou AN, Papadopoulou LC. CAR T-cell Therapy: A New Era in Cancer Immunotherapy. Curr Pharm Biotechnol. 2018; 19:5–18. https://doi.org/10.2174/1389201019666180418095526 PMID: 29667553.

5. Wei J, Han X, Bo J, Han W. Target selection for CAR-T therapy. J Hematol Oncol. 2019; 12:62. https://doi.org/10.1186/s13045-019-0758-x PMID: 31221182.

6. Liu B, Yan L, Zhou M. Target selection of CAR T cell therapy in accordance with the TME for solid tumors. Am J Cancer Res. 2019; 9:228–41. PMID: 30906625

7. Breyanzi (Package Insert). Juno Therapeutics, Inc., a Bristol Myers Squibb Company. Bothell, WA: 2021 [updated Feb 2021; cited 24 Apr 2021]. https://www.fda.gov/media/145711/download.

8. Abecma (Package Insert). Celgene Corporation, a Bristol Myers Squibb Company. Summit, NJ: 2021 [updated Mar 2021; cited 24 Apr 2021]. https://www.fda.gov/media/147055/download.

9. Zheng P-P, Kros JM, Li J. Approved CAR T cell therapies: ice bucket challenges on glaring safety risks and long-term impacts. Drug Discov Today. 2018; 23:1175–82. https://doi.org/10.1016/j.drudis.2018.02.012 PMID: 29501911.

10. Laxmi V. Global viral vector manufacturing markets and technologies through 2022. bcc Research: 2018 [cited 9 Sep 2020]. https://www.bccresearch.com/market-research/pharmaceuticals/global-viral-vector-manufacturing-markets-and-technologies.html.

11. Kutner RH, Zhang X-Y, Reiser J. Production, concentration and titration of pseudotyped HIV-1-based lentiviral vectors. Nat Protoc. 2009; 4:495–505. https://doi.org/10.1038/nprot.2009.22 PMID: 19300443.

12. Segura MdLM, Kamen A, Garnier A. Downstream processing of oncoretroviral and lentiviral gene therapy vectors. Biotechnol Adv. 2006; 24:321–37. https://doi.org/10.1016/j.biotechadv.2005.12.001 PMID: 16448798.

13. Perry C, Rayat ACME. Lentiviral Vector Bioprocessing. Viruses. 2021; 13. Epub 2021/02/09. https://doi.org/10.3390/v13020268 PMID: 33572347.

14. Barczak W, Suchorska W, Rubiś B, Kulcenty K. Universal real-time PCR-based assay for lentiviral titration. Mol Biotechnol. 2015; 57:195–200. https://doi.org/10.1007/s12033-014-9815-4 PMID: 25370825.

15. Geraerts M, Willems S, Baekelandt V, Debyser Z, Gijsbers R. Comparison of lentiviral vector titration methods. BMC Biotechnol. 2006; 6:34. https://doi.org/10.1186/1472-6750-6-34 PMID: 16836756.

16. Valkama AJ, Oruetxebarria I, Lipponen EM, Leinonen HM, Käyhty P, Hynynen H, et al. Development of Large-Scale Downstream Processing for Lentiviral Vectors. Mol Ther Methods Clin Dev. 2020; 17:717–30. https://doi.org/10.1016/j.omtm.2020.03.025 PMID: 32346549.

17. Jiang W, Hua R, Wei M, Li C, Qiu Z, Yang X, et al. An optimized method for high-titer lentivirus preparations without ultracentrifugation. Sci Rep. 2015; 5:13875. Epub 2015/09/08. https://doi.org/10.1038/srep13875 PMID: 26348152.

18. Ruscic J, Perry C, Mukhopadhyay T, Takeuchi Y, Bracewell DG. Lentiviral Vector Purification Using Nanofiber Ion-Exchange Chromatography. Mol Ther Methods Clin Dev. 2019; 15:52–62. https://doi.org/10.1016/j.omtm.2019.08.007 PMID: 31649955.

19. Lizée G, Aerts JL, Gonzales MI, Chinnasamy N, Morgan RA, Topalian SL. Real-time quantitative reverse transcriptase-polymerase chain reaction as a method for determining lentiviral vector titers and measuring transgene expression. Hum Gene Ther. 2003; 14:497–507. https://doi.org/10.1089/104303403764539387 PMID: 12718761.

20. Delenda C, Gaillard C. Real-time quantitative PCR for the design of lentiviral vector analytical assays. Gene Ther. 2005; 12 Suppl 1:S36–50. https://doi.org/10.1038/sj.gt.3302614 PMID: 16231054.

21. Picanço-Castro V, Moço PD, Mizukami A, Vaz LD, Souza Fernandes Pereira de M, Silvestre RN, et al. Establishment of a simple and efficient platform for car-t cell generation and expansion: from lentiviral

54

production to in vivo studies. Hematol Transfus Cell Ther. 2020; 42:150–8. https://doi.org/10.1016/j.htct.2019.06.007 PMID: 31676276.

22. Moço PD, Abreu Neto de MS, Fantacini DMC, Picanço-Castro V. Optimized Production of Lentiviral Vectors for CAR-T Cell. Methods Mol Biol. 2020; 2086:69–76. https://doi.org/10.1007/978-1-0716-0146-4_5 PMID: 31707668.

23. Labisch JJ, Bollmann F, Wolff MW, Pflanz K. A new simplified clarification approach for lentiviral vectors using diatomaceous earth improves throughput and safe handling. J Biotechnol. 2021:11–20. https://doi.org/10.1016/j.jbiotec.2020.12.004 PMID: 33301854

24. FDA/CDER/CVM, editor. Bioanalytical method validation Guidance for industry. Guidance for industry. 2018 [cited 11 Jan 2021]. https://www.fda.gov/regulatory-information/search-fda-guidance-documents/bioanalytical-method-validation-guidance-industry.

25. Bray M-A, Carpenter A. Assay Guidance Manual. Advanced Assay Development Guidelines for Image-Based High Content Screening and Analysis. Bethesda (MD); 2004.

26. Zhang Ji-Hu, Chung Thomas D. Y., and Oldenburg Kevin R. A Simple Statistical Parameter for Use in Evaluation and Validation of High Throughput Screening Assays.

27. Moreira AS, Cavaco DG, Faria TQ, Alves PM, Carrondo MJT, Peixoto C. Advances in Lentivirus Purification. Biotechnol J. 2020:e2000019. https://doi.org/10.1002/biot.202000019 PMID: 33089626.

28. Kutner RH, Puthli S, Marino MP, Reiser J. Simplified production and concentration of HIV-1-based lentiviral vectors using HYPERFlask vessels and anion exchange membrane chromatography. BMC Biotechnol. 2009; 9:10. https://doi.org/10.1186/1472-6750-9-10 PMID: 19220915.

29. Olgun HB, Tasyurek HM, Sanlioglu AD, Sanlioglu S. High-Grade Purification of Third-Generation HIV-Based Lentiviral Vectors by Anion Exchange Chromatography for Experimental Gene and Stem Cell Therapy Applications. Methods Mol Biol. 2019; 1879:347–65. https://doi.org/10.1007/7651_2018_154 PMID: 30006865.

30. Hassanzadeh G, Naing T, Graber T, Jafarnejad SM, Stojdl DF, Alain T, et al. Characterizing Cellular Responses During Oncolytic Maraba Virus Infection. Int J Mol Sci. 2019; 20. Epub 2019/01/29. https://doi.org/10.3390/ijms20030580 PMID: 30700020.

31. Herod MR, Loundras E-A, Ward JC, Tulloch F, Rowlands DJ, Stonehouse NJ. Employing transposon mutagenesis to investigate foot-and-mouth disease virus replication. J Gen Virol. 2015; 96:3507–18. https://doi.org/10.1099/jgv.0.000306 PMID: 26432090.

32. Andreu-Moreno I. Collective Infection of Cells by Viral Aggregates Promotes Early Viral Proliferation and Reveals a Cellular-Level Allee Effect.

33. Tulloch F, Pathania U, Luke GA, Nicholson J, Stonehouse NJ, Rowlands DJ, et al. FMDV replicons encoding green fluorescent protein are replication competent. J Virol Methods. 2014; 209:35–40. Epub 2014/09/04. https://doi.org/10.1016/j.jviromet.2014.08.020 PMID: 25194890.

34. Stevenson EV, Collins-McMillen D, Kim JH, Cieply SJ, Bentz GL, Yurochko AD. HCMV reprogramming of infected monocyte survival and differentiation: a Goldilocks phenomenon. Viruses. 2014; 6:782–807. Epub 2014/02/13. https://doi.org/10.3390/v6020782 PMID: 24531335.

35. Joubert P-E, Stapleford K, Guivel-Benhassine F, Vignuzzi M, Schwartz O, Albert ML. Inhibition of mTORC1 Enhances the Translation of Chikungunya Proteins via the Activation of the MnK/eIF4E Pathway. PLoS Pathog. 2015; 11:e1005091. Epub 2015/08/28. https://doi.org/10.1371/journal.ppat.1005091 PMID: 26317997.

36. Forrest S, Lear Z, Herod MR, Ryan M, Rowlands DJ, Stonehouse NJ. Inhibition of the foot-and-mouth disease virus subgenomic replicon by RNA aptamers. J Gen Virol. 2014; 95:2649–57. Epub 2014/08/05. https://doi.org/10.1099/vir.0.067751-0 PMID: 25096816.

37. Stewart H, Bartlett C, Ross-Thriepland D, Shaw J, Griffin S, Harris M. A novel method for the measurement of hepatitis C virus infectious titres using the IncuCyte ZOOM and its application to antiviral screening. J Virol Methods. 2015; 218:59–65. https://doi.org/10.1016/j.jviromet.2015.03.009 PMID: 25796989.

38. Liao-Chan S, Daine-Matsuoka B, Heald N, Wong T, Lin T, Cai AG, et al. Quantitative assessment of antibody internalization with novel monoclonal antibodies against Alexa fluorophores. PLoS ONE. 2015; 10: e0124708. Epub 2015/04/20. https://doi.org/10.1371/journal.pone.0124708 PMID: 25894652.

39. Higashikawa F, Chang L. Kinetic analyses of stability of simple and complex retroviral vectors. Virology. 2001; 280:124–31. https://doi.org/10.1006/viro.2000.0743 PMID: 11162826.

40. Dautzenberg IJC, Rabelink MJWE, Hoeben RC. The stability of envelope-pseudotyped lentiviral vectors. Gene Ther. 2020. https://doi.org/10.1038/s41434-020-00193-y PMID: 32973351.

41. Carmo M, Alves A, Rodrigues AF, Coroadinha AS, Carrondo MJT, Alves PM, et al. Stabilization of gammaretroviral and lentiviral vectors: from production to gene transfer. J Gene Med. 2009; 11:670–8. https://doi.org/10.1002/jgm.1353 PMID: 19507176.

42. Cronin J, Zhang X-Y, Reiser J. Altering the tropism of lentiviral vectors through pseudotyping. Curr Gene Ther. 2005; 5:387–98. https://doi.org/10.2174/1566523054546224 PMID: 16101513

43. Beer C, Meyer A, Müller K, Wirth M. The temperature stability of mouse retroviruses depends on the cholesterol levels of viral lipid shell and cellular plasma membrane. Virology. 2003; 308:137–46. https://doi.org/10.1016/s0042-6822(02)00087-9 PMID: 12706097

44. Zimmermann K, Scheibe O, Kocourek A, Muelich J, Jurkiewicz E, Pfeifer A. Highly efficient concentration of lenti- and retroviral vector preparations by membrane adsorbers and ultrafiltration. BMC Biotechnol. 2011; 11:55. https://doi.org/10.1186/1472-6750-11-55 PMID: 21599966.

45. Segura M, Kamen A, Trudel P, Garnier A. A novel purification strategy for retrovirus gene therapy vectors using heparin affinity chromatography. Biotechnol Bioeng. 2005; 90:391–404. https://doi.org/10.1002/bit.20301 PMID: 15812800.

46. Merten O-W, Schweizer M, Chahal P, Kamen A. Manufacturing of viral vectors: part II. Downstream processing and safety aspects. Pharmaceutical Bioprocessing. 2014; 2:237–51.

47. Kim S-H, Lim K-I. Stability of Retroviral Vectors Against Ultracentrifugation Is Determined by the Viral Internal Core and Envelope Proteins Used for Pseudotyping. Mol Cells. 2017; 40:339–45. https://doi.org/10.14348/molcells.2017.0043 PMID: 28535668.
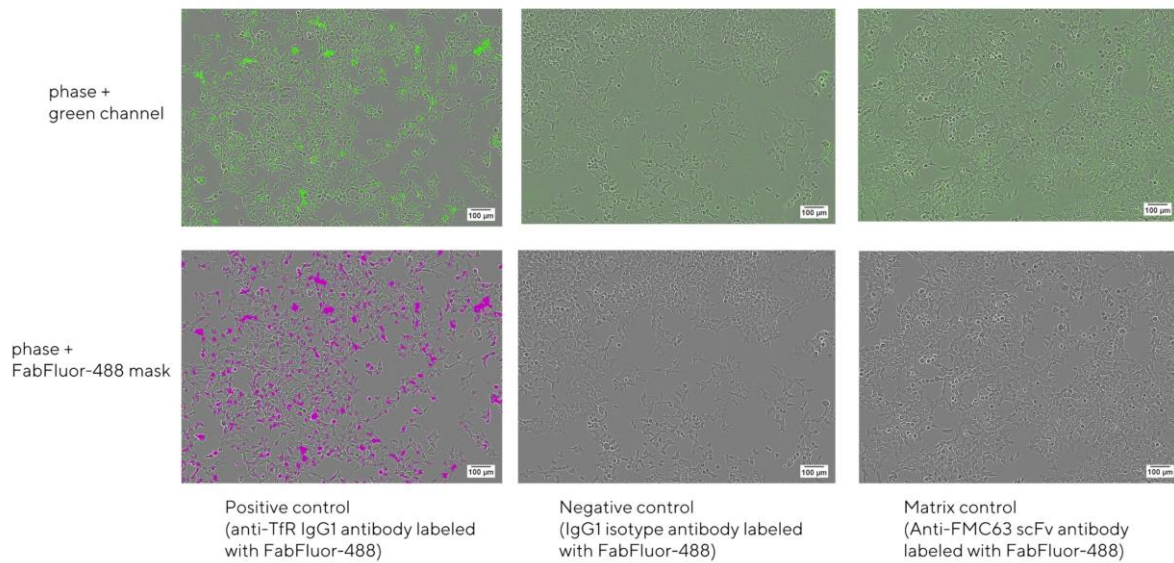
56

Supplemental figures

phase +
green channel

Positive control
(anti-TfR IgG1 antibody labeled
with FabFluor-488)

Negative control
(IgG1 isotype antibody labeled
with FabFluor-488)

Matrix control
(Anti-FMC63 scFv antibody
labeled with FabFluor-488)

phase +
FabFluor-488 mask

S1 Fig: Positive and negative controls of the staining protocol. Top row: Phase contrast image of HEK293T cells merged with green channel. Bottom row: Phase contrast image merged with FabFluor-488 mask in magenta. Left column: Anti-transferrin-receptor (TfR) IgG1 antibody labeled with FabFuor-488 as a positive control. Middle column: IgG1 isotype antibody labeled with FabFuor-488 as a negative control. Right column: Matrix control containing no lentiviral vector with anti-FMC63 scFv antibody labeled with FabFluor-488. All images were taken at 10x magnification.
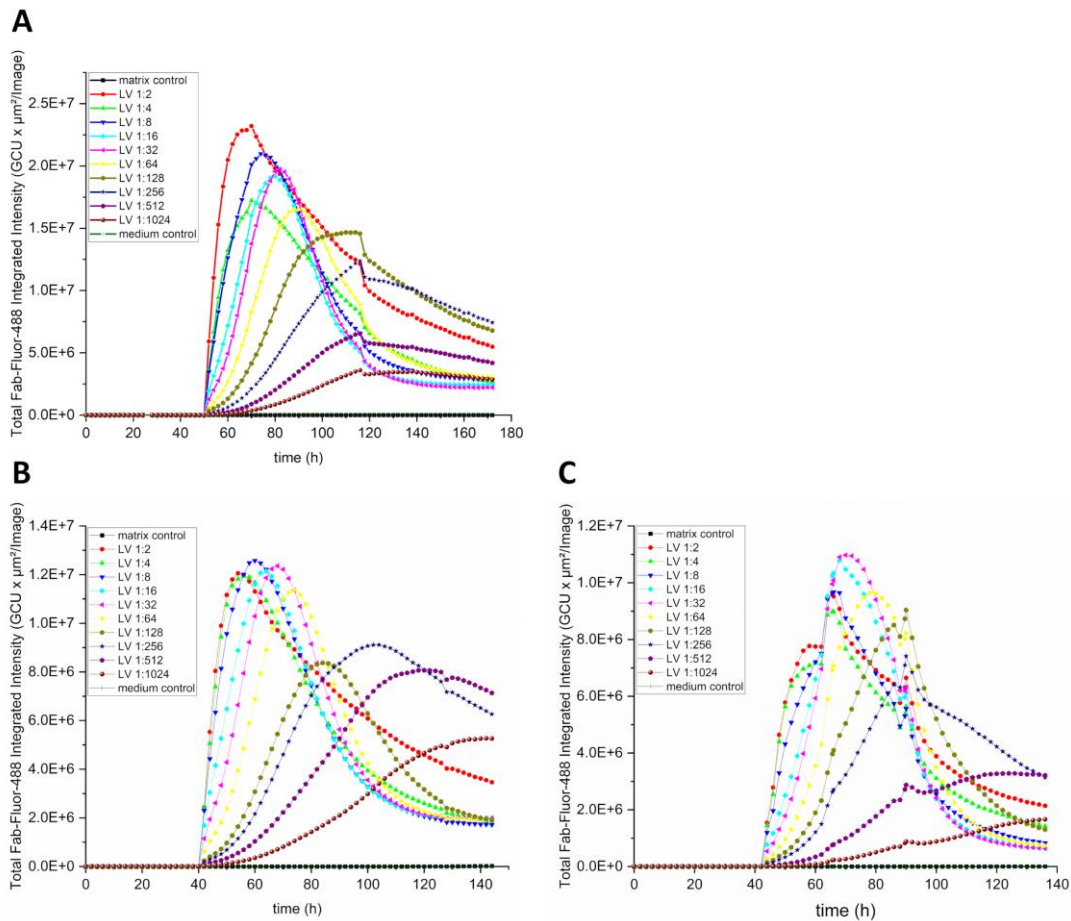
S2 Fig: Total FabFluor-488 integrated intensity of HEK293T cells infected by several lentivirus dilutions over time. FabFluor-488 fluorescence intensity was analyzed on three independently infected plates (A-C). Lentiviral vector (LV) dilutions were between 1:2 and 1:1024. Low virus dilutions showed a higher integrated intensity, its peak is reached earlier, and the signal decreases earlier compared to high virus dilutions. The negative controls (matrix and medium control) gave no signal.

S3 Fig: FabFluor-488 mask over time. HEK293T cells after infection with a 1:2 diluted lentiviral vector and staining 24 h post-infection. Phase contrast images were merged with FabFluor-488 mask, shown in magenta. The yellow arrow indicates a fully detected cell cluster 66 h post-infection that is not fully detected by the FabFluor-488 mask at later time points (90 h and 98 h post-infection). Normalized positive areas were 90.5 % (A), 68.8 % (B), and 63.3 % (C) for the representative images.

4.3 Steric exclusion chromatography of lentiviral vectors using hydrophilic cellulose membranes

The most commonly used chromatography mode for LV is AEX due to its simple and cost-effective operation [50,147]. The transfer of either AEX or affinity chromatography, routinely employed for protein purification processes, to LV purification is difficult due different biological, chemical, and physical properties of LV and proteins. Thus, it is not surprising that both methods do not translate well to LV purification as the LV lipid envelope makes them extremely labile [49]. Steric exclusion chromatography (SXC) offers the opportunity to purify LV under mild conditions and can be considered a platform technology applicable to different biomolecules [148].

The implementation of a clarification method that allowed the efficient generation of clarified material which can be used for subsequent purification steps and the development of a fast and accurate LV infectious titer assay (Section 4.1 & 4.2) laid the foundation for an extensive investigation of the SXC of LV. In the third publication, a general operation protocol for SXC was developed and critical process parameters were successfully identified and optimized (Fig. 11).
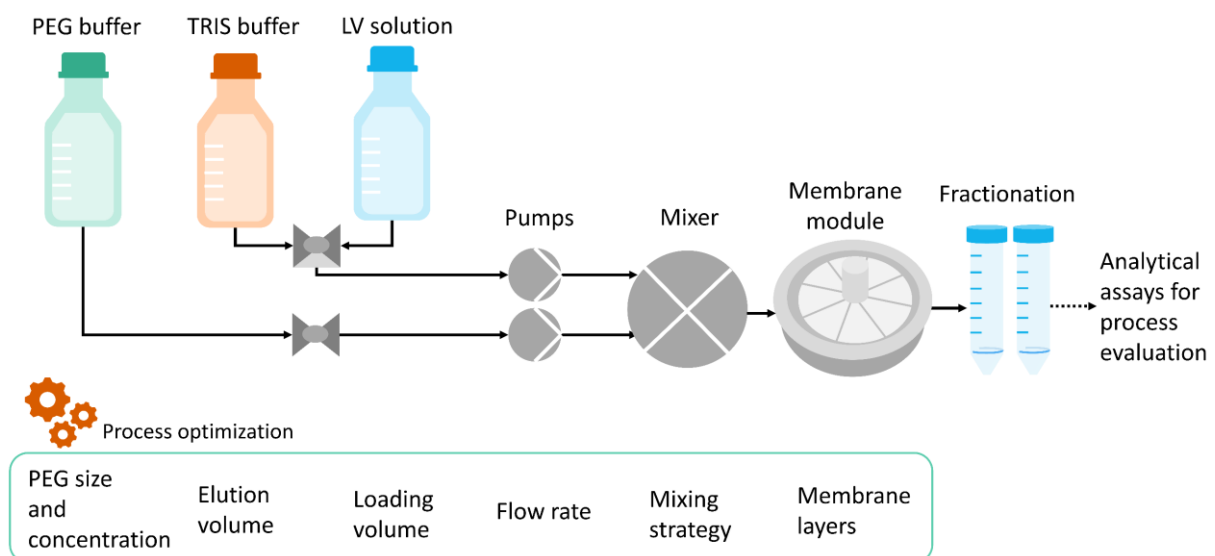
Figure 11: Chromatographic setup for steric exclusion chromatography with adjusting screws of the chromatography process which were considered for process optimization.

Stabilized cellulose membranes incorporated into a housing enabling an axial flow served as a stationary phase. After confirming that the buffers and chromatography device used have no

impact on LV infectivity two different mixing strategies of the clarified LV solution with the PEG buffer were assessed. The dynamic mixing of the LV solution with the PEG inside the system shortly before loading to the membrane column yielded significantly higher LV recoveries compared with loading a pre-mixed solution. Possible aggregation of the LV particles in the pre-mixed solution could have had a negative effect on the SXC process, although no increase in particle size was measured with dynamic light scattering. Next, a screening experiment was performed, testing different PEG molecular weights (4000 and 6000 Da) and concentrations (7.5, 10, and 12.5%), and two different membrane layer numbers. The PEG buffer composition yielding the highest LV recoveries was 12.5% final PEG 4000 concentration, leading to the ideal strength of depletion attraction between the LV particles and the membrane. The impurity removal was approximately 80% and mostly unaffected by the PEG buffer composition due to the pronounced size difference between the LV and the impurities allowing selective retention of the LV, as PEG at the chosen size and concentration is preferentially excluded from large molecules. The use of ten over five membrane layers had no significant effect on LV recoveries but resulted in a lower dsDNA removal with 12.5% PEG 4000, hence five membrane layers were chosen for further experiments. Given the thermodynamic nature of the SXC process, the flow rate was found to highly affect LV recoveries having an optimum flow rate at around 6-7 mL·min^{-1}, higher and lower flow rates resulted in a reduced LV recovery. The effect of the flow rate on impurity removal was less pronounced. With the dynamic mixing, 12.5% PEG 4000, and a flow rate of 7 mL·min^{-1}, an LV particle and infectious titer recovery of 86% and 88%, respectively, were obtained while removing approximately 80% total protein and dsDNA (host cell and plasmid DNA).

Furthermore, the pressure was identified to be a main critical process parameter. PEG buffers with high viscosity contribute to increased system pressure. During loading, a constant pressure increase was observed, likely due to pore size reduction with an increased amount of captured LV. When the membrane was loaded until the pressure maximum of the membrane device was reached, almost no LV was recovered in the eluate. Hence, overloading the membrane eventually leads to product loss. The PEG concentration measured in the eluate was 7.6 g·L^{-1}. However, subsequent downstream processing steps such as TFF have the potential to remove PEG molecules as they are significantly smaller than LV. Concluding, it was demonstrated that SXC is a gentle purification method suitable for LV purification as it preserves LV infectivity, yields high recoveries, and good impurity removal.

Steric exclusion chromatography of lentiviral vectors using hydrophilic cellulose membranes

Jennifer J. Labisch [a,b,*], Meriem Kassar [a,c], Franziska Bollmann [d], Angela Valentic [c], Jürgen Hubbuch [c], Karl Pflanz [a]

[a] Lab Essentials Applications Development, Sartorius Stedim Biotech GmbH, Göttingen, Lower Saxony, Germany
[b] Institute of Technical Chemistry, Leibniz University Hannover, Hanover, Lower Saxony, Germany
[c] Karlsruhe Institute of Technology, Institute of Process Engineering and Life Sciences, Biomolecular Separation Engineering, Karlsruhe, Baden-Württemberg, Germany
[d] Marketing Separation Technologies, Sartorius Stedim Biotech GmbH, Göttingen, Lower Saxony, Germany

ARTICLE INFO

ABSTRACT

Enveloped viral vectors like lentiviral vectors pose purification challenges due to their low stability. A gentle purification method is considered one of the major bottlenecks for lentiviral vector bioprocessing. To overcome these challenges, a promising method is steric exclusion chromatography which has been used to purify a variety of target molecules. In this study, we successfully identified optimal process parameters for steric exclusion chromatography to purify lentiviral vectors. Lentiviral vector particle recoveries and infectious recoveries of 86% and 88%, respectively, were achieved. The process parameters optimal for steric exclusion chromatography were determined as follows: polyethylene glycol with a molecular weight of 4000 Da, a polyethylene glycol concentration of 12.5%, and a flow rate of 7 mL·min^{-1} using 5 layers of stabilized cellulose membranes as a stationary phase. High protein and dsDNA removal of approximately 80% were obtained. The remaining polyethylene glycol concentration in the eluate was determined. We defined the maximum loading capacity as 7.5×10^{12} lentiviral particles for the lab device used and provide deeper insights into loading strategies. Furthermore, we determined critical process parameters like pressure. We demonstrated in our experiments that steric exclusion chromatography is a gentle purification method with high potential for fragile enveloped viral vectors as it yields high recoveries while efficiently removing impurities.

1. Introduction

Lentiviral vectors (LV) represent one of the three most commonly used viral vectors for gene transfer in gene therapy clinical trials [1] and are the most frequently used viral gene delivery platform for the *ex vivo* generation of chimeric antigen receptor (CAR)-T cells for cancer immunotherapies [2]. The LV size offers a high genetic cargo capacity. The demand for efficient LV bioprocessing is steadily increasing, incentivizing the development of suitable materials and process strategies for fragile enveloped viral vectors like LV. Downstream processing (DSP) poses many challenges since the transfer of methods developed for protein bioprocessing is unlikely due to the distinct bio- and physicochemical properties of the molecules. The purification step is considered one of the major bottlenecks for enveloped viral vectors [3,4].

Various chromatographic methods have been utilized for LV purification, such as anion exchange chromatography (AEX) [5–9], heparin affinity chromatography (AC) [10–12], immobilized metal affinity chromatography (IMAC) [12–15], and biotin-streptavidin AC [16,17]. Although promising, these methods have some disadvantages for the purification of enveloped viral vectors. The most widely used chromatographic mode for LV is AEX since it is a simple and cost-effective method. However, elution is performed either by changing the pH or by increasing the ionic strength of the elution buffer. Both treatments result in a decrease in the infectivity of LVs due to their susceptibility to high salt concentrations and to their narrow optimal pH range [4,10,18,19]. Heparin AC is performed under mild conditions; however, selectivity is rather low because DNA and many host cell proteins (HCPs) have an affinity for heparin resulting in a co-elution [4]. In addition to the high costs associated with the resin, heparin presents a major drawback

* Corresponding author at: Lab Essentials Applications Development, Sartorius Stedim Biotech GmbH, Göttingen, Lower Saxony, Germany.
E-mail address: jennifer.labisch@sartorius.com (J.J. Labisch).

since it requires an additional step to eliminate the leaked ligand. This is another issue to consider for the purification of a product intended for clinical use [20]. The desorption reagents required for other affinity chromatography methods, such as guanidine-HCl, D-biotin, and urea for IMAC, imidazole, or ethylenediaminete-traacetic acid (EDTA) for biotin-streptavidin AC, were reported to inactivate the LV [13,21]. Additionally, leakage of metal ions from the matrix and toxicity of desorption reagents are potential hazards and must be considered when LVs are used in clinical trials [22].

For enveloped viral vectors, a potential alternative to commonly performed chromatography methods is steric exclusion chromatography (SXC) as this method does not require any chemical interaction between the target species and the stationary phase. This allows for milder elution conditions and preserves viral activity. SXC was first described by Lee et al. [23] for purifying immunoglobulin M and bacteriophage M13K07 with OH-monoliths, and by Gagnon et al. [24] for purifying IgG on starch-coated magnetic nanoparticles. The application of cellulose membranes as stationary phases for SXC was first published by Marichal-Gallardo et al. [25]. SXC has been proven to effectively purify a variety of viruses: baculovirus [26], Orf virus [27], adeno-associated virus (AAV) [28], and influenza A virus [25]. Typically, screening of a suitable PEG size and concentration needs to be performed for every target molecule. Wang et al. [29] observed increasing retention of their molecule of interest, γ-globulin, by increasing the PEG 6000 concentration from 10% to 15% using a polyacrylamide cryogel monolith as a stationary phase. Marichal-Gallardo et al. [25] purified influenza A with SXC using 8% PEG 6000 and achieved a recovery of 83%. Lothert et al. [30] achieved the highest recovery of above 90% of Orf virus with 8% PEG 8000.

The SXC method principle is shown in Fig. 1A. The mechanism of SXC relies on the depletion potential, which was described by Asakura and Oosawa [31] and further investigated by Vrij [32]. Polyethylene glycol (PEG) molecules are arranged in a random coil structure that can be seen as penetrable hard spheres. When PEG is added to a solution containing viral particles, depletion zones are formed around the viral vectors and adjacent to the hydrophilic stationary phase. The depletion zone is an area that is not accessible to the polymer's center of gravity; hence, the PEG molecules are sterically excluded from this area. This leads to a loss of conformational entropy of the polymer chains that creates a thermodynamically unfavorable increase in free energy that promotes a physical reorganization of the viral vectors. When a viral particle approaches another viral particle (or the stationary phase), the PEG molecules cannot penetrate the gap. Thus, a negative osmotic pressure is created, causing the solvent to flow out between two viral particles (or between a viral particle and the stationary phase) and resulting in weak attraction. When the depletion zones of two viral particles (or of the viral particle and the stationary phase) overlap, the total excluded volume is reduced [33,34]. Excess water is transferred from the PEG-deficient zones to the bulk solvent, reducing the PEG concentration in the bulk solvent, which in turn, decreases the free energy [23]. In a dilute polymer solution, the polymer chains do not interact with one another and the interaction potential depends on the polymer concentration and polymer size, more specifically the gyration radius [35]. The optimal PEG size and concentration depend on the size of the target molecule to be purified. The viral particles are eluted with a buffer that does not contain PEG. The use of PEG-free buffer reserves the association of the viral particles with the membrane, eluting the particles as a result. Mild elution buffers are chosen in which fragile viruses are stable.

In this study, we initially describe how to use SXC for the purification of LVs, defining the optimal PEG size and concentration, as well as the optimal flow rate and maximum loading capacity.

Moreover, we analyze different loading strategies to provide deeper insights into critical process parameters.

2. Materials and methods

2.1. Lentiviral vector production, harvest, and clarification

Third generation lentiviral vectors, which carry a CD19-CAR transgene, were produced by transient transfection of suspension HEK293T/17 SF cells (ACS-4500, ATCC) with four plasmids (Aldevron) in a UniVessel® 2 L single-use bioreactor (Sartorius). Lentiviral vector production, harvest, and nucleic acid digestion with all materials used are described in detail in Labisch et al. [36]. The lentiviral vector containing cell culture broth was directly clarified using Sartoclear Dynamics® Lab V50 (0.45 μm polyethersulfone membrane version) with 5 g·L^{-1} diatomaceous earth (Sartorius) and a Microsart® e.jet vacuum pump (Sartorius). The lentiviral vector was aliquoted and stored at −80 °C.

2.2. Steric exclusion chromatography

2.2.1. Membrane and housing

A stabilized cellulose membrane Hydrosart® 10242 (Sartorius), a precursor of Sartobind membrane adsorbers, was used as a stationary phase. The porous cellulose membranes are produced in three steps: In the first step, a cellulose acetate membrane is produced from a polymer solution using an evaporation-induced phase separation process. Second, a regenerated cellulose intermediate is made by saponification and, third, the regenerated cellulose intermediate is chemically crosslinked. The membrane is reinforced with a polyester nonwoven. The membrane lot used in this work has a thickness of 230 μm (measured with a thickness gage of 0.01 mm) per layer and a mean flow pore size of 2.5–3 μm (determined with a Porolux 500 porometer). The mean airflow rate at 200 Pa, 20 cm² was 17.61 L·m^{-2}s^{-1} (determined with an air permeability tester FX3300, Textest), and the bubble point was 0.4 bar (determined with automatic filter integrity test system Sartocheck 4 plus, Sartorius). The industrial production of crosslinked cellulose membranes as well as their characterization procedures are described in detail by Tolk [37]. Stacks of 5 or 10 membrane layers with a diameter of 30 mm were incorporated into an MA15 polypropylene module and overmolded with an Arburg 221–75–350 injection molding machine. The final chromatography module has an accessible membrane diameter of 25 mm, resulting in an accessible membrane surface area of 4.91 cm² per layer. The MA15 housing is the same as used for the commercial Sartobind® Q 15. The recommended maximum pressure for this device is 0.6 MPa. The integrity of the module is tested by filtering 0.1% charcoal (Carl Roth) in water through the membrane and inspecting the distribution of charcoal on the first layer. Pressures are tested with a static and burst pressure stand (Maximator). Membrane structure was visualized with a Fei Quanta 200 scanning electron microscope. The membrane devices described were used for all experiments in this study.

2.2.2. Chromatography setup and procedure

The chromatography system ÄKTA^{TM} avant 150 (Cytiva Life Sciences) with inline UV (280 nm) and conductivity monitoring operated by UNICORN 7.1 software was used for purification of the lentiviral vectors by SXC. Additionally, a multi-angle dynamic light scattering detector (MALS) (Wyatt Technology) connected in-line and operated with Astra 8 software was included for some of the purification runs. The chemicals for the buffers, Tris, hydrochloric acid (HCl), sodium chloride (NaCl), PEG 2000, PEG 4000, and PEG 6000 were purchased by Carl Roth. Buffers were prepared in
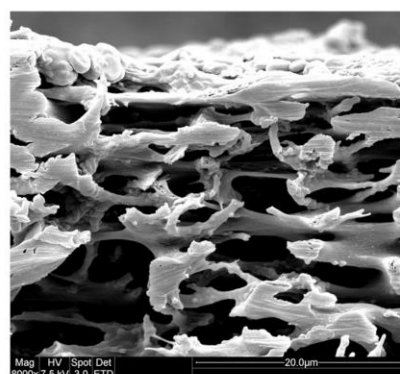
2
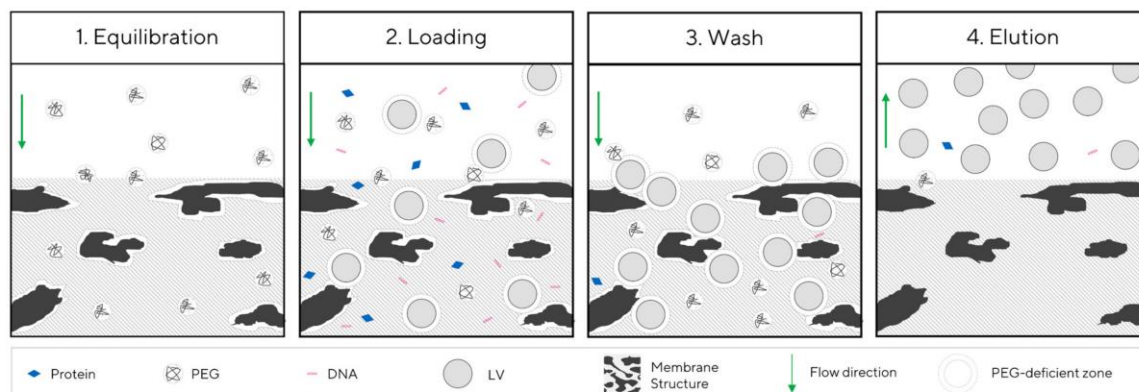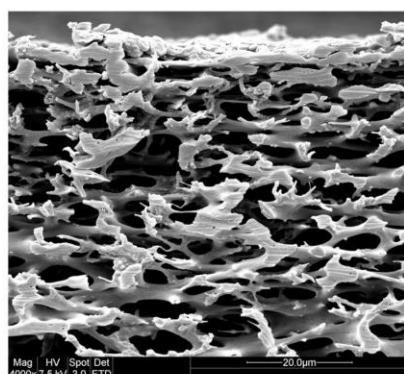
Fig. 1. SXC method principle and stationary phase. A hydrophilic membrane (shown in cross section) is equilibrated with PEG buffer. A PEG-deficient zone forms at the membrane surface, due to the inability of the PEG molecules to fully penetrate this area because of their hydrodynamic radius. During loading a PEG-deficient zone is forms around the LV particles' surface as well (A1). The LV particles associate with the stationary phase, whereas impurities are removed in the flow through (A2). The membrane is then washed with PEG buffer and the LVs remain associated with the stationary phase while unbound remaining impurities are washed out (A3). LVs dissociate from the stationary phase when eluted with Tris buffer (A4). Schematic visualization only; sizes differ in reality: in relation to the pore size, the LV is magnified 10 times and the other molecules (PEG, protein, DNA) are shown magnified 100 times. Exemplary scanning electron microscope pictures of the stabilized cellulose membrane in cross section at 4,000x (B) and 8,000x magnification showing the membrane pore structure of one membrane layer (C).

ultrapure water of Arium® Pro (Sartorius). Two buffers were employed to perform SXC: 1) a 50 mM Tris-HCl buffer with 150 mM NaCl, pH 7.4 (A1), and 2) a PEG buffer with 50 mM Tris-HCl, 150 mM NaCl pH 7.4, and PEG with a certain molecular weight and concentration depending on the experiment conditions (B1). In the following, the buffers are referred to as Tris buffer and PEG buffer.

On the day of the experiment, the LV sample was thawed in a water bath at 37 °C until only small ice clumps remained. The LV sample was then stored at 4 °C until use (30–60 min). The LV solution was used up on the day of thawing. Different LV batches were used for different experiments; therefore, the respective titer of each LV sample is indicated in the results section. The LV solutions were frozen up to 6 months before use. The LV solution was kept on ice during the experiments and the fractions were collected and cooled at 4 °C. The MA15 membrane device was first equilibrated with 20 mL of the Tris buffer and the PEG buffer that were mixed inline at a ½ dilution. For example, a PEG buffer with a concentration of 25% (w/v) PEG 4000 would then equal a final PEG concentration of 12.5%. The loading strategy experiment was performed with PEG 6000 at a concentration of 10% (Section 3.1). In Section 3.2 the first experiments were conducted to investigate the effect of the PEG concentration on the strength of the depletion attraction using PEG 4000 and PEG 6000 at final concentrations of 7.5%, 10%, and 12.5%. The second experiment of Section 3.2 was conducted to investigate the effect of PEG size on the range of the depletion attraction. Therefore, PEG size was systematically varied using PEG with three molecular weights: PEG 2000 Da, PEG 4000, and PEG 6000, as well as a mixture of PEG 2000 and PEG 4000. All buffers had a final PEG concentration of 12.5%. Further experiments (Section 3.3–3.5) were performed with 12.5% PEG 4000. The PEG molecular weights and concentrations are indicated for each experiment in the results section. The LV sample (A2) was loaded by inline mixing with the PEG buffer at a ½ dilution, if not indicated otherwise. The loading volume varied between experiments and is provided in the results section for each experiment. The membrane column was then washed with 15 mL of Tris buffer and PEG buffer that were mixed inline at a ½ dilution. The LVs were eluted with 20 mL of Tris buffer, if not indicated otherwise. Fractions were aliquoted and stored at −80 °C for analysis. The flow

3

rates, PEG size, and PEG concentration varied depending on the experiment. A new membrane device was used for every run. All experiments were performed in triplicate.

2.3. Analytics

2.3.1. Infectious titer determination using the Incucyte® S3
The infectious LV titer was quantified using the live-cell analysis system Incucyte® S3 (Sartorius). Adherent HEK293T cells (ACC 635, DSMZ) were infected with serially diluted LV samples, and the expression of the CD19-CAR was measured by an immunological real-time imaging method. The method and materials used are described in detail in Labisch et al. [19].

2.3.2. Particle titer determination with p24 ELISA
The LV particle titer was quantified by performing a p24 enzyme-linked immunosorbent assay (ELISA) using the QuickTiter™ Lentivirus titer kit (Cell Biolabs). The absorbance was read at 450 nm with a FLUOstar Omega plate reader (BMG Labtech). The absorbance at 450 nm of the samples correlated with the concentration of the p24 capsid protein. The standard curve obtained was fitted by a second-degree polynomial. The p24 concentrations determined were converted into viral particle titers by assuming that 1.25×10^7 LV particles contain 1 ng of p24 and 1 LV particle contains about 2000 molecules of p24 [38].

2.3.3. Total protein quantification
The total protein concentration was determined with the Pierce™ Coomassie Bradford protein assay kit (Thermo Fisher Scientific). The kit was used according to the manufacturer's instructions. Standards and samples were analyzed in duplicates in transparent 96-well microtiter plates (Greiner Bio-one). The absorbance was read at 595 nm with a FLUOstar Omega plate reader. The standard curve obtained was fitted by linear regression.

2.3.4. Total dsDNA quantification
The dsDNA content was determined with the Quant-iT™ PicoGreen™ dsDNA assay (Thermo Fisher Scientific). The assay was performed according to the manufacturer's instructions. Standards and samples were analyzed in duplicates in a 96-well black microplate (Corning). The samples were excited at 480 nm, and the fluorescence emission intensity was measured at 520 nm using the FLUOstar Omega microplate reader. The standard curve obtained was fitted by linear regression.

2.3.5. Determination of the PEG concentration
A modified Dragendorff method was performed to determine the remaining PEG concentration in the elution fractions. A quantity of 0.17 g bismuth subnitrate (Fluka) was dissolved in 2 mL glacial acetic acid (Fluka) in a 20 mL Erlenmeyer flask and diluted to a volume of 20 mL with deionized water (solution A). Four grams of potassium iodide (TCI) was dissolved in 10 mL of deionized water (solution B). Solutions A and B, each in a volume of 5 mL, and 20 mL of glacial acetic acid were added to a 100 mL Erlenmeyer flask and diluted to a volume of 100 mL with deionized water to obtain the Dragendorff reagent. Then 2 g of barium chloride (Fluka) was dissolved in 8 mL of deionized water. PEG 4000 standards in a concentration range from 0.1 to 1 g·L^{-1} were prepared; 0.5 mL PEG 4000 standards or SXC elution fractions were added to a 1.5 mL reaction tube. Next, 0.1 mL of barium chloride solution, 0.2 mL of Dragendorff reagent, and 0.2 mL of deionized water were added and mixed. Samples were incubated for 15 min. Standards and samples were analyzed in duplicate in transparent 96-well microtiter plates (Greiner Bio-one). The absorbance was read at 510 nm using a plate reader. The standard curve obtained was fitted by linear regression.

2.4. Statistical analysis

The statistical significance of between-group differences was evaluated by using unpaired Student's t-tests (two-tailed) with OriginPro® 2021 (OriginLab). Where applicable, experiments were evaluated with MODDE Pro 13 (Sartorius). Results are presented as mean ± standard deviation of triplicates.

3. Results and discussion

3.1. Impact of mixing shear and buffer systems on LV infectivity as well as of a suitable LV loading strategy

SXC is considered a milder chromatography method for enveloped viral vectors compared with AEX or affinity chromatography. To investigate whether the PEG buffer used for SXC has an impact on LV infectivity, an LV solution was mixed in a 1:1 ratio with 25% (w/v) PEG 4000 buffer, resulting in a final PEG concentration of 12.5%. Besides this, LV was incubated with the Tris-HCl elution buffer and the virus production medium FreeStyle293. An LV-free sample served as a negative control. The samples were incubated for 1 h at 4 °C first, then LV infectivity was determined according to Section 2.3.1. The samples were incubated for 1 h since the maximum duration of one SXC run was 35 min and within 1 h the fractions were aliquoted and stored at −80 °C until analysis. The incubation was performed at 4 °C as LV was kept on ice during SXC runs and fractions were cooled at 4 °C before freezing. Further stability data of the LV at different temperatures and incubation times were previously published [19]. The incubation of LV with the PEG buffer or the Tris-HCl buffer did not reduce the infective titer significantly ($p \le 0.05$) compared to the sample incubated with medium as shown in Fig. 2A. The LV is present in the production medium after harvest and clarification. The medium sample, therefore, serves as a control. We showed that PEG buffer and Tris-HCl buffer do not reduce the biological activity of LV.

To analyze the effect of LV pass-through in the chromatography system on the LV infectivity, several bypass runs were performed. As the LV material needed to be mixed with the PEG buffer before loading, we chose to explore different mixing strategies available: The first option involved mixing the LV solution with PEG buffer externally in a bottle by using a magnetic stirrer with a magnetic stir bar and by loading the ready-mixed solution via the sample valve of the chromatography system. The second option entailed mixing the two solutions internally in the chromatography system using its dynamic mixer. We investigated both strategies with the aim of obtaining high virus recoveries. Moreover, the MALS detector was either connected to or disconnected from the system to further analyze the effect of the additional pressure caused by the detector. The differences in infective titer recoveries of the bypass runs are negligible (Fig. 2B), regardless of whether internal or external mixing was performed. The connection of the MALS detector increased the pressure from 0.21 MPa to 0.38 MPa. When a membrane adsorber is connected, a higher pressure must be considered. All in all, the chromatography system, as well as the dynamic mixer itself, did not have a significant impact on the LV infectious titers, achieving recoveries of 90% or more. A possible explanation could be that the viscosity of the PEG buffer somewhat reduces shear stress, for instance that is generated by the dynamic mixer; therefore, the impact of shear stress might be low. Our observation is consistent with Ruscic et al. [39], who reported no significant LV loss by the fast liquid chromatography system used in their study for ion exchange chromatography.

In a second experiment, the different loading strategies of internal and external mixing as described above were tested by performing SXC. The experiments were carried out using PEG with a molecular weight of 6000 Da at a final concentration of 10% and
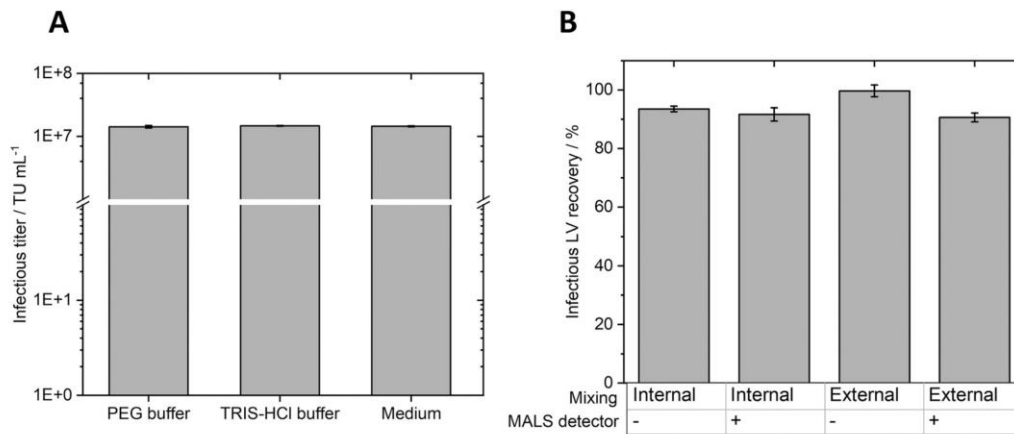
Fig. 2. Shear and buffer impact on LV infectivity. Infectious titers after incubation of LV with different buffers or medium for 1 h at 4 °C (A). Infectious titer recoveries for bypass experiments with the chromatography system and the MALS detector using two different mixing strategies of the LV and the PEG buffer (B).
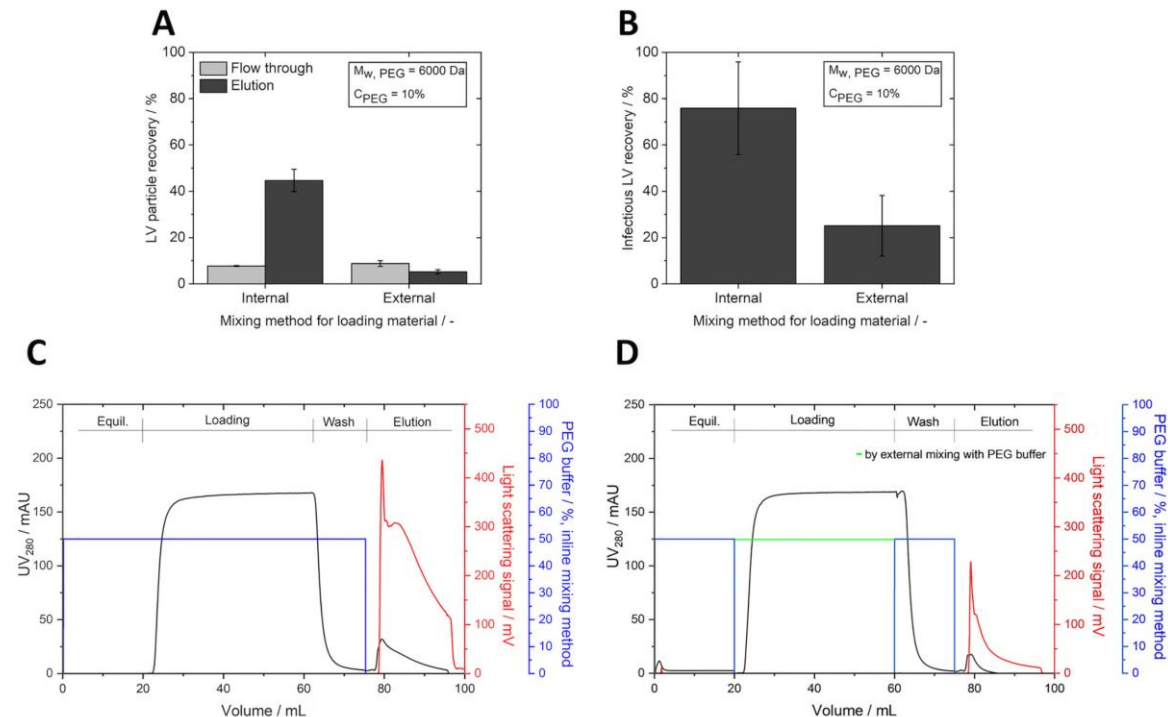

Fig. 3. Comparison of mixing methods for LV loading. LV particle recovery (A) and infectious recovery (B) in the elution fraction of different mixing strategies during the loading step. Chromatograms of SXC runs with internal (C) or external mixing (D) of LVs with PEG buffer. The UV signal is shown in black, the light scattering signal in red; the percentage of PEG buffer added during inline mixing in blue, and during external mixing in green.

a flow rate of 7 mL·min^{-1}. We chose PEG 6000 based on previous publications [23–25,28,40,41] as a starting point to investigate the ideal loading strategy before identifying a suitable PEG size and concentration. Internal mixing resulted in a significantly higher particle recovery ($p \leq 0.001$) of $45 \pm 5\%$ compared with $5 \pm 1\%$ for external mixing of LV with PEG buffer. In the flow through fractions, similar LV particle recoveries of about 8% were detected for both mixing strategies (Fig. 3A). The wash fraction was not plotted since LV particle recovery in the wash fractions was

below or equal to 2% for all runs. The infectious LV recovery for internal mixing was $76 \pm 20\%$, significantly higher ($p \leq 0.05$) than that of $25 \pm 13\%$ for external mixing (Fig. 3B). We did not analyze the infectious titer in the flow through and wash fractions, because only a very small amount of LV particles was recovered in these fractions, and this is difficult to detect by an infectivity assay. First, the volume of the flow through section is large; thus, the LV in the flow through fractions is highly diluted; and second, the p24 detected in the flow through and wash fraction might also be

5

J.J. Labisch, M. Kassar, F. Bollmann et al.

stem from non-infectious LV debris, resulting in a signal below the detection limit. Two representative chromatograms (Fig. 3C and D) confirm the observation of the titer assays. When internal mixing was performed during loading, the elution peak showed a higher light scattering signal, indicating a larger number of eluted particles compared with the elution peak when the LV was mixed externally and then loaded. When the LV solution is mixed with PEG, the unfavorable excess in free energy caused by the formation of PEG-deficient zones can be either reduced by LV self-association or by the association of LV with the stationary phase. Internal mixing can possibly promote association with the stationary phase because the LV is mixed with PEG shortly before reaching the stationary phase. By contrast, external mixing may lead to LV aggregation since the incubation time is longer before reaching the membrane surface. The formation of aggregates may hinder the subsequent elution of LV particles, resulting in low LV recoveries. These observations are consistent with other studies that reported particle aggregation when adeno-associated viral vectors were mixed with the PEG buffer externally [28]. This phenomenon was first postulated by Lee et al. [23], who performed inline mixing due to a potentially preferred association of the target molecule with the stationary phase, preventing aggregation of the target molecules with one another. On the other hand, external mixing of baculovirus with PEG buffer and loading via a loop has been reported to yield high vector recoveries [26]. Although the preferred use of inline mixing was discussed and reported before, this is the first study presenting comparative data. Based on these findings, all further experiments were performed by mixing the LV with the PEG buffer internally in the chromatography system.

3.2. Optimal PEG size and concentration for LV purification

The aim of this investigation was to determine an optimal PEG size and concentration at which both high LV particle and infectious recoveries, as well as high dsDNA and protein removal, are achieved. The first experiment (Fig. 4) was conducted to investigate the effect of PEG concentration on the strength of the depletion attraction. PEG with molecular weights of 4000 Da and 6000 Da and concentrations of 7.5%, 10.0%, and 12.5% were tested systematically. SXC devices described in Section 2.2.1 with 5 and 10 membrane layers were used. Two different numbers of layers were tested because the surface area required to capture LV successfully was not yet known, or whether a certain number of layers was required to prevent LV breakthrough. LV solution was loaded in the same volumes of 25 mL LV solution for 5-layer and 10-layer membrane devices, corresponding to 6.25×10^{12} total viral particles (2.50×10^{11} VP·mL^{-1}) and 9.25×10^{7} infectious viral particles (3.70×10^{6} TU·mL^{-1}). The ratio between physical particles compared to functional particles of the product was 6.7×10^{4} VP·TU^{-1}. This solution equaled a 50 mL loading volume as the LV was mixed in a dilution of ½ with PEG buffer. The percentages of LV particle recovery in the flow through and elution fractions were plotted against the corresponding PEG concentration (Fig. 4A and B). The wash fraction was not plotted since LV particle recovery in the wash fractions was below 3% for all runs.

The LV particle recovery in the elution fractions rose as the PEG 4000 concentration increased (Fig. 4A). For a 5-layer membrane device, only $32 \pm 13\%$ of the LV particles were recovered in the elution fraction at a PEG 4000 concentration of 7.5%, whereas a high percentage of $69 \pm 3\%$ of LV particles were lost in the flow through fraction. For the concentrations of PEG 4000 analyzed we have a dilute concentration regime of the polymer solution. In dilute polymer solutions, the range of depletion attraction depends on the polymer size, while the strength of the interaction depends on the polymer concentration [42]. When PEG 4000 was used at a concentration of 7.5%, the ratio of PEG molecules

to LV particles was too low to achieve the depletion attraction of all LV particles, and a high amount of LV was lost in the flow through fraction. Using a 10-layer membrane resulted in a significantly lower LV loss ($p \leq 0.001$) in the flow through fraction, but recovery in the elution fraction was similar to 7.5% PEG 4000 using an SXC device with 5 membrane layers. One possible reason could be that the critical proximity required between the LV and the membrane is less frequently present with 5 layers. With 10 layers, the LV particles must pass through more membrane layers, which means an increased chance that an LV particle might encounter the membrane, then drop below the critical proximity required to result in capture. Concentrations of 10.0% and 12.5% PEG 4000 yielded significantly higher LV particle recoveries ($p \leq 0.01$) in the elution $72 \pm 7\%$ and $86 \pm 18\%$, respectively, compared with the 7.5% PEG 4000 concentration. Large error bars and recoveries above 100% are often reported when working with lentiviral vectors, or viral vectors in general, with error bars of 20–30% and even higher being reported in recent publications [6,39]. This is attributed to the inherent variability of the titer assays. Moreover, only a small amount of LV was lost in the flow through fraction (1–5%). A higher ratio of PEG molecules to LV particles induced a higher osmotic pressure around the LV particles, resulting in particle attraction. This led to a higher fraction of LV particles retained at the hydrophilic surface of the membrane with increasing PEG 4000 concentration and thus higher LV particles recovered in the elution fraction. A comparable trend is observed when using a 10-layer membrane device. Considering the experimental error there is no significant difference in the recovery of LV particles in the elution fraction when using 5 or 10 membrane layers for all PEG 4000 concentrations tested. No pronounced effect of PEG 6000 concentration on LV particle recovery was observed for the 5-layer membrane device with recoveries in the elution fraction ranging from $38 \pm 6\%$ to $52 \pm 2\%$ (Fig. 4B). When a 10-layer membrane device was used, the highest LV particle recovery of $51 \pm 7\%$ was achieved at a 7.5% PEG 6000 concentration. A further increase in the PEG 6000 concentration led to a significant decrease in LV particle recovery ($p \leq 0.01$) in the elution down to $26 \pm 2\%$. The particle recovery was almost twice as low as the highest recovery obtained with PEG 4000. When PEG 6000 was used at the concentrations investigated, the viscoelastic properties of the PEG buffer started approaching those of a semi-dilute polymer solution as obtained by the scheme of polymer solutions published by Baumgaertel and Willenbacher [43]. This means the PEG molecules begin to interact with one another and the movement of PEG chains is restricted, depending on the movement of another polymer chain [44]. In this regime, the range of depletion attraction is independent of the polymer size, and the strength of the interaction is a decreasing function of the concentration [34]. This may explain the lower LV particle recoveries and an overall higher variability in LV recoveries in previously performed experiments using PEG 6000 (data not shown). When PEG 6000 was used, negligible LV particle recoveries in the flow through fractions were measured, with values below 3% regardless of the number of membrane layers. The PEG-free depletion zone around the LV particle correlates to the PEG size. When PEG 4000 is used at a concentration of 7.5%, the total excluded volume of PEG is lower than when PEG 6000 with the same concentration is used. Therefore, a lower amount of LV particles was lost in the flow through fraction using PEG 6000.

Infectious titer recoveries were not significantly different using different concentrations of PEG 6000 and 5 or 10 membrane layers (Fig. 4D), whereas, for PEG 4000, a similar trend was observed (Fig. 4C), as described for the particle titer. The infectious titer recovery rose significantly ($p \leq 0.01$) from 67% to 84–88% when the PEG 4000 concentration was increased from 7.5% to 10.0% or to 12.5% using 5 membrane layers. Using 10 membrane layers and PEG 4000 at a concentration of 12.5% resulted in a significantly
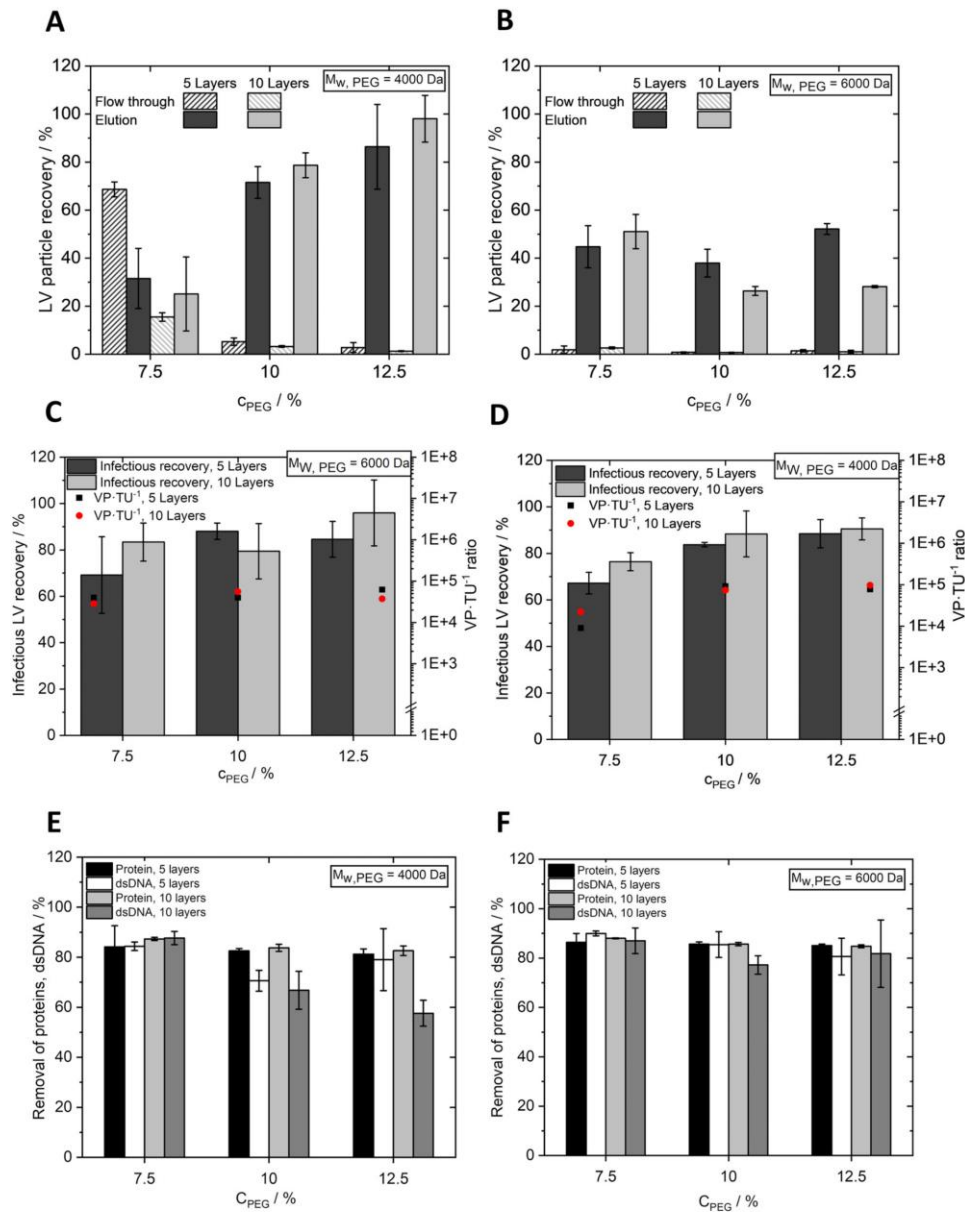
6

Fig. 4. LV titer recoveries and impurity removal using different PEG sizes and concentrations. LV particle recovery in flow through and elution fractions using PEG with molecular weights of 4000 Da (A) and 6000 Da (B), respectively, plotted against three different PEG concentrations. Infectious LV recovery and viral particle to transducing unit ratio (VP·TU^{-1}) in the elution fraction using PEG with molecular weights of 4000 Da (C) and 6000 Da (D), respectively, plotted against the different PEG concentrations. Protein and dsDNA removal using PEG with molecular weights of 4000 Da (E) and 6000 Da (F), respectively, plotted against the different PEG concentrations. SXC devices with 5 and 10 membrane layers were used.

increased infectious titer recovery ($p \leq 0.05$) compared with a PEG concentration of 7.5% (91% recovery compared with 76%). As above described, a higher ratio of PEG molecules to LV particles increases the strength of depletion attraction, inducing a higher osmotic pressure around the LV particles, resulting in particle attraction. This led to a higher fraction of infectious LV particles retained at the hydrophilic surface of the membrane with increasing PEG 4000 concentration and thus higher infectious LV recovery in the

elution fraction. Contrary to conventional chromatography methods for LV purification, which often significantly reduce the biological activity of enveloped viral vectors [3], SXC provides gentle purification conditions, which is advantageous for fragile enveloped viral vectors. All buffers used during SXC had a pH that preserves LV activity [18] and a low salt concentration that does not reduce LV infectivity [19]. Presumably, PEG may reduce, to some extent, the impact of shear stress applied to LV particles during purification.

7

According to flow mechanics of non-Newtonian fluids, viscoelastic properties induced by the addition of shear-thickening agents such as polymers hinder the deformation of suspended particles as polymer chains deform [45,46]. Another advantage is that, due to the mild elution conditions for SXC, no additional processing steps after elution are required, such as dilution of the eluate or immediate desalting as performed for AEX [39,47,48]. A recent publication by Valkama et al. reported an LV recovery of 33% with AEX [6]. Other studies performing AEX with LV typically reported recoveries below 60% [3,4]. This outlines the necessity for optimized purification methods for LV and the great potential of SXC that yields LV recoveries above 80%.

The protein and dsDNA removal for PEG 4000 and PEG 6000 at different concentrations were measured and shown in Fig. 4E and 4F. The dsDNA and protein concentrations of the loading material were 321 ng·mL^{-1} and 204 µg·mL^{-1}, respectively. Overall high removal of protein and dsDNA impurities of approximately 80% was observed. The removal of impurities was similar for different PEG sizes and concentrations. The reason for this is discussed in the following: The polymers PEG 2000, 4000, and 6000 have a gyration radius of 1.6 nm, 2.5 nm, and 3.1 nm [44], respectively, and are preferentially excluded from the vicinity of large molecules like LV particles. A typical host cell protein is the heat shock protein 70 [49] which has a hydrodynamic radius of approximately 3.5 nm. During LV production, DNase (DENARASE, c-LEcta) was used to cleave dsDNA into fragments with an expected length of approximately 5–8 bp according to the specifications of the manufacturer. With one base pair being approximately 340 pm long [50], this results in a length of 1.7 nm to 2.7 nm. However, the pronounced size difference between the LV particles (100 nm in diameter) and the contaminants allows selective retention of the larger LV particles. Therefore, nearly none of the small impurities are retained so they are efficiently removed in the flow through fraction. The impurity removal with SXC was 80–90%, which equals a log removal of 0.7 to 1. For AEX DNA removals of greater than 90% were achieved [47,51] and 2-log removal of HCPs and DNA was reported [39]. Although the impurity removal with AEX is higher compared with SXC, the advantage of SXC lies towards the LV recovery of above 80%. For AEX LV recoveries are typically below 60% [3,4,6]. Heparin affinity chromatography of LV removed 94% and 56% of protein and DNA impurities, respectively, while recovering 53% of infectious LV particles [11]. Heparin affinity chromatography yields overall a lower impurity removal and LV recovery compared with SXC. Affinity chromatography yielded a 2-log reduction of host cell DNA and protein impurities, which is higher than for SXC, but recovered only 60% of infectious LV [17]. Moreover, no ligand leaching occurs during SXC because hydrophilic cross-linked cellulose membranes without ligands are used, which eliminates additional purification costs as required for affinity chromatography [20,22]. To evaluate the most suited chromatography technique, not only the impurity removal must be considered, but the virus recovery, as well as other aspects like potential ligand leakage. The favor of SXC over traditional techniques is the high LV recovery in combination with good impurity removal.

An optimal PEG concentration was identified at 12.5% using PEG 4000. Based on this finding, the next experiment was performed to investigate the effect of PEG size on the range of the depletion attraction. Therefore, PEG size was systematically varied using PEG with three molecular weights: one lower than 4000 Da (PEG 2000) and one higher (PEG 6000). The range of the depletion interaction depends on the size of the polymer. It has been hypothesized that a more polydisperse distribution of the molecular weight of the polymers may lead to a higher depletion of the colloidal particles [52]. To analyze this, a PEG buffer with a final concentration of 12.5% was prepared using a mixture of PEG 2000 and PEG 4000 with a molarity ratio of 1:2 and compared with other monodisperse PEG buffers having the same concentration (Fig. 5A and B). A mixture of PEG 4000 and PEG 6000 was not tested as this buffer has a higher viscosity that in turn leads to a higher pressure compared with a monodisperse PEG 4000 buffer. Therefore, we tested a mixture of PEG 4000 with a lower molecular weight PEG to investigate if the performance is comparable to the monodisperse PEG 4000 buffer and at the same time resulting in a lower pressure (Fig. 7A) that is advantageous for the process as discussed in more detail in Section 3.4. For this experiment, another LV batch was used as for the previous experiments. The flow rate was set to 7 mL·min^{-1} and the loading volume was 50 mL (equal to 25 mL of LV solution), which equaled 9.1 × 10^{11} total viral particles (3.64 × 10^{10} VP·mL^{-1}) and 4.1 × 10^{7} infectious viral particles (1.64 × 10^{6} TU·mL^{-1}). The ratio between physical particles compared to functional particles of the product was 2.2 × 10^{4} VP·TU^{-1}.

At a constant PEG concentration of 12.5%, the LV particle recovery in the flow through fractions decreased significantly from 21 ± 4% to 1 ± 0.5% as the molecular weight of PEG increased (Fig. 5A). With a mixture of PEG 2000 and PEG 4000, the amount of LV lost in the flow through fractions is between the values measured for PEG 2000 and PEG 4000. This can be explained by the PEG-free depletion zone around the LV particles that becomes larger as the PEG size increases. Therefore, PEG 2000 (12.5%) led to twice as high LV particle loss in the flow through fraction compared with the mixtures of PEG 2000 and PEG 4000 having the same concentration. A different molar ratio with a higher proportion of PEG 4000 may result in less LV particle loss in flow through than with a molarity of 1:2. A higher PEG concentration is required to achieve the same depletion strength with smaller PEG sizes. The highest LV particle recovery in the elution was obtained for PEG 4000 (86 ± 18%). Using PEG 6000 at the same concentration, a significant drop in LV recovery ($p \leq 0.05$) in the elution fraction was observed (52 ± 2%). This is due to the viscoelastic properties of PEG 6000 as explained above. Fig. 5B shows overall high infectious virus particle recoveries ranging from 75% to 94% for different PEG molecular weights. Considering the error bars, the effect of the molecular weight of PEG on infectious LV recovery was negligible. The dsDNA and protein concentrations of the loading material were 477 ng·mL^{-1} and 241 µg·mL^{-1}, respectively. Overall high protein and dsDNA removal between 77 ± 4% to 88 ± 4% was achieved (Fig. 5C), regardless of the PEG molecular weight used, which has been already discussed above.

Comparing our results of the investigation on the ideal PEG size and concentration to previous SXC studies, we observed a similar trend using PEG 4000 as described by Wang et al. [29] using PEG 6000: increased retention of the biomolecule of interest with increasing PEG concentration. However, it must be considered that γ-globulin is a small molecule (hydrodynamic radius 4.5 nm) compared with LVs and smaller molecules require larger PEG sizes to achieve efficient depletion retention. Other studies with viral vectors having a similar size like LV were performed and achieved an influenza A virus recovery of 83% with 8% PEG 6000 [25] and recovery above 90% of Orf virus with 8% PEG 8000 [30]. These findings do not agree with results obtained in our present study in which high recoveries were not obtained with PEG 6000 at a concentration ranging from 7.5% to 12.5% and a flow rate of 7mL·min^{-1}. However, it must be considered that a membrane device with a regenerated cellulose membrane with a pore size of 1 µm (Whatman®) was used and the flow rate was set at 10 mL·min^{-1}. Different process parameters, such as the flow rate or the specifications of the stationary phase used, can impact SXC performance. These different process parameters may explain why we observed optimal recoveries with different PEG buffers. Larger PEG sizes like PEG 8000 were not tested in our study due to pressure concerns, as discussed later in Section 3.4.
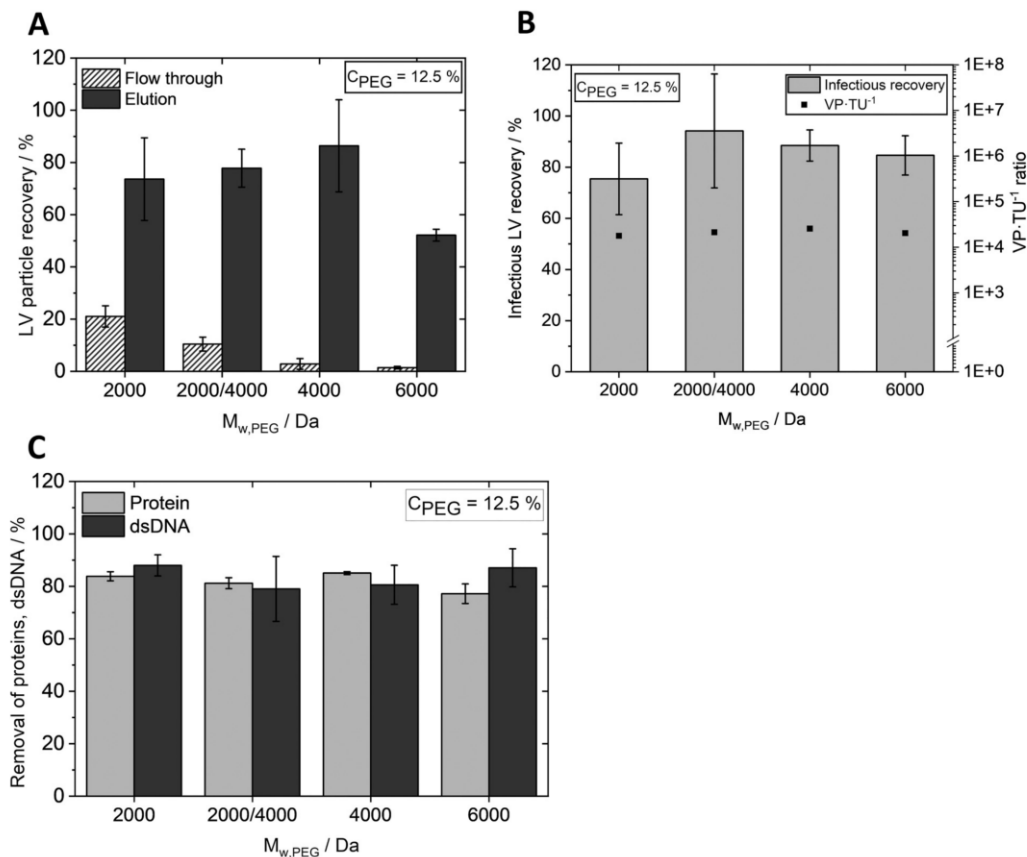
8

Fig. 5. LV titer recoveries and impurity removal using different PEG molecular weights at a constant PEG concentration. LV particle recovery in flow through and elution fractions (A), infectious LV recovery and viral particle to transducing unit ratio (VP·TU^{-1}) (B), and protein and dsDNA removal (C) plotted against the different molecular weights of PEG at a constant PEG concentration of 12.5%.

In terms of LV particle and infectious recovery, as well as impurity removal, the best results were achieved with PEG of a molecular weight of 4000 Da at a concentration of 12.5% using the 5-layer membrane device. The following experiments were performed with these parameters.

3.3. Optimal flow rate

To gain insight into the dynamic aspects of SXC, different flow rates were investigated to define an optimal flow rate at which high LV particle recoveries and infectious particle recoveries as well as high contaminant removal values are achieved. The purification step was performed systematically at flow rates of 3, 6, and 9 mL·min^{-1}. The flow rate was the same for all steps (loading, wash, elution). PEG 4000 at a final concentration of 12.5% and an SXC device with 5 membrane layers were used. An LV solution of 25 mL (equals 50 mL loading volume) was loaded, corresponding to 5.60×10^{12} total viral particles (2.24×10^{11} VP·mL^{-1}) and 9.25×10^{7} infectious viral particles (3.70×10^{6} TU·mL^{-1}). The ratio between physical particles compared to functional particles of the solution was 6.1×10^{4} VP·TU^{-1}. The main effect plots obtained by MODDE Pro 13 in Fig. 6, depict the predicted values of the selected responses when the factor varies from low to high level. The experimental data (worksheet) is indicated in the plot as well.

LV particle recovery in the elution fraction increased significantly ($p \leq 0.001$) from $28 \pm 7\%$ to $75 \pm 11\%$ when the flow rate was increased from 3 mL·min^{-1} to 6 mL·min^{-1}, but decreased significantly ($p \leq 0.05$) at a flow rate of 9 mL·min^{-1} down to $47 \pm 9\%$ (Fig. 6A). LV particle recoveries in the wash and flow through fractions were below 4% for all runs (data not shown). A comparable trend was observed for infectious LV recovery, which increased significantly ($p \leq 0.001$) from $42 \pm 4\%$ to $79 \pm 5\%$ when the flow rate was increased from 3 mL·min^{-1} to 6 mL·min^{-1} and then decreased significantly ($p \leq 0.05$) to $61 \pm 8\%$ at a flow rate of 9 mL·min^{-1} (Fig. 6D). The highest predicted LV particle recovery and infectious LV recovery are obtained for flow rates between 6 and 7 mL·min^{-1}. At a low flow rate, it takes more time for LV particles to reach the membrane of the chromatography device. It is possible that during this unfavorable state of free energy, self-association of the particles occurs before they reach the stationary phase. The subsequent elution of large aggregates is difficult. Another hypothesis is that the lower pressure at 3 mL·min^{-1} was too low to reverse aggregation of the LV particles that bound to the membrane, thus challenging their proper elution. The residence time of LV particles in the stationary phase with 9 mL·min^{-1} was possibly too short, hindering their retention. Moreover, at 9 mL·min^{-1}, the pressure limit was nearly reached, which is disadvantageous for the process. Lothert et al. [26] used the same membrane as
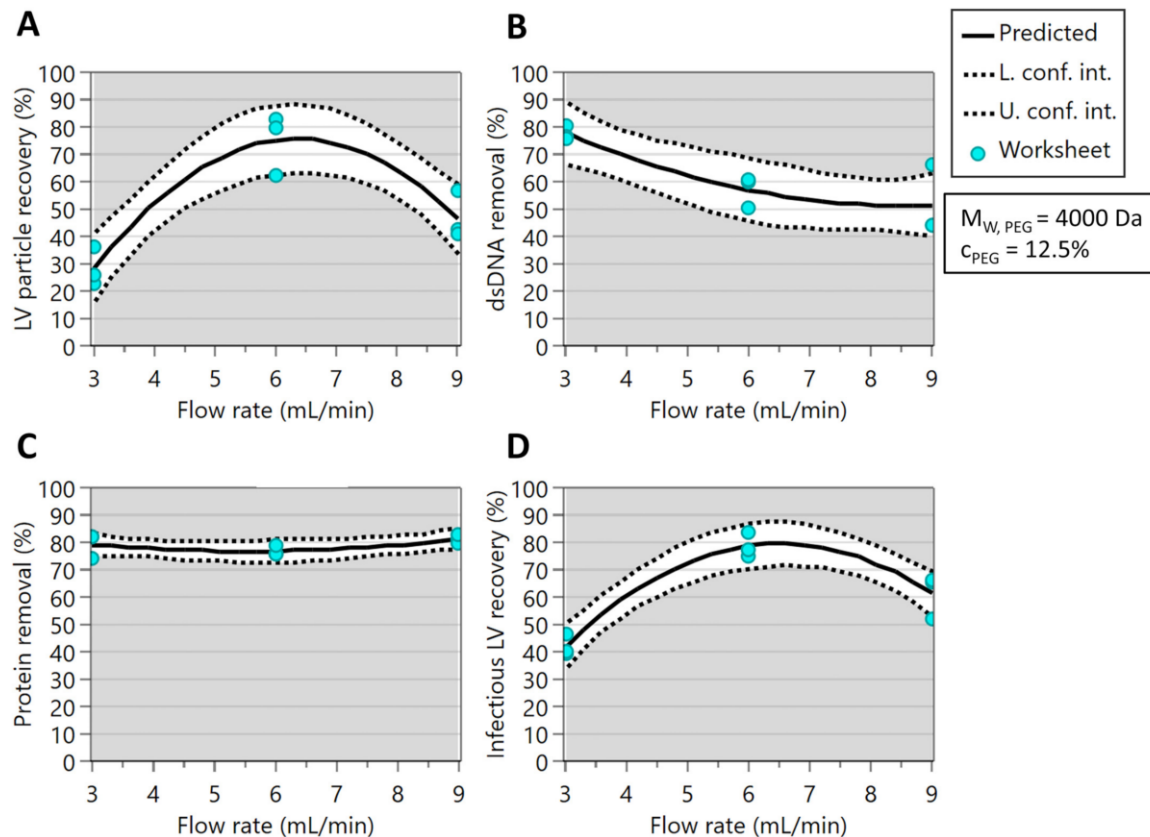
Fig. 6. Main effect plots of the flow rate. Predicted LV particle recovery (A), dsDNA removal (B), protein removal (C), and infectious LV recovery (D) for flow rates between 3 and 9 mL•min^{-1}. The measured data (worksheet) are displayed as blue dots. Solid lines show the predicted values; dotted lines, the lower and upper confidence intervals.

the one employed in our study as a stationary phase and observed that the flow rate had a high impact on virus retention and that the optimal flow rate depended on the PEG size and concentration used. We assert that optimal process conditions for flow rate and PEG buffer also depend on the stationary phase, e.g., membrane material, pore size, and thickness. Relatively high values of dsDNA and protein removal were obtained. A significant decrease in dsDNA removal ($p \leq 0.05$) from $78 \pm 2\%$ to $51 \pm 13\%$ was measured as the flow rate increased (Fig. 6B). The dsDNA removal rates at 6 mL·min^{-1} and 9 mL·min^{-1} did not significantly differ from one another ($p \leq 0.05$). Regardless of the flow rate, high protein removal values ranging from $77 \pm 2\%$ to $81 \pm 1\%$ were achieved (Fig. 6C). With respect to both LV recovery and impurity removal, a flow rate between 6 and 7 mL·min^{-1} was defined as optimal.

3.4. Pressure profiles and maximum loading volumes for SXC

We hypothesized that pressure is a critical factor to consider when performing SXC, therefore we had a closer look at pressure profiles. In order to better understand which factors are the main drivers of pressure, we analyzed the pressures for various parameters, including different PEG buffers, flow rates, and loading volumes (Fig. 7A–C). The maximum pressure of the chromatography system was set to 0.6 MPa. The pre-column pressure was always around 0.17 MPa below the system pressure. The MALS detector

was not employed for these experiments as the use of this detector causes additional pressure that would have exceeded the maximum pressure under the conditions used.

The use of a lower molecular weight and concentration of PEG resulted in a lower viscosity of the PEG buffer which is reflected by the lower system pressure observed (Fig. 7A). PEG buffers are viscous, and as the viscosity and flow rate increase, the pressure rises (Fig. 7B). Lower pressures can be advantageous for extremely labile LV particles and the process itself. Therefore, smaller PEG sizes and lower PEG concentrations should be considered. PEG buffers with a molecular weight of greater than 6000 Da were thus excluded in this study. A polydisperse PEG buffer using a mixture of two different PEG molecular weights is an option when low operating pressures are required due to process limitations. A pressure profile for loading either 100 mL or 140 mL of the LV solution is shown in Fig. 7C. This profile indicates that the pressure continuously increased during the loading step, whereas it decreased rapidly during the elution step. As a pressure increase was observed during the loading step, the volume loaded, must also be considered to reduce operating pressure. We consider the amount of LV loaded is limited by the pressure increase during loading. We hypothesize that the pressure increase observed during loading occurs due to an increase in the amount of virus captured in the membrane, which leads to membrane fouling and, therefore, to a decrease in the membrane pore size. Consequently, operating SXC near the pressure limit is disadvantageous. A lower pressure,

10
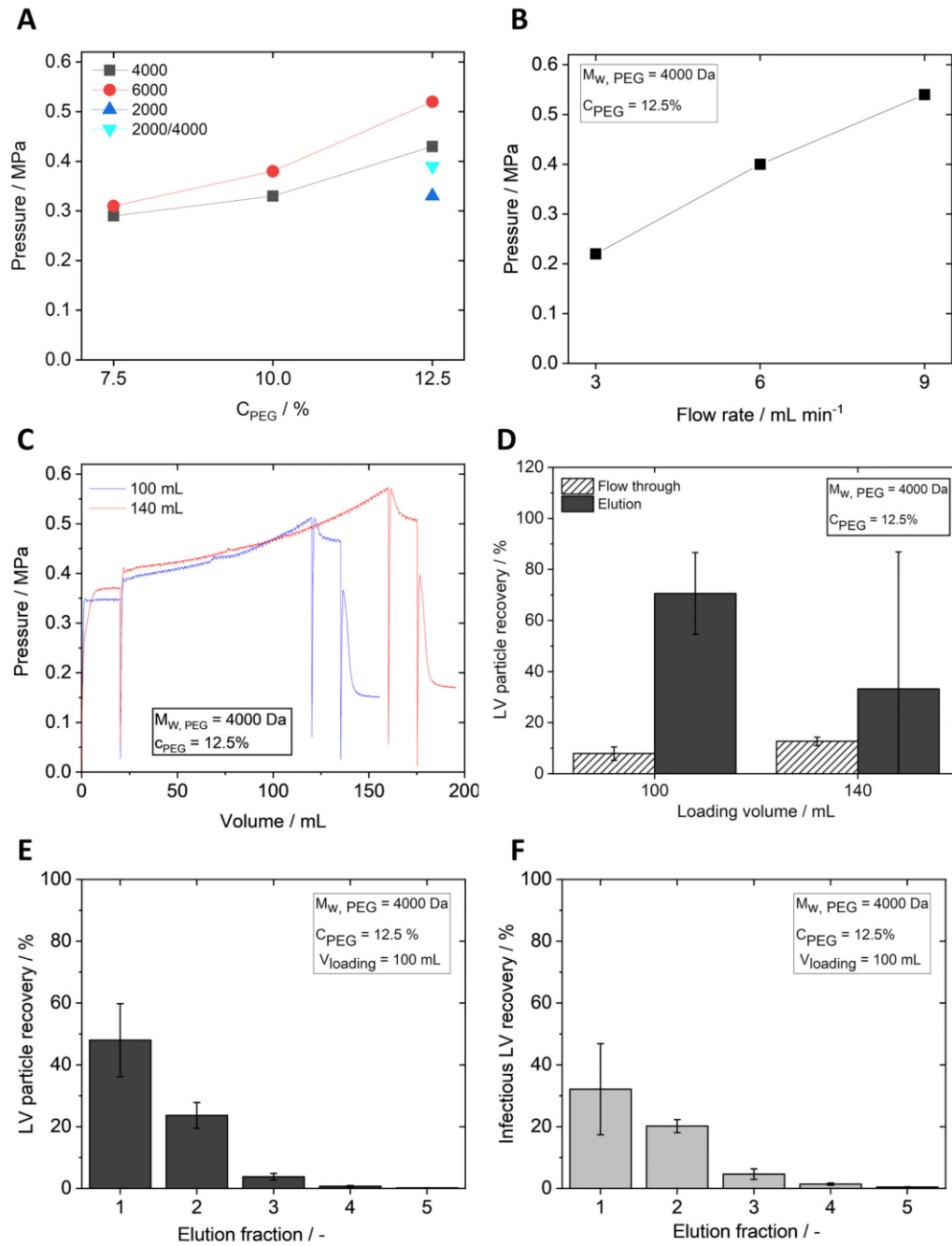
Fig. 7. Pressures and maximum loading volumes for SXC. System pressures during SXC runs using different PEG buffers (A), flow rates (B), and loading volumes (C). For A, B, the pressures at the end of the loading step are indicated. Recovered LV particles loading either 100 mL or 140 mL (equals 50 mL or 70 mL of LV solution loaded, respectively) (D). LV particle recovery (E) and infectious recovery (F) for the corresponding elution fraction loading of 100 mL (equals 50 mL LV solution). Each volume for the elution fractions was 10 mL.

11

achieved by selecting a suitable PEG buffer and an appropriate flow rate, would allow a higher number of loaded LV particles before the maximum pressure is reached.

In the next experiment, we investigated the effects of different loading volumes on LV recovery and determined the maximum loading capacity of the SXC device (Fig. 7D). The number of viral particles loaded was 7.5×10^{12} and 1.05×10^{13} total viral particles (1.50×10^{11} VP·mL^{-1}) for loading volumes of 100 mL and 140 mL (equals 50 mL and 70 mL LV solution), respectively. The LV particle recovery in the elution fraction was $71 \pm 16\%$ when 100 mL was loaded. When we attempted to load 140 mL, the pressure limit was reached at the end of the loading step for two of three replicates. The elution step, at which the pressure decreases, was performed for all runs, but only the elution of one out of three replicates was successful. While an LV particle recovery of 95% was obtained for the successfully eluted replicate, the two other replicates yielded an LV particle recovery of only 2–3%. Therefore, the LV particle recovery for the loading volume of 140 mL (Fig. 7D) shows an extremely high error bar. As it is not possible to elute LVs adequately after the maximum pressure has been reached, the membrane should not be overloaded. We hypothesize that when overloading the membrane aggregates are formed that block the membrane pores, thereby making it impossible to elute the viral particles as liquid flow through the membrane is restricted. Consequently, overloading the membrane and approaching the pressure limit hinders subsequent elution of the LV particles. Therefore, we recommend a maximum load of 7.5×10^{12} VP (in this case, 100 mL loading volume) per MA15 SXC 5-layer membrane device; with respect to the total available surface area of the device, the capacity is 3.06×10^{11} viral particles per cm². The pressure is of high importance, especially from a process perspective as maximum pressures of 0.3 to 0.4 MPa are typical for large-scale DSP processes, whereas the maximum pressure for the small-scale study was higher, at 0.6 MPa. This must be considered to scale up a purification process.

In a separate experiment we investigated the required elution volume when the loading volume was increased to 100 mL (3.42×10^{12} viral particles (6.84×10^{10} VP·mL^{-1}) and 9.57×10^{7} infectious particles loaded (1.91×10^{6} TU·mL^{-1}). The ratio between physical particles compared to functional particles of the product was 3.6×10^{4} VP·TU^{-1}). Five elution fractions of 10 mL each were collected, and LV recovery was analyzed for each fraction separately (Fig. 7E and F) because the MALS detector could not be used, as described above. In the first and second fractions, LV particle recoveries of $48 \pm 12\%$ and $24 \pm 4\%$ were achieved. An LV particle recovery of 4% or below was obtained in the remaining fractions (Fig. 7E). In total, a particle recovery of $77 \pm 8\%$ was achieved across all elution fractions. An analog trend was observed for the infectious recovery as depicted in Fig. 7F. Infectious recovery values of $32 \pm 15\%$ and $20 \pm 2\%$ were achieved for the first and second elution fractions; infectious recovery values of 5% or below were obtained for the remaining fractions. In total, an infectious recovery of $59 \pm 16\%$ was achieved for all elution fractions. The LV particles and the infectious LV were mainly recovered in the first two to three elution fractions. Elution with 20 to 30 mL can therefore be considered sufficient for a 5-layer membrane SXC device. When collecting the first 20 mL of the eluate, a volumetric concentration factor of 2.5 of the LV was achieved. This is an advantage compared with AEX which includes typically a 5-fold dilution of the eluate to preserve the infectivity of LV and a subsequent feed volume reduction step [5,39,47] or an immediate desalting step after the elution step [48]. Some protocols even include a dilution of LV with loading buffer before AEX to meet the conductivity requirements of the method [39]. Thus, AEX chromatography results in higher buffer consumption and a weakened concentration of the LV [3]. We, therefore, regard it as an advantage that no pre or post-
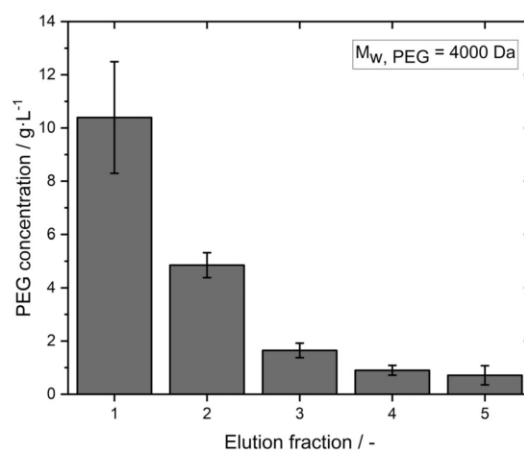
Fig. 8. PEG concentration in SXC elution fractions. PEG with a molecular weight of 4000 Da and 12.5% (w/v) was used to purify 100 mL of LV solution. The volume for each elution fraction was 10 mL.

treatment of the LV material is required for SXC as this simplifies and accelerates the downstream process.

3.5. Remaining PEG concentration in the eluate

The remaining PEG concentration in SXC eluate fractions is an important aspect to analyze since PEG poses immunogenicity concerns and should be cleared from the final drug product [53,54]. The PEG concentration of the SXC eluate was not determined in previous publications and is reported in this study for the first time. We analyzed the PEG 4000 concentration of five elution fractions of 10 mL each using a modified Dragendorff reagent. The PEG concentration decreased as the elution fraction increased (Fig. 8). Presumably, these are the PEG molecules that were contained in the dead volume of the device and were washed out as a result. For purification by SXC, two fractions (20 mL) were typically collected because most LV is recovered in these first two fractions, as depicted in Fig. 7E and 7F. For the first two fractions, this resulted in an average PEG concentration of 7.6 g·L^{-1}, which is about 6.1% of the PEG concentration used during loading; this corresponds to 152 mg PEG per 8.61×10^{11} viral particles. Since only about 6% of the starting PEG concentration was present in the first two fractions, this indicates that PEG does not bind to the membrane and is removed in the flow through and wash fractions. In this case, the biomolecules of interest, LV, are not PEGylated; some PEG is still present in the eluate and must be removed in subsequent DSP steps. Buffer exchange and concentration are typically performed after the purification step by ultrafiltration and diafiltration. Membranes with a molecular weight cut-off (MWCO) of 100 to 750 kDa [3] are used for LV concentration. The MWCO defines the lowest molecular weight at which more than 90% of the target molecule, in this case, the LV is retained. For viruses the molecular weight is not as relevant as diameter, therefore the best MWCO is given for the virus diameter [55]. Since PEG is about 20-times smaller compared to LV (2.5 nm gyration radius for PEG 4000 and 100 nm diameter for LV), it is expected that PEG is washed out in the permeate during ultrafiltration. For example, if retention of PEG is desired an MWCO of 1 kDa would be selected which is 100 to 750-times smaller than the MWCO employed for LV. It is preferable to select a smaller PEG size as it can be removed more easily as opposed to larger PEG sizes. For pharmaceutical purposes, the detection of residual PEG of the final product remains necessary.

4. Conclusion

The demand for efficient LV bioprocessing is increasing and emphasizes the need for downstream process strategies for fragile enveloped viral vectors like LV. The purification step is considered one of the main challenges due to the low stability of LV. SXC has great potential for overcoming the current bottleneck. In this study, we successfully identified optimal process parameters for SXC of lentiviral vector purification. The ideal process conditions for performing SXC to purify LV are 12.5% PEG 4000, and a flow rate between 6 and 7 mL·min^{-1} for the specific membrane and device used in this study. Under these conditions, we achieved the highest LV particle recoveries and infectious recoveries of 86% and 88%, respectively. At the same time, high protein and dsDNA removal rates were observed at 81% and 79%, respectively. We defined the maximal loading capacity for the device used as 7.5×10^{12} lentiviral particles and showed that a concentration of the LV can be achieved when the first 20 mL of the eluate are collected. Moreover, we discussed pressure concerns in detail. The maximum pressure of the device and the pressure increase during loading must be considered during the selection of process parameters. Overloading the membrane is critical as adequate LV elution was not possible after the maximum pressure was reached. The remaining PEG concentration in the eluate was investigated. Further experiments are required to analyze the removal of the remaining PEG in the subsequent downstream processing steps. Given the results presented, SXC demonstrates a high potential for purification of LV and other enveloped viral vectors. A more in-depth mechanistic understanding of the SXC principle is required to develop a successful scale-up model of this method.

Declaration of Competing Interest

The authors declare that they have no known competing financial interests or personal relationships that could have appeared to influence the work reported in this paper.

CRediT authorship contribution statement

Jennifer J. Labisch: Conceptualization, Methodology, Investigation, Formal analysis, Visualization, Writing – original draft. **Meriem Kassar:** Methodology, Formal analysis, Writing – review & editing. **Franziska Bollmann:** Supervision, Writing – review & editing. **Angela Valentic:** Supervision, Writing – review & editing. **Jürgen Hubbuch:** Supervision. **Karl Pflanz:** Supervision, Project administration.

Acknowledgements

References

[1] John Wiley & Sons, IncGene Therapy Clinical Trials Worldwide, John Wiley & Sons, Inc, Hoboken, NJ, USA, 2021 Journal of Gene Medicine https://a873679.fmphost.com/fmi/webd/GTCT Accessed 11 November 2021.

[2] J. Rininger, A. Fennell, L. Schoukroun-Barnes, C. Peterson, J. Speidel, Capacity analysis for viral vector manufacturing: is there enough? BioProcess Int. 17 (2019).

[3] C. Perry, A.C.M.E. Rayat, Lentiviral vector bioprocessing, Viruses 13 (2021), doi:10.3390/v13020268.

[4] A.S. Moreira, D.G. Cavaco, T.Q. Faria, P.M. Alves, M.J.T. Carrondo, C. Peixoto, Advances in lentivirus purification, Biotechnol. J. (2020) e2000019, doi:10.1002/biot.202000019.

[5] M. Bauler, J.K. Roberts, C.C. Wu, B. Fan, F. Ferrara, B.H. Yip, S. Diao, Y.I. Kim, J. Moore, S. Zhou, M.M. Wielgosz, B. Ryu, R.E. Throm, Production of lentiviral vectors using suspension cells grown in serum-free media, Mol. Ther. Methods Clin. Dev. 17 (2020) 58–68, doi:10.1016/j.omtm.2019.11.011.

[6] A.J. Valkama, I. Oruetxebarria, E.M. Lipponen, H.M. Leinonen, P. Käyhty, H. Hynynen, V. Turkki, J. Malinen, T. Miinalainen, T. Heikura, N.R. Parker, S. Ylä-Herttuala, H.P. Lesch, Development of large-scale downstream processing for lentiviral vectors, Mol. Ther. Methods Clin. Dev. 17 (2020) 717–730, doi:10.1016/j.omtm.2020.03.025.

[7] H.B. Olgun, H.M. Tasyurek, A.D. Sanlioglu, S. Sanlioglu, High-grade purification of third-generation HIV-based lentiviral vectors by anion exchange chromatography for experimental gene and stem cell therapy applications, Methods Mol. Biol. 1879 (2019) 347–365, doi:10.1007/7651_2018_154.

[8] S. Tinch, K. Szczur, W. Swaney, L. Reeves, S.R. Witting, A scalable lentiviral vector production and purification method using Mustang Q chromatography and tangential flow filtration, Methods Mol. Biol. 1937 (2019) 135–153, doi:10.1007/978-1-4939-9065-8_8.

[9] A.S. Moreira, T.Q. Faria, J.G. Oliveira, A. Kavara, M. Schofield, T. Sanderson, M. Collins, R. Gantier, P.M. Alves, M.J.T. Carrondo, C. Peixoto, Enhancing the purification of lentiviral vectors for clinical applications, Sep. Purif. Technol. 274 (2021) 118598, doi:10.1016/j.seppur.2021.118598.

[10] M. Segura, A. Kamen, P. Trudel, A. Garnier, A novel purification strategy for retrovirus gene therapy vectors using heparin affinity chromatography, Biotechnol. Bioeng. 90 (2005) 391–404, doi:10.1002/bit.20301.

[11] M.M. Segura, A. Garnier, Y. Durocher, H. Coelho, A. Kamen, Production of lentiviral vectors by large-scale transient transfection of suspension cultures and affinity chromatography purification, Biotechnol. Bioeng. 98 (2007) 789–799, doi:10.1002/bit.21467.

[12] M. Zhao, M. Vandersluis, J. Stout, U. Haupts, M. Sanders, R. Jacquemart, Affinity chromatography for vaccines manufacturing: finally ready for prime time? Vaccine 37 (2019) 5491–5503, doi:10.1016/j.vaccine.2018.02.090.

[13] K. Ye, S. Jin, M.M. Ataai, J.S. Schultz, J. Ibeh, Tagging retrovirus vectors with a metal binding peptide and one-step purification by immobilized metal affinity chromatography, J. Virol. 78 (2004) 9820–9827, doi:10.1128/JVI.78.18.9820-9827.2004.

[14] M.C. Cheeks, N. Kamal, A. Sorrell, D. Darling, F. Farzaneh, N.K.H. Slater, Immobilized metal affinity chromatography of histidine-tagged lentiviral vectors using monolithic adsorbents, J. Chromatogr. A 1216 (2009) 2705–2711, doi:10.1016/j.chroma.2008.08.029.

[15] J.H. Yu, D.V. Schaffer, Selection of novel vesicular stomatitis virus glycoprotein variants from a peptide insertion library for enhanced purification of retroviral and lentiviral vectors, J. Virol. 80 (2006) 3285–3292, doi:10.1128/JVI.80.7.3285-3292.2006.

[16] R. Chen, N. Folarin, V.H.B. Ho, D. McNally, D. Darling, F. Farzaneh, N.K.H. Slater, Affinity recovery of lentivirus by diaminopelargonic acid mediated desthiobiotin labelling, J. Chromatogr. B Anal. Technol. Biomed. Life Sci. 878 (2010) 1939–1945, doi:10.1016/j.jchromb.2010.05.019.

[17] L. Mekkaoui, F. Parekh, E. Kotsopoulou, D. Darling, G. Dickson, G.W. Cheung, L. Chan, K. MacLellan-Gibson, G. Mattiuzzo, F. Farzaneh, Y. Takeuchi, M. Pule, Lentiviral vector purification using genetically encoded biotin mimic in packaging cell, Mol. Ther. Methods Clin. Dev. 11 (2018) 155–165, doi:10.1016/j.omtm.2018.10.008.

[18] F. Higashikawa, L. Chang, Kinetic analyses of stability of simple and complex retroviral vectors, Virology 280 (2001) 124–131, doi:10.1006/viro.2000.0743.

[19] J.J. Labisch, G.P. Wiese, K. Barnes, F. Bollmann, K. Pflanz, Infectious titer determination of lentiviral vectors using a temporal immunological real-time imaging approach, PLoS ONE 16 (2021) e0254739, doi:10.1371/journal.pone.0254739.

[20] O.W. Merten, M. Schweizer, P. Chahal, A. Kamen, Manufacturing of viral vectors: part II. Downstream processing and safety aspects, Pharm. Bioprocess. 2 (2014) 237–251, doi:10.4155/PBP.14.15.

[21] S.L. Williams, D. Nesbeth, D.C. Darling, F. Farzaneh, N.K.H. Slater, Affinity recovery of moloney murine leukaemia virus, J. Chromatogr. B Anal. Technol. Biomed. Life Sci. 820 (2005) 111–119, doi:10.1016/j.jchromb.2005.03.016.

[22] T. Rodrigues, M.J.T. Carrondo, P.M. Alves, P.E. Cruz, Purification of retroviral vectors for clinical application: biological implications and technological challenges, J. Biotechnol. 127 (2007) 520–541, doi:10.1016/j.jbiotec.2006.07.028.

[23] J. Lee, H.T. Gan, S.M.A. Latiff, C. Chuah, W.Y. Lee, Y.S. Yang, B. Loo, S.K. Ng, P. Gagnon, Principles and applications of steric exclusion chromatography, J. Chromatogr. A 1270 (2012) 162–170, doi:10.1016/j.chroma.2012.10.062.

[24] P. Gagnon, P. Toh, J. Lee, High productivity purification of immunoglobulin G monoclonal antibodies on starch-coated magnetic nanoparticles by steric exclusion of polyethylene glycol, J. Chromatogr. A 1324 (2013) 171–180, doi:10.1016/j.chroma.2013.11.039.

[25] P. Marichal-Gallardo, M.M. Pieler, M.W. Wolff, U. Reichl, Steric exclusion chromatography for purification of cell culture-derived influenza A virus using regenerated cellulose membranes and polyethylene glycol, J. Chromatogr. A 1483 (2017) 110–119, doi:10.1016/j.chroma.2016.12.076.

[26] K. Lothert, G. Sprick, F. Beyer, G. Lauria, P. Czermak, M.W. Wolff, Membrane-based steric exclusion chromatography for the purification of a recombinant baculovirus and its application for cell therapy, J. Virol. Methods 275 (2020) 113756, doi:10.1016/j.jviromet.2019.113756.

[27] K. Lothert, F. Pagallies, T. Feger, R. Amann, M.W. Wolff, Selection of chromatographic methods for the purification of cell culture-derived Orf virus for its application as a vaccine or viral vector, J. Biotechnol. 323 (2020) 62–72, doi:10.1016/j.jbiotec.2020.07.023.

[28] P. Marichal-Gallardo, K. Börner, M.M. Pieler, V. Sonntag-Buck, M. Obr, D. Bejarano, M.W. Wolff, H.G. Kräusslich, U. Reichl, D. Grimm, Single-use capture purification of adeno-associated viral gene transfer vectors by membrane-based steric exclusion chromatography, Hum. Gene Ther. 32 (2021) 959–974, doi:10.1089/hum.2019.284.

[29] C. Wang, S. Bai, S.P. Tao, Y. Sun, Evaluation of steric exclusion chromatography on cryogel column for the separation of serum proteins, J. Chromatogr. A 1333 (2014) 54–59, doi:10.1016/j.chroma.2014.01.059.

[30] K. Lothert, F. Pagallies, F. Eilts, A. Sivanesapillai, M. Hardt, A. Moebus, T. Feger, R. Amann, M.W. Wolff, A scalable downstream process for the purification of the cell culture-derived Orf virus for human or veterinary applications, J. Biotechnol. 323 (2020) 221–230, doi:10.1016/j.jbiotec.2020.08.014.

[31] S. Asakura, F. Oosawa, On interaction between two bodies immersed in a solution of macromolecules, J. Chem. Phys. 22 (1954) 1255–1256, doi:10.1063/1.1740347.

[32] A. Vrij, Polymers at interfaces and the interactions in colloidal dispersions, Pure Appl. Chem. 4 (1976) 471–483, doi:10.1351/pac197648040471.

[33] Q. He, Investigation of stabilization mechanisms for colloidal suspension using nanoparticles. Electronic Theses and Dissertations, 2014. 10.18297/etd/593.

[34] H.N.W. Lekkerkerker, R. Tuinier, Colloids and the Depletion Interaction, Springer, Netherlands, Dordrecht, 2011, doi:10.1007/978-94-007-1223-2.

[35] R. Tuinier, J. Rieger, C.G. de Kruif, Depletion-induced phase separation in colloid–polymer mixtures, Adv. Colloid Interface Sci. 103 (2003) 1–31, doi:10.1016/S0001-8686(02)00081-7.

[36] J.J. Labisch, F. Bollmann, M.W. Wolff, K. Pflanz, A new simplified clarification approach for lentiviral vectors using diatomaceous earth improves throughput and safe handling, J. Biotechnol. (2021) 11–20, doi:10.1016/j.jbiotec.2020.12.004.

[37] J.A. Tolk, *Mikrofiltrationsmembranen Auf Basis regenerierter Cellulose*. Dissertation, Hannover, 2017.

[38] P. Escarpe, N. Zayek, P. Chin, F. Borellini, R. Zufferey, G. Veres, V. Kiermer, Development of a sensitive assay for detection of replication-competent recombinant lentivirus in large-scale HIV-based vector preparations, Mol. Ther. 8 (2003) 332–341, doi:10.1016/S1525-0016(03)00167-9.

[39] J. Ruscic, C. Perry, T. Mukhopadhyay, Y. Takeuchi, D.G. Bracewell, Lentiviral vector purification using nanofiber ion-exchange chromatography, Mol. Ther. Methods Clin. Dev. 15 (2019) 52–62, doi:10.1016/j.omtm.2019.08.007.

[40] K. Lothert, A.F. Offersgaard, A.F. Pihl, C.K. Mathiesen, T.B. Jensen, G.P. Alzua, U. Fahnøe, J. Bukh, J.M. Gottwein, M.W. Wolff, Development of a downstream process for the production of an inactivated whole hepatitis C virus vaccine, Sci. Rep. 10 (2020) 16261, doi:10.1038/s41598-020-72328-5.

[41] M.D. Hein, H. Kollmus, P. Marichal-Gallardo, S. Püttker, D. Benndorf, Y. Genzel, K. Schughart, S.Y. Kupke, U. Reichl, OP7, a novel influenza A virus defective interfering particle: production, purification, and animal experiments demonstrating antiviral potential, Appl. Microbiol. Biotechnol. 105 (2021) 129–146, doi:10.1007/s00253-020-11029-5.

[42] F. Matter, A.L. Luna, M. Niederberger, From colloidal dispersions to aerogels: how to master nanoparticle gelation, Nano Today 30 (2020) 100827, doi:10.1016/j.nantod.2019.100827.

[43] M. Baumgaertel, N. Willenbacher, The relaxation of concentrated polymer solutions, Rheol. Acta 35 (1996) 168–185, doi:10.1007/BF00396044.

[44] M.Z. Jora, M.V.C. Cardoso, E. Sabadini, Dynamical aspects of water-poly(ethylene glycol) solutions studied by 1H NMR, J. Mol. Liq. 222 (2016) 94–100, doi:10.1016/j.molliq.2016.06.101.

[45] G. Böhme, Strömungsmechanik Nichtnewtonscher Fluide, 2nd ed., Vieweg+Teubner Verlag, Wiesbaden, 2000, doi:10.1007/978-3-322-80140-1.

[46] M. Rubinstein, R.H. Colby, Polymer Physics, Oxford Univ. Press, Oxford, 2014.

[47] V. Bandeira, C. Peixoto, A.F. Rodrigues, P.E. Cruz, P.M. Alves, A.S. Coroadinha, M.J.T. Carrondo, Downstream processing of lentiviral vectors: releasing bottlenecks, Hum, Gene Ther. Methods 23 (2012) 255–263, doi:10.1089/hgtb.2012.059.

[48] R.H. Kutner, S. Puthli, M.P. Marino, J. Reiser, Simplified production and concentration of HIV-1-based lentiviral vectors using HYPERFlask vessels and anion exchange membrane chromatography, BMC Biotechnol. 9 (2009), doi:10.1186/1472-6750-9-10.

[49] S.S. Rane, R.J. Dearman, I. Kimber, S. Uddin, S. Bishop, M. Shah, A. Podmore, A. Pluen, J.P. Derrick, Impact of a heat shock protein impurity on the immunogenicity of biotherapeutic monoclonal antibodies, Pharm. Res. 36 (2019) 51, doi:10.1007/s11095-019-2586-7.

[50] B. Alberts, A. Johnson, J. Lewis, D. Morgan, M. Raff, K. Roberts, P. Walter, Molecular Biology of the Cell, 6th ed., Garland Science, New York, 2015.

[51] O.-.W. Merten, S. Charrier, N. Laroudie, S. Fauchille, C. Dugué, C. Jenny, M. Audit, M.A. Zanta-Boussif, H. Chautard, M. Radrizzani, G. Vallanti, L. Naldini, P. Noguiez-Hellin, A. Galy, Large-scale manufacture and characterization of a lentiviral vector produced for clinical *ex vivo* gene therapy application, Hum. Gene Ther. 22 (2011) 343–356, doi:10.1089/hum.2010.060.

[52] S. Yang, H. Tan, D. Yan, E. Nies, A.C. Shi, Effect of polydispersity on the depletion interaction in nonadsorbing polymer solutions, Phys. Rev. E Stat. Nonlinear Soft Matter Phys. 75 (2007) 61803, doi:10.1103/PhysRevE.75.061803.

[53] N. d'Avanzo, C. Celia, A. Barone, M. Carafa, L. Di Marzio, H.A. Santos, M. Fresta, Immunogenicity of polyethylene glycol based nanomedicines: mechanisms, clinical implications and systematic approach, Adv. Ther. 3 (2020) 1900170, doi:10.1002/adtp.201900170.

[54] M. Swierczewska, K.C. Lee, S. Lee, What is the future of PEGylated therapies? Expert Opin. Emerg. Drugs 20 (2015) 531–536, doi:10.1517/14728214.2015.1113254.

[55] R. Singh, Membrane Technology and Engineering for Water Purification (Second Edition), in: Application, Systems Design and Operation, 2015, pp. 1–80, doi:10.1016/B978-0-444-63362-0.00001-X.

14

4.4 Scaling up of steric exclusion membrane chromatography for lentiviral vector purification

Scale-up of steric exclusion chromatography remains a task yet to be solved. All published studies on SXC have been conducted on a laboratory scale. Only one large-scale approach was reported for an Orf virus purification using OH-monoliths, but results were not reproducible and the scale-up was immediately transferred from a small scale of a few milliliters up to 200 L without process understanding of the scale-up [137].
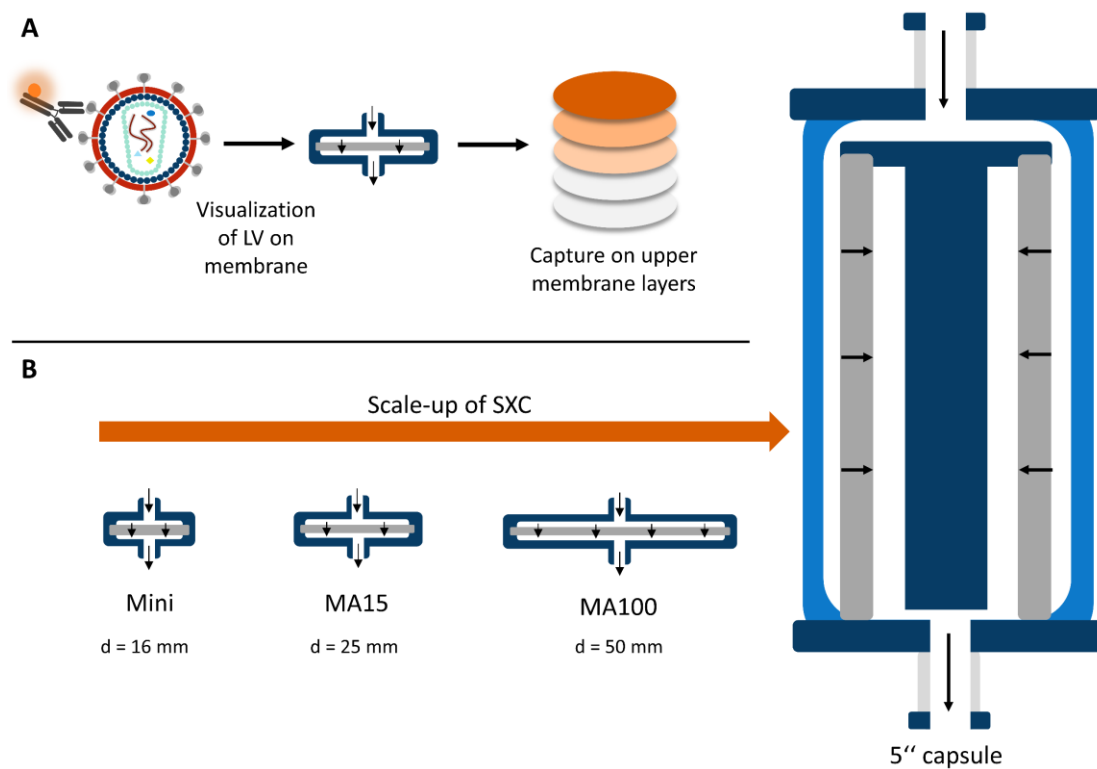
Figure 12: (A) Visualization of labeled LV on the membrane and (B) scale-up of steric exclusion chromatography using four different device scales.

In the fourth part of this work, the scale-up requirements of SXC were investigated. This manuscript is currently submitted to the Journal Membranes (MDPI) and the general concepts of this work are registered as a patent application (patent application number: S15837EU). The first and fundamental part of this work was the visualization of the LV on the stationary phase membrane after the loading and washing step, before the elution (Fig. 12). This revealed that the LV is mainly located on the upper two membrane layers. This is contrary to the former assumption that the whole membrane volume is used for the capture of the target molecule. This raises the question of how to scale up an SXC membrane device, since

increasing the membrane layer number would not result in a capacity increase. Consequently, an increase in the membrane surface area of the first membrane layer must be targeted.

The identified optimal process conditions (PEG buffer composition, flow rate) for the small-scale device that was used in the third part of this work, were applied to a device that had a four-fold larger membrane area. The LV recoveries were unexpectedly low indicating that the process conditions were not suitable for the larger device. As the SXC process is thermodynamically driven, and the flow rate was previously found to be a crucial factor, scaling of the flow rate was presumably the important factor in this case. Since the LV capture was observed at the upper membrane layers scaling the flow rate with the membrane surface area was attempted which would result in the same flow velocity through the pores if the fluid is equally distributed. It was found that when applying the same surface area-specific flow rate to the large device the LV recoveries increased significantly from about 10% at lower velocity to 73% at scaled velocity and were not significantly different from the recoveries obtained with the small device at the same surface area-specific flow rates. Moreover, the impurity removal was comparable between the device scales.

Another investigated aspect was the amount of loaded LV. No LV breakthrough was observed, however when the membrane was overloaded it was not possible to elute the LV anymore which presumably remained on the membrane. The configuration of the device lid highly affected liquid distribution on the membrane. A distributor structure that enables uniform liquid distribution is preferred, as the membrane area is then uniformly loaded with LV and this in turn led to higher LV recoveries and smaller standard deviations.

To further analyze the presented approach of scaling the flow rate according to the membrane surface area of the first layer, further scale-down experiments with an axial device and scale-up experiments with a radial 5'' capsule were performed. With the scaling approach of using a minimum surface-area specific flow rate, reproducible SXC LV recoveries for four different module sizes with an overall scaling factor of 98 were achieved. Further, the results indicate that a certain critical, potentially minimum surface area-specific flow rate is necessary to achieve reproducible LV recoveries for the four different device scales tested.

All in all, in this chapter the scale-up of SXC with a scaling factor of 98 was realized by scaling the flow rate related to the surface area of the first membrane layer of the chromatography units.

Article

Scaling Up of Steric Exclusion Membrane Chromatography for Lentiviral Vector Purification

Jennifer Julia Labisch [1,2,*] ⓘ, **Richard Paul** [1,3] ⓘ, **G. Philip Wiese** [1,3] ⓘ and **Karl Pflanz** [1]

[1] Lab Essentials Applications Development, Sartorius Stedim Biotech GmbH, August-Spindler-Straße 11, 37079 Göttingen, Germany
[2] Institute of Technical Chemistry, Leibniz University Hannover, Callinstraße 5, 30167 Hannover, Germany
[3] Chemical Process Engineering, Rheinisch-Westfälische Technische Hochschule (RWTH) Aachen University, Forckenbeckstraße 51, 52074 Aachen, Germany
* Correspondence: jennifer.labisch@sartorius.com

Abstract: Lentiviral vectors (LVs) are widely used in clinical trials of gene and cell therapy. Low LV stability incentivizes constant development and the improvement of gentle process steps. Steric exclusion chromatography (SXC) has gained interest in the field of virus purification but scaling up has not yet been addressed. In this study, the scaling up of lentiviral vector purification by SXC with membrane modules was approached. Visualization of the LVs captured on the membrane during SXC showed predominant usage of the upper membrane layer. Furthermore, testing of different housing geometries showed a strong influence on the uniform usage of the membrane. The main use of the first membrane layer places a completely new requirement on the scaling of the process and the membrane modules. When transferring the SXC process to smaller or larger membrane modules, it became apparent that scaling of the flow rate is a critical factor that must be related to the membrane area of the first layer. Performing SXC at different scales demonstrated that a certain critical minimum surface area-dependent flow rate is necessary to achieve reproducible LV recoveries. With the presented scaling approach, we were able to purify 980 mL LVs with a recovery of 68%.

Keywords: steric exclusion chromatography; membrane chromatography; scaling up of membrane modules; lentiviral vector purification; polyethylene glycol; depletion potential

1. Introduction

Lentiviral vectors (LVs) have long been used in the biopharmaceutical industry, primarily in gene-modified cell therapy [1,2]. Stable integration of the LV genome and long-term expression of the transgene have achieved successful therapeutic outcomes for certain diseases, such as acute lymphoblastic leukemia (ALL) [3]. The first pediatric patient with ALL that was treated with LV-based gene-modified cell therapy has now been cancer-free for ten years [4]. In clinical trials, LVs are used to treat a wide range of diseases, including cancers, immune disorders, metabolic disorders, and rare congenital diseases [3,5]. New potential applications for LVs have emerged. Recently, the use of LVs gained importance as a possible vaccination platform that uses integrating as well as non-integrating LVs to target infectious diseases [6,7]. The broad range of diseases that can be treated with LVs and emerging applications will lead to an increased need for efficient LV bioprocessing [8]. Many challenges are faced during LV manufacturing, especially purification (which requires further optimization) [9].

A study on the use of steric exclusion chromatography (SXC) for LV purification was recently published [10]. A variety of viruses have been previously purified by SXC, including baculovirus [11], Orf virus [12,13], AAV [14], and influenza A virus [15]. SXC is a gentle purification method offering high potential for the purification of large, enveloped, fragile viral vectors as it does not require any chemical interaction between the target species and the stationary phase and preserves viral infectivity. The basic principle of SXC is based

on depletion interaction [16] and has been discussed in previous publications [10,17,18]. Briefly, the viral vector feed solution is mixed with PEG buffer and loaded onto a hydrophilic stationary phase, e.g., a regenerated cellulose membrane. Upon the addition of PEG, depletion zones around the viral particles and the stationary phase are formed. The resulting depletion interaction results in the association of viral vectors with the stationary phase. The viral particles are eluted with a PEG-free buffer, reserving the association of the viral particles with the stationary phase.

So far, SXC has only been performed at small scales. SXC studies relying on membranes as a stationary phase used stacked membrane layers assembled in their housing (e.g., a stainless-steel holder for multi-use or an overmolded plastic housing for single-use) so that the flow was directed frontally from above, resulting in a dead-end flow [19]. Membrane devices of a diameter between 13 mm and 25 mm with 10 to 20 layers of stacked membranes have been employed in previous publications on SXC [11,12,14,15,20–23]. However, a deep mechanistic understanding of the requirements of the membrane device is lacking, especially concerning the potential scaling up of SXC. Both the location of viral vector association in the membrane and the effect of different membrane device geometries or sizes on the performance of SXC have yet to be investigated, leaving unanswered questions as to how scaling up could be achieved.

In this study, we show LV location on a stabilized cellulose membrane which served as a stationary phase. Based on these results, we developed a scaling up approach with different device scales and geometries. We reveal the critical aspect of a scaled flow rate, as well as the importance of module design, for successful LV recovery using SXC in a scale-up format.

2. Materials and Methods

2.1. Lentiviral Vector Production, Harvest, and Clarification

Third-generation lentiviral vectors were produced by transient transfection of suspension HEK293T/17 SF cells (ACS-4500, ATCC) with four plasmids in a UniVessel® 10 L bioreactor operated by a BIOSTAT® B-DCU (Sartorius, Göttingen, Germany). The pH electrode was calibrated, and the vessel was assembled (containing a 2 × 3 blade segment impeller, ring-up sparger) and filled with water equivalent to 30% of its volume. The bioreactor was autoclaved at 121 °C. After autoclaving, the bioreactor was emptied and filled to 80% of the final volume with FreeStyle medium (Thermo Fisher Scientific, Waltham, MA, USA) + 0.0002% Antifoam C (Sigma Aldrich, St. Louis, MO, USA) + 1x insulin-transferrin-selenium (Thermo Fisher Scientific, Waltham, MA, USA). The bioreactor was connected to the BIOSTAT®, the DO probe was calibrated, and the pH electrode was re-calibrated. Cultivation setpoints were the following: stirrer speed 202 rpm, 30% DO, 37 °C, pH 7.1. Gassing rates and gassing cascades are given in the supplementary section. The bioreactor was left overnight to adjust pH and pO2. The next day, the bioreactor was inoculated with 9% of the final bioreactor volume to a final viable cell density of 0.3×10^6 cells·mL^{-1}. After inoculation, and once daily onwards, the bioreactor was sampled for viable cell density and viability determination with a Cedex HiRes (Roche, Basel, Switzerland) and offline pH measurement. The pH probe was re-calibrated when a difference of >0.1 was detected between the externally and internally measured pH. Three days after inoculation, transfection was performed. Subsequently, 0.5 mg of total plasmid DNA was used per liter of final culture volume in a mass ratio of 5:2.5:1:1 (pALD-Lenti-GFP:pALD-GagPol:pALD-VSV-G:pALD-REV1; Aldevron, Fargo, ND, USA) and was prepared in FreeStyle medium without additives. In a separate flask, 4 mL of PEIpro per mg of total plasmid DNA was diluted in FreeStyle medium (5% of the final bioreactor volume each). The two solutions were mixed and, after incubation for 15 min, added to the bioreactor. The following reagents were added to the bioreactor 18 h after transfection: an anti-clumping agent (1:500 (*v/v*)), the enhancer sodium butyrate (final concentration of 10 mM, Sigma Aldrich, St. Louis, MO, USA), and 1 mL of 2% Antifoam C. A nuclease treatment for nucleic acid digestion was performed with 10 U·mL^{-1} DENARASE® (c-Lecta, Leipzig, Germany) and 2 mM

MgCl$_2$ (final concentrations) directly in the bioreactor for 1 h at 37 °C. After nucleic acid digestion, the cell culture broth (which contained the lentiviral vector) was clarified using Sartoclear Dynamics® Lab V50 (0.45 µm polyethersulfone membrane version) with 5 g/L of diatomaceous earth (Sartorius, Göttingen, Germany). The lentiviral vector was aliquoted and stored at −80 °C.

2.2. Steric Exclusion Chromatography

2.2.1. Membrane and Housing

An uncharged stabilized cellulose membrane Hydrosart® 10242 (Sartorius, Göttingen, Germany) was used as a stationary phase. For crosslinking, diglycidyl ethers were used as described in detail in [24]. Crosslinking leads to a change in the chemical nature and thus the properties of the membrane, in particular the swelling properties. Pure regenerated cellulose membranes adsorb about 16% of water and thus change its expansion by about 16%. After crosslinking, swelling is reduced by more than half. As a result, the membrane is easier to install and use in the device. Membrane production, characterization, and integrity testing of membrane devices have been previously described by Labisch et al. [10]. The membrane lot used in this study had a thickness of 220 µm per layer and a mean flow pore size of 2.5–3 µm. Stacks of 5 membrane layers were incorporated into the respective polypropylene module housing and either overmolded with an Arburg 221-75-350 injection molding machine or incorporated into a stainless-steel holder so that membranes could be accessed easily during LV visualization experiments (Section 2.3.6). The recommended maximum pressure for axial devices is 0.6 MPa (0.4 MPa for the radial 5″ device). SXC devices are shown in Figure 1, and specifications are listed in Table 1.
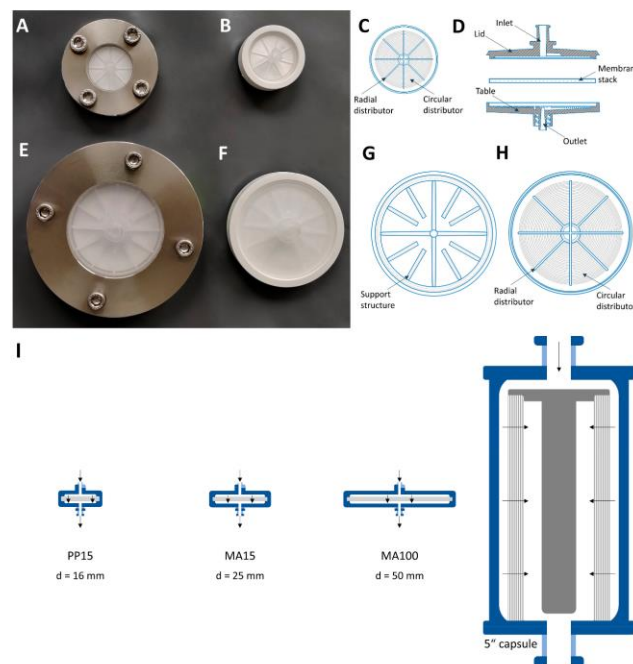
Figure 1. SXC membrane devices. MA15 in a (**A**) stainless-steel holder or (**B**) overmolded. (**C**) The inner structure of the MA15 lid and table with radial and circular distribution channels and (**D**) a cross-sectional view of an SXC membrane device. MA100 in a (**E**) stainless-steel holder or (**F**) overmolded. (**G**) Inner support geometry of the MA100 lid and (**H**) structure of the MA100 table with radial and circular distribution channels. (**I**) Device size comparison of the scale-up approach of SXC using 4 different modules.

Table 1. Specifications for SXC chromatography with different device scales.

Specification	PP15	MA15	MA100	5″ Capsule
Equilibration volume	8 mL	20 mL	80 mL	2 L
Loading volume	20 mL	40 mL	160 mL or higher	1.96 L
Loaded LV volume	10 mL	25 mL	80 mL or higher	0.98 L
Wash volume	8 mL	15 mL	60 mL	2 L
Elution volume	10 mL	20 mL	80 mL or higher	0.98 L
Device geometry	axial	axial	axial	radial
Diameter of axial devices	16 mm	25 mm	50 mm	-
Surface area per layer	$2.01\ cm^2$	$4.91\ cm^2$	$19.63\ cm^2$	$192\ cm^2$
Membrane volume	$0.22\ cm^3$	$0.565\ cm^3$	$2.257\ cm^3$	$75\ cm^3$
Scaling factor	1	2.5	10	98

The membrane housing of the MA100 used in this study has a lid and a table with distinct geometries. The lid has a coarse structure with thicker bridges that prevent the membrane from pressing tightly against it which is intended to give the liquid room to spread (Figure 1G). The table has 8 radial distribution channels and 20 circular distribution channels that collect the fluid toward the outlet (Figure 1H). The PP15 and MA15 devices have the same distribution channel geometry in the lid and table (Figure 1C).

2.2.2. Chromatography Setup and Procedure

An ÄKTA™ avant 150 (Cytiva Life Sciences, Uppsala, Sweden) chromatography system with inline UV (280 nm) and conductivity monitoring operated by UNICORN 7.1 software was used to purify the lentiviral vectors via SXC using the PP15, MA15, and MA100 modules. For the large-scale SXC experiments with the 5″ capsule (Sartorius, Göttingen, Germany) and 4 mm bed height (approx. 18 layers), a multi-use rapid cycling chromatography system (MU RCC, Sartorius, Göttingen, Germany) was used with a PuraLev® i30SU pump (Levitronix, Zürich, Switzerland) installed inline that was operated at 600 rpm, which served as a dynamic mixer for the buffers and feed solution. All chemicals (Tris, hydrochloric acid (HCl), sodium chloride (NaCl), PEG 4000) were purchased from Carl Roth (Karlsruhe, Germany). Buffers were prepared in ultrapure water from the Arium® Pro (Sartorius, Göttingen, Germany). Two buffers were prepared: (1) a 50 mM Tris-HCl buffer with 150 mM NaCl, pH 7.4 (A1), and (2) 25% PEG 4000 in 50 mM Tris-HCl, 150 mM NaCl, pH 7.4 (B1). In the following section, the buffers are referred to as Tris buffer and PEG buffer. The same buffer compositions were used for all experiments based on the buffer optimization experiments previously published [10].

The volumes for equilibration, loading, wash, and elution for all device scales are listed in Table 1. On the day of the experiment, the LV sample was thawed in a water bath at 37 °C until only small ice clumps remained. The sample was then stored at 4 °C until use (30–60 min). The entire LV solution was used on the day of thawing. Different LV batches were used for different experiments; therefore, the respective titer of each LV sample is indicated in the results section. The LV solution was kept on ice during the experiments and the fractions were collected and cooled at 4 °C (automatic fractionation with the ÄKTA avant and manual fractionation with the MU RCC). The membrane device was first equilibrated with the Tris buffer and the PEG buffer, which were mixed inline at a ½ dilution. The PEG buffer with a concentration of 25% (w/v) PEG 4000 then reached a final PEG concentration of 12.5%. The LV sample (A2) was loaded by being mixed inline with the PEG buffer at a ½ dilution in the downflow direction. The loading volume varied between experiments with the MA100 device and is therefore provided in the results section for each experiment. The membrane was washed with Tris buffer and PEG buffer, which were mixed inline at a ½ dilution. The LVs were eluted with Tris buffer in the upflow direction. Fractions were aliquoted and stored at −80 °C for analysis. The flow rates and SXC membrane device design varied depending on the experiment and are mentioned in the respective results section. To perform SXC experiments with the

ÄKTA chromatography system at high flow rates (<10 mL·min^{-1}), an open configuration was used for the chromatography system. In this open configuration the fractions were manually collected directly after the installed chromatography device, without running through the whole system to reduce the pressure. A new membrane device was used for each run (single use).

2.3. Analytics

2.3.1. Infectious Titer Determination

The infectious LV titer was quantified with the Incucyte® S3 live-cell analysis system (Sartorius, Göttingen, Germany). Adherent HEK293T cells (ACC 635, DSMZ) were infected with serially diluted LV samples, and GFP expression was measured through real-time imaging as described in detail by Labisch et al. [25] with the following modifications: no staining was performed and transgene expression (GFP) was read out 48 h post-infection. Samples were analyzed in duplicate.

2.3.2. Particle Titer Determination

The LV particle titer was quantified with an enzyme-linked immunosorbent assay (ELISA) using the QuickTiter™ Lentivirus titer kit (Cell Biolabs, San Diego, CA, USA) that quantifies the p24 capsid protein. Absorbance was read at 450 nm with a FLUOstar Omega plate reader (BMG Labtech, Ortenberg, Germany). The standard curve obtained was fitted by a second-degree polynomial. The p24 concentrations determined were converted into viral particle titers by assuming that 1.25×10^{7} LV particles contain 1 ng of p24 and 1 LV particle contains about 2000 molecules of p24 [26].

2.3.3. Total Protein Quantification

Total protein concentration was determined with the Pierce™ Coomassie Bradford protein assay kit (Thermo Fisher Scientific, Waltham, MA, USA) according to the manufacturer's instructions. Standards and samples were analyzed in duplicate in transparent 96-well microtiter plates (Greiner Bio-one, Kremsmünster, Austria). Absorbance was read at 595 nm with a microplate reader. The standard curve obtained was fitted by linear regression.

2.3.4. Total dsDNA Quantification

The total dsDNA amount (host cell and plasmid DNA) was quantified with the Quant-iT™ Pico-Green™ dsDNA assay (Thermo Fisher Scientific, Waltham, MA, USA) according to the manufacturer's instructions. Standards and samples were analyzed in duplicate in black 96-well microplates (Corning, Corning, NY, USA). The samples were excited at 480 nm, and fluorescence emission intensity was measured at 520 nm using a microplate reader. The standard curve obtained was fitted by linear regression.

2.3.5. SDS-PAGE and Silver Staining

Proteins were fractionated by SDS-PAGE in 4–15% Mini-PROTEAN® TGX Stain-Free protein gels (Bio-Rad, Hercules, CA, USA). SDS-PAGE was performed according to the manufacturer's instructions. Precision Plus protein standard (Bio-Rad) served as a marker. The gel was run at a constant voltage of 300 V for 15–20 min. Protein bands were visualized with a Pierce Silver Stain Kit (Thermo Fisher Scientific, Waltham, MA, USA).

2.3.6. Lentiviral Vector Visualization

Staining was performed to visualize the location of the LVs on the membrane before and after elution. The LV sample was incubated for 1 h at 4 °C with a mouse monoclonal antibody to VSV-G (F-6) labeled with Alexa Fluor® 546 (Santa Cruz Biotechnology, Santa Cruz, CA, USA) in a dilution of 1:2000. Five layers of the Hydrosart® membranes were placed between the table and lid of the chromatography device that was incorporated in the stainless-steel holder (Figure 1A,E). The screws were tightened to 3 Nm. The SXC run

was performed as described above and stopped after the wash step before elution. The membranes were separated and visualized with a UVP ChemStudio (Analytik Jena, Jena, Germany) by applying the green light source (550 nm), the ethidium bromide filter, and an exposure time of 60 s. An untreated membrane layer that was not incorporated into the membrane holder device was used as a negative control.

2.4. Statistical Analysis

The statistical significance of between-group differences was evaluated using an unpaired Student's *t*-test (two-tailed) in OriginPro® 2021 (OriginLab, Northampton, MA, USA). Where applicable, experiments were evaluated with MODDE Pro 13 (Sartorius, Göttingen, Germany).

3. Results and Discussion

3.1. Lentiviral Vector Visualization on a Membrane

To date, it is unclear where the target product (in this case, the LV) is located on the membrane after loading by SXC, and the literature lacks studies of particle localization in the stationary phase during SXC. Visualizing LVs on the stationary phase could contribute to the understanding of the SXC process and process requirements.

We stained lentiviral vectors with an anti-VSV-G antibody labeled with Alexa Fluor® 546 as described in Section 2.3.6. The labeled LVs were loaded on a membrane that was incorporated into an MA15 housing and placed in a stainless-steel holder (Figure 1A). SXC was performed using a PEG buffer with a final PEG 4000 concentration of 12.5% and a flow rate of 7 mL·min^{-1}. A volume of 50 mL was loaded, corresponding to a 25 mL LV solution with 1.5×10^{11} VP·mL^{-1}. The SXC runs were stopped either after the loading and wash step (Figure 2A) or after the elution step (Figure 2B) for optical visualization.
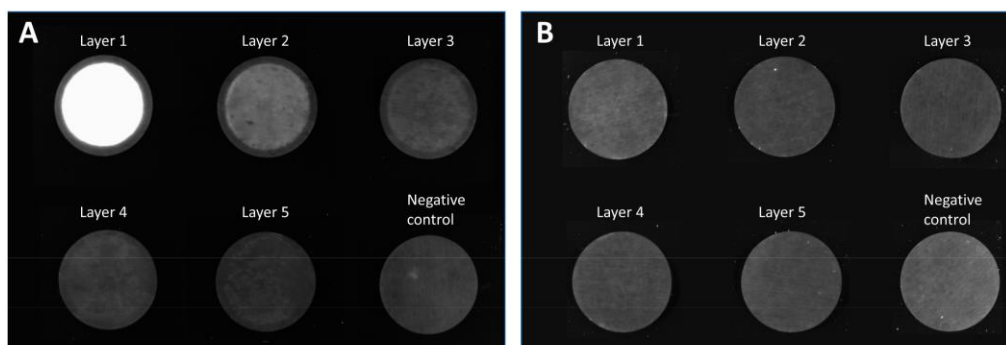
Figure 2. Membrane layers of an MA15 device after loading lentiviral vectors labeled with an anti-VSV-G Alexa Fluor® 546 antibody. Membrane layers were separated after the (**A**) loading and wash step of steric exclusion chromatography or (**B**) after the elution step. A membrane that was not incorporated into the device served as a negative control.

Figure 2 shows the visualization of captured viral vectors on the membrane after being loading by SXC. LV particles were mainly present on the first and second layers of the membrane. Some LV particles can be detected on layer three, but no fluorescence was detected on layers four or five. The particles were homogeneously distributed on the membrane layers. Only the clamping edge, which is not in contact with the liquid, was not stained accordingly. These findings indicate that with SXC, we capture very few viral particles in the depth of the unit. Therefore, using 15 layers—as is often described in the literature [11,15]—does not appear to offer any added value compared to the use of 5 layers. Furthermore, column volume, which is specified for other conventional membrane chromatography devices, plays a minor role in the SXC method. Although it is a

straightforward approach, visualization of the viral vectors on the membrane indicates that adding more membrane layers (thereby increasing the membrane volume) does not appear to be a valuable scaling method. The surface area of the first layer is a more important feature for SXC. We assume that once the first layer is saturated, the access to further layers is restrained, and a multilayer of LV particles is built that reduces pore size. Thus, a pressure increase is observed during loading, as previously reported [10,22]. After elution, no fluorescence was detected on the membrane, indicating that (almost) all LVs were eluted.

3.2. Identifying Critical Process Parameters for the Scaling Up of SXC

SXC has so far only been performed at small scales using axial membrane devices with a diameter of up to 25 mm. By increasing the membrane surface area four-fold (MA100 module), we aimed to identify critical process parameters for successful scaling up of the purification of lentiviral vectors via SXC. Previous research with a small-scale MA15 device determined 12.5% PEG 4000 as an ideal buffer for the purification of LVs with SXC [10]. Therefore, this buffer composition was used and not further modified in the following experiments. In the same study using the MA15, an optimal flow rate of 6–7 mL·min^{-1} (tested flow rate range 3–9 mL·min^{-1}) was identified, achieving infectious LV recovery above 80%. In a first attempt, we tested flow rates between 3–9 mL·min^{-1} using the MA100 device and an LV batch with a titer of 1.25×10^7 TU·mL^{-1}. Figure 3A shows that lower than expected infectious LV recoveries were observed. We concluded that the optimal flow rate for the MA100 device is not within this range.
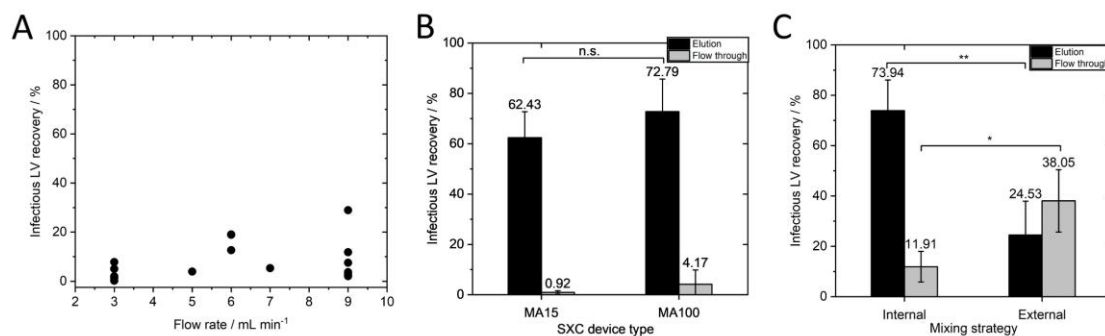
Figure 3. Identification of critical process parameters to achieve a high infectious LV recovery for SXC scale-up. (**A**) Infectious LV recovery for different flow rates between 3 and 9 mL·min^{-1}. (**B**) Infectious LV recoveries of MA15 and MA100 with the same surface area-dependent flow rate of 1.43 mL·min^{-1}·cm^{-2} (MA15 N = 6, MA100 N = 11). (**C**) Infectious LV recovery for internal and externally mixed LV-PEG-solution, N = 3. Data in B and C represent mean $\pm$ standard deviation. *p*-values are indicated as follows: * $p \leq 0.05$, ** $p \leq 0.01$, n.s.—not significant.

For membrane chromatography, the flow rate is typically given in membrane volumes per minute. As discussed in Section 3.1, scaling up by only increasing the membrane volume but not the surface area of the first membrane does not seem to be useful with respect to the surface-oriented capture of the vector particles. Thus, specification of the flow rate per membrane surface area (of one layer) would be more reasonable than flow rate per membrane volume. For this reason, we did not scale flow rate with membrane volume as a first attempt. It was shown in a previous study that scaling the flow rate according to membrane volume is not necessary for axial devices with the same diameter [10]. In the aforementioned study, MA15 devices with 5 and 10 membrane layers achieved LV recoveries that were not significantly different when applying the same flow rate of 7 mL·min^{-1}, which is the same surface area-dependent flow rate of 1.43 mL·min^{-1}·cm^{-2}. It should be noted that scaling with the surface-area dependent flow rate was still unknown and not discussed in the previous study, as no different device sizes were tested. This

parameter is investigated in our study for the first time. However, 7 mL·min^{-1} was half the flow rate in membrane volumes per minute for the 10-layer unit compared to the 5-layer unit (6.2 MV·min^{-1} for the 10-layer MA15 and 12.4 MV·min^{-1} for the 5-layer MA15). If flow rate had to be scaled with membrane volume, this would have been noticed in the experiment, and the non-significant differences indicated that this was not necessary. For this reason, the flow rates for the MA100 device were not adjusted according to membrane volume, though the same volumetric flow rates were used since an adjustment based on the membrane area of the first layer was only considered in the next step. Given the dynamic depletion flocculation process of SXC, we hypothesized that the flow rate is dependent on the surface area of one membrane layer. The previously determined optimal flow rate of 7 mL·min^{-1} for the MA15 device corresponds to a surface area-dependent flow rate of 1.43 mL·min^{-1}·cm^{-2}. We aimed to apply the same surface area-dependent flow rate for the MA100 device. As the membrane surface area of one layer is four times larger, a flow rate of 1.43 mL·min^{-1}·cm^{-2} for the MA100 device corresponds to 28 mL·min^{-1}.

However, the pressure limit was reached when applying 28 mL·min^{-1} with the viscous PEG buffer. The UV cell and fractionator of the chromatography system contribute to the pressure. To circumvent this technical limitation, we opened the chromatography system after the column position and fractionated manually. This adjustment allowed us to apply a flow rate of 1.43 mL·min^{-1}·cm^{-2} (28 mL·min^{-1}) for the MA100 device. We performed SXC runs with an LV batch with a titer of 1.73×10^7 TU·mL^{-1} at 1.43 mL·min^{-1}·cm^{-2} with the MA15 and MA100 device and detected no significant differences in infectious titer (Figure 3B). The MA100 yielded an infectious LV recovery of 72.79 ± 12.92%. These results confirm our hypothesis that the flow rate must be scaled to the surface area of one membrane layer. The flow velocity through the stationary phase seems to be a decisive factor in purification success. When the same flow rate in mL·min^{-1} is applied to the MA100 device, the same feed is distributed to a larger surface area and, thus, to a higher number of pores compared to the MA15 device. Since the average pore diameter remains unchanged, the flow velocity inside the pores decreases and falls below the optimal flow velocity inside the stationary phase to achieve efficient LV capture during loading and release during elution. Another possible explanation, recently discussed in [13], is that a limited spontaneous encounter for the LV and the stationary phase could lead to a less efficient depletion interaction. In our case, a certain flow rate through the membrane pores might be necessary to increase the probability of an encounter between the LVs and the stationary phase.

Internal and external mixing of the LV solution with PEG buffer was performed for the MA100 SXC runs as was previously performed for the MA15 runs [10]. Briefly, LV solution (titer of 1.64×10^7 TU·mL^{-1}) was mixed with PEG buffer in a flask with a magnetic stirrer. After 1 h of incubation at 4 °C, the sample was loaded onto the membrane (external mixing) or was loaded via pump A and pump B of the chromatography system and mixed in the dynamic mixer shortly before reaching the membrane device. Infectious LV recovery was significantly higher ($p \leq 0.01$) when internal mixing was performed (Figure 3C) than when external mixing was performed (73.94 ± 12.13% and 24.53 ± 13.43%, respectively). These findings support the results of Labisch et al. and Eilts et al., in which the same effect was observed for other module sizes [10,13]. Moreover, a significantly higher amount of LVs (38.05 ± 12.37%) was lost in the flow through ($p \leq 0.05$) when LVs were loaded after external mixing. The external mixing of PEG buffer with the LV solution and incubation could have led to LV aggregation as depletion interaction can occur between LVs and the stationary phase during the SXC loading step, as well as between the viral particles themselves [27]. Forming aggregates, the system's free energy is already reduced, leading to a less effective depletion interaction between the LV and the membrane and loss in the flow through. These observations underline the highly dynamic nature of this chromatography method, as already observed by the importance of flow rate.

Total protein and dsDNA removal using the MA15 and MA100 devices at the same surface area-dependent flow rate of 1.43 mL·min^{-1}·cm^{-2} was next investigated (Figure 4).

The total dsDNA and protein concentrations of the loading material and elution fractions are listed in Table 2.
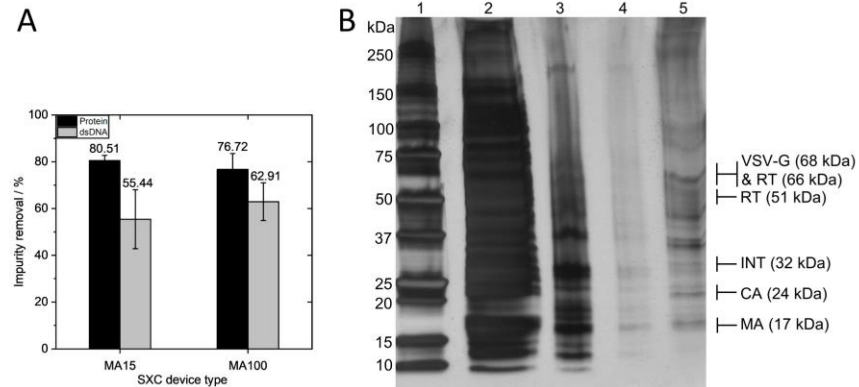

Figure 4. Impurity removal via steric exclusion chromatography. (**A**) Total protein and dsDNA removal using the MA15 and MA100 devices with the same surface area-dependent flow rate of 1.43 mL·min^{-1}·cm^{-2} (MA15 N = 6, MA100 N = 11). (**B**) SDS-PAGE gel with silver staining of SXC fractions: 1—marker, 2—loading material, 3—flow through, 4—wash, 5—elution. Protein bands refer to VSV-G envelope protein, reverse transcriptase (RT) subunit p51 and p66, integrase (INT), capsid (CA), and matrix (MA). Data in A represent mean ± standard deviation.

Table 2. Total protein and dsDNA concentration in loading material and elution fractions for SXC chromatography with the MA15 or MA100 device.

Device	Protein in Loading Material/µg·mL^{-1}	Protein in Elution Fraction/µg·mL^{-1}	dsDNA in Loading Material/ng·mL^{-1}	dsDNA in Elution Fraction/ng·mL^{-1}
MA15	268.45 ± 10.06	52.26 ± 5.65	283.49 ± 87.07	55.44 ± 12.58
MA100	253.38 ± 39.95	57.38 ± 15.15	356.35 ± 81.43	62.91 ± 8.06

Overall, high removal of proteins was observed, with 80.51 ± 2.22% (0.7 log removal) for the MA15 device and 76.72 ± 6.81% (0.64 log removal) for the MA100 device. A silver-stained SDS-PAGE gel confirmed the measurement, showing a high amount of protein contaminants in the loading material and the removal of the majority of the protein impurities in the flow through (Figure 4B). The elution fraction shows protein bands for the structural proteins of the lentiviral vector and little contaminating protein. Total dsDNA removal was 55.44 ± 12.58% (0.35 log removal) for the MA15 device and 62.91 ± 8.06% (0.43 log removal) for the MA100 device. These results demonstrate that comparable impurity removals are obtained for both device types. The effective removal of impurities derives from the pronounced size differences between the LV and the contaminating proteins and DNA, as discussed extensively elsewhere [10].

Next, we tested different loading volumes ranging from 100 to 700 mL (corresponding to 50 to 350 mL LV solutions) on the MA100 device. The LV batch had a titer of 1.35 × 10^7 TU·mL^{-1} and 1.14 × 10^{10} VP·mL^{-1}. Previous SXC experiments with the MA100 were performed by loading 200 mL. Flow through and elution fractions of all runs were analyzed. No increase in the amount of LVs in the flow through was observed as the loading volume increased, which is exemplarily shown in Figure 5A,D.
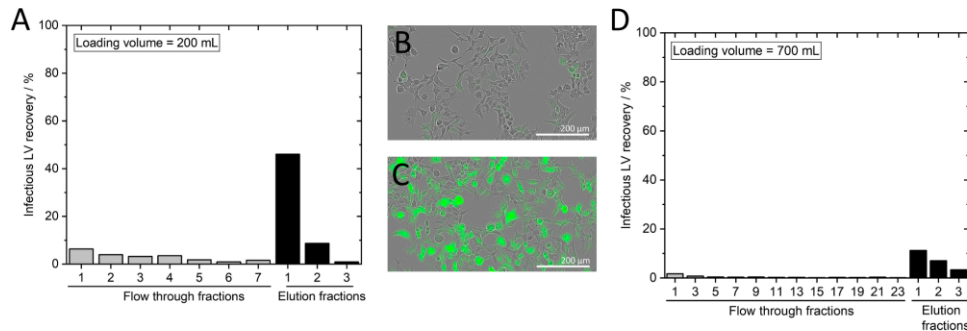
Figure 5. Identification of loading capacity. Infectious LV recovery for loadings of (**A**) 200 mL and (**D**) 700 mL. Phase contrast image merged with a green fluorescence channel image of HEK293T cells after incubation with a (**B**) flow through fraction or (**C**) elution fraction.

These findings are supported by captured images of HEK293T cells expressing no GFP after transduction with the flow through fractions (Figure 5B). In contrast, HEK293T cells transduced with LVs from the elution fractions showed GFP expression (Figure 5C). When a high LV amount was loaded (Figure 5D), the elution of the captured LVs was hardly possible, resulting in a low recovery in the elution fraction. The highest LV recovery was achieved by loading around 200 mL (Figure 5A). Therefore, we define a loading capacity of 1.35×10^9 TU and 1.14×10^{12} VP. In contrast to conventional chromatography methods, SXC does not rely on a stationary phase having functional groups, and thus limited binding sites, which typically results in a breakthrough that is observed once all binding sites are occupied. During our SXC runs, no LV breakthrough was observed. Thus, membrane capacity for SXC cannot be defined at 10% LV breakthrough; instead, different loading volumes and the success of LV elution are analyzed to determine the loading capacity at which the LV recovery in the elution is satisfactory. In the previous experiments (Figure 3B), 4.10×10^8 TU and 1.60×10^9 TU were loaded onto the MA100 and MA15 device, respectively, showing that approximately four times as many LVs could be loaded onto the MA100 device compared to the MA15 device. The loaded amount of LVs was lower than in the previous study, in which CAR-T-based LVs were used with a higher LV titer in the loading material [10]. These differences in the upstream material are likely the reason for the different outcomes, and it might be necessary to determine the ideal loading volume for each target product separately. Another reason could be the uneven LV distribution on the membrane with the MA100 standard housing discussed in Section 3.3, which might lead to the inefficient elution of overloaded membrane areas.

To further analyze the presented approach of scaling the flow rate according to the membrane surface area of the first layer, we performed scale-down experiments with an axial PP15 device for three different flow rates (N = 3 each) and a scale-up experiment with a radial 5″ device for two different flow rates (N = 1 each). Additionally, further runs at different flow rates with the MA15 and MA100 modules were performed (N = 3) to complement the data.

According to the literature, this is the first study using a membrane capsule for SXC and includes the largest membrane module that has been used for this method to date, with a loaded LV volume of 0.98 L. Pressure limitation was often discussed as a potential hurdle for SXC scale-up. As previously reported, the viscous buffers result in higher pressure compared to conventional chromatography methods such as anion exchange chromatography, and pressure increases during loading have often been reported [10,22,23]. We observed a pressure increase during the two scale-up runs with the 5″ capsules of 0.4 to 0.8 bar (run 1) and 0.5 to 0.7 bar (run 2). As the pressure limit of the device is 4 bar, pressure was not a limiting factor during the scale-up runs under the tested conditions.

The infectious and particle recoveries and impurity removals for the four different device scales are shown in Figure 6 and are plotted against different surface area-specific flow rates.
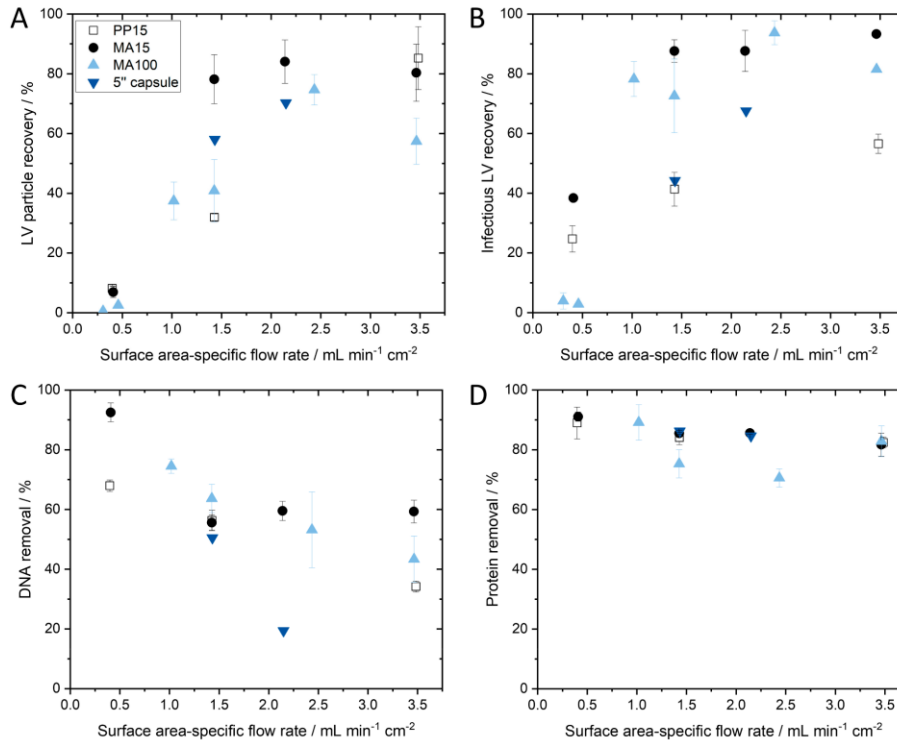

Figure 6. (**A**) Particle and (**B**) infectious LV recovery and (**C**) dsDNA and (**D**) protein removal in SXC experiments plotted against different surface area-specific flow rates for different module sizes. Replicates for each device and flow rate are as follows: PP15, N = 3 for all flow rates; MA15, N = 3 for all flow rates; MA100, for 1.43 mL·min^{-1}·cm^{-2} N = 11, for all other flow rates N = 3; 5″ capsule, N = 1.

Plotting the infectious and particle titer recoveries of the tested device scales against different surface-area specific flow rates shows that if the flow rate falls under a critical minimum flow rate, then LV recovery decreases significantly (Figure 6A,B). It appears that LV recovery asymptotically approaches a maximum. A decrease in LV recovery at flow rates above 3.5 mL·min^{-1}·cm^{-2} is possible; however, there is a technically feasible limit due to the maximum flow rate of the system and the maximum pressure of the module. Further investigation is necessary to confirm this observation, but it is clear that a surface area-dependent flow rate that is too low significantly reduces LV recovery. In general, a surface area-dependent flow rate of approximately 1.4 mL·min^{-1}·cm^{-2} or higher is necessary for successful scaling up of SXC. The reason why a critical minimum flow rate is necessary can be explained when considering the capture mechanism on the membrane. An association (capture) of the LVs on the membrane takes place when the depletion zones of the LVs and the membrane overlap. This occurs through random encounters between the LV and the membrane while passing through the membrane. When the flow rate is increased, the turbulence within the membrane increases as well, which in turn is expected to increase the likelihood of LVs encountering other LVs or the membrane for depletion interaction. We expect that the effect approaches a maximum probability of encounters that can be observed in an asymptotical trend.

When scaling the flow rate and loaded LV volume according to the membrane area of the chromatography module, the processing time for a complete chromatography run remains constant; thus, SXC runs with an MA15 or a 5″ capsule both take approximately 20 min at 1.43 mL·min^{-1}·cm^{-2}. This short processing time is especially beneficial for fragile enveloped viruses and viral vectors and enables a fast and efficient DSP process. With the scaling approach of using a minimum surface-area dependent flow rate, we were able to achieve reproducible SXC LV recovery at four different module sizes. The highest LV volume purified by SXC was 980 mL, with a recovery of 68% representing an overall scaling factor of 98 compared to the smallest device (PP15) (Table 1). dsDNA removal shows a decreasing trend with increasing surface area-specific flow rate (Figure 6C). To achieve both high LV recovery and dsDNA removal, a surface area-specific flow rate between 1.4 and 2.5 mL·min^{-1}·cm^{-2} is preferred, which subsequently achieves approximately 51% dsDNA removal. Protein removal was unaffected by flow rate and was consistent for the different module sizes, with a protein removal of about 84% (Figure 6D). Good overall impurity removals were achieved and a subsequent ultrafiltration and diafiltration step will likely follow the DSP process to remove residual PEG and further increase the purity of the product.

3.3. Influence of the Design of the Membrane Housing on SXC Performance

After identifying critical process parameters for the scaling up of SXC, we investigated the impact of the design of the membrane housing of the MA100 module on LV capture in the membrane and SXC performance.

The membrane chromatography devices used in this study are operated by an axial flow from above through a membrane stack and have a low bed height (height of superimposed membrane layers). Besides a lower bed height, the incident flow area is larger than the resin columns. A uniform flow distribution over the entire membrane area is required to avoid channeling and to enable the whole membrane area to be used efficiently. Even flow distribution is achieved by a distributor structure inside the lid, which spreads the fluid over the membrane, and a collector structure inside the table, which collects the fluid. As housing geometry significantly influences fluid transport through the membrane, housing design should play a major role during chromatography process development [28,29].

Axial devices are limited by their central inlet, resulting in a velocity profile; however, they still have the advantage of simple production and are therefore preferred at small scales.

Lentiviral vector visualization with the MA100 housing was carried out to assess LV distribution on the membrane before and after elution. SXC was performed at a flow rate of 1.43 mL·min^{-1}·cm^{-2}. A volume of 160 mL was loaded, which corresponds to a volume of 80 mL of LV solution with a particle titer of 7.27×10^9 VP·mL^{-1} and an infectious titer of 2.71×10^7 TU·mL^{-1}. For the first SXC run with labeled LVs, a standard housing configuration was used with the lid and table having distinct structures (Figure 1G,H). Figure 7A displays an uneven distribution on the membrane layers with a consistent appearance throughout all membrane layers. As previously observed with the MA15 device (Figure 2), the LVs are mainly located on the upper layers, although some LVs also reach the bottom membrane layers. The fluid does not seem to have been distributed evenly over the membrane. This uneven fluid distribution has favored membrane channeling and an imbalanced utilization of the membrane layer, thus leading to the overloading of some areas. These overloaded areas can potentially lead to the poorer detachment of particles, causing them to remain aggregated on the membrane.
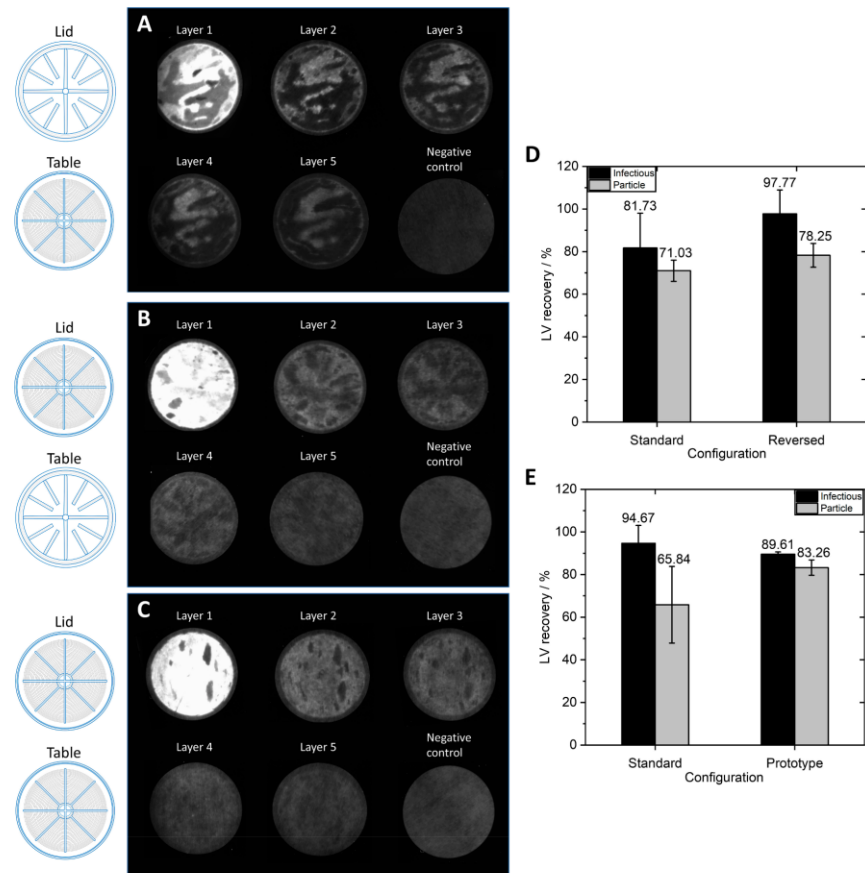
Figure 7. Influence of different MA100 configurations on the location of labeled LVs (anti-VSV-G Alexa Fluor® 546 antibody) on the membrane after loading and on the recovery of infectious and particle LVs. Membrane layers were separated after the loading and washing steps of steric exclusion chromatography. The lid and table configurations of the housing are indicated on the left and include a (**A**) standard configuration, (**B**) reversed configuration, and (**C**) prototype configuration. (**D,E**) Infectious and particle LV recovery for the three configurations of the MA100 housing operated at 1.43 mL·min^{-1}·cm^{-2} (N = 3 each). Data represent mean ± standard deviation.

For the second SXC run, the device's configuration was reversed; the table (Figure 1H) was used as a lid and vice versa. Therefore, the incoming fluid was distributed by the radial and circular distribution channels. Figure 7B shows that the LVs are more evenly distributed on the membrane layers. LV presence on the first membrane layer is visible, comparable to the findings when using the MA15 module (Figure 2). The changed lid and table configuration in this run highly improved fluid distribution over the membrane. These findings demonstrate that a lid with radial and circular distribution channels is better suited than a coarse structure with thick bridges when seeking to spread the fluid over the membrane (Figure 1G). The dark spots within the bright areas indicate the presence of air bubbles that did not allow the fluid to access the membrane in this area. Air bubbles prevent the utilization of the surface area they occupy, reducing the recovery of target species. A higher pressure drop across the membrane could eliminate air bubbles; alternatively, an optimized module design might be necessary.

A prototype was constructed with radial and circular distribution channels in the lid and the table. This housing configuration also resulted in evenly distributed LVs on the membrane (Figure 7C). Some air bubbles were present in the device (dark spots). Comparing Figure 7B,C, the LVs appear to be better distributed with the prototype housing. A possible reason is that the fluid is not only evenly distributed on top of the membrane stack but is also collected from the membrane more efficiently and directed to the outlet of the table with the distribution channel design. This LV visualization experiment shows that the membrane module's design is crucial to achieving evenly distributed fluid on the membrane so that the whole membrane area can be utilized.

The three device configurations explained above were used to purify LVs via SXC. For this experiment, the membranes, lid, and table of the MA100 module were incorporated into a stainless-steel holder (Figure 1E). Thus, comparability to the overmolded MA100 devices used for previous experiments is limited. The LV recoveries for different MA100 housing configurations are shown in Figure 7D,E. The standard configuration was used for all previous experiments and served as a comparison for the reversed and prototype configurations. The virus solution purified with the standard and reversed configuration (Figure 7D) had a total particle titer of 1.02×10^{10} VP·mL^{-1} and an infectious titer of 2.39×10^{7} TU·mL^{-1}. The virus solution purified with the prototype device and the standard configuration (Figure 7E) had a total particle titer of 4.32×10^{9} VP·mL^{-1} with a concentration of 3.03×10^{7} TU·mL^{-1}.

The reversed configuration generated higher infectious LV recovery and total LV particle recovery compared to the standard configuration, although differences were not significant. The LV recoveries of the prototype configuration were also not significantly different from the standard configuration, though standard deviations were lower with the prototype configuration. These findings indicate that utilizing a distribution structure on the inlet and outlet side allows for generally more stable reproduction of LV recoveries. The prototype and reversed configuration reduce the dead volume on the inlet side, which decreases back-mixing effects and promotes a narrower residence time distribution [28]. Concerning the high LV recoveries, the uniform LV distribution on the membrane, and the lowest dead volume, the prototype device with a flow distributor plate in the lid and table is the favored configuration for an axial MA100 device. Further device optimizations are necessary to avoid the entrapment of air bubbles in the module. Moreover, other module geometries, such as the capsule format with a radial flow, showed promising results in our study and have the advantage of a homogenous flow distribution that has been previously discussed in several studies [28,30,31] and that can be easily scaled [32].

4. Conclusions

Steric exclusion chromatography has been demonstrated to have potential as a gentle purification method for large enveloped viral vectors. However, scaling up has not yet been investigated, raising the question of how to approach this challenge. Visualization of the LVs on the membrane showed that SXC is a surface-oriented process, meaning that LVs are mainly captured on the upper membrane layer. We demonstrated that flow rate must be scaled with the membrane area of the first layer. Scale-down and scale-up experiments demonstrate that a certain critical minimum surface area-dependent flow rate is necessary to achieve reproducible LV recoveries with the four different device scales tested. These devices had an overall scaling factor of 98. For the largest scale runs, a radial device geometry was successfully used to purify 980 mL of LVs, and further scaling up could be realized by using larger capsules or cassette modules. Investigating various loading volumes showed no LV breakthrough with increasing volume. However, the elution of LVs from overloaded membrane areas was hardly possible, indicating an optimal amount of LVs to be loaded. Altering the design of the MA100 module housing improved flow distribution and led to a uniform distribution of LVs on the membrane. The use of improved housing prototypes could offer the possibility of loading more LVs, as overloading of membrane areas is more likely to be avoided. Overall, we have demonstrated the scalability of SXC

using membrane modules, providing a basis for potential future industrial applications of the method.

References

1. Albinger, N.; Hartmann, J.; Ullrich, E. Current status and perspective of CAR-T and CAR-NK cell therapy trials in Germany. *Gene Ther.* **2021**, *28*, 513–527. [CrossRef] [PubMed]
2. Labbé, R.P.; Vessillier, S.; Rafiq, Q.A. Lentiviral vectors for T cell engineering: Clinical applications, bioprocessing and future perspectives. *Viruses* **2021**, *13*, 1528. [CrossRef] [PubMed]
3. Bulcha, J.T.; Wang, Y.; Ma, H.; Tai, P.W.L.; Gao, G. Viral vector platforms within the gene therapy landscape. *Signal Transduct. Target. Ther.* **2021**, *6*, 53. [CrossRef] [PubMed]
4. Neff Newitt, V. The Incredible Story of Emily Whitehead & CAR T-Cell Therapy. *Oncol. Times* **2022**, *44*, 19–21. [CrossRef]
5. Milone, M.C.; O'Doherty, U. Clinical use of lentiviral vectors. *Leukemia* **2018**, *32*, 1529–1541. [CrossRef]
6. Ku, M.-W.; Charneau, P.; Majlessi, L. Use of lentiviral vectors in vaccination. *Expert Rev. Vaccines* **2021**, *20*, 1571–1586. [CrossRef]
7. Gurumoorthy, N.; Nordin, F.; Tye, G.J.; Wan Kamarul Zaman, W.S.; Ng, M.H. Non-Integrating Lentiviral Vectors in Clinical Applications: A Glance Through. *Biomedicines* **2022**, *10*, 107. [CrossRef]
8. Roots Analysis Business Research & Consulting. *Viral Vectors, Non-Viral Vectors and Gene Therapy Manufacturing Market, 2021–2030: Research Report*, 4th ed; Roots Analysis Business Research & Consulting: Punjab, India, 2021. Available online: https://www.rootsanalysis.com/reports/view_document/viral-vectors-non-viral-vectors-and-gene-therapy-manufacturing-market-/274.html (accessed on 7 August 2022).
9. Perry, C.; Rayat, A.C.M.E. Lentiviral vector bioprocessing. *Viruses* **2021**, *13*, 268. [CrossRef]
10. Labisch, J.J.; Kassar, M.; Bollmann, F.; Valentic, A.; Hubbuch, J.; Pflanz, K. Steric exclusion chromatography of lentiviral vectors using hydrophilic cellulose membranes. *J. Chromatogr. A* **2022**, *17*, 463148. [CrossRef]
11. Lothert, K.; Sprick, G.; Beyer, F.; Lauria, G.; Czermak, P.; Wolff, M.W. Membrane-based steric exclusion chromatography for the purification of a recombinant baculovirus and its application for cell therapy. *J. Virol. Methods* **2020**, *275*, 113756. [CrossRef]
12. Lothert, K.; Pagallies, F.; Feger, T.; Amann, R.; Wolff, M.W. Selection of chromatographic methods for the purification of cell culture-derived Orf virus for its application as a vaccine or viral vector. *J. Biotechnol.* **2020**, *323*, 62–72. [CrossRef]
13. Eilts, F.; Lothert, K.; Orbay, S.; Pagallies, F.; Amann, R.; Wolff, M.W. A summary of practical considerations for the application of the steric exclusion chromatography for the purification of the Orf viral vector. *Membranes* **2022**, *12*, 1070. [CrossRef]
14. Marichal-Gallardo, P.; Börner, K.; Pieler, M.M.; Sonntag-Buck, V.; Obr, M.; Bejarano, D.; Wolff, M.W.; Kräusslich, H.-G.; Reichl, U.; Grimm, D. Single-use capture purification of adeno-associated viral gene transfer vectors by membrane-based steric exclusion chromatography. *Hum. Gene Ther.* **2021**, *32*, 959–974. [CrossRef]
15. Marichal-Gallardo, P.; Pieler, M.M.; Wolff, M.W.; Reichl, U. Steric exclusion chromatography for purification of cell culture-derived influenza A virus using regenerated cellulose membranes and polyethylene glycol. *J. Chromatogr. A* **2017**, *1483*, 110–119. [CrossRef]
16. Lekkerkerker, H.N.W.; Tuinier, R. *Colloids and the Depletion Interaction*; Springer: Dordrecht, The Netherlands, 2011.
17. Lee, J.; Gan, H.T.; Latiff, S.M.A.; Chuah, C.; Lee, W.Y.; Yang, Y.-S.; Loo, B.; Ng, S.K.; Gagnon, P. Principles and applications of steric exclusion chromatography. *J. Chromatogr. A* **2012**, *1270*, 162–170. [CrossRef]
18. Gagnon, P.; Toh, P.; Lee, J. High productivity purification of immunoglobulin G monoclonal antibodies on starch-coated magnetic nanoparticles by steric exclusion of polyethylene glycol. *J. Chromatogr. A* **2013**, *1324*, 171–180. [CrossRef]

19. Orr, V.; Zhong, L.; Moo-Young, M.; Chou, C.P. Recent advances in bioprocessing application of membrane chromatography. *Biotechnol. Adv.* **2013**, *31*, 450–465. [CrossRef]
20. Hein, M.D.; Kollmus, H.; Marichal-Gallardo, P.; Püttker, S.; Benndorf, D.; Genzel, Y.; Schughart, K.; Kupke, S.Y.; Reichl, U. OP7, a novel influenza A virus defective interfering particle: Production, purification, and animal experiments demonstrating antiviral potential. *Appl. Microbiol. Biotechnol.* **2021**, *105*, 129–146. [CrossRef]
21. Eilts, F.; Steger, M.; Lothert, K.; Wolff, M.W. The suitability of latex particles to evaluate critical process parameters in steric exclusion chromatography. *Membranes* **2022**, *12*, 488. [CrossRef]
22. Lothert, K.; Pagallies, F.; Eilts, F.; Sivanesapillai, A.; Hardt, M.; Moebus, A.; Feger, T.; Amann, R.; Wolff, M.W. A scalable downstream process for the purification of the cell culture-derived Orf virus for human or veterinary applications. *J. Biotechnol.* **2020**, *323*, 221–230. [CrossRef]
23. Lothert, K.; Offersgaard, A.F.; Pihl, A.F.; Mathiesen, C.K.; Jensen, T.B.; Alzua, G.P.; Fahnøe, U.; Bukh, J.; Gottwein, J.M.; Wolff, M.W. Development of a downstream process for the production of an inactivated whole hepatitis C virus vaccine. *Sci. Rep.* **2020**, *10*, 16261. [CrossRef]
24. Tolk, J.A. Mikrofiltrationsmembranen auf Basis Regenerierter Cellulose. Dissertation, Gottfried Wilhelm Leibniz Universität, Hannover, Germany, 2017.
25. Labisch, J.J.; Wiese, G.P.; Barnes, K.; Bollmann, F.; Pflanz, K. Infectious titer determination of lentiviral vectors using a temporal immunological real-time imaging approach. *PLoS ONE* **2021**, *16*, e0254739. [CrossRef] [PubMed]
26. Escarpe, P.; Zayek, N.; Chin, P.; Borellini, F.; Zufferey, R.; Veres, G.; Kiermer, V. Development of a sensitive assay for detection of replication-competent recombinant lentivirus in large-scale HIV-based vector preparations. *Mol. Ther.* **2003**, *8*, 332–341. [CrossRef] [PubMed]
27. Cavazzana-Calvo, M.; Payen, E.; Negre, O.; Wang, G.; Hehir, K.; Fusil, F.; Down, J.; Denaro, M.; Brady, T.; Westerman, K.; et al. Transfusion independence and HMGA2 activation after gene therapy of human β-thalassaemia. *Nature* **2010**, *467*, 318–322. [CrossRef] [PubMed]
28. Hagemann, F.; Wypysek, D.; Baitalow, K.; Adametz, P.; Thom, V.; Wessling, M. Why device design is crucial for membrane adsorbers. *J. Chromatogr. Open* **2022**, *2*, 100029. [CrossRef]
29. Ghosh, R.; Wong, T. Effect of module design on the efficiency of membrane chromatographic separation processes. *J. Membr. Sci.* **2006**, *281*, 532–540. [CrossRef]
30. Teepakorn, C.; Grenier, D.; Fiaty, K.; Charcosset, C. Characterization of hydrodynamics in membrane chromatography devices using magnetic resonance imaging and computational fluid dynamics. *Chem. Eng. Res. Des.* **2016**, *113*, 61–73. [CrossRef]
31. Teepakorn, C.; Fiaty, K.; Charcosset, C. Effect of geometry and scale for axial and radial flow membrane chromatography: Experimental study of bovine serum albumin adsorption. *J. Chromatogr. A* **2015**, *1403*, 45–53. [CrossRef]
32. Charcosset, C. Membrane processes in biotechnology: An overview. *Biotechnol. Adv.* **2006**, *24*, 482–492. [CrossRef]

5 Conclusion and outlook

Lentiviral vectors have become a standard gene delivery tool in CAR-T cell therapy with even more gene therapy applications in the pipeline. The quickly increasing demand is challenging the industry to supply the required LV quantities. Existing protein downstream operation units cannot be simply transferred to LV processes and extensive optimization of existing methods as well as research into new, alternative methods is essential.

The PhD thesis focused on the development of a lab-scale downstream process of LV produced by a suspension culture process from harvest and clarification to purification, as well as advancing respective vector analytics. Diatomaceous earth (DE) was used as a filter aid for vacuum-based clarification of LV produced by mammalian suspension cell culture. While the adaption of the filter aid amount was essential to reduce LV loss, the filter capacity, thus sample throughput, was largely increased compared to the classical approach of centrifugation and filtration. Further investigations on clarification with DE could be done to compare different DE grades (porosities) that could have an impact on LV retention. Potentially larger DE pores could reduce LV retention in the filter aid since LV are large molecules that can be likely entrapped in small pores. The upscaling of the method for vacuum-driven clarification with DE is at the moment limited to the simultaneous clarification of 12 L which covers the typical research scale of LV. As DE is used in the production of blood-based pharmaceutical components (e.g., plasma fractionation) scalable process solutions are available, e.g., by FILTROX. For larger LV batches a series of filters with decreasing pore size is applicable, which are operated with a constant flow provided by a peristaltic pump until a pressure limit is reached. The comparison to clarification with DE would be an interesting aspect to investigate, however, for small volumes, a quick approach with minimum equipment needs is favored.

Viral vector quantification is currently regarded as one of the major bottlenecks in vector process development, as reliable high throughput methods are needed to be developed, and orthogonal methods are required since there is no one fits all solution for vector quantification and results depend highly on the method used. Especially determination of the infectious titer is important as this is the key value for LV to assess the success of a process step as only infectious vectors are functional and have a therapeutic effect. Semi-automated solutions, such as the infectious titer assay with real-time live-cell image analysis developed in this thesis,

enable high throughput sample analysis with low handling. The development of an advanced infectious titer assay with high sample throughput was decisive for subsequent process development as this facilitated the analysis of a high sample number generated through the subsequent chromatography step development. The trend for analytical measurements for process development activities goes towards further automation of processes, e.g., the implementation of pipetting robots and automated data evaluation. Those are further key aspects that will decrease the analysis time of samples and data. Artificial intelligence (AI) will also play a role in future data analysis, e.g., image analysis. AI would offer a label-free classification of live and dead cells by cell morphology analysis, further reducing labor and consumable costs. The use of several viral vector quantification assays will likely remain present in the near future as there is no gold standard virus quantification method available and the comparison of obtained values by orthogonal methods increases the reliability. Moreover, depending on the gene of interest that is transferred with the lentiviral vector, not all infectious titer quantification methods can be applied. Image analysis or flow cytometry, which were used in this study, is only applicable if a fluorescent reporter protein or a cell surface protein (stained with a respective fluorescent antibody) is the gene of interest. If other genes of interest are used, which lack the possibility of a visual readout, the infectious titer can only be determined via qPCR. What remains clear is that great efforts have been made, but there is still a long way to go to reliably evaluate viral vector process development experiments.

Steric exclusion chromatography is a chromatography technique that is to date not used in industrial applications. In this PhD thesis, SXC demonstrated huge potential to be used as a purification technique for LV. Moreover, SXC is a potential platform approach as it can be adapted for the purification of other target molecules like virus-like particles, exosomes, and other large enveloped viral vectors like VSV and Orf that are yet difficult to purify with conventional chromatography techniques. The main advantage is the mild operating conditions requiring no high salt concentrations or pH changes known to reduce LV infectivity. In addition, no direct chemical binding is exploited, meaning that SXC is a very flexible method and applicable to different virus serotypes or virus types in general regardless of the size, shape, and protein composition of the viral vector, eliminating the need to develop a new purification process for each vector type. However, process conditions like PEG buffer composition, flow rate, and loading capacity need to be adapted for each biomolecule. The

possibility to load the virus feed directly after clarification on the membrane eliminates the need for an intermediate buffer adjustment before SXC. Still, if a feed material with a significantly lower vector concentration compared with the vector concentrations used in the published paper, a previous concentration step might be necessary to achieve efficient depletion interaction.

In general, every hydrophilic stationary phase could be potentially used for SXC. This work focused on stabilized regenerated cellulose membranes, but previous publications of SXC used monoliths likewise. From a process perspective, the use of disposable membranes reduces process times and offers the possibility of sterilized membrane units which is not given when using monoliths that need to be regenerated and come with high costs. Other hydrophilic membrane materials or the same membrane material but with other characteristics may be tested in the future as this could help to further understand the method mechanism. For instance, different membrane pore sizes or membrane functionalizations could be screened and the effect of these characteristics on the SXC performance or process requirements, e.g., flow rates, could then be evaluated. It must be clearly understood that the process conditions established in this work are optimal for LV purification with a certain stationary phase, however other biomolecules and stationary phases will likely result in other process conditions. In this work, overmolded devices were produced, while other studies used manually punched membranes and assembled devices. To allow the widespread use of SXC, a commercially available device with a certified production process is necessary to supply off-the-shelf units and ensure minimal variability of the units and the SXC process itself. Moreover, SXC using membranes as a stationary phase was so far performed with axial and radial module geometries of up to 192 cm² (surface area of one membrane layer), further, scale-up can be realized by using larger capsules or preferentially cassette modules.

PEG has been widely used in the pharmaceutical industry to PEGylate biomolecules to increase their pharmacokinetic profiles. What once has been the gold standard is now viewed with skepticism because several immunogenic responses occurred after systemic PEG administration. Hence the remaining PEG concentration in the eluted viral vector product needs to be removed in subsequent DSP steps to gain the acceptability of manufacturers and regulatory authorities. For CAR-T applications that are performed *ex vivo,* the presence of PEG in the LV product is less likely to be a problem compared with *in vivo* gene therapy as in CAR-T

cell therapy only the transduced cells and not the viral vector itself are administered to the patient. Measurement of the remaining PEG concentrations will probably be required as a standard analytical assay before the final product release. In conclusion, the introduction and additional improvement of SXC in laboratory-scale downstream processes and the transfer to large scales could offer interesting prospects for LV downstream processing development.

The lack of studies on mechanistic understanding of SXC scale-up hindered the acceptance of the method to date. In this work, it was shown that capture of the LV happens on the very first membrane layers and not in the depth of the stationary phase. This results in a completely new understanding of the process operation. Scale-up can therefore be realized by increasing the surface area of the first membrane layer and scaling the flow rate to the surface area of the device. Hence, device design will play a major role, with cassette design potentially being the choice for large scales. Further studies testing larger devices and different device designs remain an important task for future investigations to advance the commercialization of SXC.

6 References

[1] J.T. Bulcha, Y. Wang, H. Ma, P.W.L. Tai, G. Gao, Viral vector platforms within the gene therapy landscape, Signal Transduct. Target. Ther. 6 (2021) 53. https://doi.org/10.1038/s41392-021-00487-6.

[2] John Wiley & Sons, Inc, Gene therapy clinical trials worldwide, John Wiley & Sons, Inc, Hoboken, NJ, USA, Journal of Gene Medicine, 2021. https://a873679.fmphost.com/fmi/webd/GTCT (accessed 30 September 2022).

[3] M. Irving, E. Lanitis, D. Migliorini, Z. Ivics, S. Guedan, Choosing the right tool for genetic engineering: Clinical lessons from chimeric antigen receptor-T cells, Hum. Gene Ther. 32 (2021) 1044–1058. https://doi.org/10.1089/hum.2021.173.

[4] N. Albinger, J. Hartmann, E. Ullrich, Current status and perspective of CAR-T and CAR-NK cell therapy trials in Germany, Gene Ther. 28 (2021) 513–527. https://doi.org/10.1038/s41434-021-00246-w.

[5] M. Sheykhhasan, H. Manoochehri, P. Dama, Use of CAR T-cell for acute lymphoblastic leukemia (ALL) treatment: a review study, Cancer Gene Ther. (2022). https://doi.org/10.1038/s41417-021-00418-1.

[6] R.P. Labbé, S. Vessillier, Q.A. Rafiq, Lentiviral vectors for T cell engineering: Clinical applications, bioprocessing and future perspectives, Viruses 13 (2021). https://doi.org/10.3390/v13081528.

[7] V. Neff Newitt, The Incredible Story of Emily Whitehead & CAR T-Cell Therapy, Oncology Times 44 (2022) 1,19-21. https://doi.org/10.1097/01.COT.0000824668.24475.b0.

[8] M.M. Segura, A.A. Kamen, A. Garnier, Overview of current scalable methods for purification of viral vectors, Methods Mol. Biol. 737 (2011) 89–116. https://doi.org/10.1007/978-1-61779-095-9_4.

[9] S.J. Flint, V.R. Racaniello, G.F. Rall, T. Hatziioannou, A.M. Skalka, Principles of virology, Fifth Edition, Wiley; ASM Press, Hoboken, NJ, Washington, DC, 2020.

[10] S. Modrow, D. Falke, U. Truyen, H. Schätzl, Molekulare Virologie, third ed., Spektrum Akademischer Verlag, Heidelberg, 2010.

[11] P.E. Pellett, S. Mitra, T.C. Holland, Basics of virology, Handb. Clin. Neurol. 123 (2014) 45–66. https://doi.org/10.1016/B978-0-444-53488-0.00002-X.

[12] M.C. Milone, U. O'Doherty, Clinical use of lentiviral vectors, Leukemia 32 (2018) 1529–1541. https://doi.org/10.1038/s41375-018-0106-0.

[13] W. Dong, B. Kantor, Lentiviral vectors for delivery of gene-editing systems based on CRISPR/Cas: Current state and perspectives, Viruses 13 (2021). https://doi.org/10.3390/v13071288.

[14] M.d.L.M. Segura, A. Kamen, A. Garnier, Downstream processing of oncoretroviral and lentiviral gene therapy vectors, Biotechnol. Adv. 24 (2006) 321–337. https://doi.org/10.1016/j.biotechadv.2005.12.001.

[15] R.F. Shearer, D.N. Saunders, Experimental design for stable genetic manipulation in mammalian cell lines: lentivirus and alternatives, Genes Cells 20 (2015) 1–10. https://doi.org/10.1111/gtc.12183.

[16] N.P. Sweeney, C.A. Vink, The impact of lentiviral vector genome size and producer cell genomic to gag-pol mRNA ratios on packaging efficiency and titre, Mol. Ther. Methods Clin. Dev. 21 (2021) 574–584. https://doi.org/10.1016/j.omtm.2021.04.007.

[17] S.-H. Kim, K.-I. Lim, Stability of retroviral vectors against ultracentrifugation is determined by the viral internal core and envelope proteins used for pseudotyping, Mol. Cells 40 (2017) 339–345. https://doi.org/10.14348/molcells.2017.0043.

[18] K. Zimmermann, O. Scheibe, A. Kocourek, J. Muelich, E. Jurkiewicz, A. Pfeifer, Highly efficient concentration of lenti- and retroviral vector preparations by membrane adsorbers and ultrafiltration, BMC Biotechnol. 11 (2011) 55. https://doi.org/10.1186/1472-6750-11-55.

[19] I.J.C. Dautzenberg, M.J.W.E. Rabelink, R.C. Hoeben, The stability of envelope-pseudotyped lentiviral vectors, Gene Ther. (2020). https://doi.org/10.1038/s41434-020-00193-y.

[20] F. Higashikawa, L. Chang, Kinetic analyses of stability of simple and complex retroviral vectors, Virology 280 (2001) 124–131. https://doi.org/10.1006/viro.2000.0743.

[21] C.-C. Ma, Z.-L. Wang, T. Xu, Z.-Y. He, Y.-Q. Wei, The approved gene therapy drugs worldwide: from 1998 to 2019, Biotechnol. Adv. 40 (2020) 107502. https://doi.org/10.1016/j.biotechadv.2019.107502.

[22] A. Mizukami, K. Swiech, Platforms for clinical-grade CAR-T cell expansion, Methods Mol. Biol. 2086 (2020) 139–150. https://doi.org/10.1007/978-1-0716-0146-4_10.

[23] A.N. Miliotou, L.C. Papadopoulou, CAR T-cell therapy: a new era in cancer immunotherapy, Curr. Pharm. Biotechnol. 19 (2018) 5–18. https://doi.org/10.2174/1389201019666180418095526.

[24] Business Wire, bluebird bio announces FDA approval of ZYNTEGLO®, the first gene therapy for people with beta-thalassemia who require regular red blood cell transfusions, 2022. https://www.businesswire.com/news/home/20220817005667/en/bluebird-bio-Announces-FDA-Approval-of-ZYNTEGLO%C2%AE-the-First-Gene-Therapy-for-People-with-Beta-Thalassemia-Who-Require-Regular-Red-Blood-Cell-Transfusions (accessed 19 August 2022).

[25] M.-W. Ku, P. Charneau, L. Majlessi, Use of lentiviral vectors in vaccination, Expert Rev. Vaccines 20 (2021) 1571–1586. https://doi.org/10.1080/14760584.2021.1988854.

[26] N. Gurumoorthy, F. Nordin, G.J. Tye, W.S. Wan Kamarul Zaman, M.H. Ng, Non-Integrating Lentiviral Vectors in Clinical Applications: A Glance Through, Biomedicines 10 (2022). https://doi.org/10.3390/biomedicines10010107.

[27] A. Gutierrez-Guerrero, F.-L. Cosset, E. Verhoeyen, Lentiviral vector pseudotypes: Precious tools to improve gene modification of hematopoietic cells for research and gene therapy, Viruses 12 (2020). https://doi.org/10.3390/v12091016.

[28] V. Morante, M. Borghi, I. Farina, Z. Michelini, F. Grasso, A. Gallinaro, S. Cecchetti, A. Di Virgilio, A. Canitano, M.F. Pirillo, R. Bona, A. Cara, D. Negri, Integrase-defective lentiviral vector is an efficient vaccine platform for cancer immunotherapy, Viruses 13 (2021). https://doi.org/10.3390/v13020355.

[29] L. Apolonia, The old and the new: Prospects for non-integrating lentiviral vector technology, Viruses 12 (2020). https://doi.org/10.3390/v12101103.

[30] Roots Analysis Business Research & Consulting, Viral vectors, non-viral vectors and gene therapy manufacturing market, 2021-2030: Research report, 4th ed., 2021. https://www.rootsanalysis.com/reports/view_document/viral-vectors-non-viral-vectors-and-gene-therapy-manufacturing-market-/274.html (accessed 7 August 2022).

[31] J. Rininger, A. Fennell, L. Schoukroun-Barnes, C. Peterson, J. Speidel, Capacity analysis for viral vector manufacturing: Is there enough?, Bioprocess Int. 17 (2019).

[32] M.G. Moleirinho, R.J.S. Silva, P.M. Alves, M.J.T. Carrondo, C. Peixoto, Current challenges in biotherapeutic particles manufacturing, Expert Opin. Biol. Ther. 20 (2020) 451–465. https://doi.org/10.1080/14712598.2020.1693541.

[33] E. Martínez-Molina, C. Chocarro-Wrona, D. Martínez-Moreno, J.A. Marchal, H. Boulaiz, Large-scale production of lentiviral vectors: Current perspectives and challenges, Pharmaceutics 12 (2020). https://doi.org/10.3390/pharmaceutics12111051.

[34] O.W. Merten, M. Hebben, C. Bovolenta, Production of lentiviral vectors, Mol. Ther. Methods Clin. Dev. 3 (2016) 16017. https://doi.org/10.1038/mtm.2016.17.

[35] M.V. Ferreira, E.T. Cabral, A.S. Coroadinha, Progress and perspectives in the development of lentiviral vector producer cells, Biotechnol. J. 16 (2021) e2000017. https://doi.org/10.1002/biot.202000017.

[36] A.P. Manceur, H. Kim, V. Misic, N. Andreev, J. Dorion-Thibaudeau, S. Lanthier, A. Bernier, S. Tremblay, A.-M. Gélinas, S. Broussau, R. Gilbert, S. Ansorge, Scalable lentiviral vector production using stable HEK293SF producer cell lines, Hum. Gene Ther. Methods 28 (2017) 330–339. https://doi.org/10.1089/hgtb.2017.086.

[37] H.E. Gouvarchin Ghaleh, M. Bolandian, R. Dorostkar, A. Jafari, M.F. Pour, Concise review on optimized methods in production and transduction of lentiviral vectors in order to facilitate immunotherapy and gene therapy, Biomed. Pharmacother. 128 (2020) 110276. https://doi.org/10.1016/j.biopha.2020.110276.

[38] A. McCarron, M. Donnelley, C. McIntyre, D. Parsons, Challenges of up-scaling lentivirus production and processing, J. Biotechnol. 240 (2016) 23–30. https://doi.org/10.1016/j.jbiotec.2016.10.016.

[39] T.A. Grein, T. Weidner, P. Czermak, Concepts for the production of viruses and viral vectors in cell cultures, in: S.J.T. Gowder (Ed.), New Insights into Cell Culture Technology, InTech, 2017.

[40] A. McCarron, M. Donnelley, C. McIntyre, D. Parsons, Transient lentiviral vector production using a packed-bed bioreactor system, Hum. Gene Ther. Methods 30 (2019) 93–101. https://doi.org/10.1089/hgtb.2019.038.

[41] J. Sheu, J. Beltzer, B. Fury, K. Wilczek, S. Tobin, D. Falconer, J. Nolta, G. Bauer, Large-scale production of lentiviral vector in a closed system hollow fiber bioreactor, Mol. Ther. Methods Clin. Dev. 2 (2015) 15020. https://doi.org/10.1038/mtm.2015.20.

[42] O.-W. Merten, M. Schweizer, P. Chahal, A.A. Kamen, Manufacturing of viral vectors for gene therapy: part I. Upstream processing, Pharmaceutical Bioprocessing 2 (2014) 183–203. https://doi.org/10.4155/pbp.14.16.

[43] M. Bauler, J.K. Roberts, C.-C. Wu, B. Fan, F. Ferrara, B.H. Yip, S. Diao, Y.-I. Kim, J. Moore, S. Zhou, M.M. Wielgosz, B. Ryu, R.E. Throm, Production of lentiviral vectors using suspension cells grown in serum-free media, Mol. Ther. Methods Clin. Dev. 17 (2020) 58–68. https://doi.org/10.1016/j.omtm.2019.11.011.

[44] P. Kramberger, L. Urbas, A. Štrancar, Downstream processing and chromatography based analytical methods for production of vaccines, gene therapy vectors, and bacteriophages, Hum. Vaccin. Immunother. 11 (2015) 1010–1021. https://doi.org/10.1080/21645515.2015.1009817.

[45] M.M. Segura, M. Mangion, B. Gaillet, A. Garnier, New developments in lentiviral vector design, production and purification, Expert Opin. Biol. Ther. 13 (2013) 987–1011. https://doi.org/10.1517/14712598.2013.779249.

[46] World Health Organization, WHO expert committee on biological standardization, fifty-fourth report, Geneva, Switzerland, 2003.

[47] US Food and Drug Administration, Guidance for industry: characterization and qualification of cell substrates and other biological materials used in the production of viral vaccines for infectious disease indications, Rockville, USA, 2010.

[48] X. Wang, A.K. Hunter, N.M. Mozier, Host cell proteins in biologics development: Identification, quantitation and risk assessment, Biotechnol. Bioeng. 103 (2009) 446–458. https://doi.org/10.1002/bit.22304.

[49] A.S. Moreira, D.G. Cavaco, T.Q. Faria, P.M. Alves, M.J.T. Carrondo, C. Peixoto, Advances in lentivirus purification, Biotechnol. J. (2020) e2000019. https://doi.org/10.1002/biot.202000019.

[50] C. Perry, A.C.M.E. Rayat, Lentiviral vector bioprocessing, Viruses 13 (2021). https://doi.org/10.3390/v13020268.

[51] S.B. Carvalho, R.J.S. Silva, A.S. Moreira, B. Cunha, J.J. Clemente, P.M. Alves, M.J.T. Carrondo, A. Xenopoulos, C. Peixoto, Efficient filtration strategies for the clarification of influenza virus-like particles derived from insect cells, Separation and Purification Technology 218 (2019) 81–88. https://doi.org/10.1016/j.seppur.2019.02.040.

[52] H.B. Olgun, H.M. Tasyurek, A.D. Sanlioglu, S. Sanlioglu, High-grade purification of third-generation HIV-based lentiviral vectors by anion exchange chromatography for experimental gene and stem cell therapy applications, Methods Mol. Biol. 1879 (2019) 347–365. https://doi.org/10.1007/7651_2018_154.

[53] W. Jiang, R. Hua, M. Wei, C. Li, Z. Qiu, X. Yang, C. Zhang, An optimized method for high-titer lentivirus preparations without ultracentrifugation, Sci. Rep. 5 (2015) 13875. https://doi.org/10.1038/srep13875.

[54] M.C. Rosales Gerpe, L.P. van Lieshout, J.M. Domm, J.P. van Vloten, J. Datu, J.C. Ingrao, D.L. Yu, J. de Jong, T.J. Moraes, P.J. Krell, B.W. Bridle, S.K. Wootton, Optimized pre-clinical grade production of two novel lentiviral vector pseudotypes for lung gene delivery, Hum. Gene Ther. 31 (2020) 459–471. https://doi.org/10.1089/hum.2019.211.

[55] L. Besnard, V. Fabre, M. Fettig, E. Gousseinov, Y. Kawakami, N. Laroudie, C. Scanlan, P. Pattnaik, Clarification of vaccines: An overview of filter based technology trends and best practices, Biotechnol. Adv. 34 (2016) 1–13. https://doi.org/10.1016/j.biotechadv.2015.11.005.

[56] B. Raghavan, M. Collins, S. Walls, A. Lambropoulos, S. Bergheim-Pietza, Optimizing the clarification of industrial scale viral vector culture for gene therapy, Cell Gene Therapy Insights 5 (2019) 1311–1322. https://doi.org/10.18609/cgti.2019.137.

[57] D. Hoffmann, J. Leber, D. Loewe, K. Lothert, T. Oppermann, J. Zitzmann, T. Weidner, D. Salzig, M. Wolff, P. Czermak, Purification of new biologicals using membrane-based processes, in: Current trends and future developments on (bio-) membranes, 2019, pp. 123–150.

[58] D. Boudeffa, B. Bertin, A. Biek, M. Mormin, F. Leseigneur, A. Galy, O.-W. Merten, Toward a scalable purification protocol of GaLV-TR-pseudotyped lentiviral vectors, Hum. Gene Ther. Methods 30 (2019) 153–171. https://doi.org/10.1089/hgtb.2019.076.

[59] A.R. Cooper, S. Patel, S. Senadheera, K. Plath, D.B. Kohn, R.P. Hollis, Highly efficient large-scale lentiviral vector concentration by tandem tangential flow filtration, J. Virol. Methods 177 (2011) 1–9. https://doi.org/10.1016/j.jviromet.2011.06.019.

[60] E. Papanikolaou, G. Kontostathi, E. Drakopoulou, M. Georgomanoli, E. Stamateris, K. Vougas, A. Vlahou, A. Maloy, M. Ware, N.P. Anagnou, Characterization and comparative performance of lentiviral vector preparations concentrated by either one-step ultrafiltration or ultracentrifugation, Virus Res. 175 (2013) 1–11. https://doi.org/10.1016/j.virusres.2013.03.015.

[61] P.M. Doran, Bioprocess engineering principles, second edition, Academic Press, Waltham, Mass., 2013.

[62] M. Grauf, B. Lagrange, K. Schöne, Simplified small-scale harvest of CHO cells for mAb analytics, Genetic Engineering & Biotechnology News 38 (2018) 22–23. https://doi.org/10.1089/gen.38.05.07.

[63] FILTROX, Alluvial filtration: An economical solution for midstream clarification, 2020. https://www.filtrox.com/blog/tag/alluvial-filtration/ (accessed 30 September 2022).

[64] B. Raghunath, W. Bin, P. Pattnaik, J. Janssens, Best practices for optimization and scale-up of microfiltration TFF processes, BioProcess J 11 (2012) 30–40. https://doi.org/10.12665/J111.Raghunath.

[65] T. Williams, O. Goodyear, L. Davies, C. Knevelman, M. Bransby, J. Miskin, K. Mitrophanous, Lentiviral vector manufacturing process enhancement utilizing TFDF™ technology, Cell Gene Therapy Insights 6 (2020) 455–467. https://doi.org/10.18609/cgti.2020.053.

[66] O.-W. Merten, M. Schweizer, P. Chahal, A. Kamen, Manufacturing of viral vectors: part II. Downstream processing and safety aspects, Pharmaceutical Bioprocessing 2 (2014) 237–251. https://doi.org/10.4155/PBP.14.15.

[67] V. Bandeira, C. Peixoto, A.F. Rodrigues, P.E. Cruz, P.M. Alves, A.S. Coroadinha, M.J.T. Carrondo, Downstream processing of lentiviral vectors: releasing bottlenecks, Hum. Gene Ther. Methods 23 (2012) 255–263. https://doi.org/10.1089/hgtb.2012.059.

[68] A.J. Valkama, I. Oruetxebarria, E.M. Lipponen, H.M. Leinonen, P. Käyhty, H. Hynynen, V. Turkki, J. Malinen, T. Miinalainen, T. Heikura, N.R. Parker, S. Ylä-Herttuala, H.P. Lesch, Development of large-scale downstream processing for lentiviral vectors, Mol. Ther. Methods Clin. Dev. 17 (2020) 717–730. https://doi.org/10.1016/j.omtm.2020.03.025.

[69] M. Soldi, L. Sergi Sergi, G. Unali, T. Kerzel, I. Cuccovillo, P. Capasso, A. Annoni, M. Biffi, P.M.V. Rancoita, A. Cantore, A. Lombardo, L. Naldini, M.L. Squadrito, A. Kajaste-Rudnitski, Laboratory-Scale Lentiviral Vector Production and Purification for Enhanced Ex Vivo and In Vivo Genetic Engineering, Mol. Ther. Methods Clin. Dev. 19 (2020) 411–425. https://doi.org/10.1016/j.omtm.2020.10.009.

[70] A. Jungbauer, Chromatographic media for bioseparation, Journal of Chromatography A 1065 (2005) 3–12. https://doi.org/10.1016/j.chroma.2004.08.162.

[71] M. Barut, A. Podgornik, P. Brne, A. Strancar, Convective interaction media short monolithic columns: enabling chromatographic supports for the separation and purification of large biomolecules, J. Sep. Sci. 28 (2005) 1876–1892. https://doi.org/10.1002/jssc.200500246.

[72] P. Nestola, C. Peixoto, R.R.J.S. Silva, P.M. Alves, J.P.B. Mota, M.J.T. Carrondo, Improved virus purification processes for vaccines and gene therapy, Biotechnol. Bioeng. 112 (2015) 843–857. https://doi.org/10.1002/bit.25545.

[73] J.H. Yu, D.V. Schaffer, Selection of novel vesicular stomatitis virus glycoprotein variants from a peptide insertion library for enhanced purification of retroviral and lentiviral vectors, J. Virol. 80 (2006) 3285–3292. https://doi.org/10.1128/JVI.80.7.3285-3292.2006.

[74] R. Chen, N. Folarin, V.H.B. Ho, D. McNally, D. Darling, F. Farzaneh, N.K.H. Slater, Affinity recovery of lentivirus by diaminopelargonic acid mediated desthiobiotin labelling, J. Chromatogr. B Analyt. Technol. Biomed. Life Sci. 878 (2010) 1939–1945. https://doi.org/10.1016/j.jchromb.2010.05.019.

[75] L. Mekkaoui, F. Parekh, E. Kotsopoulou, D. Darling, G. Dickson, G.W. Cheung, L. Chan, K. MacLellan-Gibson, G. Mattiuzzo, F. Farzaneh, Y. Takeuchi, M. Pule, Lentiviral vector purification using genetically encoded biotin mimic in packaging cell, Mol. Ther. Methods Clin. Dev. 11 (2018) 155–165. https://doi.org/10.1016/j.omtm.2018.10.008.

[76] M. Segura, A. Kamen, P. Trudel, A. Garnier, A novel purification strategy for retrovirus gene therapy vectors using heparin affinity chromatography, Biotechnol. Bioeng. 90 (2005) 391–404. https://doi.org/10.1002/bit.20301.

[77] M.M. Segura, A. Garnier, Y. Durocher, H. Coelho, A. Kamen, Production of lentiviral vectors by large-scale transient transfection of suspension cultures and affinity chromatography purification, Biotechnol. Bioeng. 98 (2007) 789–799. https://doi.org/10.1002/bit.21467.

[78] K. Ye, S. Jin, M.M. Ataai, J.S. Schultz, J. Ibeh, Tagging retrovirus vectors with a metal binding peptide and one-step purification by immobilized metal affinity chromatography, J. Virol. 78 (2004) 9820–9827. https://doi.org/10.1128/JVI.78.18.9820–9827.2004.

[79] M. Schweizer, O.-W. Merten, Large-scale production means for the manufacturing of lentiviral vectors, Curr. Gene Ther. 10 (2010) 474–486. https://doi.org/10.2174/156652310793797748.

[80] V. Slepushkin, N. Chang, Y. Gan, B. Jiang, E. Deausen, D. Berlinger, G. Binder, K. Andre, L. Humeau, B. Dropulic, Large-scale purification of a lentiviral vector by size exclusion

chromatography or mustang Q ion exchange capsule, BioProcess J 2 (2003) 89–95. https://doi.org/10.12665/J25.Dropulic.

[81] G.-A. Junter, L. Lebrun, Polysaccharide-based chromatographic adsorbents for virus purification and viral clearance, J. Pharm. Anal. 10 (2020) 291–312. https://doi.org/10.1016/j.jpha.2020.01.002.

[82] Resins, monoliths, or membranes. Which chromatographic method should you use?, 2021. https://www.sartorius.com/en/knowledge/science-snippets/resins-monoliths-or-membranes-which-chromatographic-method-should-you-use-1077712 (accessed 13 September 2022).

[83] V. Orr, L. Zhong, M. Moo-Young, C.P. Chou, Recent advances in bioprocessing application of membrane chromatography, Biotechnol. Adv. 31 (2013) 450–465. https://doi.org/10.1016/j.biotechadv.2013.01.007.

[84] C. Teepakorn, K. Fiaty, C. Charcosset, Effect of geometry and scale for axial and radial flow membrane chromatography: Experimental study of bovine serum albumin adsorption, J. Chromatogr. A 1403 (2015) 45–53. https://doi.org/10.1016/j.chroma.2015.05.023.

[85] S. Fischer-Früholz, M. Leuthold, S. Weisshaar, F. Taft, M. Hirai, Membrane chromatography cassettes for bind and elute applications of viruses and large proteins, 2018. https://dc.engconfintl.org/vt_vii/76 (accessed 20 April 2022).

[86] A.L. Zydney, New developments in membranes for bioprocessing – A review, Journal of Membrane Science 620 (2021) 118804. https://doi.org/10.1016/j.memsci.2020.118804.

[87] S. Tinch, K. Szczur, W. Swaney, L. Reeves, S.R. Witting, A scalable lentiviral vector production and purification method using Mustang Q chromatography and tangential flow filtration, Methods Mol. Biol. 1937 (2019) 135–153. https://doi.org/10.1007/978-1-4939-9065-8_8.

[88] R.H. Kutner, S. Puthli, M.P. Marino, J. Reiser, Simplified production and concentration of HIV-1-based lentiviral vectors using HYPERFlask vessels and anion exchange membrane chromatography, BMC Biotechnol. 9 (2009). https://doi.org/10.1186/1472-6750-9-10.

[89] A.S. Moreira, T.Q. Faria, J.G. Oliveira, A. Kavara, M. Schofield, T. Sanderson, M. Collins, R. Gantier, P.M. Alves, M.J.T. Carrondo, C. Peixoto, Enhancing the purification of lentiviral vectors for clinical applications, Separation and Purification Technology 274 (2021) 118598. https://doi.org/10.1016/j.seppur.2021.118598.

[90] M.P. Marino, M. Panigaj, W. Ou, J. Manirarora, C.-H. Wei, J. Reiser, A scalable method to concentrate lentiviral vectors pseudotyped with measles virus glycoproteins, Gene Ther. 22 (2015) 280–285. https://doi.org/10.1038/gt.2014.125.

[91] M.R. Greene, T. Lockey, P.K. Mehta, Y.-S. Kim, P.W. Eldridge, J.T. Gray, B.P. Sorrentino, Transduction of human CD34+ repopulating cells with a self-inactivating lentiviral vector for SCID-X1 produced at clinical scale by a stable cell line, Hum. Gene Ther. Methods 23 (2012) 297–308. https://doi.org/10.1089/hgtb.2012.150.

[92] N.J. Darton, D. Darling, M.J. Townsend, D.J. McNally, F. Farzaneh, N.K.H. Slater, Lentivirus capture directly from cell culture with Q-functionalised microcapillary film chromatography, J. Chromatogr. A 1251 (2012) 236–239. https://doi.org/10.1016/j.chroma.2012.06.072.

[93] D.J. McNally, D. Darling, F. Farzaneh, P.R. Levison, N.K.H. Slater, Optimised concentration and purification of retroviruses using membrane chromatography, J. Chromatogr. A 1340 (2014) 24–32. https://doi.org/10.1016/j.chroma.2014.03.023.

[94] R. Ghosh, S. Koley, S. Gopal, A.L. Rodrigues, J.S. Dordick, S.M. Cramer, Evaluation of lentiviral vector stability and development of ion exchange purification processes, Biotechnol. Prog. (2022) e3286. https://doi.org/10.1002/btpr.3286.

[95] H.P. Lesch, A. Laitinen, C. Peixoto, T. Vicente, K.-E. Makkonen, L. Laitinen, J.T. Pikkarainen, H. Samaranayake, P.M. Alves, M.J.T. Carrondo, S. Ylä-Herttuala, K.J. Airenne, Production and

purification of lentiviral vectors generated in 293T suspension cells with baculoviral vectors, Gene Ther. 18 (2011) 531–538. https://doi.org/10.1038/gt.2010.162.

[96] M.G. Moleirinho, S. Feast, A.S. Moreira, R.J.S. Silva, P.M. Alves, M.J.T. Carrondo, T. Huber, C. Fee, C. Peixoto, 3D-printed ordered bed structures for chromatographic purification of enveloped and non-enveloped viral particles, Separation and Purification Technology 254 (2021) 117681. https://doi.org/10.1016/j.seppur.2020.117681.

[97] A. Podgornik, A. Štrancar, Convective interaction media (CIM) – Short layer monolithic chromatographic stationary phases, in: Biotechnology annual review, Elsevier, 2005, pp. 281–333.

[98] A. Podgornik, S. Yamamoto, M. Peterka, N.L. Krajnc, Fast separation of large biomolecules using short monolithic columns, J. Chromatogr. B Analyt. Technol. Biomed. Life Sci. 927 (2013) 80–89. https://doi.org/10.1016/j.jchromb.2013.02.004.

[99] M.C. Cheeks, N. Kamal, A. Sorrell, D. Darling, F. Farzaneh, N.K.H. Slater, Immobilized metal affinity chromatography of histidine-tagged lentiviral vectors using monolithic adsorbents, J. Chromatogr. A 1216 (2009) 2705–2711. https://doi.org/10.1016/j.chroma.2008.08.029.

[100] J. Turnbull, B. Wright, N.K. Green, R. Tarrant, I. Roberts, O. Hardick, D.G. Bracewell, Adenovirus 5 recovery using nanofiber ion-exchange adsorbents, Biotechnol. Bioeng. 116 (2019) 1698–1709. https://doi.org/10.1002/bit.26972.

[101] J. Ruscic, C. Perry, T. Mukhopadhyay, Y. Takeuchi, D.G. Bracewell, Lentiviral vector purification using nanofiber ion-exchange chromatography, Mol. Ther. Methods Clin. Dev. 15 (2019) 52–62. https://doi.org/10.1016/j.omtm.2019.08.007.

[102] S. Asakura, F. Oosawa, On interaction between two bodies immersed in a solution of macromolecules, The Journal of Chemical Physics 22 (1954) 1255–1256. https://doi.org/10.1063/1.1740347.

[103] A. Vrij, Polymers at interfaces and the interactions in colloidal dispersions, Pure and Applied Chemistry 4 (1976) 471–483. https://doi.org/10.1351/pac197648040471.

[104] H.N.W. Lekkerkerker, R. Tuinier, Colloids and the depletion interaction, Springer Netherlands, Dordrecht, 2011.

[105] J. Lee, H.T. Gan, S.M.A. Latiff, C. Chuah, W.Y. Lee, Y.-S. Yang, B. Loo, S.K. Ng, P. Gagnon, Principles and applications of steric exclusion chromatography, J. Chromatogr. A 1270 (2012) 162–170. https://doi.org/10.1016/j.chroma.2012.10.062.

[106] Q. He, Investigation of stabilization mechanisms for colloidal suspension using nanoparticles. Electronic Theses and Dissertations, 2014.

[107] R. Tuinier, J. Rieger, C.G. de Kruif, Depletion-induced phase separation in colloid–polymer mixtures, Advances in Colloid and Interface Science 103 (2003) 1–31. https://doi.org/10.1016/S0001-8686(02)00081-7.

[108] A.A. D'souza, R. Shegokar, Polyethylene glycol (PEG): a versatile polymer for pharmaceutical applications, Expert Opin. Drug Deliv. 13 (2016) 1257–1275. https://doi.org/10.1080/17425247.2016.1182485.

[109] P. Gagnon, P. Toh, J. Lee, High productivity purification of immunoglobulin G monoclonal antibodies on starch-coated magnetic nanoparticles by steric exclusion of polyethylene glycol, J. Chromatogr. A 1324 (2013) 171–180. https://doi.org/10.1016/j.chroma.2013.11.039.

[110] P. Marichal-Gallardo, M.M. Pieler, M.W. Wolff, U. Reichl, Steric exclusion chromatography for purification of cell culture-derived influenza A virus using regenerated cellulose membranes and polyethylene glycol, J. Chromatogr. A 1483 (2017) 110–119. https://doi.org/10.1016/j.chroma.2016.12.076.

[111] S.-L. Sim, T. He, A. Tscheliessnig, M. Mueller, R.B.H. Tan, A. Jungbauer, Protein precipitation by polyethylene glycol: a generalized model based on hydrodynamic radius, J. Biotechnol. 157 (2012) 315–319. https://doi.org/10.1016/j.jbiotec.2011.09.028.

[112] T. Arakawa, S.N. Timasheff, Mechanism of poly(ethylene glycol) interaction with proteins, Biochemistry 24 (1985) 6756–6762. https://doi.org/10.1021/bi00345a005.

[113] C. Wang, S. Bai, S.-P. Tao, Y. Sun, Evaluation of steric exclusion chromatography on cryogel column for the separation of serum proteins, J. Chromatogr. A 1333 (2014) 54–59. https://doi.org/10.1016/j.chroma.2014.01.059.

[114] A. Levanova, M.M. Poranen, Application of steric exclusion chromatography on monoliths for separation and purification of RNA molecules, J. Chromatogr. A 1574 (2018) 50–59. https://doi.org/10.1016/j.chroma.2018.08.063.

[115] P. Marichal-Gallardo, K. Börner, M.M. Pieler, V. Sonntag-Buck, M. Obr, D. Bejarano, M.W. Wolff, H.-G. Kräusslich, U. Reichl, D. Grimm, Single-use capture purification of adeno-associated viral gene transfer vectors by membrane-based steric exclusion chromatography, Hum. Gene Ther. 32 (2021) 959–974. https://doi.org/10.1089/hum.2019.284.

[116] K. Lothert, G. Sprick, F. Beyer, G. Lauria, P. Czermak, M.W. Wolff, Membrane-based steric exclusion chromatography for the purification of a recombinant baculovirus and its application for cell therapy, J. Virol. Methods 275 (2020) 113756. https://doi.org/10.1016/j.jviromet.2019.113756.

[117] M.D. Hein, H. Kollmus, P. Marichal-Gallardo, S. Püttker, D. Benndorf, Y. Genzel, K. Schughart, S.Y. Kupke, U. Reichl, OP7, a novel influenza A virus defective interfering particle: production, purification, and animal experiments demonstrating antiviral potential, Appl. Microbiol. Biotechnol. 105 (2021) 129–146. https://doi.org/10.1007/s00253-020-11029-5.

[118] K. Lothert, F. Pagallies, F. Eilts, A. Sivanesapillai, M. Hardt, A. Moebus, T. Feger, R. Amann, M.W. Wolff, A scalable downstream process for the purification of the cell culture-derived Orf virus for human or veterinary applications, J. Biotechnol. 323 (2020) 221–230. https://doi.org/10.1016/j.jbiotec.2020.08.014.

[119] K. Lothert, F. Pagallies, T. Feger, R. Amann, M.W. Wolff, Selection of chromatographic methods for the purification of cell culture-derived Orf virus for its application as a vaccine or viral vector, J. Biotechnol. 323 (2020) 62–72. https://doi.org/10.1016/j.jbiotec.2020.07.023.

[120] K. Lothert, A.F. Offersgaard, A.F. Pihl, C.K. Mathiesen, T.B. Jensen, G.P. Alzua, U. Fahnøe, J. Bukh, J.M. Gottwein, M.W. Wolff, Development of a downstream process for the production of an inactivated whole hepatitis C virus vaccine, Sci. Rep. 10 (2020) 16261. https://doi.org/10.1038/s41598-020-72328-5.

[121] M. White, R. Whittaker, C. Gándara, E.A. Stoll, A guide to approaching regulatory considerations for lentiviral-mediated gene therapies, Hum. Gene Ther. Methods 28 (2017) 163–176. https://doi.org/10.1089/hgtb.2017.096.

[122] M. Poorebrahim, S. Sadeghi, E. Fakhr, M.F. Abazari, V. Poortahmasebi, A. Kheirollahi, H. Askari, A. Rajabzadeh, M. Rastegarpanah, A. Linē, A. Cid-Arregui, Production of CAR T-cells by GMP-grade lentiviral vectors: latest advances and future prospects, Crit. Rev. Clin. Lab. Sci. 56 (2019) 393–419. https://doi.org/10.1080/10408363.2019.1633512.

[123] C. Delenda, C. Gaillard, Real-time quantitative PCR for the design of lentiviral vector analytical assays, Gene Ther. 12 Suppl 1 (2005) S36-50. https://doi.org/10.1038/sj.gt.3302614.

[124] W. Barczak, W. Suchorska, B. Rubiś, K. Kulcenty, Universal real-time PCR-based assay for lentiviral titration, Mol. Biotechnol. 57 (2015) 195–200. https://doi.org/10.1007/s12033-014-9815-4.

[125] L. Sastry, T. Johnson, M.J. Hobson, B. Smucker, K. Cornetta, Titering lentiviral vectors: comparison of DNA, RNA and marker expression methods, Gene Ther. 9 (2002) 1155–1162. https://doi.org/10.1038/sj.gt.3301731.

[126] K. Lothert, F. Eilts, M.W. Wolff, Quantification methods for viruses and virus-like particles applied in biopharmaceutical production processes, Expert Rev. Vaccines 21 (2022) 1029–1044. https://doi.org/10.1080/14760584.2022.2072302.

[127] S. Heider, C. Metzner, Quantitative real-time single particle analysis of virions, Virology 462-463 (2014) 199–206. https://doi.org/10.1016/j.virol.2014.06.005.

[128] G. Lizée, J.L. Aerts, M.I. Gonzales, N. Chinnasamy, R.A. Morgan, S.L. Topalian, Real-time quantitative reverse transcriptase-polymerase chain reaction as a method for determining lentiviral vector titers and measuring transgene expression, Hum. Gene Ther. 14 (2003) 497–507. https://doi.org/10.1089/104303403764539387.

[129] M. Geraerts, S. Willems, V. Baekelandt, Z. Debyser, R. Gijsbers, Comparison of lentiviral vector titration methods, BMC Biotechnol. 6 (2006) 34. https://doi.org/10.1186/1472-6750-6-34.

[130] Y. Wang, S. Bergelson, M. Feschenko, Determination of lentiviral infectious titer by a novel droplet digital PCR method, Hum. Gene Ther. Methods 29 (2018) 96–103. https://doi.org/10.1089/hgtb.2017.198.

[131] L.J. Ausubel, C. Hall, A. Sharma, R. Shakeley, P. Lopez, V. Quezada, S. Couture, K. Laderman, R. McMahon, P. Huang, D. Hsu, L. Couture, Production of CGMP-Grade Lentiviral Vectors, Bioprocess Int. 10 (2012) 32–43.

[132] V. Picanço-Castro, P.D. Moço, A. Mizukami, L.D. Vaz, M. de Souza Fernandes Pereira, R.N. Silvestre, J.T.C. de Azevedo, A. de Sousa Bomfim, M.S. de Abreu Neto, K.C.R. Malmegrim, K. Swiech, D.T. Covas, Establishment of a simple and efficient platform for car-t cell generation and expansion: from lentiviral production to in vivo studies, Hematol. Transfus. Cell Ther. 42 (2020) 150–158. https://doi.org/10.1016/j.htct.2019.06.007.

[133] P.J. Klasse, Molecular determinants of the ratio of inert to infectious virus particles, Prog. Mol. Biol. Transl. Sci. 129 (2015) 285–326. https://doi.org/10.1016/bs.pmbts.2014.10.012.

[134] A.J. Marozsan, E. Fraundorf, A. Abraha, H. Baird, D. Moore, R. Troyer, I. Nankja, E.J. Arts, Relationships between infectious titer, capsid protein levels, and reverse transcriptase activities of diverse human immunodeficiency virus type 1 isolates, J. Virol. 78 (2004) 11130–11141. https://doi.org/10.1128/JVI.78.20.11130-11141.2004.

[135] O.-W. Merten, S. Charrier, N. Laroudie, S. Fauchille, C. Dugué, C. Jenny, M. Audit, M.-A. Zanta-Boussif, H. Chautard, M. Radrizzani, G. Vallanti, L. Naldini, P. Noguiez-Hellin, A. Galy, Large-scale manufacture and characterization of a lentiviral vector produced for clinical ex vivo gene therapy application, Hum. Gene Ther. 22 (2011) 343–356. https://doi.org/10.1089/hum.2010.060.

[136] K. Cornetta, L. Duffy, C.J. Turtle, M. Jensen, S. Forman, G. Binder-Scholl, T. Fry, A. Chew, D.G. Maloney, C.H. June, Absence of replication-competent lentivirus in the clinic: analysis of anfused T cell products, Mol. Ther. 26 (2018) 280–288. https://doi.org/10.1016/j.ymthe.2017.09.008.

[137] L.M. Skrdlant, R.J. Armstrong, B.M. Keidaisch, M.F. Lorente, D.L. DiGiusto, Detection of replication competent lentivirus using a qPCR assay for VSV-G, Mol. Ther. Methods Clin. Dev. 8 (2018) 1–7. https://doi.org/10.1016/j.omtm.2017.09.001.

[138] A.L. Gimpel, G. Katsikis, S. Sha, A.J. Maloney, M.S. Hong, T.N.T. Nguyen, J. Wolfrum, S.L. Springs, A.J. Sinskey, S.R. Manalis, P.W. Barone, R.D. Braatz, Analytical methods for process and product characterization of recombinant adeno-associated virus-based gene therapies, Mol. Ther. Methods Clin. Dev. 20 (2021) 740–754. https://doi.org/10.1016/j.omtm.2021.02.010.

[139] J.J. Labisch, F. Bollmann, M.W. Wolff, K. Pflanz, A new simplified clarification approach for lentiviral vectors using diatomaceous earth improves throughput and safe handling, J. Biotechnol. (2021) 11–20. https://doi.org/10.1016/j.jbiotec.2020.12.004.

[140] J.J. Labisch, G.P. Wiese, K. Barnes, F. Bollmann, K. Pflanz, Infectious titer determination of lentiviral vectors using a temporal immunological real-time imaging approach, PLoS ONE 16 (2021) e0254739. https://doi.org/10.1371/journal.pone.0254739.

[141] J.J. Labisch, M. Kassar, F. Bollmann, A. Valentic, J. Hubbuch, K. Pflanz, Steric exclusion chromatography of lentiviral vectors using hydrophilic cellulose membranes, Journal of Chromatography A 17 (2022) 463148. https://doi.org/10.1016/j.chroma.2022.463148.

[142] M. Immarino, J. Nti-Gyabaah, M. Chandler, D. Roush, K. Göklen, Impact of cell density and viability on primary clarification of mammalian cell broth: An analysis using disc-stack centrifugation and charged depth filtration, Bioprocess Int. (2007) 38–50.

[143] J.J. Labisch, A. Pickl, F. Bollmann, K. Pflanz, Lab-scale harvest and clarification of lentiviral vectors using vacuum filtration units, 2021.

[144] J. Stephenson, C. Bladen, I. Wilkinson, Rapid mammalian cell harvest without centrifugation for antibody purification using the Sartoclear Dynamics® Lab filtration system, 2018.

[145] H.E.G.M. Bakr, Diatomite: Its characterization, modifications and applications, Asian J. of Materials Science 2 (2010) 121–136. https://doi.org/10.3923/ajmskr.2010.121.136.

[146] T. van der Meer, B. Minow, B. Lagrange, F. Krumbein, F. Rolin, Diatomaceous earth filtration: Innovative single-use concepts for clarification of high-density mammalian cell cultures, Bioprocess Int. (2014).

[147] A.D. Minh, A.A. Kamen, Critical assessment of purification and analytical technologies for enveloped viral vector and vaccine processing and their current limitations in resolving co-expressed extracellular vesicles, Vaccines (Basel) 9 (2021). https://doi.org/10.3390/vaccines9080823.

[148] K. Lothert, Steric exclusion chromatography: Advancement of a laboratory-based platform technology into a key component of viral vector and vaccine production processes. Dissertation, Gießen, 2022.

7 Appendix

7.1 Abbreviations

AAV	Adeno-Associated Virus
AEX	Anion Exchange Chromatography
AI	Artificial Intelligence
CAR	Chimeric Antigen Receptor
CD19	Cluster of Differentiation 19
DE	Diatomaceous earth
DoE	Design of Experiment
dsDNA	Double-stranded Desoxyribonucleic Acid
DSP	Downstream Processing
ELISA	Enzyme-Linked Immunosorbent Assay
GMP	Good Manufacturing Practice
HEK	Human Embryonal Kidney
HIV	Human Immunodeficiency Virus
Ig	Immunoglobulin
LV	Lentiviral Vector
NaCl	Sodium Chloride
PEG	Polyethylene Glycol
qPCR	Quantitative Polymerase Chain Reaction
SEC	Size Exclusion Chromatography
SXC	Steric Exclusion Chromatography
TFF	Tangential Flow Filtration
VSV-G	Vesicular Stomatitis Virus Glycoprotein

7.2 List of figures

Curriculum vitae

Personal data

Name	Jennifer Julia Labisch
Date of birth	19.08.1994
Place of birth	Hannover, Germany

Education

Since 01/2020	Doctoral student at the Institute of Technical Chemistry, Gottfried Wilhelm Leibniz University, Hannover
10/2017-11/2019	Master of Science in Molecular Biotechnology, Johann Wolfgang Goethe University, Frankfurt am Main
10/2014-09/2017	Bachelor of Science in Molecular Biotechnology, Bielefeld University, Bielefeld
07/2005-06/2013	General Matriculation Standard at Wilhelm-Raabe-Schule, Hannover

Professional experience

Since 01/2020	Scientist, Lab Essentials Applications Development, Sartorius Stedim Biotech GmbH, Göttingen
05/2019-11/2019	Master Thesis, Lab Essentials Applications Development and Regenerative Medicine, Sartorius Stedim Biotech GmbH, Göttingen
10/2018-12/2018	Internship, Membrane Technology, Sartorius Stedim Biotech GmbH, Göttingen
04/2017-07/2017	Bachelor Thesis, Pre-clinical pharmacology and immunology, Fraunhofer ITEM, Hannover

Publications and conference contributions

Publications

(1) J.J. Labisch, F. Bollmann, M.W. Wolff, K. Pflanz. A new simplified clarification approach for lentiviral vectors using diatomaceous earth improves throughput and safe handling, Journal of Biotechnology, Volume 326, 2021, DOI: doi.org/10.1016/j.jbiotec.2020.12.004

- J.J. Labisch (90%): Conceptualization, methodology, investigation, formal analysis, visualization, writing (original draft)
- F. Bollmann, M.W. Wolff (in total 5%): Supervision, writing (review and editing)
- K. Pflanz (5%): Supervision, project administration

(2) J.J. Labisch, G.P. Wiese, K. Barnes, F. Bollmann, K. Pflanz. Infectious titer determination of lentiviral vectors using a temporal immunological real-time imaging approach, PLoS ONE 16(7), e0254739, 2021, DOI: doi.org/10.1371/journal.pone.0254739

- J.J. Labisch (85%): Conceptualization, methodology, investigation, formal analysis, visualization, writing (original draft)
- G.P. Wiese (10%): Investigation, formal analysis, visualization
- K. Barnes, F. Bollmann, K. Pflanz (in total 5%): Supervision, writing (review and editing), project administration

(3) J.J. Labisch, M. Kassar, F. Bollmann, A. Valentic, J. Hubbuch, K. Pflanz. Steric exclusion chromatography of lentiviral vectors using hydrophilic cellulose membranes, Journal of Chromatography A, Volume 1674, Article 463148, 2022,
DOI: doi.org/10.1016/j.chroma.2022.463148

- J.J. Labisch (85%): Conceptualization, methodology, investigation, formal analysis, visualization, writing (original draft)
- M. Kassar (10%): Methodology, formal analysis, writing (review and editing)
- F. Bollmann, A. Valentic, J. Hubbuch, K. Pflanz (in total 5%): Supervision, writing (review and editing), project administration

(4) J.J. Labisch, R. Paul, G.P. Wiese, K. Pflanz. Scaling up of steric exclusion membrane chromatography for lentiviral vector purification, Membranes, 13(2):149, 2023,

DOI: doi.org/10.3390/membranes13020149, patent application number: S15837EU

- J.J. Labisch (85%): Conceptualization, methodology, investigation, formal analysis, visualization, writing (original draft)
- R. Paul, G.P Wiese (in total 10%): Methodology, formal analysis
- K. Pflanz (5%): Supervision, conceptualization, project administration, writing (review and editing)

(5) L. Crowley, J.J. Labisch, M. Leskovec, M. Tajnik Sbaizero, K. McLaughlin, P. Nestola, A. Boulais. Purifying viral vectors - A review of chromatography solutions, published in "Bioprocess development and analytics for viral vector-based therapeutics" by the editors Saurabh Gautam, Abhilash Chiramel, and Roland Pach, publisher: Springer Nature Switzerland AG, accepted manuscript, currently in press

- L. Crowley (30%): Writing (original draft)
- J.J. Labisch (30%): Writing (original draft)
- M. Leskovec, M. Tajnik Sbaizero (in total 25%): Writing (original draft)
- K. McLaughlin, P. Nestola, A. Boulais (in total 15%): Writing (review and editing)

(6) F. Eilts, J.J. Labisch, S. Orbay, Y.M.J. Harsy, M. Steger, F. Pagallies, R. Amann, K. Pflanz, M.W. Wolff. Stability studies for the identification of critical process parameters for a pharmaceutical production of the Orf virus. Submitted to the Journal Vaccine on 19.10.2022.

- F. Eilts (40%): Conceptualization, validation, investigation, visualization, writing (original draft)
- J.J. Labisch (15%): Conceptualization, investigation, writing (review and editing)
- S. Orbay (10%): Investigation, writing (review and editing)
- Y.M.J. Harsy (10%): Investigation, formal analysis, writing (review and editing)
- M. Steger (10%): Investigation, writing (review and editing)
- F. Pagallies (5%): Resources, writing (review and editing)
- R. Amann, K. Pflanz, M.W. Wolff (in total 10%): Writing (review and editing), supervision, funding acquisition

Conference contributions

J.J. Labisch, M. Kassar, K. Pflanz. Steric exclusion chromatography of lentiviral vectors using hydrophilic cellulose membranes. 17th International Ph.D. Seminar on Chromatographic Separation Science (SoCSS), 2022, June 27-29, Karlsruhe, Germany (Oral presentation).

J.J. Labisch, M. Kassar, K. Pflanz. Steric exclusion chromatography as a purification technique for large enveloped viral vectors - lentiviral vectors as a case study. 18th International Symposium on Preparative and Industrial Chromatography and Allied Techniques (SPICA), 2022, October 11-14, Lisbon, Portugal (Poster presentation).